Development of Scalable Solutions for the Valorization of Brewer's Co-Products

Vom Promotionsausschuss der

Technischen Universität Hamburg

Zur Erlangung des akademischen Grades

Doktor-Ingenieurin (Dr.-Ing)

genehmigte Dissertation (Monographie)

von
Marie Schottroff

aus
Hamburg

2025

Examination Board

1st Examiner: Prof. Dr. Andreas Liese
2nd Examiner: Prof. Dr. Kerstin Kuchta
Chair of the Examination Board: Prof. Dr. Anna-Lena Heins

Date of the Oral Examination

16.10.2025

Identifier

DOI: https://doi.org/10.15480/882.16261
Handle: https://hdl.handle.net/11420/59273

Acknowledgements

First of all, I would like to express my sincere gratitude to Prof. Dr. Andreas Liese, who not only supervised my work but also continuously supported my personal growth. Through your dedication and personal commitment, you have created an environment of collaboration and teamwork — one in which not only science is created, but genuine friendships are formed.

I would also like to thank Dr. Mark Schneeberger, whose valuable input and support were essential to the realization of this project. Thank you for believing in the idea of this industrial PhD project right from the beginning. My sincere appreciation goes to the GEA Brewery Systems GmbH Application Development team as well as the Technology Organization under the leadership of Carsten Waubke for their ongoing support.

I would like to extend my sincere gratitude to the whole team of the Institute of Technical Biocatalysis. You welcomed me with open arms, supported me in every question or doubt I had and made the overall experience special. I will never forget the memories created and will be grateful for every moment shared. Special thanks go out to Maren Breuer and Anna Gorte for always supporting everyone and everything that happened in the lab.

Further, I would like to express a special thank you to Leon Klose and Patrick Bahns for reviewing this thesis and for their openness to discuss new ideas at all times.

I am also grateful to the committed students who contributed to this work through their efforts and dedication. My thanks go to Hauke Riebesehl, Klara-Marie Jäger, Josefine Häussling Löwgren, Felix Pitschk, Aein Sanajian, Sara Mansouri Mashhadi, Maral Dibaei Moghanjoghi, Sahar Khosravi and Michelle David. I wish you all the best for your future endeavors and hope to meet you again!

And lastly, but most importantly, I would like to thank my family and husband for supporting me unconditionally. I am forever grateful for everything you do.

Abstract

With the growing importance of sustainable industry transformation, the valorization of once considered waste streams is gaining traction. The brewing industry remains one of the largest food waste producers in the beverage sector, with brewer's spent grain (BSG) and brewer's spent yeast (BSY) being the two most abundant by-products generated [1]. To date, these by-products have been sold as low-cost animal feed or disposed of in landfills. Although the scientific community has extensively investigated potential valorization options, industrial adoption of the proposed processes remains scarce. This work aims to identify scalable solutions for the valorization of BSG and BSY for industrial scale adoption.

For BSY, the valorization strategy focuses on the production of a yeast extract with intrinsic proteolytic activity. Mechanical cell disruption methods such as high-pressure homogenization, glass bead treatment and ultrasonication have been shown to lead to reproducible proteolytic activities in the BSY extracts. The release of protease activity followed first order kinetics for ultrasonication, suitable for identifying optimal process conditions to release maximum activity. For high pressure homogenization, protein extraction yields in the order of magnitude of 60% by mass were achieved simultaneously to the release of proteolytic activity. Thermal yeast autolysis was shown to be unsuitable for the production of proteolytic BSY extracts due to missing trends of released activity with time and temperature. The characterization of the produced BSY extracts revealed the presence of cysteine, aspartate, serine and metalloproteases. The addition of 10 mM zinc sulfate showed to increase the proteolytic activity in the BSY extracts above 10%, presumably due to zinc dependent metalloproteases present. An application of the proteolytic extract showed relative hydrolysis rates above 80% on BSG protein to smaller peptides under optimized conditions.

For BSG, high-shear mixing has been demonstrated to be a suitable wet-milling technology for particle size reduction as well as potentially opening up the lignocellulosic matrix. At dry mass contents of 10%, protein extraction efficiencies were highest for 10 min high-shear mixed BSG. On a 50 g scale, both enzymes Alcalase® and Formea® Sol resulted in protein yields above 65%. The scale-up of the extraction with Alcalase® to a 35 kg scale resulted in protein extraction yields above 80% for different BSG types. The protein extraction on a pilot-scale followed a process intensification approach, since both the particle size reduction as well as the enzymatic hydrolysis took place in the same high-shear mixing device. With steam or hot water available, also inactivation and sterilization steps can be performed. The valorization of the fiber fraction of BSG was evaluated based on the extraction of arabino- and xylo-oligosaccharides through liquid hot water treatment and through the enzymatic extraction of C5 and C6 sugars to form a sugar-rich fermentation medium. For both cases, optimal extraction conditions for the given experimental setup were identified through design of experiment approaches. The sugar extraction resulted in a process applicable on the high-shear mixing device, enabling a route to a sequential BSG valorization process with first a protein extraction and secondly a sugar extraction. The solid residue from a protein extraction process was finally applied in a 5% by weight BSG-PLA composite to produce a 3D-printable filament. The knowledge gained from this work can be used for further upscaling experiments and can help to overcome the challenges of introducing valorization processes for BSG and BSY on an industrial scale.

Kurzfassung

Mit der wachsenden Bedeutung der nachhaltigen Transformation der Industrie gewinnt die Verwertung von einst als Abfall betrachteten Strömen an Bedeutung. Die Brauindustrie ist einer der größten Lebensmittelabfallproduzenten im Getränkesektor, wobei Treber und Althefe die beiden am häufigsten anfallenden Nebenprodukte sind [1]. Bis heute werden diese als kostengünstiges Tierfutter verkauft oder auf Deponien entsorgt. Obwohl die wissenschaftliche Gemeinschaft umfangreiche Ergebnisse zu potenziellen Verwertungsoptionen aufzeigen konnte, bleibt die industrielle Umsetzung der vorgeschlagenen Prozesse aus. Diese Arbeit zielt darauf ab, skalierbare Lösungen für die Verwertung von Treber und Althefe für die industrielle Anwendung zu identifizieren.

Für die Althefe konzentrierte sich die Verwertungsstrategie auf die Herstellung eines Hefeextrakts mit intrinsischer proteolytischer Aktivität. Mechanische Zellaufschlussmethoden wie Hochdruckhomogenisierung, Glasperlen- und Ultraschallbehandlung führten zu reproduzierbaren proteolytischen Aktivitäten. Die Freisetzung der Proteaseaktivität folgte bei der Ultraschallbehandlung einer Kinetik erster Ordnung, was geeignet ist, um optimale Prozessbedingungen für maximale Aktivität im Extrakt zu identifizieren. Bei der Hochdruckhomogenisierung wurden gleichzeitig zur Freisetzung der proteolytischen Aktivität Proteinausbeuten in der Größenordnung von 60% erzielt. Die thermische Hefeautolyse erwies sich aufgrund fehlender Trends der freigesetzten Aktivität in Abhängigkeit von Zeit und Temperatur als ungeeignet für die Herstellung proteolytischer Hefeextrakte. Die Charakterisierung der produzierten Hefeextrakte zeigte das Vorhandensein von Cystein-, Aspartat-, Serin- und Metalloproteasen. Die Zugabe von 10 mM Zinksulfat erhöhte die proteolytische Aktivität in den Extrakten um mehr als 10%, vermutlich aufgrund der Anwesenheit von zinkabhängigen Metalloproteasen. Eine Anwendung des proteolytischen Extrakts zeigte eine relative Hydrolyserate von Treberprotein zu kleineren Peptiden von größer 80% unter optimierten Bedingungen.

Für Treber konnte gezeigt werden, dass Hochscherkaftmischen eine geeignete Technologie zur Partikelgrößenreduktion sowie potenziell zur Öffnung der lignocellulosehaltigen Matrix darstellt. Bei einem Trockensubstanzgehalt von 10% war die Proteinausbeute nach 10 min Hochscherkraftmischen maximal. Auf einer 50 g-Skala führten sowohl die Enzyme Alcalase® als auch Formea® Sol zu Proteinausbeuten von über 65%. Der Scale-up der Extraktion mit Alcalase® auf eine 35 kg-Skala ergab Proteinausbeuten von über 80% für verschiedene Trebertypen. Die Proteinextraktion im Pilotmaßstab folgte einem Prozess-intensivierungsansatz, da sowohl die Partikelgrößenreduktion als auch die enzymatische Hydrolyse im selben Hochscherkraftmischer stattfanden. Mit Dampf oder heißem Wasser können auch Inaktivierungs- und Sterilisationsschritte angeschlossen werden. Die Verwertung der Faserfraktion von BSG wurde basierend auf der Extraktion von Arabino- und Xylo-Oligosacchariden durch Heißwasserbehandlung und durch die enzymatische Extraktion von C5- und C6-Zuckern zur Bildung eines zuckerreichen Fermentationsmediums bewertet. Für beide Fälle wurden optimale Extraktionsbedingungen für das gegebene experimentelle Setup durch statistische Versuchsplanung identifiziert. Die Zuckerextraktion führte zu einem auf dem Hochscherkraftmischer anwendbaren Prozess, der einen Weg zu einem sequentiellen Treberverwertungsprozess ermöglicht, bei dem zuerst eine Proteinextraktion und anschließend eine Zuckerextraktion erfolgt. Der feste Rückstand aus einem Proteinextraktionsprozess wurde schließlich in einem 5% Treber-PLA-Komposit zur Herstellung eines 3D-druckbaren Filaments verwendet. Das aus dieser Arbeit gewonnene Wissen kann für weitere Upscaling-Experimente genutzt werden und dazu beitragen, die Herausforderungen bei der Einführung von Verwertungsprozessen für Treber und Althefe im industriellen Maßstab zu überwinden.

Table of Contents

List of Figures

List of Tables

List of Abbreviations

ANOVA	Analysis of variance
AOS	Arabino-oligosaccharide
AP	Acidification power
BSG	Brewer's spent grain
BSY	Brewer's spent yeast
CAPEX	Capital expenditure
CFU	Colony forming unit
CMC	Carboxymethylcellulose
CWD	Cell wall debris
DCM	Dichloromethane
DH	Degree of hydrolysis
dm	Dry matter content
DNS	3,5-Dinitrosalicylic acid
DoE	Design of experiment
EGTA	Ethylene glycol-bis(β-aminoethyl ether)-*N,N,N′,N′*-tetra acetic acid
EDTA	Ethylenediaminetetraacetic acid
E/S	Enzyme to substrate ratio
FAO	Food and Agriculture Organization of the United Nations
FDM	Fused deposition modelling
Fr	Froude number
FP	French press
FTIR	Fourier-transform infrared spectroscopy
GB	Glass bead
GOS	Gluco-oligosaccharide
HC	Hemicellulose
HPH	High-pressure homogenization
HSM	High-shear mixing
IA	Iodoacetamide
IEP	Isoelectric point
ICP	Intracellular pH
IP	Insoluble protein
KPC	Potassium phosphate citrate buffer
LHW	Liquid hot water
NaPC	Sodium phosphate citrate buffer
NEM	*n*-Ethyl-maleimide
Ne	Newton number
Nu	Nusselt number
MS	Monosaccharide
OPEX	Operational expenditure
PID	Proportional integral derivative
PLA	Polylactic acid
PMSF	Phenylmethylsulfonyl fluoride
Pr	Prandtl number
PS	Polysaccharide
PTFE	Polytetrafluoroethylene
Re	Reynolds number
RNA	Ribonucleic acid
SDS	Sodium dodecyl sulfate
StDev	Standard deviation
TCA	Trichloroacetic acid
US	Ultrasound
WHO	World Health Organization
XOS	Xylo-oligosaccharide

List of Symbols

Latin Symbols

A	-	Absorbance
A_R	1/s	Pre-exponential factor
c	mol/L	Concentration
c_P	J/kg K	Specific heat capacity
d	µm	Diameter
D	m	Inner reactor diameter
E	-	Emission
E_a	J/mol	Activation energy
E_t	MPa	Tangent modulus
E_Y	MPa	Young's modulus
F	-	Dilution factor
g	m/s²	Gravitational constant
k	1/s	Reaction rate constant
l	m	Characteristic length
m	kg	Mass
n	mol	Molar amount
N	1/s	Agitator speed
R	J/mol K	Universal gas constant
R_o	-	Severity factor
t	min or h	Time
T	K	Absolute temperature
u	m/s	Fluid velocity
v	U/g	Mass specific enzyme activity
V	L	Volume
w	-	Mass fraction
Y	-	Yield

Greek Symbols

α	W/m² K	Heat transfer coefficient
ε	%	Strain
ε_b	%	Breakage strain
ϑ	°C	Temperature
λ	W/m K	Thermal conductivity
σ	MPa	Stress
σ_m	MPa	Maximum tensile strength
µ	Pa s	Dynamic viscosity
ρ	kg m^{-3}	Density

1 Introduction

Agricultural and food industries generate relevant amounts of organic residues during raw materials processing. Despite the increasing focus onto circular economy, aiming to minimize waste through regeneration, reuse, and innovation, these by-products often go underutilized, displaying low or no commercial value. The beverage industry is responsible for the largest share of food waste produced at 26% [2]. With a global annual production of 1.88 billion hectoliters in 2023, the brewing industry is a major contributor to this food waste [3]. The valorization of this waste by the brewing sector itself or by external industries would be a major step towards sustainable industry practices. The following chapters provide an introduction to the relevant theoretical framework used in the context of this work and highlight the main challenges on the way to a sustainable industry transformation.

1.1 The Brewing Process

The brewing process is one of the oldest fermentative processes known to mankind. The earliest consumption of beer is dated back as much as 12,000 BC [4]. Although the processes and equipment used have changed over time, the four basic ingredients remain the same: A starch-containing grain, water, hops and yeast. In short, the grains are mixed with water and heated to defined temperature stages to activate intrinsic amylases, that degrade starch into water-soluble oligomers and monosaccharides. The sugar-rich water is referred to as wort and separated from the grain residue through lautering. The wort is further processed through boiling, where also the hops are added for the typical bitterness flavor. Insoluble proteins aggregated during boiling as well as solid hop residues are removed from the wort in a whirlpool process. The aerated wort is then transferred to cooled fermentation vessels, where the yeast is added. The yeast metabolizes contained sugars into ethanol. After fermentation, the so-called green beer is stored for defined periods of time prior to stabilization and final metering. The following Figure 1 gives an overview of the equipment used for the described brewing process. [5]

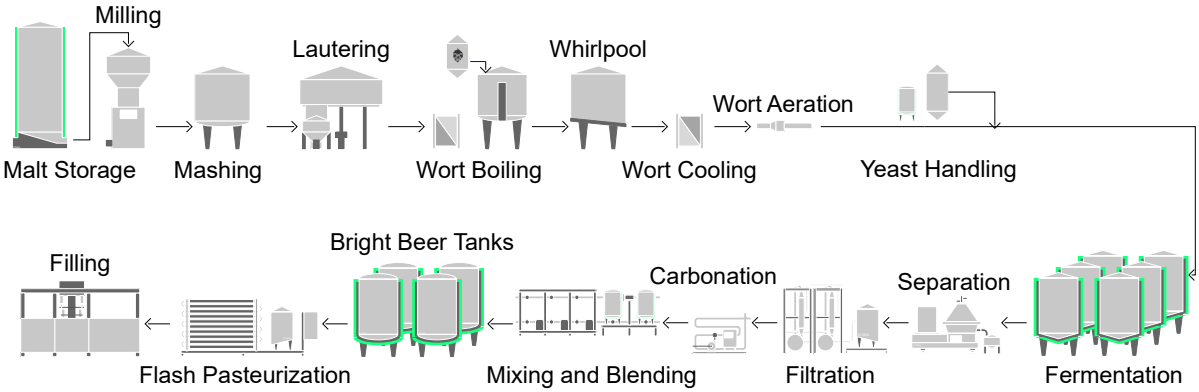

Figure 1: Graphical representation of the brewing process.

From the short description of the brewing process above, it is evident, that a liquid product, the beer, is produced from three solid starting materials: grains, hops and yeast. Per every 100 L of beer produced, around 20 kg of brewer's spent grain (BSG) is produced [6,7]. BSG is the insoluble part of the malt separated during lautering. By mass, this already accounts for 85% of all solid wastes produced during the brewing process [8]. For brewer's spent yeast (BSY), the yeast fraction separated after fermentation and not used for re-pitching, the total mass is estimated to be 1.5-1.8 kg per 100 L of beer produced [9]. In contrast to challenges such as reduction of the overall thermal and electrical energy demand, no classical engineering tools

such as re-use, coupling or change of unit operation allow for omitting the production of BSG and BSY, as they are intrinsic to the process. However, this could also be a chance for the brewing sector. Global beer production has been stagnant or even declined over the past 10 years, producing a need for the breweries to find new ways of revenue [3]. This could enable a fast adoption of promising valorization processes for the by-products produced. The main challenge lies in the design of processes, that allow a fast adoption on the industrial scale, as well as the cooperation of different industries to establish new supply chains.

1.2 Brewer's Spent Grain

Brewer's spent grain is the remaining solid fraction after lautering. It consists mainly of water-insoluble protein, structural carbohydrates and lignin in the husk, pericarp and seed coat [10]. The compositional profile of BSG is commonly reported on the basis of its major constituents: Protein, cellulose, hemicellulose, lignin, ash and lipid. Some research groups add residual starch as another component of interest. The following Table 1 summarizes the commonly reported ranges for these major components in BSG.

Table 1: Commonly reported compositional profile of BSG [7,11–13].

Component	Mass fraction [% w/w]
Protein	17 – 30
Cellulose	20 – 30
Hemicellulose	12 – 25
Lignin	12 – 28
Ash	1 – 5
Lipid	1 – 10
Starch	0 – 26

The wide ranges in chemical composition are a result of the broad malt variety used in the brewing sector, as well as different harvest time, malting and mashing conditions and the potential presence of adjuncts such as maize or rice [10]. An additional factor plays the lack of globally harmonized analytical methods for the determination of biomass compositional profiles.

Although BSG is considered food-grade immediately after leaving the brewing process, its current use is limited to animal feed, biogas production, and landfills [14]. Approximately 70% of all BSG produced is sold at a market price of 35 €/t [12,15]. Due to its promising compositional profile, many efforts have been made in the scientific community to identify appropriate valorization approaches [7,8,12]. One of the main areas of focus has been to leverage the food grade status of BSG as soon as it leaves the process. This approach would be in line with the EU Farm to Fork Strategy as well as the UN Sustainable Development Goals "2 - Zero Hunger" and "12 - Responsible Consumption and Production" [16,17].

A quickly developed approach was the use of BSG as a whole. The BSG was dried and subsequently milled, before being incorporated into food-products such as baked goods, yogurts, sausages or snacks [6,7]. It has been reported, that the incorporation of BSG increased the dietary fiber and protein contents, which is generally considered as desirable properties. Negative impacts have been reported at BSG levels above 15% by mass, since properties such as flavor, texture and color of the final product are influenced [7]. With this, a major limitation of this approach has come to light: The little mass of BSG, that can be incorporated into food-products in contrast to the mass of BSG produced on a daily basis. NAIBAHO ET AL. additionally highlighted missing consumer acceptance and market readiness for a broad application of BSG in a wide variety of food-products [6]. To date, this approach

has been realized in several smaller breweries focusing on the production of small quantities of brewery labelled snacks and ready-to-eats.

Next to the use of BSG as a whole, the use of isolated fractions thereof has been an area of high attention in the scientific community. Especially the extraction of protein has been studied intensely [7,18–20]. The majority of BSG protein consist of globulins, albumins, glutelins and hordeins. Around 7.5% by mass of the total protein content of barley malt is extracted during mashing, mostly from the water- and salt-soluble albumin and globulin fractions. This leaves hordeins and glutelins as the major protein fractions in BSG. While glutelins are known to be soluble in weak alkaline environments, hordeins can be solubilized in hydro-alcoholic solutions. [13] This has resulted in many studies focusing on chemical protein extraction methods using alkaline or ethanol solutions for protein solubilization. Extracted fractions have been reported to present high water-holding capacities [21]. However, the overall highest protein extraction yields were obtained from enzymatic extractions, either through the application of different proteases or a combination with carbohydrases [20]. Produced peptide-rich hydrolysates have been linked to antioxidant and emulsifying properties [21]. Although the extraction and pre-treatment methods required for high protein yields are known, they have yet to be widely adopted on an industrial scale.

In addition to the protein fraction, the lignocellulosic fiber matrix of BSG has received increasing attention for food-grade valorization approaches [7,22–24]. The fiber fraction of BSG consists of cellulose, hemicellulose and lignin, representing 45-65% of dry BSG [7]. An exemplary representation of this structure is given in the following Figure 2.

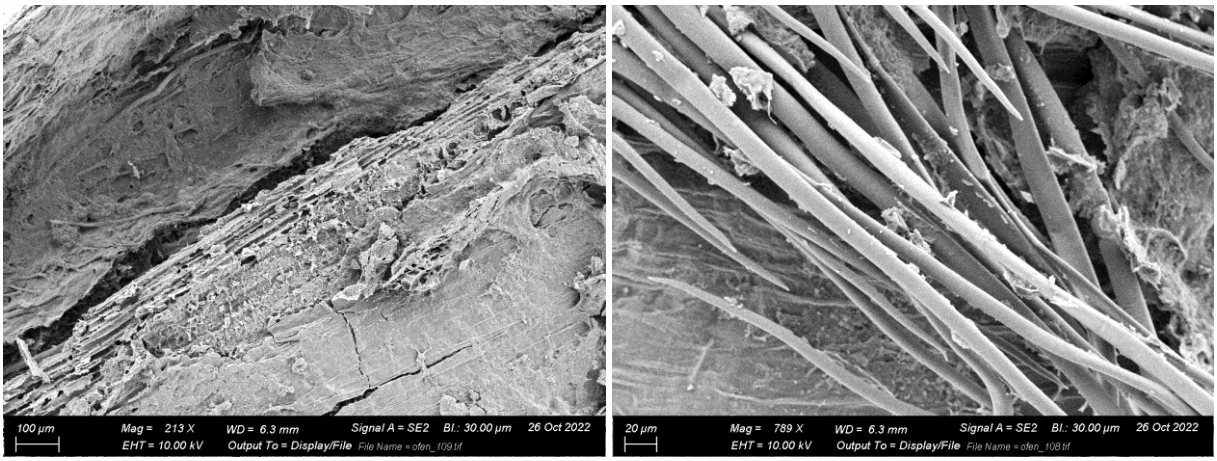

Figure 2: Scanning electron microscope images of BSG fiber structure. Left: 213x magnification of BSG lignocellulosic surface structure. Right: Close-up of 789x magnified cellulose fibrils.

Cellulose is a linear homopolymer consisting of β-1,4-glycosidically linked glucose monomers. Hemicellulose consists mainly of arabinoxylan and a xylose backbone [13]. Lignin as the third part of the fiber fraction is a phenolic macromolecule. It is made up of three aromatic monomers: p-coumaryl alcohol, coniferyl alcohol and sinapyl alcohol [25]. The fiber fraction can be divided into a soluble and an insoluble part. The soluble fraction includes high branched arabinoxylans, xyloglucans and β-glucans, while the insoluble fraction consists of lignin, cellulose, glucomannans and low branched arabinoxylans [13]. Studies for the valorization thereof for the food sector have mostly focused on the extraction of antioxidant polyphenol fractions and prebiotic arabino- and xylo-oligosaccharides [7,22,24]. Hydrothermal treatments have been proposed as suitable extraction technologies. For all fractionation approaches, different pretreatment options have been applied to open up the lignocellulosic matrix of BSG and enhance access to contained components. Commonly applied pretreatment strategies

include drying, milling, wet-milling, autoclaving, defatting, ultrasonication, microwave treatment and pulsed electric field application [20,26].

In addition to valorization strategies within the food sector, other approaches have included the use of BSG for biotechnological processes such as the production of protein-enriched animal feed, lactic acid, or enzymes in solid-state or submerged fermentations [27–29]. In addition, biorefinery approaches for the production of bulk chemicals have been proposed [8,30]. Application of BSG in functional materials, e.g. as biosorbents as well as brick additives and in packaging materials have been studied [8,31–33]. And lastly, the recovery of energy from BSG in the form of biogas, through combustion or pyrolysis have been discussed [8,12].

1.3 Brewer's Spent Yeast

Brewer's spent yeast is the yeast fraction not used for further beer fermentations. The cells are still viable when leaving the process. Common yeast strains used for beer brewing can be divided into two categories: top-fermenting ale yeast strains (*S. cerevisiae*) and bottom-fermenting lager yeast strains (*S. pastorianus*) [34]. The main characteristics of these yeast strains are shown in the following Table 2.

Table 2: Main characteristics of brewing yeast strains *S. cerevisiae* and *S. pastorianus* [35].

Parameter	*S. cerevisiae*	*S. pastorianus*
Optimum fermentation temperature	12 – 25 °C	5 – 15 °C
Flocculation	Weakly flocculent (flotation behavior)	Strongly flocculent (sedimentary behavior)
Glucose induced inhibition of maltose uptake	Yes	No
Fermentation of maltotriose	Little	High

In industrial sized breweries, it is common practice to reuse employed yeast fractions for 4-6 times before disposal [36]. However, only a small fraction of the total spent yeast is used to restart the next fermentation batch, while the majority is discarded [37]. During beer fermentation, yeast cells are exposed to a number of external stress factors such as oxidative, osmotic and nutritional stress. This implies, that the yeast metabolic state and thus its compositional profile is not uniform over different fermentation cycles [38]. The compositional profile and potential applications of BSY thus depend not only on the yeast strain employed, but also on the number of pitching cycles, stress factors the cells were exposed to and beer type that was produced. A mean compositional profile of BSY is given in the following Table 3.

Table 3: Commonly reported compositional profile of BSY [36,37,39].

Component	Mass fraction [% w/w]
Protein	40 – 75
RNA	1 – 21
Ash	5 – 14
Lipid	0.2 – 4
Carbohydrates	12 – 26

To date, 40-60% of BSY are used as low-cost animal feed with a focus on swine and cattle [40,41]. However, due to its high protein content, research on valorization processes for BSY has focused on its direct use for human consumption [37,42,43]. Recent approaches have focused on the use of BSY as a fermentation substrate and the extraction of valuable fractions such as proteins, peptides and glucans as functional foods [37,44]. In addition,

peptide-rich extracts of BSY have been associated with multiple bioactivities, including antimicrobial, antioxidant and antihypertensive properties [40,45]. Next to the extraction of bioactive peptides from BSY, intrinsic bioactivities from enzymes of the yeast cells offer potential for valorization. Of particular interest are yeast-derived enzymes, most promisingly protease and invertase enzymes [40]. As proteases constitute the largest category within the industrial enzyme markets, the demand for novel, cost-effective and food-grade enzymes is high [46,47]. These bioactive molecules could potentially act as green hydrolysis feedstocks for use in the food and health sectors, where the production of peptide-rich products from (plant) protein sources is a highly sought after area of research [48–50]. However, there has been little research into the extraction of intracellular enzymes from BSY [51–53]. Most existing studies focus on the extraction of specific enzymes for analytical investigation of enzyme type and its properties to gain knowledge on the yeast strain and its metabolism [54–56]. The focus on extraction of enzymes in a crude yeast extract to make use of their activity in subsequent processes is not well established. This paragraph was adapted from SCHOTTROFF ET AL. (2025) [57]

Most of the yeast proteases can be found in the vacuole compartment. A graphical representation of a BSY cell is given in Figure 3.

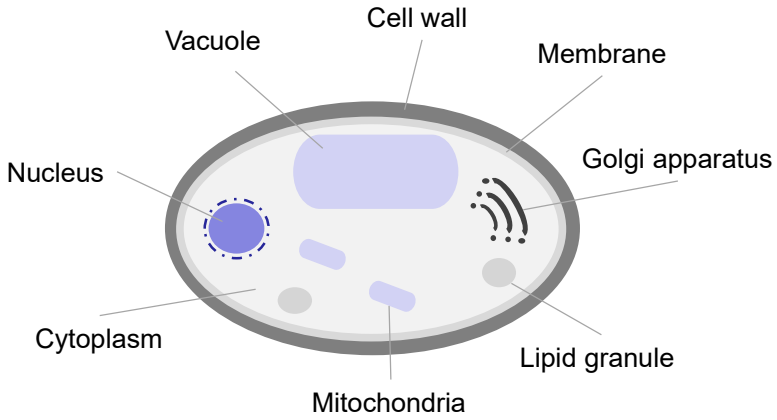

Figure 3: Graphical representation of a brewer's spent yeast cell and its organelles.

One of the principal functions of the vacuole is protein degradation through different types of exo- and endoproteases [35,58]. Damaged or superfluous proteins are degraded into basic amino acids, which are stored in or extracted from the vacuole for further use. The vacuole contained proteases also play a central role in the stress-induced yeast autolysis process. Non-specific intracellular proteolysis is triggered under starvation or pH and temperature shock conditions [35,58,59]. Yeast vacuolar proteases have been studied extensively for laboratory *S. cerevisiae* strains [56,58,60–63]. The following Table 4 summarizes the seven known vacuolar proteases.

Table 4: Known vacuolar proteases of *S. cerevisiae* [56,58,63].

Protease	EC number	Type
Proteinase A	3.4.23.6	Aspartyl Endoprotease
Proteinase B	3.4.22.9	Serine Endoprotease
Carboxypeptidase Y	3.4.16.5	Serine Carboxypeptidase
Carboxypeptidase S	3.4.17.4	Zinc Metalloprotease
Aminopeptidase I	3.4.11.22	Zinc Metalloprotease
Aminopeptidase Y	3.4.11.15	Metalloprotease
Dipeptidylaminopeptidase B	3.4.14.2	Serine Dipeptidase

Generally, endoproteases such as proteinase A and B hydrolyze protein-internal peptide bonds, whereas exoproteases such as carboxy- and aminopeptidases hydrolyze peptide bonds between C- or N-terminal amino acids [35,64]. The residual activity of BSY contained proteases can be influenced by endogenous and external activators and inhibitors. In the case of aspartyl and metalloproteases, an activated water molecule acts as a nucleophile during hydrolysis of the peptide bond of the substrate. Aspartyl proteases contain an aspartic acid residue in their active site and display optimum catalytic activity at acidic pH. Metalloproteases of *S. cerevisiae* possess a glutamic acid residue in their active site and require divalent metal ions for hydrolysis. Ions like Zn^{2+}, Ca^{2+} and Mg^{2+} are known to act as potential activators during catalysis. [58,64]

The extraction of valuable fractions from BSY requires the disruption of the yeast cell wall.The cell wall makes up about 15-20% of the total dry weight of a cell and consists of the polysaccharides glucan, mannan and chitin as well as protein and lipids [65]. Cell disruption methods are generally divided into three groups: Physical, chemical and enzymatic methods. Physical methods include the use of ultrasound, high-pressure homogenization, cell milling, decompression and pulsed electric fields [42,66]. Chemical methods include the use of chelating agents, detergents and solvents able to cause permeabilization or lysis of the yeast cells [66]. Enzymatic disruption methods can be divided into autolysis processes, whereby endogenous yeast enzymes degrade the cell triggered by external stress factors such as starvation or pH and temperature shocks [65]. The application of external lytic enzymes such as lysozymes, glucanases and lipases form the second group of the enzymatic cell disruption methods [42].

1.4 Scale-up of Processes

The commercialization of processes requires the transfer from lab-scale findings to industrial sized requirements. One of the main challenges in the design of lab-scale studies is the identification of critical parameters for large scale applications. Among others, the following points need to be addressed:

- Equipment design changes due to change of operation mode from batch to continuous, from glass vessels to stainless-steel applications or due to non-linearities among scale [67].
- Safety considerations in terms of equipment modifications, standard operating procedures and personal protective equipment used [67].
- Spatial requirements on site in terms of unit operations chosen and equipment design.
- Regulatory requirements in terms of the product, the process, the surroundings of the process or disposal of side-streams [67].
- Consideration of OPEX and CAPEX investments early on to determine the product quality and unit operations required as well as the overall business case.

Scale-up in itself is the increase of production scale, often from laboratory to pilot and finally the industrial size. From an engineering perspective, the main challenge during scale-up of lab-scale results arises due to non-linearities among scale in heat and mass transfer as well as energy requirements [67]. This implies, that often the lab-scale equipment used cannot simply be increased in size. Instead, the design of the reactor itself, including heating and mixing equipment may need to be adjusted. To ensure, that lab-scale yields and quality parameters can still be achieved with a different set of equipment used, a dimension analysis can be introduced. This mathematical tool is used to describe chemical or physical processes via linearly independent variables [68]. The resulting dimensionless numbers can be used to describe systems at different scales, that possess the same chemical or physical properties.

In the scope of fluid dynamics and mixing, relevant dimensionless numbers include the Reynolds, Newton and Froude numbers. In the field of heat transfer, relevant dimensionless numbers include the Nusselt and Prandtl numbers.

The Reynolds number represents the relation of inertial to viscous forces in a fluid flow and is used to describe the flow regime. For a fluid flow through a radial pipe, the critical Reynolds number marking the transition from laminar to turbulent flow regime is commonly stated as 2300. [69] For stirred tank vessels, this number is not as clearly defined, as it strongly depends on the impeller geometry. The critical Reynolds number for these cases is commonly found above 20000 [70]. The Reynolds number is defined as per equation (1).

$$Re = \frac{\rho \cdot u \cdot l}{\mu} \tag{1}$$

With *Re* representing the dimensionless Reynolds number, *ρ* the density in [kg/m³], *u* the fluid velocity in [m/s], *l* the characteristic length in [m] and *μ* the dynamic viscosity in [Pa s].

The Newton or Power number describes the ratio of power consumption relative to the fluid properties and impeller speed. It is thus commonly used in the design of stirred tank reactors together with the Reynolds number to determine desired mixing conditions at low power inputs. The Newton number is defined as per equation (2). [71]

$$Ne = \frac{P}{\rho \cdot N^3 \cdot D^5} \tag{2}$$

With *Ne* representing the dimensionless Newton number, *P* the power of the agitator [W], *ρ* the fluid density [kg/m^3], *N* the agitator speed [1/s] and *D* the diameter of the agitator [m].

The Froude number describes the relation of inertial forces to gravitational forces. In the field of process engineering, it is commonly used in multiphase flow applications to describe the mixing regime in open tanks. The number is defined as per equation (3). [69]

$$Fr = \frac{u^2}{g \cdot l} \tag{3}$$

With *Fr* representing the dimensionless Froude number, *u* the fluid velocity in [m/s], *g* the gravitational constant in [m/s^2] and *l* the characteristic length in [m].

The Nusselt number is a dimensionless heat transfer coefficient and thus describes the ratio of convective to conductive heat transfer. The determination of the Nusselt number strongly depends on the characteristic length and the correlation used to describe the convective heat transfer coefficient. The Nusselt number is defined as per equation (4). [69]

$$Nu = \frac{\alpha \cdot l}{\lambda} \tag{4}$$

With *Nu* representing the dimensionless Nusselt number, *α* the heat transfer coefficient in [W/m² K], *l* the characteristic length in [m] and *λ* the thermal conductivity in [W/m K].

The Prandtl number describes the ratio of momentum diffusivity to thermal diffusivity and is a thermophysical property ratio. It is commonly used in the description of heat transfer properties of fluids. The Prandtl number is defined as per equation (5). [69]

$$Pr = \frac{\mu \cdot c_P}{\lambda} \tag{5}$$

With *Pr* representing the dimensionless Prandtl number, *μ* the dynamic viscosity in [Pa s], c_P the specific heat capacity in [J/kg K] and *λ* the thermal conductivity in [W/m K].

1.5 Challenges in By-Product Valorization in the Brewing Industry

Both the know-how on scaling processes from a small to a larger scale and the knowledge on potential BSG and BSY valorization processes in the scientific community exist. Still, industrial sized valorization plants remain scarce. A potential reason might lie in the lack of interdisciplinary teams in the development of BSG and BSY valorization processes. On an industry level, the development of new processing options or products includes laboratory staff, an engineering team and the business development units [67]. This allows an early on adjustment of process needs to both product, processing and economic aspects. Most of the knowledge generated on BSG and BSY valorization exists inside of the scientific community, rarely incorporating industrial partners during study design. Using this knowledge directly by the industry is challenging, as most of the reported BSG and BSY valorization efforts were conducted on the lab-scale without stating dimensionless numbers for upscaling experiments [20,37]. Bringing the vast knowledge on BSG and BSY valorization to the industry thus requires further efforts in terms of proof of principle upscaling trials, clearly stating data relevant for process transfer including energy requirements and dimensionless numbers as well as demonstrating the technological readiness level of newly applied technologies. In addition, the proposed valorization strategy must be able to process a relevant amount of the BSG produced with each brew. In a 1,000,000 hL/a brewery with 300 d/a of production, the wet BSG amount on a production day accumulates to 8 t/h. This example highlights the need for scalable processing equipment with short processing times. An additional benefit could arise for unit operations allowing for high solids loadings.

Other factors relevant to the industry include the knowledge on achieved purity levels, the overall reproducibility and which by-products are generated. This knowledge is essential in developing an understanding of the product produced, waste handling procedure required and also helps gain insights into the overall business case [67]. In addition, it enables the industry to start establishing supply chains and investigating the consumer acceptance of proposed products. In terms of the overall business case, there are already publications moving towards techno-economic analyses, being a very important step towards demonstrating the economic viability of the proposed processes [24,72,73].

In addition to these knowledge-based gaps, there are further challenges in the valorization of BSG and BSY, that need to be addressed. Both present high moisture contents when leaving the brewing process. BSG after lautering is reported to contain 70-80% water, whereas yeast is harvested as a beer slurry with a water content of 86-90% by mass [7,74]. This for one implies high transport costs to a valorization site in a wet state, which challenges the business case for processing plants outside the immediate vicinity of breweries. Additionally, especially BSG is prone to microbial spoilage during storage in the wet state, with a stability of only two days at ambient conditions [14]. Drying BSG and BSY is associated with high energy demands and thus costs, without increasing the value of the biomass itself. This creates the need to either directly valorize the BSG or BSY fractions inside of the brewery complex or to produce a stable intermediate for subsequent industries. Both options need to yield higher value components justifying the added CAPEX and OPEX for the stabilization or valorization line of the brewery.

Overall, the great potential of using these two co-products in new processes could be the next step towards more sustainable beer production, if the extensive knowledge of potential valorization processes for BSG and BSY is combined with the data required for industrial adoption.

2 Aim of the Thesis

The main objective of the thesis is to develop and evaluate valorization strategies for both BSG and BSY to overcome current challenges in existing valorization processes. The focus is set on the following strategies:

- In-house valorization of BSG and BSY inside of the brewery to omit the need for costly transport in the wet state or energy intensive drying steps without added value to the product fractions. In addition, the direct processing minimizes the risk of microbial degradation during storage.
- Production of stabilized intermediates enriched in either protein, fiber or with intrinsic biological activity for subsequent industries, rather than producing finally purified end-consumer products. This limits the footprint required for the valorization plant and gives the brewing company the flexibility to meet local market demands.
- Application of a holistic approach, making use of every fraction of BSG and BSY.
- Only scalable solutions and wet processing options are investigated to avoid energy intensive drying steps as well as making use of the already contained water.
- Process intensification approaches are used, that limit the required footprint of the overall plant.

For the valorization of BSY, the production of a hydrolytic extract is investigated. This extract could act as a hydrolysis feedstock for the brewery itself or for subsequent industries in the food sector. For the production thereof, the technologies thermal yeast autolysis, ultrasonication, high-pressure homogenization and glass bead treatment are applied. In addition to the release of proteolytic activity, the overall protein extraction efficiency is evaluated. The produced BSY extract is characterized to identify suitable application ranges for enzymatic hydrolysis. A proof of principle application of this extract is conducted on BSG protein to potentially produce a peptide-rich product and enable a co-valorization of both BSG and BSY in a single process.

For the valorization of BSG, different fractionation approaches are studied. In line with the process intensification strategy, a high-shear mixing device is introduced and evaluated for the wet-milling of BSG and subsequent hydrolysis reactions. The enzymatic extraction of protein as well as monosaccharides from BSG is studied on both the lab- and pilot-scale. In addition, the extraction of arabino- and xylo-oligosaccharides through liquid hot water treatment is evaluated. The remaining solid residue is analyzed on its potential to be used in material applications.

3 Materials and Methods

3.1 Chemicals & Materials

Unless otherwise stated, all chemicals were purchased from Carl Roth (Karlsruhe, Germany) or Sigma Aldrich (Steinheim, Germany) in a purity ≥ 98%. The gel used for electrophoresis of proteins ServaGel™ TG PRiME™ 8% was purchased from SERVA (Heidelberg, Germany). Brewer's spent yeast was produced in the 1 hL microbrewery Campus Perle of the Hamburg University of Technology, which was kindly made available for this work, before being stored for a maximum of 24 h at 4 °C prior to cell disruption. The SafLager™ W-34/70 yeast strain used, a *Saccharomyces pastorianus* variant, was purchased from Fermentis by Lesaffre (Marcq-en-Baroeul Cedex, France). Brewer's spent grain was produced in the same 1 hL microbrewery, before being stored at -20 °C in polypropylene bags until use. Unless otherwise stated, all brewing malts are from WEYERMANN® (Bamberg, Germany). The hops used were Magnum and Hercules by Hopsteiner (Mainburg, Germany) and Amarillo by Barth Haas (Nuremberg, Germany). All protease enzymes and enzyme blends were kindly provided by Novonesis (Bagsvaerd, Denmark). Polylactic acid (PLA) with a specific density of 1240 kg/m³ was purchased from 3devo (Utrecht, Netherlands).

3.2 Raw Material Production

A standardized American lager beer was brewed in the 1 hL microbrewery Campus Perle of the Hamburg University of Technology. The set up of the brewery is given in the following Figure 4.

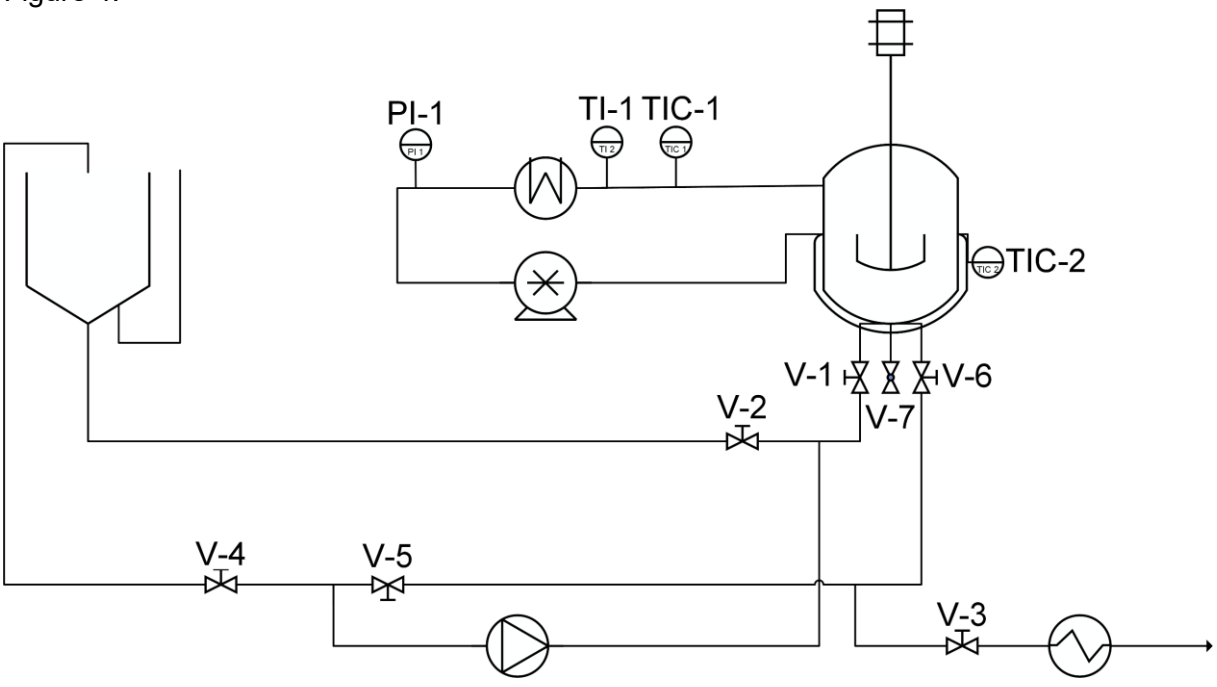

Figure 4: Piping and instrumentation diagram of the 1 hL microbrewery Campus Perle.

The gravity after boiling was set to 12.5 °P. The bottom-fermenting lager yeast strain *S. pastorianus* type SafLager® W34/70 by Fermentis was used for all fermentations. Fermentations were run at 12.8 °C until a constant residual sugar content was determined for two consecutive days, as can be seen for an exemplary brew in Figure 5. This paragraph was adapted from SCHOTTROFF ET AL. (2025) [57].

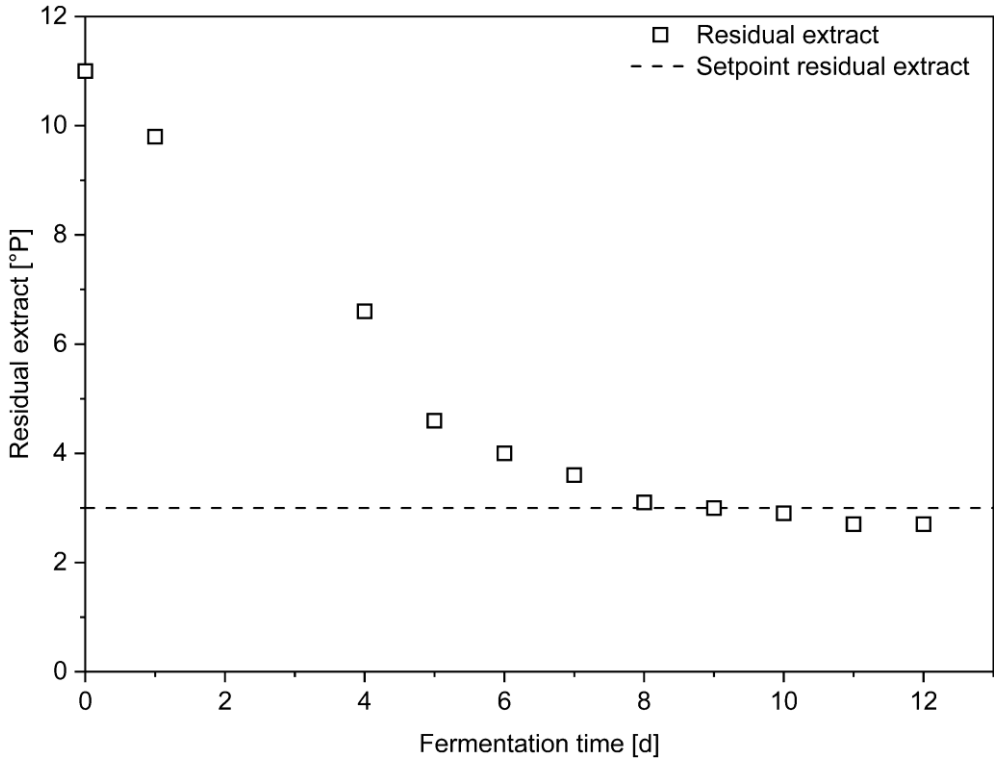

Figure 5: Lager beer fermentation at 12°C stopped after reaching a residual extract of ≤3 °P.

The beer suspension was subsequently cooled to 7 °C for 24 h to allow the yeast to sediment in the cylindroconical bottom of the tank. The BSY slurry was harvested after beer separation and stored at 4 °C for a maximum of 24 h before cell disruption. This paragraph was adapted from SCHOTTROFF ET AL. (2025) [57]. During lautering, the BSG was washed twice with tap water to wash out remaining wort components required for the brewing process. The left spent grains were collected in 2 L polypropylene bags and frozen at -20 °C until further use.The exact recipe used is given in the following Table 5.

Table 5: Standardized lager beer recipe RubyRoast produced at the Campus Perle microbrewery.

Parameter	Value	Unit
Beer type	Premium American Lager	-
Total malt weight used	25	kg
Pilsner malt	18.25	kg
CARARED malt	6.25	kg
CARAAROMA malt	0.5	kg
Total hops weight used	145.4	g
Mosaic hops	49.1	g
Herkules hops	49.1	g
Cascade hops	47.2	g
Gravity after boiling	12-12.5	°P
Yeast strain used	SafLager™ W-34/70*	-
Fermentation temperature	12	°C
Fermentation time	11-17	d
Final Gravity after fermentation	≤ 3	°P

**S. pastorianus* variant by Fermentis [75]

3.3 Raw Material and Product Characterization

The following chapters summarize all analytical assays, procedures and devices used for characterization of the raw materials or any fractions thereof.

3.3.1 Water Content Determination

The moisture content of each sample was determined on a Mettler Toledo Moisture Analyzer HE53 (Gießen, Germany). 1 g of wet sample was placed in an aluminum pan and heated to 105 °C until constant weight. The weight loss during drying was deemed the water content of the sample.

3.3.2 Protein Content Determination

Pierce Assay

A colorimetric assay was used to qualitatively assess the protein contents in liquid phases. The basis for the Pierce bicinchoninic acid is a reduction of Cu^{2+} to Cu^{+} by protein in an alkaline medium [76]. In short, 150 µL of Pierce reagent were mixed with 10 µL of sample, followed by 5 min incubation at 30 °C in the dark in a microwell plate. Absorbance was read at 660 nm in triplicates with an extinction coefficient of 0.0367 L/mmol/cm in a Tecan Infinite 200 Pro microplate reader (Maennedorf, Switzerland). Calibration was done with bovine serum albumin. This paragraph was adapted from SCHOTTROFF ET AL. (2025) [57].

Determination of amino acid profile

The amino acid profiles of dried, solid samples were determined according to LAMP ET AL. (2018) [77]. In short, quantification of proteinogenic amino acids was carried out chromatographically after analytical acid hydrolysis. 0.2-0.3 g of the dried sample were hydrolyzed at 110 °C for 24 h with 25 mL of 6 M HCl in a convective oven. After cooling, the sample pH was adjusted to pH 1 using 10 M NaOH. 2 mL of internal standards L-norvaline and sarcosine each at 2.5 mM were added and mixed. Samples were filtered through a 0.45 µm polyether sulfone syringe filter and transferred to HPLC vials. For chromatographic analysis, an Agilent Infinity 1260 HPLC (Santa Clara, CA, USA) with fluorescence detector was used, where the non-polar stationary phase is a C18 column and the mobile phase a gradient system of an aqueous buffer solution of 0.5 M sodium borate buffer at pH 8.4 and an organic phase of acetonitrile, methanol and water at a volumetric ratio of 45:45:10. Derivatization was done with *o*-phthaldialdehyde for aspartic acid, glutamic acid, serine, histidine, glycine, threonine, arginine, alanine, tyrosine, methionine, phenylalanine, isoleucine, leucine and lysine and with 9-fluorenylmethyloxycarbonyl chloride for proline. This paragraph was adapted from SCHOTTROFF ET AL. (2025) [57].

The amino acids cysteine and tryptophan were only determined for the raw materials. For the cysteine determination, the samples were oxidized with 0.5 mL of a 30% hydrogen peroxide solution and 4.5 mL of a 0.05 M phenol and formic acid solution for 26 h at 20 °C. The reaction was stopped with the addition of 0.84 g of sodium pyrosulfite. Subsequently, the acid hydrolysis was conducted as described earlier. For tryptophan, an alkaline hydrolysis was conducted with the addition of 5 mL of a 4.2 M NaOH and 0.2 mM thiodiglycol solution at 110 °C for 20 h. The pH was subsequently adjusted to a value of pH 3 with 6 M HCl. The following procedure was equivalent to the procedure described for the acid hydrolysis with the difference, that only norvaline was used as an internal standard. Both amino acids cysteine and tryptophan were only determined for the starting materials due to the toxicity of the required chemicals and low concentrations in both BSG and BSY. Literature data for BSY states only low mass fractions in the range of 2.84% for a combined value of cysteine and methionine and 1.10% for tryptophan [78]. Literature data for BSG states also only low mass fractions with 0.22% for cysteine and 0.14% for tryptophane, respectively [7,79].

The protein extraction yield was based on the determined amino acid profile and defined according to the following equation.

$$Y_P = \frac{m_H \cdot w_{P,H}}{m_{BSY} \cdot w_{P,BSY}} \quad (6)$$

With Y_P denoting the dimensionless extraction yield, m_H the dried mass of the hydrolysate [g], $w_{P,H}$ the protein content in the hydrolysate per dry matter hydrolysate [w/w], m_{BSY} the dry matter mass of BSY [g] and $w_{P,BSY}$ the protein content in BSY per dry matter of BSY [w/w]. Whenever the protein content of the hydrolysate could not be determined directly due to limits in available sample mass after drying, it was calculated via a mass balance as given in equation (7) based on the determined protein content in the solid residue after drying.

$$m_H w_{P,H} = 1 - m_{SR} \cdot w_{P,SR} \quad (7)$$

With m_{SR} denoting the dried mass of the solid residue [g] and $w_{P,SR}$ the protein content in the solid residue per dry matter in [w/w].

CHNS Elemental Analysis

The elemental analysis for carbon, hydrogen, nitrogen and sulfur (CHNS) was used as an indirect determination for the protein content in samples, that did not present sufficient dry mass for an amino acid HPLC analysis. The protein content was determined indirectly from the nitrogen content using conversion factors. A conversion factor of 6.25 was used for BSG and 5.50 for BSY [80,81]. The elemental analysis was conducted by the central lab of the Hamburg University of Technology using a Vario Macro Cube by Elementar (Langenselbold, Germany).

3.3.3 Determination of the Degree of Hydrolysis

The determination of the degree of hydrolysis was based on the assay developed by ADLER-NISSEN and BENJAKUL AND MORRISSEY with modifications [82,83]. In short, 125 µL of the sample was pipetted into a 5 mL Eppendorf tube. 2 mL of 0.21 M NaPC at pH 8.2 were added. Subsequently 1 mL of 0.01% w/v trinitrobenzene sulfonic acid was added and the mixture vortexed for homogenization. The reaction mixture was incubated for 20 min in the dark at 50 °C and the reaction subsequently stopped via the addition 2 mL 0.1 M Na_2SO_4. After cooling down for 20 min at room temperature, 150 µL of the mixture were transferred into a 96-well plate and the absorbance measured at 420 nm. A standard curve with L-leucine was used.

The maximum possible degree of hydrolysis was determined from 0.2 g of dried biomass. 25 mL of 6 M HCl was added and an acid hydrolysis was carried out for 24 h at 110 °C in a convective oven. After cooling, the sample pH was adjusted to pH 6 using 10 M NaOH. The liquid hydrolysate was filtered into a 2 mL vessel using a 0.45 µm polyether sulfone syringe filter. The sample was then subjected to the same procedure as described above.

The degree of hydrolysis was calculated using the following equation (8).

$$DH = \frac{h}{h_{max}} \quad (8)$$

With DH representing the dimensionless degree of hydrolysis, h the free α-amino acid content of the sample [mmol] and h_{max} the maximum possible free α-amino acid content of the starting biomass [mmol].

3.3.4 Sugar and Structural Carbohydrate Content Determination

The determination of monomeric sugars, organic acids as well as furfural and hydroxymethylfurfural was conducted according to the lab analytical procedure NREL/TP-510-42623 of the National Renewable Energy Laboratory of the US Department of Energy [84]. In short, the pH of each sample was adjusted to a value of pH 5-6 with calcium carbonate. The sample was then filtered and subjected to HPLC analysis in an Agilent Infinity 1260 system (Santa Clara, CA, USA) equipped with a refractive index detector (RID). The mobile phase used was a 5 mM H_2SO_4 solution containing 1% v/v acetonitrile. The method run time was set to 65 min at a flow rate of 0.7 mL/min. 10 µL of sample were injected and the refractive index was analyzed at a detector and column temperature of 55 °C. Calibration was done for cellobiose, glucose, xylose, arabinose, formic acid, acetic acid, furfural and hydroymethylfurfural in a concentration range of 0-24 g/L.

Structural carbohydrates were determined with the same HPLC settings, but after analytical hydrolysis according to NREL/TP-510-42618 [85]. In short, the determination of structural carbohydrates started with 300 mg of dried, solid sample dissolved in 3 mL of 72% by weight H_2SO_4 and incubated at 30 °C for 60 min. The acid was then diluted with ultrapure water to a final acid concentration of 4% w/w. A 5 mL aliquot was transferred to a pressure tube for subsequent autoclaving at 121 °C for 60 min in a VARIOKLAV® BlueLine by HP Kabortechnik (Oberschleißheim, Germany). After cooling, the sample was vacuum-filtered to remove the solids and the pH was adjusted to pH 5-6. The samples were filtered again using a 0.2 µm nylon syringe filter and transferred to HPLC vials for analysis of monomeric sugar contents. To account for the release of water during formation of polysaccharides when converting the sugar concentrations to the structural carbohydrate concentrations, anhydro correction factors of 0.90 for glucose and 0.88 for xylose and arabinose were used [85].

For the determination of oligosaccharides in liquid samples, a 5 mL aliquot thereof was transferred to a pressure tube. 174 µL of a 72% by weight H_2SO_4 solution was added to result in an acid concentration of 4% w/w. These samples were autoclaved at 121 °C for 60 min together with sugar recovery standards to account for the loss of monomeric sugars during analytical hydrolysis. The sugar recovery standards contained 20 g/L glucose, 10 g/L xylose and 2 g/L arabinose. The pH of the samples and the sugar recovery standards was adjusted to pH 5-6 prior to filtration into HPLC vials using a 0.2 µm nylon syringe filter. Next to the hydrolyzed samples, a filtered aliquot of each untreated sample was analyzed for monosaccharide concentrations. The determined difference in monosaccharide contents from untreated and hydrolyzed samples corrected for the loss of monomeric sugars detected via the sugar recovery standards was then used to determine the overall oligosaccharide concentrations. The same anhydro correction factors than for the structural carbohydrates were used.

3.3.5 Lignin Content Determination

The lignin content was determined from the acid hydrolysate of the determination procedure for the structural carbohydrates as described in chapter 3.3.4. The determination was based on the spectrophotometric analysis of this liquid sample at 340 nm according to NREL/TP-510-42618 [85].

3.3.6 Lipid Content Determination

The lipid content of BSG and BSY samples was based on a Soxhlet extraction using *n*-hexane as a solvent. 5 g of dried biomass were placed in a cellulose thimble and covered with cotton wool. The thimble was placed in a Soxhlet extractor filled with 300 mL *n*-hexane and let run for 6 h under boiling conditions. Water was used as a cooling medium in the top-mounted reflux condenser. After extraction, *n*-hexane was evaporated using a rotary evaporator and the

remaining solid residue dried at 60 °C until constant weight. The lipid content was then determined gravimetrically from the weight of the remaining solid residue.

3.3.7 Ash Content Determination

The ash content was determined in a muffle furnace according to DIN ISO 18122. In short, 1 g dried biomass was transferred to a ceramic bowl and heated to 550 °C until constant weight. The sample was left to cool in a desiccator, before the remaining ash weight was determined gravimetrically.

3.3.8 RNA Determination

For BSY, the RNA content was determined using the hot perchloric acid method according to RUT [86]. In short, 200 mg of dried BSY was soaked in 10 mL 0.5 M perchloric acid solution for 30 min at 90 °C. Samples were subsequently cooled in a water-ice-bath and centrifuged at 3857 x g in an Universal 320R centrifuge by Andreas Hettich GmbH (Tuttlingen, Germany). The supernatants were decanted off and diluted 1:1000 v/v with 0.5 M perchloric acid. Absorbance was read at 270 nm and 290 nm in a UVIKON XL spectrophotometer by Goebel Instrumentelle Analytik GmbH (Au in der Hallertau, Germany). The RNA content was then calculated according to equation (9).

$$w_{RNA} = \frac{(A_{270} - A_{290}) \cdot F}{16.3 \cdot M} \tag{9}$$

With w_{RNA} representing the mass-based RNA content [w/w], A_{270} and A_{290} the absorbance values at the respective wavelength 270 nm and 290 nm [-], F the dilution factor [-] and M the mass of the sample [mg].

3.3.9 Yeast Vitality Assays

To assess the metabolic state of the yeast prior to cell disruptions, two yeast vitality assays were used: The acidification power test and the determination of the intracellular pH.

Acidification Power Test

Yeast vitality was assayed using an acidification power test adapted from GABRIEL ET AL. [87]. The vitality is defined as the ability to both metabolize endogenous glycogen and exogenous glucose substrates. The magnitude of spontaneous acidification (AP_{10}) through hydrolysis of internal glycogen bonds is measured over a period of 10 minutes with a starting pH of 6.3. For this, the harvested BSY-beer slurry was washed twice with ultrapure water at pH 6.3 at 154 x g for 1 min and 20 °C in an Universal 320R centrifuge by Andreas Hettich GmbH (Tuttlingen, Germany). 3 g of the resulting BSY cell pellet were resuspended in 15 mL ultrapure water at pH 6.3. The change in pH of this suspension was recorded every minute for a total of 10 min. The magnitude of glucose induced acidification power (AP_{20}) was also measured for a period of 10 minutes directly after the AP_{10} measurement, where 4.5 mL of a 50% glucose solution at pH 6.3 were added. Both values are defined as per the following equations (10) and (11). This paragraph was adapted from SCHOTTROFF ET AL. (2025) [57].

$$AP_{10} = 6.3 - pH(t = 10\ \text{min}) \tag{10}$$

$$AP_{20} = 6.3 - pH(t = 20\ \text{min}) \tag{11}$$

Intracellular pH

Yeast vitality was additionally assayed via an intracellular pH (ICP) determination. The method is based on the membrane passing esterase substrate fluorescein diacetate [88]. Through pH dependent intracellular enzyme activity, the fluorescent dye fluorescein is produced [89]. This dye can be detected in yeast cells at the excitation wavelengths of 441 nm and 488 nm and

the emission wavelength of 518 nm. For the assay, 0.5 g yeast cell pellet were suspended in 3 mL ice-cold 50 mM sodium phosphate citrate (NaPC) buffer at pH 3. The suspension was centrifuged at 3600 x g for 4 min at 4 °C in a Universal 320R centrifuge by Andreas Hettich GmbH (Tuttlingen, Germany) and the supernatant discarded. The procedure was repeated two times, before the cell pellet was suspended in 750 µL ice-cold buffer. 75 µL of a 10 mM carboxyfluorescein diacetate in DMSO were added and the mixture vortexed for 1 min. 250 µL of the suspension were pipetted into a 15 mL reaction vessel and 8 mL of ice-cold buffer were added. The mixture was incubated for 14 min at 30 °C in the dark. The sample was subsequently washed twice with 6 mL of buffer. The liquid supernatants were discarded. The cell pellet was suspended in 3 mL buffer at room temperature and 3 aliquots of 150 µL were pipetted into a black well plate prior to fluorescence detection. The calibration was done with pipetting 15 µL of a 100 mM carboxyfluorescein solution into 135 µL of a 50 mM NaPC buffer with a respective pH of 4.8-6.4 in 0.2 steps. The ICP was calculated according to equation (12).

$$ICP = ln\left(\frac{E_{488}}{E_{441}}\right) \quad (12)$$

With E_{488} representing the concentration and pH dependent emission at an excitation wavelength of 488 nm [-] and E_{441} the only concentration dependent emission at 441 nm excitation [-].

3.3.10 SDS-PAGE

Protein sizes were evaluated qualitatively via a sodium dodecyl sulfate-polyacrylamide gel electrophoresis (SDS-PAGE). The polyacrylamide concentration in the gels was 8%. The protein marker used, visualized protein sizes between 10-245 kDa. For sample preparation, 20 µL of sample were mixed with 10 µL of ultrapure water and 10 µL of SDS buffer solution. Sample proteins were then denatured at 80 °C for 5 min. 10 µL of the samples were pipetted into the gel chambers submerged in the SDS running buffer consisting of 30 g/L Tris-(hydroxymethyl)-aminomethan, 144 g/L Glycine and 10 g/L SDS. The voltage was set to 170 V for 30-60 min. The gel was then washed with ultrapure water and stained for 1 h with Coomassie blue under constant shaking. This paragraph was adapted from SCHOTTROFF ET AL. (2025) [57].

3.3.11 Particle Size Analysis

Particle size distributions were determined with a Camsizer XT by Retsch Technology (Haan, Germany) through particle imaging. Only dried BSG samples were used. An active air jet was used for an even distribution of the particles. Particle size distributions were determined once only, as sample was constantly fed into the feeding pipe until no further change of the particle size distribution was visible. The detection range was set to 0-7500 µm for raw BSG and 0-3000 µm for high-shear mixed BSG. Given particle size distributions are based on the volume density distributions evaluated for d_{area}, the diameter of an equivalent circle with the same area.

3.4 Enzymatic Activity Assays

The following chapters summarizes the assays and experimental setups used to determine enzyme activities.

3.4.1 Casein Protease Activity Assay

Quantification of enzyme activity was done via a non-specific protease assay as described by CUPP-ENYARD ET AL. [90]. The activity was determined spectrophotometrically at 660 nm in triplicates with an extinction coefficient of 9.8505 L/mmol/cm. One unit is defined as the production of a color equivalent to 1 µmol of tyrosine per minute at pH 7.5 and 37 °C. The reaction was started by adding 1 mL of enzyme solution to vials containing 5 mL of a 0.65%

by mass casein solution prepared in 50 mM potassium phosphate citrate buffer (KPC) pH 7.5 preheated to 37 °C. No enzyme solution was added to the blank. The reaction was stopped after 10 min by adding 5 mL of a 110 mM trichloroacetic acid solution. 1 mL of enzyme solution was then added to the blank. All vials were incubated for another 30 min at 37 °C, before 2 mL were filtered over 0.45 µm polyether sulfone syringe filters into a suitable vial. 5 mL of a 500 mM sodium carbonate and 1 mL of 0.5 M Folin's phenol reagent were added. After another 30 min incubation at 37 °C, samples were filtered again and 1 mL was transferred into suitable cuvettes for absorbance measurement at 660 nm. A standard curve was recorded with L-tyrosine. Activity was calculated as shown below. This paragraph was adapted from SCHOTTROFF ET AL. (2025) [57].

$$v_V = \frac{n_{tyrosine} \cdot V_{assay}}{t \cdot V_{enzyme} \cdot V_{cuvette}} \tag{13}$$

$$v = \frac{v_V}{c_{BSY,DM}} \tag{14}$$

Where v_v is the volumetric activity [U/mL], $n_{tyrosine}$ is the equivalent amount of tyrosine in the assay determined from the slope of the calibration curve [µmol], V_{assay} is the assay volume [mL], t is the reaction time [min], V_{enzyme} is the enzyme solution volume used [mL], $V_{cuvette}$ is the cuvette volume [mL], v is the mass specific activity [U/g] based on BSY dry matter and $c_{BSY,DM}$ is the concentration of BSY dry matter in the enzyme solution [g/mL].

3.4.2 3,5-Dinitrosalicylic Acid Assay for Cellulase and Xylanase Activity

For the determination of carbohydrase activity, a 3,5-dinitrosalicylic acid (DNS) assay was used. The assay is a photometric assay based on the amount of reducing sugars released during incubation with an enzyme sample [91]. The color change of the DNS reagent to 3-amino-5-nitrosalicylic acid due to the presence of reducing sugars can be photometrically detected at 546 nm. For the assay, the DNS reagent solution consisted of 30% w/w Rochelle salts, 1% w/v DNS and 0.4 M NaOH. For cellulase activity determination, carboxymethylcellulose (CMC) was used as a substrate. A 1% w/w CMC solution was prepared in 0.1 M acetate buffer at pH 5. For xylanase activity determination, Birchwood xylan was used as a substrate. A 1% w/w substrate solution in 0.1 M sodium phosphate citrate buffer at pH 5 was used. The pipetting scheme given in Table 6 was used for each sample.

Table 6: Pipetting scheme for DNS assay procedure.

Sample type	Volume substrate solution [µL]	Volume of acetate buffer [µL]	Volume of enzyme solution [µL]
Blank	0	2000	0
Enzyme blank	1000	1000	0
Substrate blank	0	1500	500
Enzyme sample	1000	500	500

The substrate and acetate buffer mixture was heated to 50 °C prior to enzyme addition. The mixture was incubated for exactly 10 min at 50 °C and 550 rpm once the enzyme was added. After incubation, 1 mL of each solution was mixed with 1 mL of DNS reagent solution. The mixture was vortexed and inactivated at 80 °C for 10 min. The samples were left to cool on ice for 5 min prior to spectrophotometric analysis at 546 nm. For the calibration curves, 1 mL of a glucose or xylose solution, respectively, was mixed with 1 mL of DNS reagent. The samples were heated to 80 °C for 10 min and their absorbance was determined at 546 nm. The activity of the enzyme sample was calculated according to equation (12).

$$v_v = \frac{A_{546} \cdot V_{assay}}{t \cdot V_{enzyme} \cdot F} \quad (15)$$

Where v_v is the volumetric activity [U/mL], A_{546} is the absorbance read at 546 nm [-], V_{assay} is the total assay volume [mL], t the assay time [min], V_{enzyme} the volume of the enzyme [mL] and F the slope of the standard curve [min/µmol].

3.5 Cell Disruption Methods

For an identification of suitable methods to produce proteolytically active BSY extracts, different cell disruption methods were investigated. The following chapters summarize the experimental procedures followed for each method. The general work flow for each method is represented in the following Figure 6. This figure as well as the description of the individual cell disruption methods are adapted from SCHOTTROFF ET AL. (2025) [57]. The icons used are from © amethyststudio, Icons8, nessign, sparklestroke, effort_project and Victoruler via Canva.com.

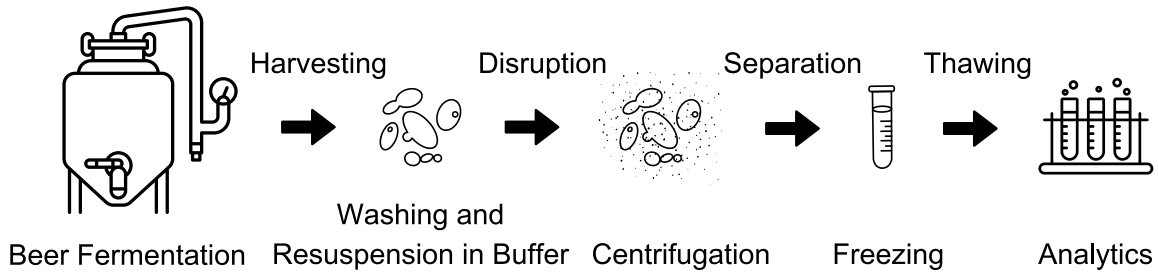

Figure 6: Schematic overview of the experimental procedure from beer fermentation to proteolytically active BSY extracts.

The BSY slurry obtained after harvest was centrifuged at 3019 x g at 4 °C for 10 min in a Beckman Coulter Avanti J25 centrifuge (Brea, CA, USA) to separate beer from the yeast. The cell pellet was resuspended in ultrapure water and centrifuged again under the same conditions. The washing process was repeated a total of two times before resuspending the cell pellet at a ratio of 1:2 w/v in 0.1 M sodium phosphate citrate buffer at pH 6 or pH 7, respectively. This BSY suspension was subjected to the different cell disruption methods and analyzed on released protease activity, protein content and contained protein sizes.

3.5.1 Thermal Yeast Autolysis

For the thermal yeast autolysis, 20 mL of the BSY suspension were transferred to baffled Erlenmeyer flasks and placed in a preheated incubator type ecotron by Infors HT (Bottmingen, Switzerland) at a temperature of 45, 50 or 55 °C respectively. Shaking was set to 200 rpm. The autolysis samples were left for a maximum of 4 h. At each sampling time, one flask was removed and the content was centrifuged at 3857 x g and 4 °C for 20 min in a Universal 320R centrifuge by Andreas Hettich GmbH (Tuttlingen, Germany). The liquid supernatant was carefully transferred to a fresh test tube. The remaining cell wall debris was dried at 60 °C to constant weight.

3.5.2 Ultrasound Treatment

20 mL of the buffered yeast suspension were transferred to a 50 mL reaction vessel. A 20 kHz sonotrode type GM 2070 by Bandelin electronic GmbH and Co. KG (Berlin, Germany) was placed in the middle of the suspension. The reaction vessel was placed in an ice water bath, before starting the ultrasound treatment at 100% power input for the desired cell disruption time. Every 2 min, the temperature of the suspension was checked. If a threshold of 15 °C was

surpassed, the suspension was kept on ice for 5 min before resuming the cell disruption treatment. BSY extract was separated from the cell wall debris via centrifugation at 3857 x g and 4 °C for 20 min in a Universal 320R centrifuge by Andreas Hettich GmbH (Tuttlingen, Germany). The liquid supernatant was carefully transferred to a fresh test tube. The remaining cell wall debris was dried at 60 °C to constant weight.

3.5.3 Glass Bead Treatment

Glass beads of 0.5 mm diameter were added in a ratio of 1:1 w/w cell pellet to glass beads to 20 mL of the buffered yeast suspension. The mixture was vortexed on a Vortex-Genie 2 by Scientific Industries, Inc. (Bohemia, NY, USA) at 100% power input for the desired cell disruption time. Every 5 min, the mixture was cooled in an ice water bath for 5 min. BSY extract was separated from the cell wall debris via centrifugation at 3857 x g and 4 °C for 20 min in a Universal 320R centrifuge by Andreas Hettich GmbH (Tuttlingen, Germany). The liquid supernatant was carefully transferred to a fresh test tube. The remaining cell wall debris was dried at 60 °C to constant weight. A glass bead treatment of 15 min under the above stated conditions is referred to as standardized cell disruption method throughout subsequent chapters of this work.

3.5.4 French Press

For the high-pressure cell disruption, 20 mL of buffered BSY suspension were taken up by the French pressure cell type Aminco FA-078 by SLM (USA) and disrupted at 900-1200 bar for 10 cycles. The pressure was set with a hand lever and varied in between cycles. BSY extract was separated from the cell wall debris via centrifugation at 3857 x g and 4 °C for 20 min in a Universal 320R centrifuge by Andreas Hettich GmbH (Tuttlingen, Germany). The liquid supernatant was carefully transferred to a fresh test tube. The remaining cell wall debris was dried at 60 °C to constant weight.

3.5.5 High-Pressure Homogenization

High-pressure homogenization was performed in a GEA PandaPlus NS 1001L homogenizer (Parma, Italy). For each run, 300 mL of buffered BSY suspension were disrupted for up to 10 passes through the two-stage high-pressure valve. The homogenized suspension was pumped back to the feeder after each pass through the valve. A countercurrent tubular heat exchanger with water as the cooling medium was used to maintain the temperature below 20 °C after each pass. The BSY extract was separated from the cell wall debris by centrifugation at 3857 x g and 4 °C for 20 min in a Universal 320R centrifuge by Andreas Hettich GmbH (Tuttlingen, Germany). The liquid supernatant was carefully transferred to a fresh test tube. The remaining cell wall debris was dried at 60 °C to constant weight.

3.5.6 High-shear mixing

High-shear mixing was performed in a 100 L GEA Batch Formula® (Skanderborg, Denmark). A detailed description of the device can be found in chapter 3.7.1. The yeast was kindly supplied by Holsten Brewery in Hamburg, Germany and originated from a Pilsner brew. The yeast was processed the same day as it was harvested. No active cooling was present on-site during high-shear mixing. The following Table 7 summarizes the experimental conditions applied.

Table 7: Experimental conditions for high-shear mixing of BSY for cell disruption.

Parameter	Description
BSY type	Bottom-fermenting yeast in Pilsner beer
Mass BSY slurry	32.6 kg
Mass dry matter of BSY	3.0 kg
HSM time	0, 2, 5, 7, 10, 12, 15 min
HSM power	100% (7 kW, 2104 rpm)
Agitation power	50% (1 kW, 27 rpm)
Control cell disruptions	0.5 mm GB in beer and in 0.1 M NaPC pH 6, 15 min, 4 °C

A 100 mL aliquot of the high-shear mixed yeast was taken from the bottom mounted sampling valve. The BSY extract was separated from the cell wall debris by centrifugation at 3857 x g and 4 °C for 20 min in a Universal 320R centrifuge by Andreas Hettich GmbH (Tuttlingen, Germany). The liquid supernatant was carefully transferred to a fresh test tube. The remaining cell wall debris was dried at 60 °C to constant weight. The cell disruptions were conducted directly in beer due to a missing large-scale centrifuge for washing of the yeast slurry prior to high-shear mixing. To account for this deviation, two control cell disruptions on lab-scale were conducted. The first was a glass bead cell disruption as described in chapter 3.5.3 and the second was conducted under the same conditions but also directly in beer.

3.6 BSY Extract Characterization Methods

3.6.1 Screening of Protease Activity at Different pH Values

A pH screening was performed to determine a suitable pH range for cell disruption. All cell disruptions were performed following the above procedure of glass bead treatment for 15 min explained in detail in chapter 3.5.3. The buffers used during cell disruption are summarized in Table 1. The protease activity was determined directly after the cell disruptions. This paragraph as well as Table 8 were adapted from SCHOTTROFF ET AL. (2025) [57].

Table 8: List of buffers used during pH screening experiments.

pH [-]	Buffer [0.1 M]
3 – 7	Na_2HPO_4 + $C_6H_8O_7$
8 – 9	$C_4H_{11}NO_3$ + HCl
10	Na_2CO_3 + $NaHCO_3$

3.6.2 Temperature Stability Assay

A temperature range of 20-60 °C was assayed in 5 °C steps. Each temperature was run in triplicates in 1.5 mL reaction tubes at 500 rpm in a thermoshaker. Samples were taken every hour. An initial sample at 0 h was assayed as a blank and the determined absorbance read at 440 nm and used as a basis to all subsequently taken samples to result in a relative absorbance value. The enzyme activity is assumed to correlate linearly with the absorbance read at 440 nm, as investigated by CHARNEY AND TOMARELLI for azocasein as a protease substrate [92]. The following Table 9 summarizes the pipetting scheme used.

Table 9: Enzyme activity assay procedure for temperature stability screening.

Description	Enzyme activity	Enzyme extract blank
Buffer	480 µL	480 µL
Enzyme	20 µL	20 µL
10% TCA (w/v)	-	0.5 mL
1% Azocasein (w/w)	0.5 mL	0.5 mL
Incubation	60 min, 20-60 °C*	
10% TCA (w/v)	0.5 mL	-
Centrifugation	6500 x g, 5 min	
1 M NaOH	1 mL	1 mL
Absorbance	440 nm	

*Temperature fixed for each experimental run. Temperatures 20-60 °C assayed in 5 °C steps.

3.6.3 Protease Class Identification Assay

A screening assay for the identification of protease classes in produced BSY extracts was adapted from GARCIA-CARREÑO ET AL. with modifications [47]. The measurement was based on a ratio of a sample, where a protease class specific inhibitor was added to a sample without the addition of this inhibitor. The substrate used was 1% azocasein (w/w). Hydrolysis by proteases resulted in the release of free azo-groups and thus an absorbance increase measured at 440 nm. A value of 100% relative activity indicates no change in activity through addition of the inhibitor. Values below 100% indicate a protease inhibition and are thus considered as an indicator for the presence of this protease class in the BSY extract. The used procedure is summarized in the following Table .

Table 10: Inhibition assay procedure used for protease class characterization of BSY extracts.

Description	Inhibitor	Activity blank	Enzyme blank	Solvent blank
Buffer	470 µL	480 µL	480 µL	480 µL
Enzyme	20 µL	20 µL	20 µL	20 µL
Inhibitor	10 µL	-	-	-
Inhibitor solvent	-	-	-	10 µL
Incubation	37 °C, 60 min			
10% TCA	-	-	0.5 mL	-
1% Azocasein	0.5 mL	0.5 mL	0.5 mL	0.5 mL
Incubation	37 °C, 60 min			
10% TCA	0.5 mL	0.5 mL	-	0.5 mL
Centrifugation	6500 g, 5 min			
1 M NaOH	1 mL	1 mL	1 mL	1 mL
Absorbance	440 nm			

The assay was based on the protease class specific inhibition through seven commercially available inhibitors: ethylene glycol-bis(β-aminoethyl ether)-*N,N,N′,N′*-tetraacetic acid (EGTA), ethylenediaminetetraacetic acid (EDTA), iodoacetamide (IA), Bestatin, *n*-ethyl-maleimide (NEM), Pepstatin A and phenylmethylsulfonyl fluoride (PMSF). The following Table 11 summarizes the used inhibitors and their inhibition mechanism as well as the used concentration ranges in the assay.

Table 11: Inhibition mechanisms of commercially available protease inhibitors used for a protease class screening on BSY extracts. EGTA = ethylene glycol-bis(β-aminoethyl ether)-*N,N,N',N'*-tetraacetic acid, EDTA = ethylenediaminetetraacetic acid, IA = iodoacetamide, NEM = *n*-ethyl-maleimide, PMSF = phenylmethylsulfonyl fluoride.

Inhibitor	Inhibition mechanism	Inhibitor concentrations [mM]
EGTA	Reversible, indirect inhibition through chelation of metal ions in catalytic site (Ca^{2+}, Mg^{2+})	100, 500, 1000
EDTA	Reversible, indirect inhibition through chelation of metal ions in catalytic site (Ca^{2+}, Fe^{2+})	100, 1000, 5000
IA	Reversible, competitive inhibition	90, 100, 110
Bestatin	Reversible, competitive inhibition	13, 15, 16.5
NEM	Irreversible, reaction with thiol groups in catalytic site	95, 100, 105
Pepstatin A	Reversible, competitive inhibition	0.5, 0.75, 1, 100
PMSF	Irreversible reaction with serine residues in catalytic site	10, 100, 500

These concentrations were based on supplier recommendations for protease inhibition studies. For comparability of results, all inhibitors were used once at 100 mM concentration. The only exception is Bestatin due to limited availability of this inhibitor. The same assay was used for a study of seven potential activators on metalloproteases: NaCl, $CaCl_2$, $MgCl_2$, Na_2SO_4, $MgSO_4$, $ZnSO_4$ and $MnSO_4$. All used at concentrations of 1 mM, 5 mM and 10 mM.

3.7 BSG Fractionation Methods

3.7.1 High-Shear Mixing in GEA Batch Formula®

A 100 L GEA Batch Formula® mixer as shown in Figure 7 was used as a one-pot device for BSG particle size reduction and subsequent protein and sugar extractions.

Figure 7: Graphical representation of the used 100 L GEA Batch Formula® high-shear mixer. Photo taken from GEA internal database.

The device was connected to an external electrical heater installed to supply the double walled heating mantle with water at the set temperature. The device was equipped with the rotor-stator type mixing device for particle size reduction using a 4 mm mesh sieve and a top-mounted anchor-type agitator with a diameter of 0.44 m. The installed power for each mixing device is given in the following Table 12. The vacuum pump for adding powdered ingredients to the system was not used in the scope of the present work.

Table 12: Installed agitator power on 100 L GEA Batch Formula®.

Device	Installed Power [kW]
High shear mixing device	22
Agitator	2.2
Vacuum pump	5

High-shear mixing (HSM) was always done at 100% power input from the mixing device (2104 rpm) and 50% power input from the agitator (27 rpm). BSG was always filled in from the top. An automated water dosing system added the required amount of tap water to result in a 10% by mass dry matter content inside of the mixing vessel. During high-shear mixing, no temperature control was active.

The mixing time of the top-mounted agitator at different power inputs was characterized in water. For this, 34 L of tap water were added into the 100 L HSM batch reactor. The top-mounted agitator was set to 50% (27 rpm), 75% (39 rpm) and 100% (53 rpm) power, respectively. The sample port was opened, until a water flow of 1 kg/min was achieved. A conductivity probe type GLP 100 by Greisinger electronic GmbH (Regenstauf, Germany) was positioned in the outlet flow of the sample port. 1 L of 0.01 M NaCl solution was added to the 34 L of water and the change in conductivity was recorded over time until a constant value was reached. Each agitation power was assayed in triplicates. In addition, the dimensionless Reynolds and Newton numbers were determined according to equations (16) and (17).

$$Re = \frac{N \cdot D^2 \cdot \rho}{\mu} \tag{16}$$

$$Ne = \frac{P}{\rho \cdot N^3 \cdot D^5} \tag{17}$$

With N representing the agitator speed [1/s], D the diameter of the agitator [m], ρ the density of water at 20 °C [kg/m^3], μ the dynamic viscosity of water at 20 °C [Pa s] and P the power of the agitator [W].

3.7.2 Osborne Fractionations

The procedure for the Osborne fractionations was adapted from LAMP with modifications [93]. The Osborne fractions were determined for raw BSG and 10 min high-shear mixed BSG in technical triplicates. For this, three centrifuge tubes were filled with 200 g of the respective BSG type and ultrapure water mixture with a dry matter content of 10% by mass. A magnetic stirring bar was placed in the centrifuge tube and mixing for 30 min at 500 rpm was started. The samples were subsequently centrifuged for 30 min at 3019 x g in a Beckman Coulter Avanti J25 centrifuge (Brea, CA, USA). The liquid supernatant was carefully collected. Ultrapure water was added to the remaining solid residue until 200 g total suspension weight were reached and the procedure repeated. Both liquid supernatants were combined and frozen at -20 °C. The same solid residue was subsequently extracted twice with a 20 g/L NaCl solution, followed by a 70% ethanol solution and lastly an 0.05 M NaOH solution. The procedure was each time the same: Filling up with solution until 200 g total suspension weight, extraction for 30 min followed by centrifugation. All frozen supernatants were freeze dried until constant weight. All remaining solid residues were dried at 60 °C until constant weight. All dried

samples and the starting biomass were analyzed on contained amino acid contents according to chapter 3.3.2.

3.7.3 Protein Extraction Studies

Protein extractions were done on a 50 g lab-scale and a 35 kg pilot-scale. The influence of high-shear mixing on BSG protein extraction was evaluated on the lab-scale for four different protein extraction methods. The most promising approaches were scaled-up to the pilot-scale to investigate transferability of the results. Additionally, the influence of brewing-type variations on protein extraction efficiencies were evaluated.

Protein Extraction Studies on Lab-Scale

The influence of high-shear mixing on protein extraction efficiency was evaluated on the lab-scale using 200 mL Schott bottles as the reaction vessels. Heating was maintained in a water bath with 200 rpm shaking. Each extraction condition was run with 0, 5 and 10 min HSM BSG with 50 g total suspension weight and 10% by mass of BSG dry weight. The pH of each sample was recorded before and after each experiment. In the case of 0 min HSM BSG, the larger BSG particles were removed after the extractions with a stainless-steel sieve. This step was not required for HSM BSG extraction runs. The remaining liquid was centrifuged at 3857 x g for 20 min at 4 °C in a Universal 320R centrifuge by Andreas Hettich GmbH (Tuttlingen, Germany). The clear hydrolysate was filtered with an 0.45 µm polyether sulfone syringe filter and frozen at -20 °C for later determination of the degree of hydrolysis and an SDS-PAGE analysis. The solid residues from both the sieving and the centrifugation were combined and dried at 60 °C until constant weight. The weight was recorded to determine the degree of solubilization. The protein content was determined for the starting biomass and the solid residues via the amino acid HPLC as described above. Four different protein extraction methods were used: extractions with tap water, with 0.1 M NaOH at pH 11, enzyme-assisted extractions at pH 8 and liquid hot water treatments. For the first two methods, the following Table 13 summarizes the experimental conditions applied.

Table 13: Experimental conditions for BSG protein extractions with tap water and 0.1 M NaOH.

Solvent	Temperature [°C]	pH [-]	Time [min]
H_2O	60	6.2*	0 60 120
0.1 M NaOH	60	11	0 60 120

*pH not adjusted for water extractions. pH ranging from 6.15-6.25 during extractions.

For the liquid hot water treatment, the detailed experimental setup is described in the following chapter 3.7.4. In short, a total suspension weight of 30 mL with a BSG dry matter content of 10% by mass was used. The reactor cartridges were inserted into the stainless-steel reactor vessels and the heating mantle was connected. The system was pressurized to 50 bar using nitrogen gas. The temperature set-points of 150 °C and 180 °C were set for three reactors each and the automated temperature control loop started. Once 95% of the setpoint was reached, the extraction timer of 10 min was started. The extraction was stopped by placing the reactors in an ice-water bath and cooling the mixture to 20 °C.

The following Table 14 summarizes the experimental conditions used for the enzyme-assisted extractions using Alcalase®. The proteolytic activity was determined as 2229.2 ± 46.9 U/mL using the casein assay described in chapter 3.4.1. Inactivation of the enzyme was done after the extractions by heating the sample to 80 °C for 10 min.

Table 14: Experimental conditions for BSG protein extractions with commercial protease Alcalase®.

Alcalase® additon [µL/g]	Temperature [°C]	pH [-]	Time [min]
10	60	8	0 60 120
20	60	8	0 60 120

After these initial screening experiments, the effect of different enzymes and enzyme-combinations thereof were tested to gain insights into the protein extraction efficiency. The following Table 15 summarizes the enzymes and their respective dosages used. Inactivation of the enzyme was done after the extractions by heating the sample to 80 °C for 10 min.

Table 15: Enzyme combinations and dosages used for BSG protein extractions.

Enzyme	Enzyme type	Dosage [µL/g]
Blank	-	0
Alcalase®	Endo-protease	10
Formea® Sol	Endo-protease	10
Viscozyme®	Cellulase and glucanase blend	10
Viscozyme® + Alcalase®		10 (each)*
Viscozyme® + Formea® Sol		10 (each)*
Celluclast®	Cellulase blend	10
Celluclast® + Alcalase®		10 (each)*
Celluclast® + Formea® Sol		10 (each)*

*Proteases added 15 min after the cellulases at 60 °C

Each enzyme had the following activities summarized in Table 16 determined with the assays described in chapter 3.4.

Table 16: Enzyme activity and Pierce protein content of stock solutions for BSG protein extractions. Alcalase® and Formea® Sol as protease activity using casein assay and Viscozyme® and Celluclast® as cellulase activity via DNS activity assay.

Enzyme	Activity [U/mL]	Protein content [mg/mL]*
Alcalase®	3621 ± 53	26.6 ± 7.9
Formea® Sol	4395 ± 10	21.6 ± 2.4
Viscozyme®	22755 ± 63	28.6 ± 4.2
Celluclast®	19649 ± 1052	23.7 ± 2.2

*Determined via Pierce assay at 660 nm and BSA as a standard.

All protein contents are in the same order of magnitude. The activity of the two protease enzymes Alcalase® and Formea® Sol and the activity of the two carbohydrase blends Viscozyme® and Celluclast® were each in the same order of magnitude. Results are thus assumed to be comparable for the same enzyme class at the same dosing volume. The choice for Formea® Sol was a result of this new enzyme blend being available for research. Since it was originally developed for plant-based milk applications from oats, a high potential for protein solubilization for BSG is assumed. Based on the manufacturer data sheets, Table 17 summarizes the working ranges for each enzyme blend.

Table 17: Working conditions of enzymes used for BSG protein extractions.

Parameter	Alcalase®	Formea® Sol	Viscozyme®	Celluclast®
Activities	Endoprotease, α-amylase	Endo-protease, carbohydrase	Carbohydrase, protease	Cellulase
pH [-]	6.5-10	6-7	4.5-6	4-9
Temperature [°C]	60-75	50-75	30-65	45-65
Dosage [µL/g_{dm}]	≤ 10	≤ 10	≤ 10	≤ 10

*All ranges and recommendations taken from supplier Novonesis.

All enzymes can be used under the previously established conditions, with the exception of pH. To enable a use of the carbohydrase acting enzymes together with the proteolytic enzymes, it was decided not to adjust the pH of the BSG-water suspension. The result was a pH of 6.2 for all extractions. To account for this deviation from previous experiments, the single enzymes as well as a BSG negative control without the addition of any enzyme were run next to the enzyme combinations.

Protein Extraction Studies on Pilot-Scale

For the pilot-scale protein extractions, a total batch-size of 35 kg was used. The BSG was filled into the high-shear mixing device from the top. The required amount of tap water was added via the automated water-supply line. The suspension was subsequently high-shear mixed for 10 min at 100% power input (2104 rpm) and 50% agitation (27 rpm). During mixing, the temperature of the suspension rose about 20 °C. The extraction timer was started once the required pH and temperature had been reached or in the case of the enzyme-assisted extractions once the enzyme had been added. Inactivation of the enzyme was done after the extractions by heating the sample to 80 °C for 10 min. Table 18 summarizes the experimental conditions applied.

Table 18: Experimental conditions during screening trials for scaling up protein extractions to 35 kg.

Parameter	Run 1	Run 2	Run 3	Run 4
Mass wet BSG [kg]	28.1	14	14	14
Mass water added [kg]	9.9	21	21	21
Solid/liquid ratio [w/w]	0.2	0.1	0.1	0.1
pH [-]	11	11	8	8
Alcalase® addition [mL/kg]*	0	0	20	10
High shear mixing time [min]	5	5	5	5
Hydrolysis time [min]	120	120	240	240
Temperature [°C]	50	50	50	50

*Alcalase® activity of 2229.2 ± 46.9 U/mL

Next to the standard RubyRoast BSG, other types of BSG were used for protein extractions to investigate the influence of brewing type variations on the protein extraction efficiency. The following Table 19 summarizes the different BSG types used. Each BSG type was extracted once with 0.1 M NaOH at pH 11 and 60 °C for 2 h and via an Alcalase® extraction at pH 8 and 60 °C with an enzyme dosage of 10 µL/g_{dm}. The Alcalase® had an activity of 3620.8 ± 52.9 U/mL. Before and after every extraction, two 50 mL samples of the suspension were taken via the bottom-mounted sample port and stored on ice. The Alcalase® containing samples were inactivated at 90 °C for 10 min. For all pilot-scale experiments, the taken samples were centrifuged at 3857 x g for 20 min at 4 °C in a Universal 320R centrifuge by Andreas Hettich GmbH (Tuttlingen, Germany). The clear hydrolysate was filtered with an 0.45 µm polyether sulfone syringe filter and frozen at -20 °C. The solid residues were dried at 60 °C until constant weight. The protein content was determined for the starting biomass and the solid residues via the amino acid HPLC as described above.

Table 19: Characteristics of different BSG types used for protein extractions on 35 kg scale.

Name	Grain Bill	Characteristics
Campus Perle	87% Pilsener malt, 6% Abbey (Kloster) malt, 5% Cara Red malt, 2% Melanoidin malt	Reference BSG, Relatively large grist due to microbrewery lauter tun set-up
Lauter tun	100% Pilsener malt	Industrial sized lauter tun (Holsten Brewery Harburg)
Lauter tun with trub addition	100% Pilsener malt	Addition of hot trub from wort kettle (Holsten Brewery Harburg)
Mash filter	100% Pilsener malt	BSG separated in mash filter, Hammer mill used for grist preparation
Wheat malt	53% Wheat malt, 45% Pilsener malt, 2% Melanoidin malt	>50% wheat malt introduces higher protein content

Application of BSY Cells on BSG under Autolysis Conditions for Protein Extraction

For the application of whole BSY cells on BSG under autolysis conditions, a fresh batch of BSY was centrifuged at 3019 x g for 10 min at 4 °C to remove the beer. The remaining cell pellet was washed twice with ultrapure water, which was removed each time via centrifugation under the above stated conditions. The BSY pellet was subsequently dissolved in 0.1 M NaPC buffer at pH 4 or 5, depending on the experimental run. A final BSY dry matter content of 7% w/w was used. For the autolysis runs, a total of 8 g of wet BSG were transferred into a 100 mL baffled Erlenmeyer flask. To this, the 7% w/v BSY suspension was added until a BSG to BSY dry matter ratio of 1:1 w/w was achieved. Additionally, single BSG and single BSY control runs in the respective 0.1 M NaPC buffer were prepared. The following Table 20 summarizes the applied conditions for the feasibility study.

Table 20: Experimental conditions for BSY autolysis on whole BSG. Acid shock = Addition of 96% H_2SO_4 at 0.01% v/v of BSY suspension in ultrapure water.

Parameter	Condition 1	Condition 2	Condition 3
Time [h]	3	23	-
Temperature [°C]	50	60	45 – 50 – 55 – 60
Acidity [-]	pH 4	pH 5	Acid shock

The sulfuric acid added in the acid shock runs had a purity of 96%, which equals 18 M. The temperature was maintained in an Infors HT ecotron incubator (Rotkreuz, Switzerland) with 150 rpm rotational shaking. For the acid shock, 96% sulfuric acid was added at a ratio of 0.01% v/v to the BSY suspension. For the temperature gradient, the temperature was increased every hour starting from 45 °C. After reaching 60 °C, the temperature was not increased further but instead maintained for the rest of the incubation period.

Once the autolysis time was over, the samples and corresponding controls were removed from the incubator and transferred to 50 mL centrifuge tubes. Solid liquid separation was achieved via centrifugation at 3857 x g for 20 min at 4 °C in a Beckman coulter J2-HS centrifuge (Brea, USA). The liquid supernatant was frozen at -20 °C and subsequently freeze-dried for a CHNS elemental analysis. The solid residue was washed twice with ultrapure water and subsequently centrifuged under the above stated conditions to remove traces of the hydrolysate. The remaining solids were dried at 60 °C and ground with a mortar and pestle prior to protein content determination via the amino acid HPLC.

Application of BSY Extract on BSG Protein

For the application of BSY proteases directly on BSG protein, a BSG protein hydrolysate was generated through alkaline and enzymatic extractions. All extractions were performed in 200 mL Schott bottles using 20 g wet BSG. A dry matter content of 10% by mass was used. Extractions were run at 60 °C for 2 h in a water bath with 125 rpm shaking. For the alkaline extractions, 0.1 M NaOH was used until the suspension had a pH of 11. For enzyme-assisted extraction, 10 µL/g_{dm} Alcalase® with an activity of 3620.8 ± 52.9 U/mL was added to a BSG water suspension with a pH of 8. Enzymes were inactivated at 80 °C for 10 min. The BSG particles were removed with a stainless-steel sieve and the remaining liquid centrifuged at 3857 x g for 20 min at 4 °C. The liquid supernatants were used as crude protein extracts and subjected to a concentration step via an isoelectric point precipitation.

The isoelectric points were defined as the pH at which the maximum amount of protein precipitated. For this, 20 mL of crude extract were adjusted to a pH from 2-6 with 1 M HCl. The samples were left for 30 min at room temperature prior to centrifugation at 3857 x g for 30 min at 10 °C. The supernatant was collected and analyzed with a Pierce assay on remaining protein content. The precipitate was dried at 60 °C and weighed. The dried samples were subsequently analyzed in the amino acid HPLC to evaluate the overall protein content. The isoelectric point determination procedure was repeated a second time in a narrower range of pH 2.5-4.5 in 0.5 steps. The identified pH values at which the maximum protein precipitated were used to concentrate the crude extracts. The pellets were subsequently re-dissolved in pH adjusted 0.1 M NaPC buffer to result in 2.4 mg/mL protein content. These extracts were used for all hydrolysis screening and optimization experiments.

The BSY extracts were produced from a fresh batch of BSY according to the standardized glass bead treatment as described in chapter 3.5.3. During the first screening experiments, the conditions given in the following Table 21 were used to identify relevant parameters for BSG protein hydrolysis by BSY proteases.

Table 21: Screening parameters used during BSG protein hydrolysis by BSY proteases.

Parameter	Range
Temperature [°C]	20 – 60
pH [-]	4 – 8
Time [h]	0.5 – 24
E/S ratio [v/v]	2–10:100
Enzyme activity [U/mL]	0.5–1

The hydrolysis reactions were carried out on a 2 mL scale in a thermoshaker at 500 rpm. Enzymes were inactivated at 80 °C for 10 min after hydrolysis. Hydrolysates were filtered with a 0.45 µm polyether sulfone syringe filter prior to analysis of the protein content via a Pierce assay. Next to the absolute Pierce protein content, a relative protein content decrease based on the initial Pierce protein content was used for comparison of the results. The definition of this parameter is given in the following equation (18).

$$x_P = \frac{w_{P,0} - w_P}{w_{P,0}} \tag{18}$$

With x_P representing the dimensionless relative protein content decrease, $w_{P,0}$ the Pierce protein content before the hydrolysis [µg/mL] and w_P the Pierce protein content after the hydrolysis [µg/mL]. With the parameter ranges identified in the screening phase, an optimization DoE was set up in the software Design Expert 12. Following a response surface methodology, a central composite design with a total of 25 experimental runs including axial and central points was chosen. Experimental parameters are summarized in the following Table 22 and were run with a 2.4 mg/mL BSG protein substrate originating from an alkaline

extraction. The BSY activity used was 1 U/mL. A full list of all experimental runs is given in the appendix in Table A-2.

Table 22: Parameter ranges used during the optimization DoE for BSG protein hydrolysis by BSY proteases.

Parameter	Value
Temperature [°C]	30 – 60
pH [-]	5.5 – 7
Time [h]	2 – 8
E/S [v/v]	10-30:100

The effect of these four factors on the response relative protein content decrease in the hydrolysate was evaluated. The same experimental procedure than during the screening phase was followed. Lastly, the influence of scale on the hydrolysis was evaluated. For this, a hydrolysis run at 30 °C, pH 6 and an E/S of 30:100 v/v for 2 h was conducted on a 2 mL and a 50 mL scale. Next to the relative protein content decrease based on the protein content prior to the hydrolysis, two new parameters were evaluated: The relative protein content decrease relative to a control without enzyme addition and a relative degree of hydrolysis. Both parameters are defined as per the following equations (19) and (20).

$$x_{P,Rel} = \frac{w_{P,C} - w_P}{w_{P,C}} \quad (19)$$

$$DH_{Rel} = \frac{DH_S - DH_C}{DH_C} \quad (20)$$

With $x_{P,Rel}$ representing the dimensionless relative protein content decrease relative to the control after hydrolysis, $w_{P,C}$ the Pierce protein content of the control [µg/mL], w_P the Pierce protein content of the sample [µg/mL], DH_{Rel} the dimensionless relative degree of hydrolysis, DH_S the absorbance at 420 nm of the degree of hydrolysis of the sample [-] and DH_C the absorbance at 420 nm of the degree of hydrolysis of the control [-].

3.7.4 Fiber Fractionation Methods

The fiber fractionation methods focused on two different approaches: The extraction of xylo- (XOS) and arabino-oligosaccharides (AOS) as well as on the extraction of monosaccharides from BSG.

Xylo- and Arabino-oligosaccharide Extractions via Liquid Hot Water Treatment

The extraction of XOS and AOS was performed on two different scales: In 30 mL batch reactors as shown in Figure 8 and in a 3 L batch reactor. Both reactors were part of the Institute of Thermal Separation Processes of the Hamburg University of Technology and were kindly made available for this work.

Figure 8: Experimental set-up of 30 mL batch reactors for liquid hot water extractions.

The smaller scale liquid hot water (LHW) reactors consisted of stainless-steel chambers equipped with Polytetrafluoroethylene (PTFE) cartridges measuring 22.9 mm in inner diameter and 95.8 mm in height, designed to hold sample volumes up to 30 mL. Each reactor is controlled via an external control loop for temperature control. For each experiment, 10 g of wet BSG were mixed with 20 mL of deionized water and heated using an electric mantle heater while continuously stirred with a magnetic stirrer bar at 500 rpm and pressurized to 50 bar. Once 95% of the target temperature was reached, the extraction timer was started. Upon completion of the set time, the reactors were rapidly cooled using an ice and water mixture. The solid and liquid fractions were then separated by centrifugation at 3857 x g for 20 min in a Universal 320R centrifuge by Andreas Hettich GmbH (Tuttlingen, Germany), and the solid residue was dried at 60 °C until constant weight. The liquid fraction was stored at 4 °C for further analysis via a sugar HPLC. The parameters of temperature and reaction time were initially screened by varying single factors. Each condition was run in technical triplicates using three reactors in parallel. The following Table 23 summarizes the experimental conditions tested during the screening phase.

Table 23: Experimental conditions during screening experiments for XOS and AOS extraction on 30 mL LHW reactor scale.

Time [min]	Temperature [°C]	Severity Factor [-]
5	180	3.05
5	190	3.35
10	140	2.18
10	150	2.47
10	160	2.77
10	170	3.06
10	180	3.36
10	190	3.65
10	200	3.94
15	170	3.24
20	140	2.48
20	150	2.77
20	160	3.07
20	170	3.36
20	180	3.66
20	190	3.95
20	200	4.25
25	160	3.16

For an easier comparison of the results obtained with existing literature, a severity factor is given for every condition tested. The severity factor is defined as per equation (21) [94].

$$\log(R_0) = \log(t) + log\left(exp\left(\frac{\vartheta - 100}{14.75}\right)\right) \quad (21)$$

With R_0 representing the dimensionless severity factor, t the LHW time [min] and ϑ the LHW temperature [°C]. For optimizing the obtained XOS and AOS extractions, a design of experiment (DoE) approach in the software Design Expert 12 by StatEase®, Inc. (Minneapolis, MN, USA) was used. Following a response surface methodology, a central composite design with a total of 19 experimental runs including axial and central points was chosen. Experimental parameters are summarized in the following Table 24. A detailed summary of all experimental runs is given in the appendix in Table A-3.

Table 24: Experimental conditions during optimization experiments for XOS and AOS extraction on 30 mL LHW reactor scale.

Parameter	Range
Temperature [°C]	160-200
Time [min]	5-25
Solid/liquid ratio [w/v]	0.05-0.15

The effect of these three factors on the responses XOS concentration, AOS concentration, combined XOS and AOS yield, xylose concentration and arabinose concentration was investigated. A total of four verification runs were conducted to analyze the accuracy of the model obtained. The chosen conditions are summarized in Table 25.

Table 25: Experimental conditions for DoE verification runs for XOS and AOS extractions.

Temperature [°C]	Solid-liquid ratio [w/v]	Reaction time [min]
190	0.05	20
180	0.125	15
170	0.1	10
160	0.1	10

The conditions identified as yielding maximum AOS and XOS concentrations through the DoE approach were used in a total of four scale-up experiments. For these experiments, a 3 L stainless steel reactor by Büchi (Essen, Germany) with an inlet diameter of 101.7 mm was used. It was designed for batch operations with a maximum operating pressure of 200 bar and a temperature range of up to 250 °C. Temperature control was maintained with an oil heating and a water cooling system. The reactor was equipped with a magnetic coupling and stirrer drive system, along with an anchor impeller with a diameter of 90 mm for effective mixing of the reaction components. Probes are integrated into the reactor for accurate measurement of temperature, pressure, and stirrer speed. Additionally, a safety valve and bottom outlet valve were included. For each experimental run, the required amount of water was added into the vessel and preheated to 90 °C. This was necessary to achieve similar heating times as in the small scale 30 mL reactors. Subsequently the required amount of BSG was added. The pressure in the reactor was maintained at subcritical conditions. The reaction was conducted at four different conditions identified during the optimization study and are summarized in the following Table 26. Each condition was tested in duplicates.

Table 26: Experimental conditions for 3 L scale experiments for XOS and AOS extractions through LHW.

Temperature [°C]	Solid-liquid ratio [w/v]	Reaction time [min]
185	0.05	5
180	0.05	5
180	0.05	10
170	0.05	20

For studying the efficiency of heat transfer in this process, the Nusselt number was determined using equation (22) valid for a stirred tank reactor equipped with an impeller stirrer [69].

$$Nu = 0.354 \cdot Re^{0.714} \cdot Pr^{0.26} \quad (22)$$

With *Nu* representing the Nusselt number, *Re* the Reynolds number and *Pr* the Prandtl number. The latter are defined as per the following equations (23) and (24).

$$Re = \frac{N \cdot D^2 \cdot \rho}{\mu} \quad (23)$$

$$Pr = \frac{c_P \cdot \mu}{\lambda} \quad (24)$$

With N representing the agitator speed [1/s], D the inner reactor diameter [m], ρ the density [kg/m^3], μ the dynamic viscosity [Pa s], c_P the specific heat capacity [J/kg K] and λ the thermal conductivity [W/m K]. All component specific parameters were used for water under subcritical conditions at 185 °C and 50 bar.

For all experiments, the combined yield of XOS and AOS based on hemicellulose content in the feedstock was calculated as per the following equation (25).

$$Y = \frac{V_{total} \cdot (C_{XOS} + C_{AOS})}{m_{BSG,dm} \cdot X_{HC}} \quad (25)$$

With Y representing the mass-based AOS and XOS yield [-], V_{total} the total liquid hydrolysate volume [mL], c_{XOS} the XOS concentraton in the hydrolysate [g/mL], c_{AOS} the AOS concentration in the hydrolysate [g/mL], $m_{BSG,dm}$ the dry matter mass of BSG at the start of the process [g] and X_{HC} the hemicellulose content by mass in the BSG starting material [w/w].

Sugar Hydrolysis Procedure

The extraction of monomeric C5 and C6 sugars from BSG was based on enzymatic extractions. A total of four different enzymes were screened on their capacity to release monomeric sugars from the BSG matrix: Cellulase from *Aspergillus niger*, Celluclast®, Cellic® Ctec and xylanase from *A. oryzae*. During a first set of screening experiments, 5 g of 5 min HSM BSG was subjected to enzymatic hydrolysis in 100 mL Schott bottles in a water bath. The following Table 27 summarizes the screening parameters tested for each enzyme.

Table 27: Screening parameters used during sugar hydrolysis from BSG.

Parameter	Value
Temperature [°C]	50
Rotating speed [rpm]	120, 170, 200
Time [h]	4, 5, 6, 24
Solid/enzyme ratio [% w/v]	5, 10, 15
pH [-]	4, 5, 6

The BSG water mixture was heated to 50 °C prior to enzyme addition. Enzymes were added at a stock solution activity of 10 U/mL. Directly after the hydrolysis time, the samples were heated to 80 °C for 10 min for enzyme inactivation. The samples were then centrifuged at 3857 x g for 20 min at 4 °C for solid liquid separation. The liquid hydrolysate was filtered with an 0.2 µm nylon syringe filter and analyzed in the sugar HPLC. The solid residue was dried at 60 °C until constant weight.

The best performing enzyme from the screening phase was Cellic® Ctec. This enzyme was used for an unoptimized proof of principle scale-up experiment in the 100 L HSM batch reactor. 15 kg of wet BSG were added to the high-shear mixer and 20 L of tap water were added via the automatic dosing line. The pH of the mixture was recorded. Subsequently, the mixture was high-shear mixed for 5 min at 100% mixing power (2104 rpm) and 50% agitation (27 rpm). The mixture was then heated to 50 °C, before the 10 U/mL enzyme stock solution was added at a ratio of 5% w/v based on BSG dry matter. A 50 mL sample was taken every 30 min for a total of 5 h hydrolysis time. The samples were stored on ice until inactivation at 80 °C for 10 min.

The samples were then centrifuged at 3857 x g for 20 min at 4 °C for solid liquid separation. The liquid hydrolysate was filtered with an 0.2 µm nylon syringe filter and analyzed in the sugar HPLC. The solid residue was dried at 60 °C until constant weight.

For optimizing the extraction yields obtained from the screening phase, a design of experiment (DoE) approach in the software Design Expert 12 was used. Following a response surface methodology, a central composite design with a total of 32 experimental runs including axial and central points was chosen. Experimental parameters are summarized in the following Table 28 and were run individually for both Celluclast® and Cellic Ctec®. A full list of all experimental runs is given in the appendix in Table A-9. Each enzyme stock solution had an activity of 100 U/mL.

Table 28: Experimental conditions during optimization experiments for C5 and C6 sugar extractions from BSG on 5 g lab-scale.

Parameter	Range
Temperature [°C]	46 – 55
Time [h]	5 – 12
Solid/enzyme ratio [% w/v]	1 – 10
pH [-]	4.5 – 5.5

The effect of these four factors on the responses C5 sugar yield, C6 sugar yield as well as on xylose, arabinose and glucose concentrations in the hydrolysate was evaluated. The same experimental procedure than during the screening phase was followed. For each enzyme, a total of two verification experiments were conducted with the conditions summarized in Table 29.

Table 29: Experimental conditions for DoE verification runs for monosaccharide sugar extractions.

No.	Parameter	Value
1	Temperature [°C]	49
	Time [h]	6
	Solid/enzyme ratio [% w/v]	1
	pH [-]	5.5
2	Temperature [°C]	54
	Time [h]	7
	Solid/enzyme ratio [% w/v]	5
	pH [-]	5

3.7.5 Application of BSG-residue in 3D-printable Filament

For the production of a 3D-printable BSG-Polylactic acid (PLA) filament, BSG residue obtained from a protein extraction process with 10 µL/g_{dm} Alcalase® on the 35 kg scale with 10 min HSM as described in chapter 3.7.3 was dried at 60 °C until constant weight. The dried BSG particles were milled in a Retsch centrifugal mill ZM 300 (Haan, Germany) equipped with an 80 µm mesh at 20000 rpm. To produce a masterbatch with 50% BSG content, dichloromethane (DCM) was added to a 200 g mixture of 50:50 w/w of dried BSG and PLA pellets under constant stirring until dissolved. The mixture was left overnight in a fume hood at room temperature to evaporate the DCM. The effect of dissolving BSG and PLA in DCM was investigated via fourier transform infrared spectroscopy (FTIR) on a Vertex 70 Bruker (Ettlingen, Germany) via attenuated total reflection (ATR) measured in the range 4000-650 cm^{-1} with a resolution of 4 cm^{-1} and 50 scans. Data was baseline corrected and a min-max normalization was conducted in post-processing.

The dried masterbatch was milled in a Retsch cutter mill SM 200 (Haan, Germany) before being mixed with PLA pellets to result in a 5% w/w dry BSG content. The PLA-BSG mixture was then pre-compounded as schematically shown in Figure 9. The icons used are from © vectorwin, Dhea Pramesti, vectoricon and Mykola Lytvynenko via Canva.com. The extrusion of the compounding step was conducted in a Haake Polylabsystem twin-screw extruder (Victoria, Australia). The temperature profile ranged from 180-200 °C in 5 °C steps along the five heating zones of the extruder. The extrusion speed was set to 100 rpm. The extruded filament strand was pelletized in an Axon ab plastics machinery pelletizer model S – 265 39 (Astrop, Sweden) before being milled in the Retsch cutter mill.

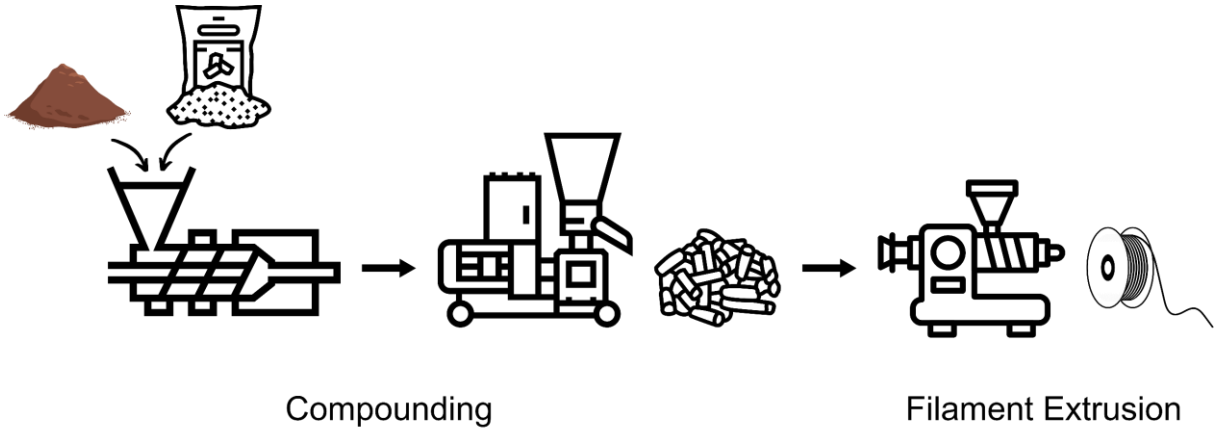

Figure 9: Schematic flow diagram of BSG and PLA filament production process.

The mixed and milled BSG-PLA composites were then extruded a second time on a 3devo filament maker ONE type Composer 350 (Utrecht, Netherlands) extruder to produce a 3D-printable filament strand. The following Table 30 summarizes the varied extrusion parameters and corresponding test ranges. The extrusion temperature was set to a single temperature.

Table 30: Parameter ranges tested during filament extrusion of BSG-PLA composites.

Parameter	Range
Extrusion temperature [°C]	180 – 200
Extruder speed [rpm]	3.5 – 5.5
Filament thickness setpoint [mm]	1.65 – 1.75
Fan speed [%]	50 – 100

All tested parameter ranges were used to produce a 5% by weight BSG-PLA filament. For each condition, a virgin PLA filament was extruded as well. The resulting filaments were used to print test specimen on a Bambulab P1S FDM printer (Shenzhen, China) equipped with an 0.6 mm hardened steel nozzle. The following Table 31 summarizes the printing parameters used.

Table 31: 3D-printing parameters used on Bambu lab P1S FDM printer.

Parameter	Value
Nozzle temperature [°C]	200
Bed temperature [°C]	75
Maximum volume speed [mm³/s]	7
Layer height [mm]	0.3
Wall loops [-]	2
Number of top and bottom layers [-]	3
Infill (cross hatch) [%]	15

The test specimen printed had dimensions according to ISO 527-2 for tensile strength measurements of plastics [95]. Subsequent tensile strength measurements were conducted in five replicates according to the same norm on a Zwick-Roell universal testing machine (Ulm, Germany) with 1 mm/s speed and a 10 kN load, which as kindly made available by the Institute of Polymers and Composites at the Hamburg University of Technology. From the obtained stress strain curves, the Young's modulus was determined as the slope of the linear portion of the stress strain curve as given in equation (26).

$$E_Y = \frac{\sigma}{\varepsilon} \tag{26}$$

With E_Y representing the Young's modulus [MPa], σ the applied stress [MPa] and ε the resulting strain of the material [%]. In addition, the tangent modulus was determined as the slope of the stress strain curve in the non-linear region as defined in equation (27).

$$E_t = \frac{d\sigma}{d\epsilon} \tag{27}$$

With E_t representing the tangent modulus [MPa], $d\sigma$ the applied difference in stress [MPa] and $d\varepsilon$ the resulting difference in strain of the material [%]. Lastly, the maximum tensile strength was determined as the maximum stress before failure and the breakage strain as the maximum relative deformation of the material. [96]

3.8 Statistical Analysis

The given data represents averages derived from three independent experiments or measurements. The results are expressed as average ± standard deviation. If no standard deviation is given, results were run as one technical replicate only. A paired two-tailed t-test was used to detect significant differences between two individual methods or groups. The significance level was either 0.05 or 0.01 and is always reported. In addition, a one-way analysis of variance (ANOVA) was performed to identify significant differences between more than two methods or groups.

4 Results and Discussion

The results obtained in the framework of the identification of suitable valorization strategies for brewer's spent grain and brewer's spent yeast are summarized in the following chapters. First, in chapter 4.1, the obtained brewing by-products are characterized on the basis of their compositional profiles. The following chapter 4.2 summarizes the findings on the production of proteolytic BSY extracts. Cell disruption methods are compared in terms of the maximum protease activity and protein content released. The results are presented in chapter 4.2.1. In order to identify potential operating conditions for subsequent hydrolysis processes using these extracts, the produced BSY fractions are characterized in detail in chapter 4.2.2. The following chapter 4.3 presents and discusses the results obtained for new BSG valorization approaches. Chapter 4.3.1 summarizes findings on protein extractions from BSG. Results from lab-scale extractions using high-shear mixing as a pretreatment strategy and applying commercial protease enzymes are scaled up to a 35 kg scale. In addition, co-valorization strategies for both BSG and BSY are evaluated. This includes a feasibility study on the use of whole BSY cells under autolysis conditions for BSG protein extraction and the application of a proteolytic BSY extract on BSG protein for peptide hydrolysis. In addition to protein extractions, results on the valorization strategies for the structural carbohydrates are presented and discussed in chapter 4.3.2. Next to hydrothermal treatments by liquid hot water extractions to isolate arabino- and xylo-oligosaccharides, enzymatic extractions using commercial cellulase enzymes on high shear mixed BSG are evaluated for their capacity to extract monomeric sugars. A valorization strategy for the remaining carbohydrate- and lignin-rich solid residue in terms of application in a filament for 3D printing is presented in chapter 4.3.3.

4.1 Raw Material Generation and Characterization

The investigation of valorization strategies for brewery by-products poses the challenge of varying compositional profiles depending on brewery-specific raw material suppliers, recipes, processing conditions and ultimately storage specifications. However, in process development it is important to keep the substrate properties and characteristics as similar as possible to allow comparison of results from different experiments. To minimize these differences, a standardized beer recipe was used to generate the by-products BSG and BSY in a reproducible manner. Even with a standardized recipe and brewing conditions, the compositional profiles of BSG and BSY will still vary from batch to batch. Therefore, the following data is only a representative example of compositional profiles of BSG and BSY used in the scope of this work.

4.1.1 Characterization of Brewer's Spent Grain

Each batch of BSG was analyzed on its pH, moisture content, particle size distribution and compositional profile. For all batches, a pH in the range of 5.5-5.8 was recorded at a moisture content of 75-80%. A pH in that range was expected, as lager beer worts are typically kept in the range of pH 5.1-5.6 during mashing for optimal starch solubilization [9]. CASTRO AND COLPINI (2021) also reported pH values around 5.5 for BSG [11]. The extraction of valuable fractions from biomass is strongly dependent on available surface area [71,97]. This is due to the physical accessibility of e.g. enzymes to hydrolysable functional groups as well as to mass transport phenomena associated with local concentration gradients. [71,98]. As a baseline, the particle size distribution of BSG was thus determined for every batch, to evaluate the influence of subsequent particle size reduction treatments on their effect on the extraction performance. The following Table 32 represents an exemplary particle size distribution obtained for BSG in the scope of this work.

Table 32: Average particle size diameters of BSG raw material from three different brewing cycles.

Diameter	$d_{x,10}$ [µm]	$d_{x,50}$ [µm]	$d_{x,90}$ [µm]
Brewer's spent grain	1723 ± 153	3280 ± 168	4910 ± 253

Basis for the determined particle size distributions was the diameter of an equivalent circle using the volume density distributions determined via image analysis. This diameter is commonly used for particle size determinations of non-spherical particles [99]. Since the mean sphericity of the prior stated particle size distributions was 45.2 ± 1.9%, this diameter was deemed suitable as a basis for comparison of the results obtained.

The compositional profile of BSG is commonly reported on the basis of its major constituents: Protein, cellulose, hemicellulose, lignin, ash and lipid. Table 1 summarizes the commonly reported ranges for these major components in BSG. A representative compositional profile of the BSG type RubyRoast used in the scope of this work is given in the following Figure 10. As can be seen, all determined values are within the broad ranges of commonly reported compositions [7,11–13]. Residual starch, if present, is contained in the sum parameter "others" for not-determined components. Quantification of residual starch was not performed because a qualitative iodine test was used as a process stop criterion during mashing. Lautering was not started until there was no color change in the reagent indicating absence of residual starch.

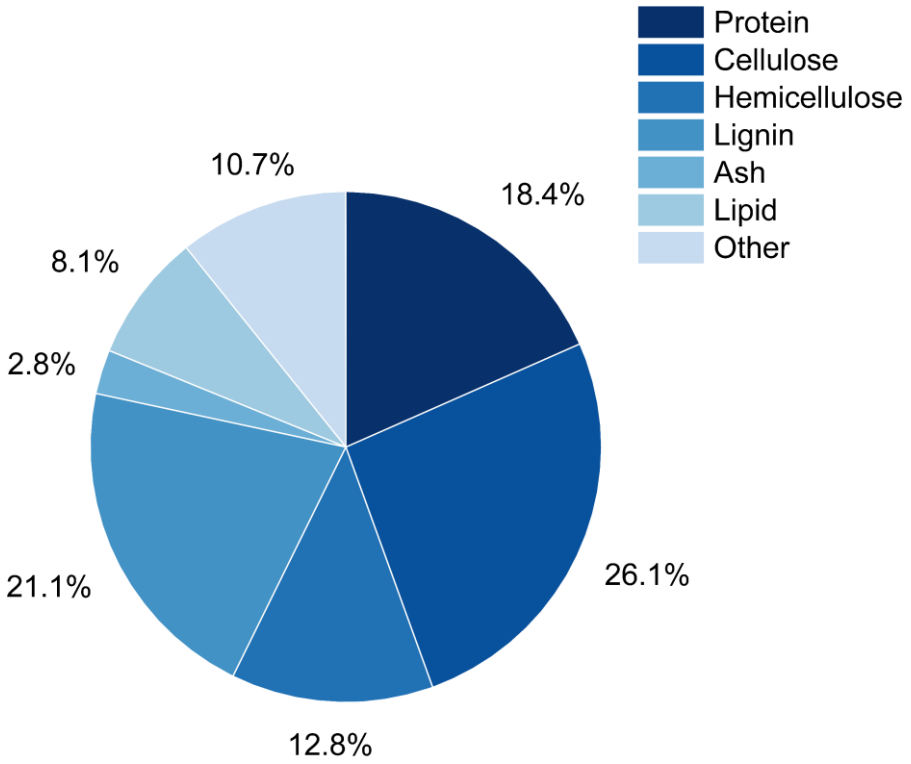

Figure 10: Compositional profile of brewer's spent grain.

A major focus of the present work is to identify protein extraction strategies that can be applied on a large industrial scale. Not only the total protein content, but also its amino acid profile is of interest, as this directly affects economic factors such as suitable market segments and thus the selling price. The following Table 33 summarizes the amino acid profile obtained for a representative RubyRoast BSG. Essential amino acids are highlighted in bold letters.

Table 33: Amino acid profile of BSG RubyRoast compared with literature data for BSG and FAO/WHO recommendations for daily intake [79,100,101].

Component	Amino acid content [% w/w]		
	Present work	GUTIÉRREZ-BARRUTIA ET AL. (2022)	FAO/WHO
Asparagine	1.59 ± 0.03	1.954 ± 0.025	-
Glutamine	4.76 ± 0.03	5.360 ± 0.226	-
Serine	0.74 ± 0.01	1.460 ± 0.011	-
Histidine	**0.13 ± 0.02**	**0.832 ± 0.016**	**1.9**
Glycine	0.52 ± 0.00	0.988 ± 0.020	-
Threonine	**1.08 ± 0.00**	**1.111 ± 0.011**	**3.4**
Arginine	0.82 ± 0.01	0.996 ± 0.022	-
Alanine	0.81 ± 0.00	2.054 ± 0.028	-
Tyrosine	**0.48 ± 0.00**	**0.939 ± 0.020**	**6.3***
Valine	**0.78 ± 0.00**	**1.453 ± 0.019**	**3.5**
Methionine	**0.41 ± 0.01**	**0.589 ± 0.012**	**2.5**
Phenylalanine	**1.02 ± 0.00**	**1.593 ± 0.028**	**6.3***
Isoleucine	**0.79 ± 0.01**	**1.108 ± 0.009**	**2.8**
Leucine	**1.35 ± 0.00**	**3.188 ± 0.150**	**6.6**
Lysine	**0.58 ± 0.01**	**0.931 ± 0.032**	**5.8**
Proline	1.37 ± 0.06	2.994 ± 0.063	-
Tryptophan	**0.13 ± 0.00**	**-**	**0.4**
Cysteine	0.50 ± 0.00	-	-
Sum	**17.83 ± 0.10**	**27.639 ± 0.264**	

*The reported value is a combined value of phenylalanine and tyrosine.

The overall amino acid content of the BSG produced at the TUHH is 9.81% by mass lower than that reported by GUTIERREZ-BARRUTIA ET AL (2022) [79]. One of the main reasons is assumed to be the biomass used. The BSG produced in the scope of this work was generated in a brew using purely barley malt, which is representative for large parts of the European market. GUTIERREZ-BARRAUTIA ET AL. (2022) used BSG obtained from a lager beer production using barley malt as well as maize as adjuncts, which is a common practice in the Americas as well as the APAC region [41]. However, the exact percentage and type of adjuncts used is not reported.

All essential amino acids can be found in the present BSG. However, experimental and literature data indicate that BSG protein alone is not suitable as a stand-alone protein supplement for human consumption meeting the recommendations by FAO and WHO for daily intake [7]. Still, it has been reported that supplementation of protein products with BSG optimizes the digestibility of the final product and improves the overall economics of the processes applied by reducing the OPEX as a readily available feedstock [7,100]. This would not only allow for the valorization of what was once considered a waste stream, but could also enable the economic feasibility of protein extractions from a variety of plant-based feedstocks.

4.1.2 Characterization of Brewer's Spent Yeast

In the scope of this work, new valorization strategies for BSY are evaluated. The major focus is set on making use of intrinsic bioactivities for application in subsequent processes. One of the major challenges of this is approach is identifying ways how to reproducibly retrieve these bioactivities, as they are strongly linked to the metabolic state of the yeast at the time of harvest. The bottom-fermenting lager yeast strain *S. pastorianus* used in the present work was harvested after two consecutive days of constant residual extract in the beer fermentation. The main harvesting criterium was thus a beer quality parameter, as would also be the case on an

industrial scale. This implies, that the fermentation duration and with that the metabolic state of the yeast at harvest will vary for each batch. In order to account for this variability, two measures of the yeast metabolic state are used: the acidification power test and the intracellular pH. The aim of introducing these parameters was to identify a potential correlation between the yeast vitality after harvest and the proteolytic activity in produced BSY extracts. The following Table 34 summarizes the obtained yeast vitality parameters for the brews of this study in relation to residual protease activity determined via the standardized glass bead treatment as a cell disruption method described in detail in chapter 3.5.3.

Table 34: Summary of determined BSY vitality through acidification power test and intracellular pH determination for standardized lager beer recipe.

Brewing date	$t_{Fermentation}$ [d]	$t_{ColdStorage}$ [d]	AP_{10} [-]	AP_{20} [-]	ICP [-]	v_s [U/g_{DM}]
13.04.2023	13	1	1.8	2.32	n.d.	5.95
19.05.2023	11	1	1.81	2.33	n.d.	4.63
26.06.2023	9	2	1.37	2.16	n.d.	2.58
23.11.2023	11	3	1.3	2.2	6.89	4.03
22.12.2024	11	3	1.51	1.85	6.49	1.67
12.04.2024	13	1	1.41	2.02	6.69	2.80
08.06.2024	12	1	0.97	1.89	6.60	1.15

As can be seen in Table 34, even for the same fermentation duration, different yeast vitality parameters are achieved. The AP_{10} value represents the intrinsic ability of yeast to metabolize glycogen while the AP_{20} value is used to characterize the ability of yeast to metabolize an exogenous glucose substrate. The data shows, that both AP_{10} and AP_{20} are positively and statistically significantly correlated with residual protease activity based on a Pearson correlation coefficient and a two-tailed t-test at a significance level of 0.05. The AP_{20} value has a stronger positive correlation with protease activity indicated by a Pearson correlation coefficient of 0.92 compared to 0.77 for the AP_{10} value. However, the method of determining the acidification power was shown to be strongly dependent on the quality of pH measurement. Depending on the age and quality of the pH probe used, different results were obtained, as the change in pH was recorded manually and only once per minute. In order to improve the reproducibility of the yeast vitality measurement, a second parameter was introduced: the intracellular pH (ICP). It could be shown, that this parameter also positively and statistically significantly correlates with the protease activity in the produced BSY extracts with a Pearson correlation coefficient of 0.90. Furthermore, it could be shown, that the AP_{20} value positively and statistically significantly correlated with the ICP. In summary, a higher ICP and a higher AP_{20} value as a measure of BSY vitality indicate a higher proteolytic activity for BSY extracts in the same order of magnitude of correlation. The AP_{10} value is a weaker indication for protease activity in BSY extracts and thus deemed unsuitable to derive clear trends for this parameter. However, both the ICP and AP_{20} values lack sufficient resolution to predict the exact protease activity in BSY extracts. A potential way of enhancing the resolution for the ICP could be a continuous flow cytometry approach, as proposed by WEIGERT ET AL. (2009) and EIGENFELD ET AL. (2023) [102,103].

Together with the yeast metabolic state and the nutrient availability during beer fermentation, the compositional profile of each BSY batch varies. Commonly stated compositional profiles are summarized in Table 3. A representative compositional profile of the BSY used in the scope of this work is given in the following Figure 11.

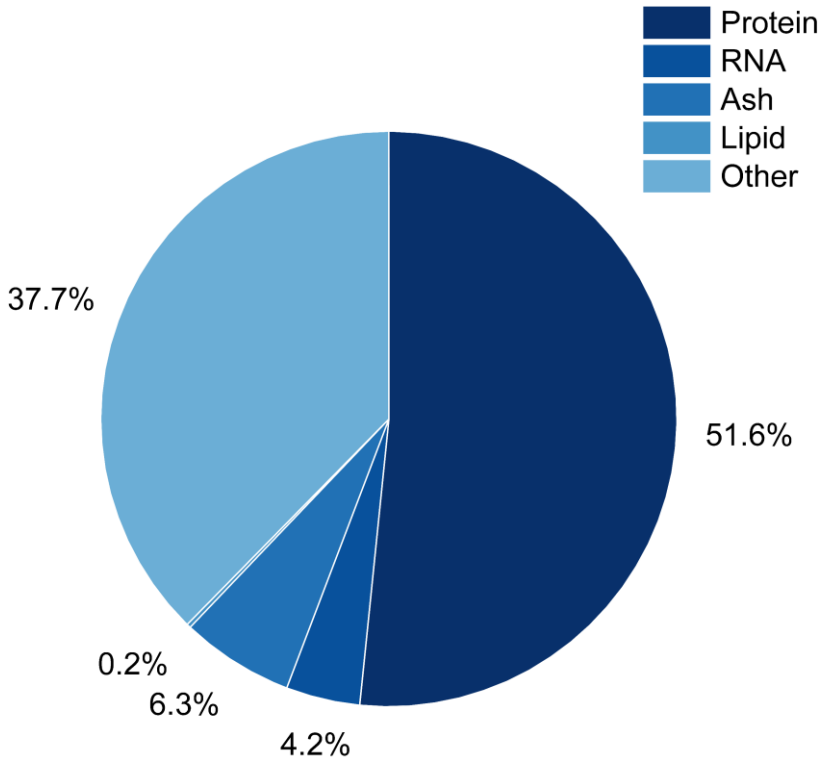

Figure 11: Compositional profile of brewer's spent yeast.

All obtained values are in the range of commonly reported mass fractions. However, due to the broad range of literature data and analytical methods available, wherever possible, relative data such as mass specific extraction yields of specific components will be stated, to allow for easier comparison of process efficiencies in between experiments. The compounds summarized under the term "Other" are assumed to comprise mostly β-glucans present in the yeast cell wall.

Next to intrinsic bioactivities such as the aforementioned protease activities in yeast extracts, an important factor for the industry is the amino acid composition, as this directly influences potential markets and applications. To allow for this evaluation, an exemplary amino acid profile of BSY is given in the following Table 35. The total amino acid content in the BSY sample sums up to 57.45 ± 0.29% by mass of dry matter. A comparison of the obtained amino acid profile with literature data on recommended essential amino acids intake for human consumption by the Food and Agriculture Organization of the United Nations (FAO) and World Health Organization (WHO) shows, that only tryptophan is supplied in recommended amounts [100,101]. It has to be noted, that other authors published data on raw BSY, that did meet the recommended doses of daily intake, e.g. CABALLERO-CORDOBA ET AL. (2000) and JAEGER ET AL (2020) [37,78]. The main reason for this is likely due to different yeast strains used as well as differences in the yeast metabolism during the brewing process. Fermentation parameters during brewing vary greatly in temperature, time, pH and oxygen content depending on the chosen recipe and yeast strain. A typical lager beer is fermented at 5-15 °C for 2-3 weeks of time, whilst a typical pale ale beer fermentation lasts for only 1-2 weeks at 12-25 °C [9,34]. In the publication of CABALLERO-CORDOBA ET AL. (2000), no mention of the applied brewing and fermentation conditions or the yeast strain used can be found. This highlights the importance of evaluating the suitability of the yeast strain under investigation for the intended valorization process.

Table 35: Amino acid profile of BSY (*S. pastorianus* strain W-34/70 by Fermentis) compared with literature data for BSY and FAO/WHO recommendations for daily intake [78,100,101].

Component	Amino acid content [% w/w]		
	Present work	CABALLERO-CORDOBA ET AL. (2000)	FAO/WHO
Asparagine	5.04 ± 0.09	-	-
Glutamine	13.49 ± 0.14	-	-
Serine	2.99 ± 0.02	-	-
Histidine	**0.83 ± 0.13**	**2.06**	**1.9**
Glycine	2.11 ± 0.11	-	-
Threonine	**2.42 ± 0.09**	**6.16**	**3.4**
Arginine	3.05 ± 0.04	-	-
Alanine	3.04 ± 0.01	-	-
Tyrosine	**2.16 ± 0.01**	**9.98***	**6.3***
Valine	**1.98 ± 0.02**	**6.20**	**3.5**
Methionine	**1.04 ± 0.01**	**2.84****	**2.5**
Phenylalanine	**2.90 ± 0.02**	**9.98***	**6.3***
Isoleucine	**2.45 ± 0.05**	**5.64**	**2.8**
Leucine	**3.95 ± 0.03**	**8.84**	**6.6**
Lysine	3.03 ± 0.03	7.13	5.8
Proline	4.14 ± 0.03	-	-
Tryptophan	**0.71 ± 0.03**	**-**	**0.4**
Cysteine	2.12 ± 0.06	-	-
Sum	**57.45 ± 0.29**	**47.19**	

*The reported value is a combined value of phenylalanine and tyrosine.
**The reported value is a combined value of methionine and cysteine.

Intermediate Summary

The aim of characterizing the produced raw materials was to present representative compositional profiles of the materials used in the present work. The key take-aways from this characterization are summarized below.

- BSG from the standardized RubyRoast recipe had a median particle size of 3-3.4 mm
- By mass, BSG contained 18% protein, 26% cellulose, 13% hemicellulose, 21% lignin, 3% ash, 8% lipids and 11% other, not determined components
- Recorded yeast vitality parameters vary with each brew and need to be reported for every batch used
- By mass, BSY contained 52% protein, 4% RNA, 6% ash, 0.2% lipids and 38% other, not determined components such as cell-wall originating β-glucans
- The recorded compositional profiles of BSG and BSY match comparative literature data
- Due to the broad ranges for compositional profiles reported in literature, mass-based extraction yields will be used whenever possible throughout this work

4.2 Brewer's Spent Yeast: Valorization as Hydrolytic Extract

Brewer's spent yeast has been proposed for the production of peptide-rich yeast extracts [104]. However, next to the extraction of bioactive peptides from BSY, intrinsic bioactivities from enzymes of yeast cells offer potential for valorization. Of particular interest are yeast-derived enzymes, most promisingly protease and invertase enzymes [40]. As proteases constitute the largest category within the industrial enzyme markets, the demand for novel, cost-effective and food-grade enzymes is high [46,47]. These bioactive molecules could potentially act as green hydrolysis feedstocks for use in the food and health sectors, where the production of peptide-rich products from (plant) protein sources is a highly sought after area of research [48–50]. However, there has been little research into the extraction of intracellular enzymes from BSY [51–53]. Most existing studies focus on the extraction of specific enzymes for analytical investigation of enzyme type and its properties to gain knowledge on the yeast strain and its metabolism [54–56]. The aim of the following chapters is thus set on investigating the potential of producing proteolytically active yeast extracts. With the dependance of applied cell disruption method on compositional profile and bioactivity in the resulting yeast extract, this study aims to identify suitable methods and operating conditions for the production of yeast extracts with maximum protease activity. The focus is set on the industrially relevant cell wall disruption methods thermal autolysis, cell milling, ultrasonication and high-pressure homogenization, enabling a fast application on larger scales. This paragraph was adapted from SCHOTTROFF ET AL. (2025) [57].

4.2.1 Screening of Cell Disruption Methods for Maximum Protease Release

The results presented in this chapter were generated by the author of this dissertation and have in part been previously published in the journal Foods by MDPI under the title "From Waste to Value: Extraction of Protease Enzymes from Brewer's Spent Yeast" by SCHOTTROFF ET AL. (2025) [57]. The results are presented together with unpublished results in this chapter to go further in depth. Proper citation will indicate, which parts have been previously published in a similar manner for transparency and attribution to the original publication.

The first step of evaluating the feasibility of using BSY as a source of protease enzymes is the identification of suitable cell disruption methods for releasing inner cell wall components. In a first set of screening experiments, four different cell disruption methods were investigated: Thermal yeast autolysis, French pressing, glass bead treatment and ultrasonication. All cell disruptions were conducted in a 0.2 M potassium phosphate citrate buffer (KPC) at pH 7. At this stage, the only quality criteria were maximizing protease activity released and reproducibility of the results. Later considerations such as co-extraction of proteins and operating expenditures relevant for scale-up considerations are investigated in subsequent chapters. The following Figure 12 summarizes the highest obtained protease activity per cell disruption method during the initial screening phase.

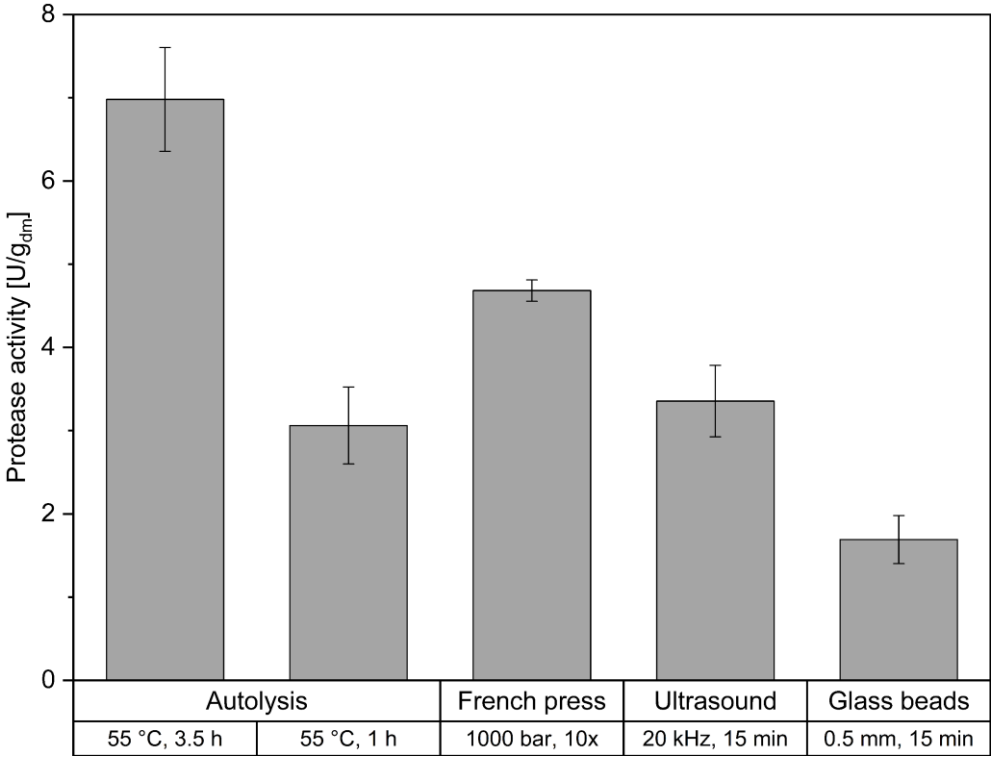

Figure 12: Highest determined protease activity per cell disruption method in 0.2 M KPC buffer at pH 7. Differences between the groups are significant at a p-value of 0.05 according to a one-way ANOVA.

As can be clearly seen, thermal yeast autolysis at 55 °C resulted in the highest overall protease activity with 7.0 ± 0.6 U/g_{dm} after 3.5 h. The second highest determined activity for this method was obtained after only 1 h treatment time with a value of 3.1 ± 0.5 U/g_{dm} and is shown directly next to it, to highlight one of the major limitations observed during cell disruption with this method: The data is inconclusive regarding trends of maximum released proteolytic activity with time and temperature as presented in Figure 13, revealed however, that above 4 h of incubation, no further increase in activity was found. Since yeast-extracted proteases are known to undergo thermal inactivation at temperatures above 45 °C, this is considered the primary reason for the absence of further increases in measured protease activity [55]. After four hours, thermal inactivation and self-degradation of the released proteases may equal or exceed their release rate during ongoing autolysis. Therefore, to optimize the investigation of this cell disruption process, the disruption time was limited to four hours. Paragraph adapted from SCHOTTROFF ET AL. (2025) [57].

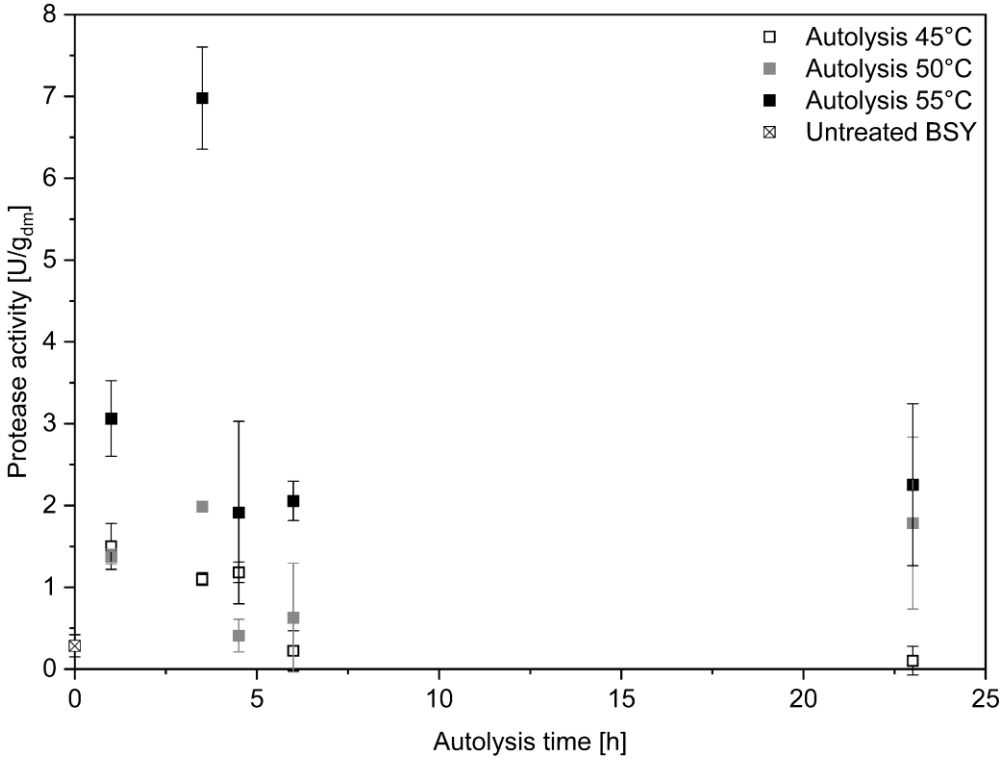

Figure 13: Protease activity in thermally autolyzed BSY extracts in 0.2 M KPC at pH 7.

The second highest proteolytic activity in the yeast extracts was obtained for the French press set-up with 4.7 ± 0.1 U/g_{dm} at 1000 bar cell disruption pressure and 10 passes through the homogenization chamber. However, the experimental set-up did not allow for reproducible results, as the homogenization pressure could not be set automatically but had to be adjusted by turning a hand lever, thus tending to overshoot the desired 1000 bar. Since this cell disruption method still proved to be principally promising for releasing proteolytic activity through action of high dynamic pressure differences, a continuous high-pressure homogenizer was used for subsequent optimization trials. Paragraph adapted from SCHOTTROFF ET AL. (2025) [57].

Both ultrasound and glass bead treatment resulted in lower, but also reproducible proteolytic activities in the yeast extracts, when run for up to 15 min. However, a linear increase in released protease activity was observed during this cell disruption time. This is consistent with the existing literature on intracellular protein release for these two cell disruption methods, suggesting first order kinetics [105–108]. For BSY, it was additionally demonstrated that after 15 minutes of cell disruption, first-order kinetics no longer apply. Instead, the overall protein release follows an asymptotic pattern, with only a slight increase in released protein content, making extended treatment times economically less justifiable [104]. To determine whether this behavior also applies to the release of protease activity, a second set of screening experiments was conducted with treatment times of up to 30 minutes. The results are shown in the following Figure 14. Paragraph adapted from SCHOTTROFF ET AL. (2025) [57].

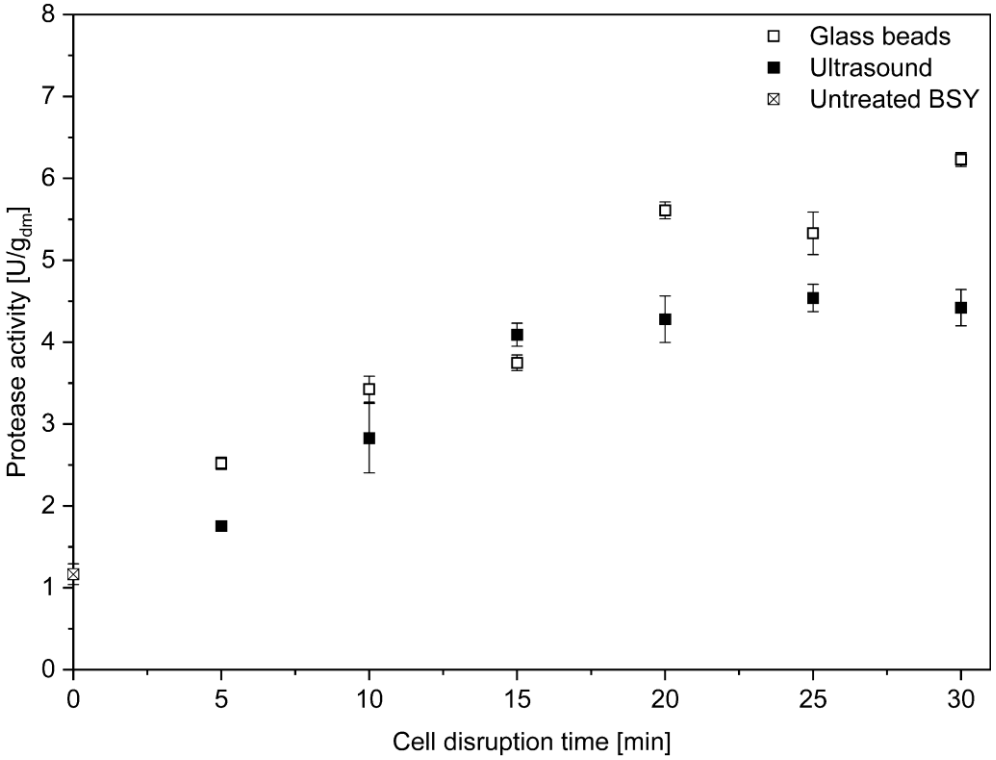

Figure 14: Protease activity in BSY extracts produced via 0.5 mm glass beads on a vortex mixer at 100% power input and 20 kHz ultrasound treatment in 0.2 M KPC at pH 7.

For ultrasound treatment, the results confirm the previously observed asymptotic behavior beyond 15 min of cell disruption for protease activity release, reaching a maximum activity of 4.54 ± 0.17 U/g_{dm} after 25 min of cell disruption. The plateau in released protease activity may be attributed to the working mechanism of ultrasound. Cell disruption occurs through bubble cavitation, generating intense local shear forces, high pressure, and temperature gradients [109,110]. The combined effects first lead to the disruption of the cell wall, followed by the breakdown of the cell membrane, ultimately resulting in the release of intracellular components. This process was described by ZHANG ET AL. (2014), who observed that cell wall-derived carbohydrates were primarily released within the first 15 minutes of yeast cell sonication before reaching a plateau at an ultrasound frequency of 20 kHz. Protein release stabilized after 20 min of ultrasound treatment, suggesting that both the cell wall and membrane had been completely degraded. [110] In this study, similar effects are assumed to contribute to the asymptotic curve observed for protease activity release, with maximum activity plateauing after 20 min of ultrasound treatment. This may be linked to the complete disruption of both the cell wall and membrane, including the vacuole compartment membrane. Since the applied frequency of 20 kHz is at the lower end of the ultrasound spectrum, it is presumed that the released proteases are not thermally or mechanically degraded during the 30 min treatment, which could explain the stable protease activity between 20 and 30 minutes [109]. However, it is also likely that extended treatment times could lead to a decline in protease activity due to prolonged exposure to high pressure, temperature gradients, and shear forces, ultimately causing structural degradation of the enzymes.

For the glass bead treatment, no clear asymptotic trend was observed in the release of protease activity. Extending the cell disruption time beyond 15 min continued to increase protease activity, with no distinct plateau reached. The highest protease activity recorded was 6.23 ± 0.09 U/g_{dm} after 30 min of cell disruption. As reported by VAN GAVER AND HUYGHEBAERT (1991), yeast cell walls do not fully disintegrate during cell milling [111]. In this study, this may be one reason why an asymptotic curve for protease release was not observed, though such a trend might become apparent with longer treatment times. Additionally, the use of a vortex

mixer instead of a flow-through system, as found in commercial bead mills, may have significantly reduced local shear forces due to the lower power input. Conversely, it is also possible that the data point at 30 minutes represents an outlier and that an asymptotic trend might still exist. Since this was not explored within the scope of this study, further experiments are needed to clarify the underlying mechanisms and trends. In particular, using a commercial cell mill is recommended for future investigations. For this study, a 15 min cell disruption time was chosen for both ultrasound and glass bead treatments to ensure better comparability of results. Paragraph adapted from SCHOTTROFF ET AL. (2025) [57].

Taking the main learnings from the initial screening experiments into account, a more thorough analysis of each cell disruption method was conducted. Autolysis times were limited to a maximum of 4 h, the French press set-up was replaced with a high-pressure homogenizer and glass bead and ultrasound treatment were conducted for a maximum of 15 min. Next to the released protease activities, other parameters such as released protein content and size were taken into account. The used buffer was also changed to 0.1 M sodium phosphate citrate (NaPC) at pH 6 based on findings presented in the subsequent chapter 4.2.2 as well as Figure A-1 in the appendix. Results for thermal yeast autolysis runs are summarized in the following Figure 15.

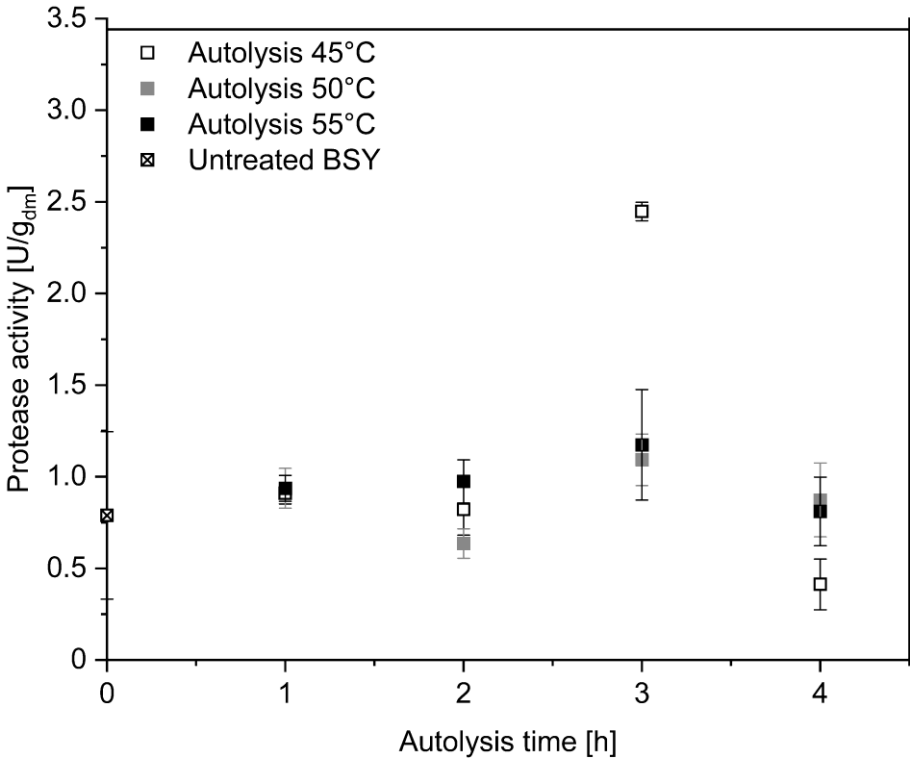

Figure 15: Protease activity in thermally autolyzed BSY extracts in 0.1 M NaPC at pH 6.

The highest proteolytic activity was determined at 45 °C after 3 h incubation with a value of 2.45 ± 0.05 U/g_{dm} followed by a drastic decrease to 0.41 ± 0.14 U/g_{dm} at the same temperature after 4 h of incubation. Thermal inactivation of proteases is considered the dominant factor, as brewing yeast strains are typically optimized for growth within a temperature range of 12–20 °C. [5]. A previous study by WOODS AND KINSELLA (1980) reported that proteases extracted from a strain of *S. carlsbergensis* exhibited no thermal inactivation at temperatures between 25-37 °C over 40 min, whereas complete inactivation occurred within 5 min at 70 °C and pH 6 [54]. Similarly, MADDOX AND HOUGH (1970) observed thermal inactivation of *S. carlsbergensis* extracted proteases at temperatures above 50 °C after 1 h incubation at pH 6.3 - 6.6 [55]. Since the present study examined a crude yeast extract containing multiple different enzymes rather than isolated fractions, it is assumed that not all proteases undergo thermal inactivation

simultaneously or at the same rate. However, it is hypothesized, that the majority of extracted proteases are inactivated between 3-4 h of autolysis. This highlights the importance of stopping the autolysis process at the point of maximum protease activity. Currently, no inline measurement for protease activity is available, which presents challenges for process automation and raises questions about the overall feasibility of this approach for producing proteolytically active yeast extracts. Paragraph adapted from SCHOTTROFF ET AL. (2025) [57].

Next to the overall released protease activity, protein extraction efficiency is an important parameter commonly used to compare different cell disruption methods with each other [104]. The following Figure 16 summarizes the results obtained for protein content in the residual cell wall debris (CWD) and overall protein extraction yield. As shown, the dry mass-specific protein content initially increases beyond that of untreated BSY cells in all autolysis experiments before declining again. This is likely due to dry matter loss caused by ongoing autolysis. At extended autolysis times, the protein content decreases as proteases released from the yeast cells break down insoluble intracellular proteins into soluble peptides and amino acids, which are subsequently released into the extracellular medium. To account for this dry matter loss, protein extraction yields were calculated via mass balance, as described in chapter 4.2.1. This approach allows for comparisons with other studies, as the mass-specific protein content can vary depending on the yeast's metabolic state at harvest and differences between yeast strains. When assessing overall protein extraction efficiency, a trend of increasing protein yield in the BSY extract over time can be observed in Figure 16 (b). Among the tested temperatures, autolysis at 50 °C resulted in the highest total protein extraction yield, reaching 32.3 ± 3.6% by mass after four hours of incubation. These findings align with previous studies, which also reported maximum protein yields at 50 °C for BSY [59,104]. However, in those studies, protein extraction was evaluated at later time points, focusing solely on protein recovery rather than residual protease activity in the extracts. Reported yields range from 10-50% after 6-8 h of incubation. Direct comparisons of absolute values remain challenging, as most studies do not provide yeast vitality measurements prior to cell disruption. This parameter is essential for assessing the metabolic state of yeast before autolysis begins and may explain variations in the time required to achieve high protein extraction yields. Additionally, details on the exact yeast strain, beer fermentation conditions, and pretreatment methods are often lacking, despite their influence on the initial protein content of the yeast. JACOB ET AL. (2019) also introduced inducers such as 0.086 mol/L sodium chloride and 0.051 mol/L ethyl acetate to enhance thermal yeast autolysis [104]. Another critical factor to consider is the method used for protein content determination. In this study, amino acid HPLC was used for all reported total protein contents, whereas the previously stated studies primarily relied on indirect methods like Kjeldahl nitrogen determination, making direct comparisons of protein yields difficult. Paragraph adapted from SCHOTTROFF ET AL. (2025) [57].

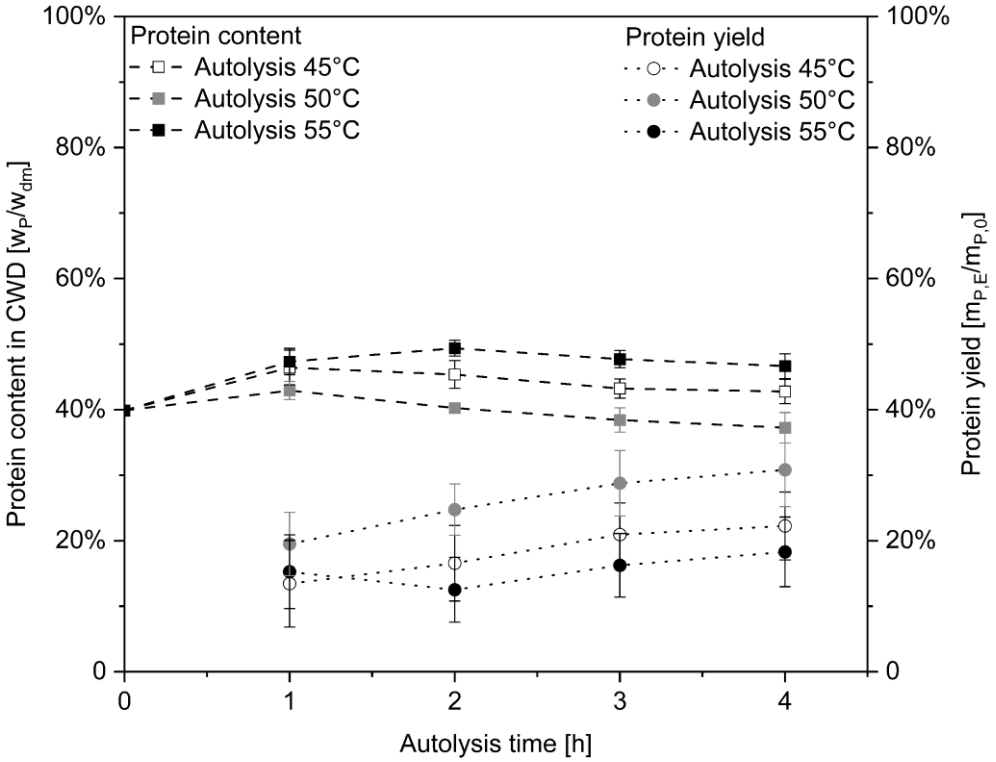

Figure 16: Protein content in residual cell wall debris fraction of thermally autolyzed yeast cells in 0.1 M NaPC at pH 6. Protein extraction yield for BSY extract calculated via mass balance. Displayed lines serve solely as a visual aid.

Residual protease activity in BSY extracts depends on the presence of intact proteins. To qualitatively evaluate the presence of proteins of different sizes, an SDS-PAGE analysis was conducted. The stained gels for the autolysis samples are shown in Figure 17, where a darker blue color indicates a higher protein concentration. The blank sample represents a non-autolyzed, cell-free supernatant obtained from a BSY cell pellet suspended in 0.1 M sodium phosphate citrate buffer (NaPC) at pH 6. Paragraph adapted from SCHOTTROFF ET AL. (2025) [57].

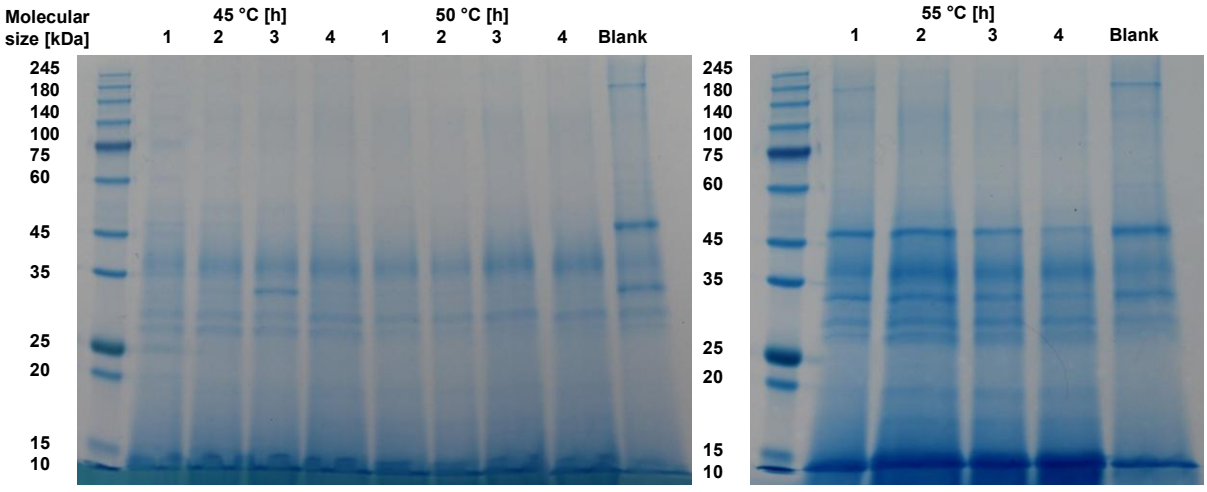

Figure 17: SDS-PAGE results for thermally autolyzed BSY extracts in 0.1 M NaPC at pH 6.

The general trend observed across all temperatures indicates that proteins larger than 45 kDa, which are visible in the blank, appear to be progressively degraded into smaller proteins and peptides over time. This degradation could be due to either thermal breakdown or the hydrolytic action of proteases released from BSY during the autolysis process. Additionally, this suggests

that the autolysis process has not advanced sufficiently to release cell wall-bound proteins, which typically range in size from 60 to 220 kDa. These larger proteins would likely have been separated into the cell pellet after centrifugation. This assumption is further supported by the residual protein content of 40-45% found in the cell wall debris after one hour of incubation. Another possibility is that these proteins are not entirely released from the cell wall but instead undergo a direct hydrolysis in place, resulting in the formation of peptides through protease activity. In all examined samples, the most prominent bands correspond to peptides smaller than 15 kDa, with additional notable bands in the 25-45 kDa range. This could be attributed to the action of vacuolar yeast proteases released during the autolysis process. In *S. cerevisiae* strains, there are seven known vacuolar proteases, which are listed together with corresponding molecular sizes in the following Table 36. Paragraph adapted from SCHOTTROFF ET AL. (2025) [57].

Table 36: Known vacuolar proteases in *S. cerevisiae* and corresponding molecular sizes [58,112].

Protease	Molecular size [kDa]
Dipeptidylaminopeptidase B	90 - 120
Carboxypeptidase S	65 - 75
Aminopeptidase Y	60 - 75
Carboxypeptidase Y	60
Aminopeptidase I	50 - 57
Proteinase A	42 - 45
Proteinase B	31 - 37

Among the listed proteases, only two are endoproteases: proteinase A and proteinase B. Proteinase A, in particular, plays a crucial role in the catalytic activation of other vacuolar proteases under stress conditions [58]. The SDS-PAGE results in this study show that whenever a protein band in the 30-35 kDa range is visible, the intensity of the protein bands up to 45 kDa increases in the following hour. This could be linked to the release of proteinase A, which then activates other vacuolar proteases that hydrolyze yeast proteins into smaller peptides. The high color intensity at the lower end of the gels may be attributed to the action of vacuolar exopeptidases, which break down proteins into smaller peptides and free amino acids. It is well known that thermally induced yeast autolysis primarily results in small peptides and amino acids, which is consistent with the findings of this study. PODPORA ET AL. (2015) reported an increase in free amino acids during BSY autolysis from 11.2% after 2 h to 77.5% after 48 h at 47 °C and pH 5.2-6.2, linking it to decomposition of proteins and peptides [113]. In addition, JACOB ET AL. (2019) reported autolysis to yield the highest free amino acid content compared to cell disruption methods cell mill and ultrasound treatment [104]. The main reason is hypothesized to be the predominant action of proteases during autolysis. Paragraph adapted from SCHOTTROFF ET AL. (2025) [57].

The results for glass bead and ultrasound treatment in terms of released protease activity in 0.1 M NaPC at pH 6 are given in Figure 18.

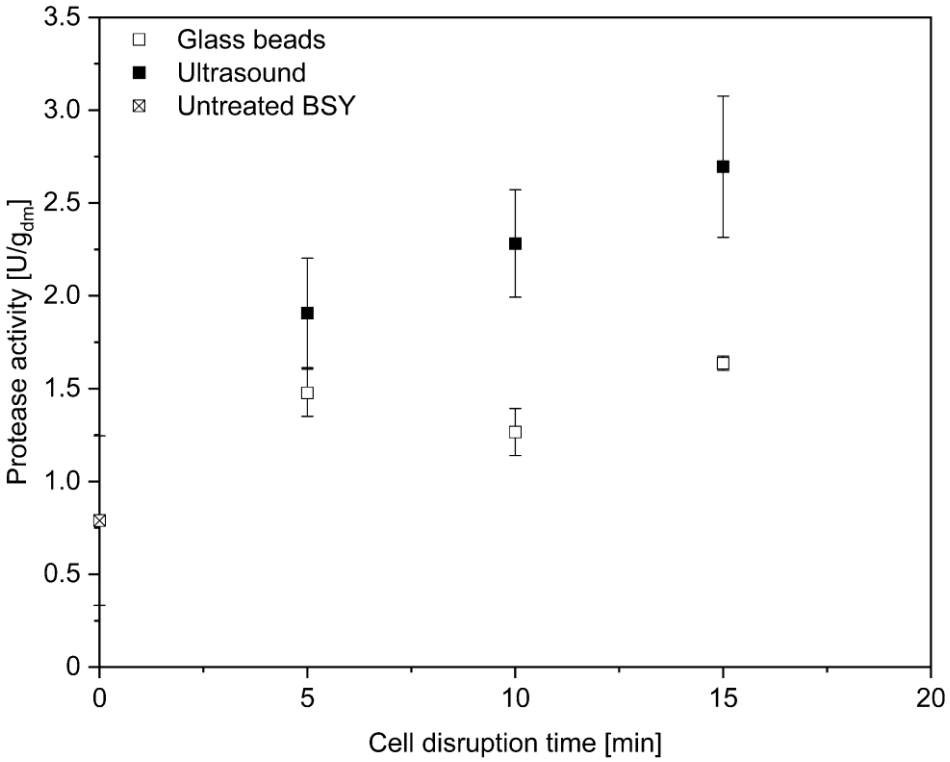

Figure 18: Protease activity in BSY extracts produced via 0.5 mm glass beads on a vortex mixer at 100% power input and 20 kHz ultrasound treatment in 0.1 M NaPC at pH 6.

As observed, all investigated cell disruptions resulted in proteolytic activity higher than for the untreated BSY supernatant. Ultrasound treatment produced higher protease activities than the glass bead treatment, with a peak activity of 2.70 ± 0.38 U/g_{dm} after 15 min. In contrast, glass bead treatment showed better reproducibility but only reached a maximum activity of 1.64 ± 0.04 U/g_{dm} after the same duration. The lower reproducibility of ultrasound treatment could be attributed to its mechanism of cell disruption. Ultrasound relies on asymmetrical bubble implosions through cavitation, which generates high shear forces that disrupt the cell wall [114]. Since the positioning of the ultrasound probe within the sample can vary, the location of these shear forces will also change. Small deviations in probe positioning between replicates might have resulted in differences in the efficiency of the disruption process. Paragraph adapted from SCHOTTROFF ET AL. (2025) [57].

The protein content in the residual cell wall debris for ultrasound treatment shows the same trend as for the autolysis samples with a dry mass specific increase from 39.9 ± 1.8% to 48.5 ± 2.6% followed by a linear decrease with progressing cell wall disruption to 41.6 ± 1.1% as can be seen in Figure 19.

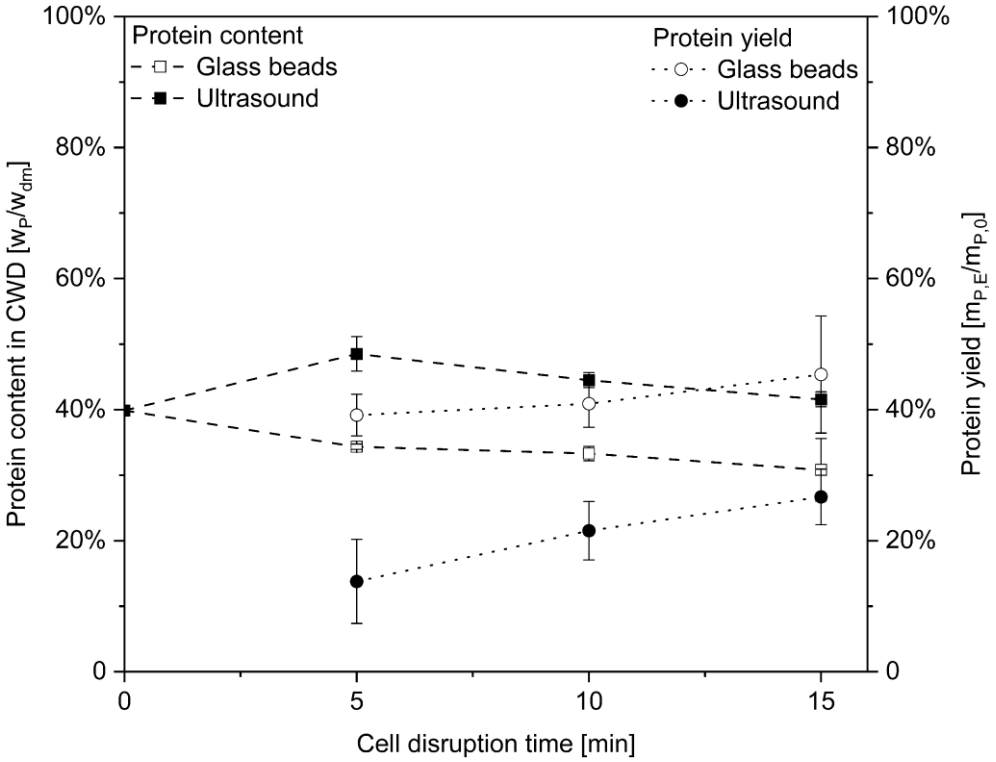

Figure 19: Protein content in residual cell wall debris fraction of glass bead and ultrasound treated yeast cells in 0.1 M NaPC at pH 6. Protein extraction yield for BSY extract calculated via mass balance. Displayed lines serve solely as a visual aid.

However, as shown in Figure 19 this behavior differs for the glass bead treatment. The protein content in the cell wall debris decreases with increasing cell disruption time, reaching a value of 30.8 ± 4.8%. This might be attributed to the mechanism of cell disruption, which is in itself unspecific. However, it could be shown, that glass bead cell disruption can be selective towards releasing intracellular compounds, depending on the glass bead diameter used. For yeast cells, glass beads with a diameter of 0.5 – 1.25 mm are commonly cited [115]. Larger diameters are typically favored for releasing periplasmic enzymes, while smaller diameters are applied to release cytoplasmic enzymes from *S. cerevisiae* [116]. This could also apply to other soluble intracellular compounds, which may not be extracted under the given disruption conditions, thus reducing the overall dry matter in the cell wall debris to a lesser extent. To test this hypothesis, measurements of carbohydrates and other intracellular components in both the BSY extracts and the cell wall debris fractions would be necessary. Since these measurements were not performed in this study, the analysis is limited to protein extraction.

As seen in Figure 19, protein extraction yields increased with longer cell disruption times. Glass bead treatment was the more effective method for cell wall disruption, resulting in a maximum protein extraction yield of 45.4 ± 8.9% by mass after 15 min, compared to 26.7 ± 4.2% by mass released through ultrasound treatment. This yield is considerably lower than those reported by other groups using these methods, particularly when compared to JACOB ET AL., who reported 80% extraction efficiency after 15 minutes of both glass bead and ultrasound treatment [104]. However, even though the same glass bead diameter and ratio to BSY suspension were used, there were differences in the experimental setups. Other research groups used a commercial cell mill, while this study had to rely on a conventional vortex mixer, which likely reduced the effective shaking frequency and, consequently, the protein extraction efficiency. Additionally, different yeast strains were used, the brewing processes differed, and no measure of yeast vitality was provided. Therefore, it is challenging to pinpoint the main cause of these significant discrepancies in results.

The qualitative analysis of released protein sizes via SDS-PAGE, shown in Figure 20, yielded results similar to those observed in the thermal autolysis analysis. Larger proteins above 45 kDa, present after 5 min of cell disruption, appear to be degraded into smaller peptides. For glass bead treatment, the sample at 10 min of cell disruption shows the lightest blue color, indicating the lowest protein content. This correlates with the protease activity measured at this time point, which was also the lowest among the three time points investigated. A possible explanation for this is that the protein release rate between five and ten minutes was lower than the protein degradation rate, due to the mechanical stress from the glass beads. As a result, most of the protein present was degraded into peptides below 15 kDa. This assumption is supported by the protein extraction yield, which increased during this time interval, while protease activity decreased, possibly due to the degradation of released proteases into non-functional peptides. The same reasoning applies to the ultrasound treatment, where an increase in color intensity in the range below 45 kDa is visible from five to ten minutes, followed by a decrease in the subsequent five-minute interval. Previous paragraphs adapted from SCHOTTROFF ET AL. (2025) [57].

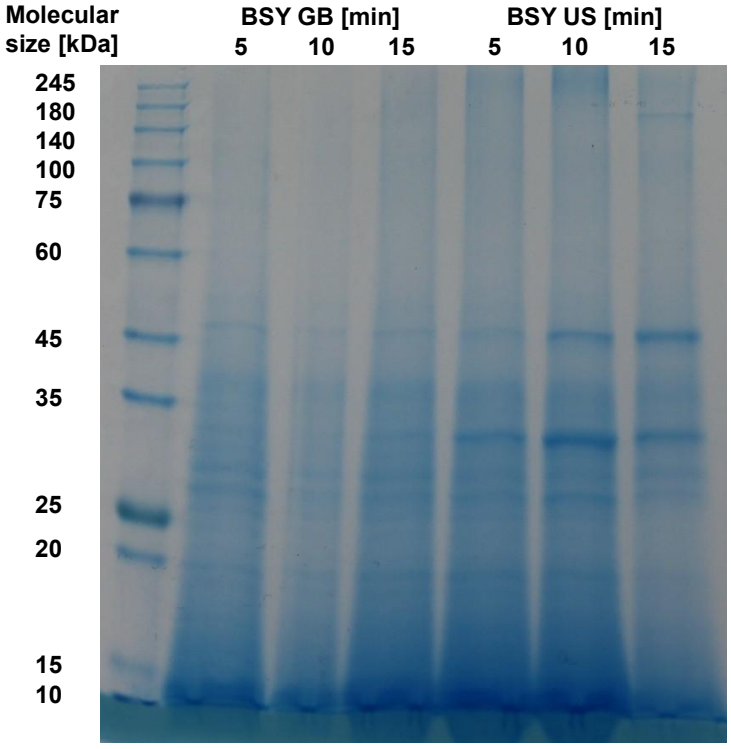

Figure 20: SDS-PAGE results for glassbead and ultrasound treated BSY extracts in 0.1 M NaPC at pH 6.

The final cell disruption method investigated was high-pressure homogenization (HPH). HPH was chosen to assess a mechanical disruption technique that is widely used on an industrial scale [115]. Since the production capacity per brew in the microbrewery Campus Perle is limited to 1.5-2 L of BSY suspension and the homogenizer has a feed volume of 300 mL per run, a second beer fermentation was started. Table 37 summarizes the differences in fermentation time until a constant residual extract of 3.5 °P was reached, as well as the differences in yeast vitality after harvest. The second BSY batch showed a lower intrinsic ability to metabolize glycogen, as indicated by the AP_{10} value, compared to the first batch. However, its ability to metabolize an exogenous glucose substrate, represented by the AP_{20} value, was higher, suggesting potentially greater proteolytic activity in the resulting BSY extracts. To account for these differences, overall comparisons between the various cell disruption methods will be made relative to the initial activity in the cell-free supernatant before cell disruption.

Table 37: Summary of fermentation, vitality and protease activity differences for two BSY batches. Protease activity determined after 15 min glass bead treatment at 4 °C using 0.5 mm glass beads on a vortex mixer at 100% power input.

BSY batch designation	Fermentation time [d]	Storage time [d]	AP_{10} [-]	AP_{20} [-]	v [U/g_{dm}]
Autolysis, GB, US	11	3	1.51 ± 0.01	1.85 ± 0.01	1.64 ± 0.04
HPH	9	2	1.36 ± 0.01	2.15 ± 0.01	2.58 ± 0.26

Before evaluating the suitability of high-pressure homogenization for the preparation of proteolytic BSY extracts, the general effectiveness of this cell disruption method was first analyzed through image-based analysis. Figure 21 summarizes the results obtained for cell disruption at 600 bar for 0 to 10 passes through the homogenization chamber. Previous paragraphs adapted from SCHOTTROFF ET AL. (2025) [57].

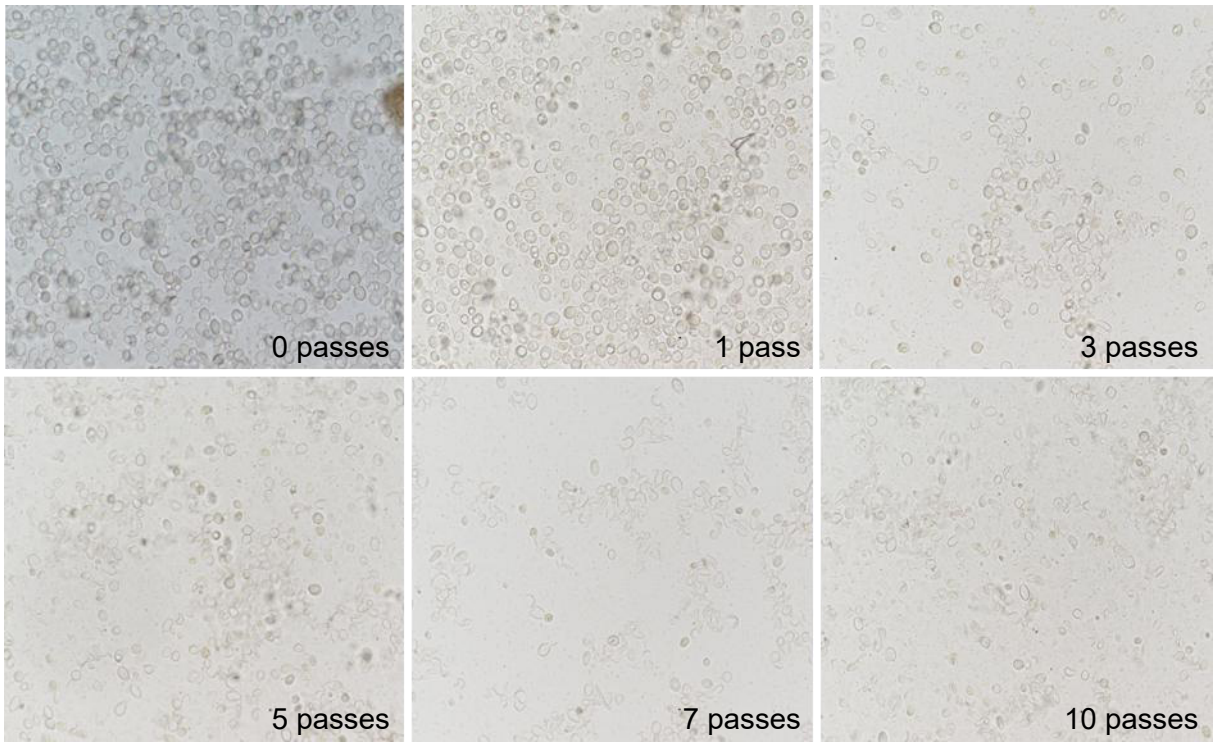

Figure 21: Image-based analysis of cell disruption progress with increasing number of passes through high pressure homogenization at 600 bar. Flux of 9 L/h maintained at max. 20 °C with countercurrent tubular heat exchanger at outlet of HPH valve. Top left to bottom right: 0, 1, 3, 5, 7 and 10 passes through homogenization valve.

It is evident that the degree of cell disruption increases with the number of passes. The cell wall is effectively disrupted using this technique. The images were digitally analyzed with the Software Nikon NIS-Elements AR (Tokyo, Japan) to assess the degree of cell disruption, and the results are summarized in Table 38. The general trend indicates, that most of the cell disruption had its effect between 1-3 passes through the homogenization chamber. After 5-10 passes, most cells appear disrupted and the cell debris dominates the images. Increasing the number of passes beyond 5-7 appears to have little added benefit for the final degree of cell disruption. Higher homogenization pressures resulted in higher degrees of cell disruption at fewer passes. Depending on the intended application of the final product, optimal conditions for cell disruption must be determined, considering both processing times and energy requirements. Paragraph adapted from SCHOTTROFF ET AL. (2025) [57].

Table 38: Grade of cell disruption from image-based analysis of high pressure homogenized BSY samples.

Homogenization pressure [bar]	Pass number [-]	Grade of cell disruption [%]
400	1	50
	3	60
	5	65
	7	75
	10	80
600	1	50
	3	75
	5	80
	7	90
	10	>95
1100	1	75
	3	80
	5	>95
	7	>95
	10	>98

There is no clear trend in the release of proteolytic activity as a function of pressure and number of passes, as shown in Figure 22.

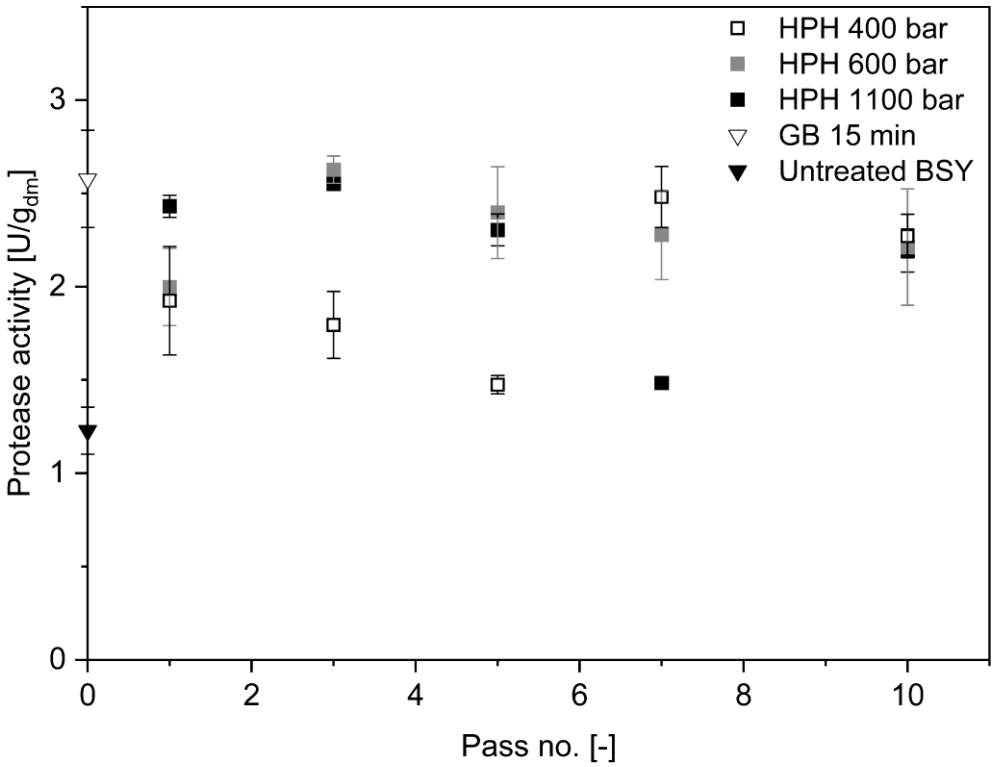

Figure 22: Protease activity in high-pressure homogenized BSY extracts in 0.1 M NaPC at pH 6.

All tested homogenization pressures and pass numbers resulted in increased proteolytic activity in the BSY extract compared to the negative control, where no homogenization was performed. Since this experiment used a different batch of BSY than the previous cell disruption methods, a glass bead cell disruption was conducted for 15 min at 4 °C, using 0.5 mm glass beads in 0.1 M NaPC at pH 6 was conducted. The released protease activity in the BSY extract from glass bead treatment with 2.6 ± 0.3 U/g_{dm} was of the same order of magnitude as that from extracts produced with HPH pressures of 600 and 1000 bar, and 1-3 passes. In general, HPH pressures above 400 bar appear to release protease activity more

effectively at pass numbers below seven. This may be due to the advanced disintegration of the cell wall caused by high dynamic pressure differences and the impact in the valve exit zone [117]. However, the overall maximum released proteolytic activity after one pass at 1100 bar did not increase with additional passes, suggesting the potential for a continuous processing route through the homogenizer. This behavior could be due to the undirected shear forces during HPH, which may lead to the degradation of proteases released during previous passes with each subsequent pass through the homogenization chamber.
In addition to proteolytic activity, another key parameter for evaluating cell disruption efficiency is the overall protein extraction efficiency. Figure 23 presents the protein content in the BSY extracts determined using a Pierce assay. The released protein content increases until three passes for 400 bar and until five passes for 600 and 1100 bar, before decreasing again. This apparent decrease in protein content may seem counterintuitive given the continued cell disruption observed in the image-based analysis. However, it is hypothesized that the maximum extractable protein content, excluding the cell wall-bound proteins, has already been released after these pass numbers. As a result, further passes through the homogenization valve likely led to fragmentation of the extracted proteins into smaller peptide fractions. Since the Pierce assay has a lower detection limit for peptides, the decrease in protein content in the supernatant may be attributed to the generation of peptides smaller than this limit, a phenomenon also noted by JACOB ET AL. when analyzing BSY autolysates using the Bradford assay [118]. Paragraph adapted from SCHOTTROFF ET AL. (2025) [57].

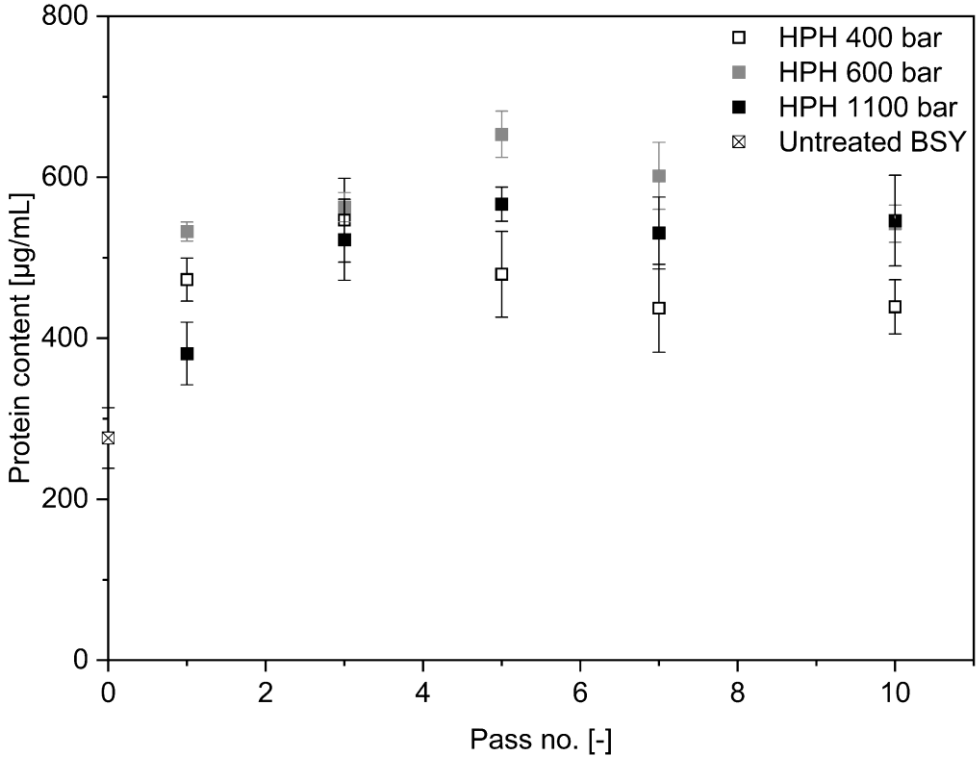

Figure 23: Pierce protein content in high-pressure homogenized BSY extracts in 0.1 M NaPC at pH 6.

This assumption is further supported by the amino acid HPLC results presented in Figure 24 (a) for the total protein contents in the extracts and cell wall debris fractions after ten passes. All investigated pressure levels resulted in protein contents of 19% for the BSY extracts and 48% for the residual cell wall debris fractions. Additionally, the overall protein extraction yields shown in Figure 24 (b) of 60% were achieved for all investigated pressure levels after ten passes. For 400 bar, this protein yield was already achieved after five passes through the homogenization valve, further supporting the assumption that cell wall disruption at all investigated pressures has already effectively released all non-cell wall-bound protein. However, due to the sample mass required for HPLC analysis, the protein content

measurements, and subsequently the yields, were only single measurements, omitting the possibility to analyze statistical relevance of the results. Paragraph adapted from SCHOTTROFF ET AL. (2025) [57].

Achieving protein extraction yields of 60% by mass for yeast is notably higher than values reported in previous studies. For example, LEE ET AL. (2024) reported protein extraction efficiencies of less than 20% for 600 bar homogenization pressure and less than 40% for 1200 bar homogenization pressure for instant dried yeast suspensions of *S. cerevisiae* of 2.3 x 10^8 CFU/mL [119]. However, a different homogenizer of the type NLM 100 by Ilsin Autoclave Co., Ltd. was used in their study. MOORE ET AL. (1990), using a single piston positive displacement pump (APV Gaulin 15 M), coupled with an APV Junior plate heat exchanger by APV Baker, found that the efficiency of yeast cell disruption in a high-pressure homogenizer strongly depends on the valve geometry and impact ring dimensions, which might explain the lower extraction yields in their study [117]. Similarly, VERDUYN ET AL. (1999), using a Panda Homogenizer by GEA Niro-Soavi, reported lower protein recoveries for *S. cerevisiae* grown on sugar cane molasses: protein recovery greater than 45% after homogenization at 1000 bar for three passes and greater than 25% after homogenization at 600 bar for six passes [120]. It should be noted that all cited publications determined protein contents via colorimetric assays or Kjeldahl measurements, using a nitrogen conversion factor of 6.25. While VERDUYN ET AL. (1999) corrected for free ammonia contents, these indirect protein content determination methods are prone to overestimating protein contents [121,122]. The commonly used conversion factor of 6.25 as a ratio to convert total nitrogen into protein contents proposed by JONES (1930) was originally intended to be used for food and feed [123]. For yeast, a more accurate nitrogen conversion factor of 5.5, accounting for non-protein nitrogen such as nucleic acids and free ammonia, was proposed by REED ET AL. (1990) [81]. Paragraph adapted from SCHOTTROFF ET AL. (2025) [57].

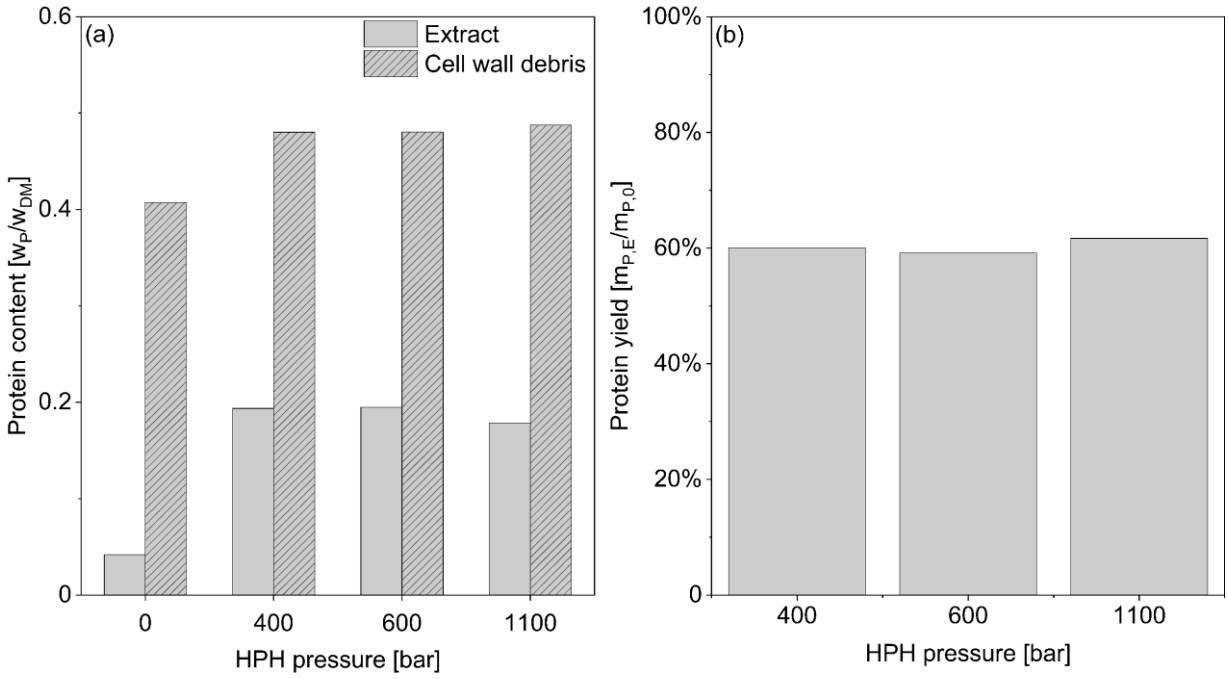

Figure 24: Protein content (a) in BSY extract and residual cell wall debris fraction of high-pressure homogenized yeast cells in 0.1 M NaPC at pH 6 determined via amino acid HPLC. Protein extraction yields (b) for BSY extracts calculated via mass balance. All protein data for a total pass number of ten. No statistical evaluation possible due to single technical replicate runs.

The conducted SDS-PAGE analysis reveals, that no distinct protein bands above 45-50 kDa are present, suggesting that larger proteins have been broken down or degraded during the homogenization process. Additionally, all protein bands below this size become more intense

in color as the number of passes increases. This observation could be related to the breakdown of proteins extracted during earlier passes through the homogenization chamber, with high mechanical stress leading to the fragmentation of these proteins into smaller peptides. The prominent bands align with previously reported protein sizes analyzed via SDS-PAGE from wine yeast *S. cerevisiae* extracts [124]. Paragraph adapted from SCHOTTROFF ET AL. (2025) [57].

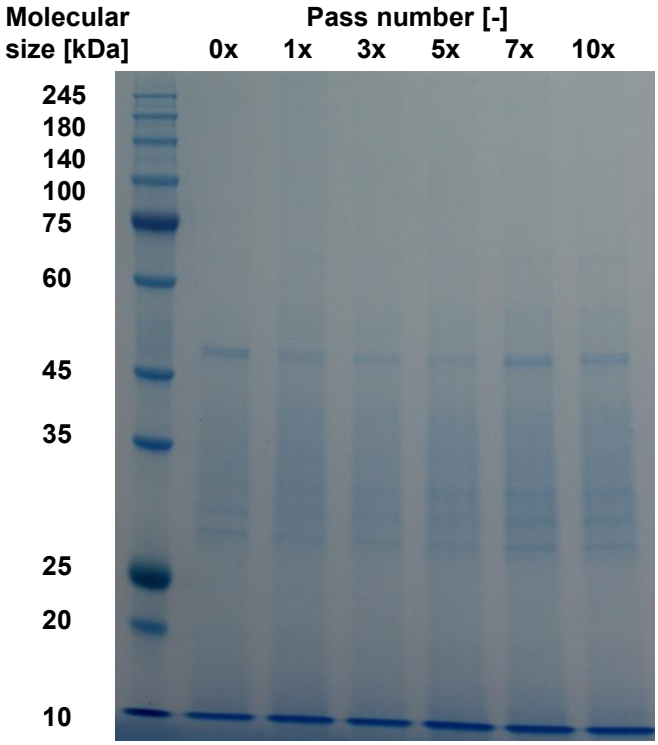

Figure 25: SDS-PAGE results for 600 bar high pressure homogenized BSY extracts in 0.1 M NaPC at pH 6.

In addition to evaluating the released protease activities and protein yields for each method, a comparison between the methods themselves is also of interest. To facilitate this comparison for the released protease activities, a normalized activity is defined and shown in Figure 26. This normalized activity is calculated as the ratio of the proteolytic activity released in the produced extract to the BSY blank activity for each brew. Only the highest activity value for each method has been considered. It has been shown that autolysis and ultrasound treatment result in extracts with similar normalized protease activity, with values of 3.10 ± 0.11 and 3.42 ± 0.83, respectively. Autolysis is acknowledged as a process that releases a substantial amount of protease enzymes, a conclusion supported by several research groups, demonstrated by the high peptide and free amino acid content. [66,104,113] The findings of this study support this hypothesis, as autolysis was found to release the highest protease activity among the four cell disruption methods investigated. However, due to the limited number of sampling points, it is still unclear whether the determined protease activity represents the maximum possible activity released during the cell disruption process. This presents an additional challenge for the application of autolysis in the production of proteolytic extracts. Various factors, such as brewing style, yeast vitality, the storage time prior to cell disruption, and the choice of buffer type, influence the resulting yeast metabolism at the onset of autolysis, leading to variability in the time of highest protease activity between batches. The lack of an inline enzyme activity assay restricts the potential for automated process control, while offline analysis is too slow to act as a stopping criterion. Paragraph adapted from SCHOTTROFF ET AL. (2025) [57].

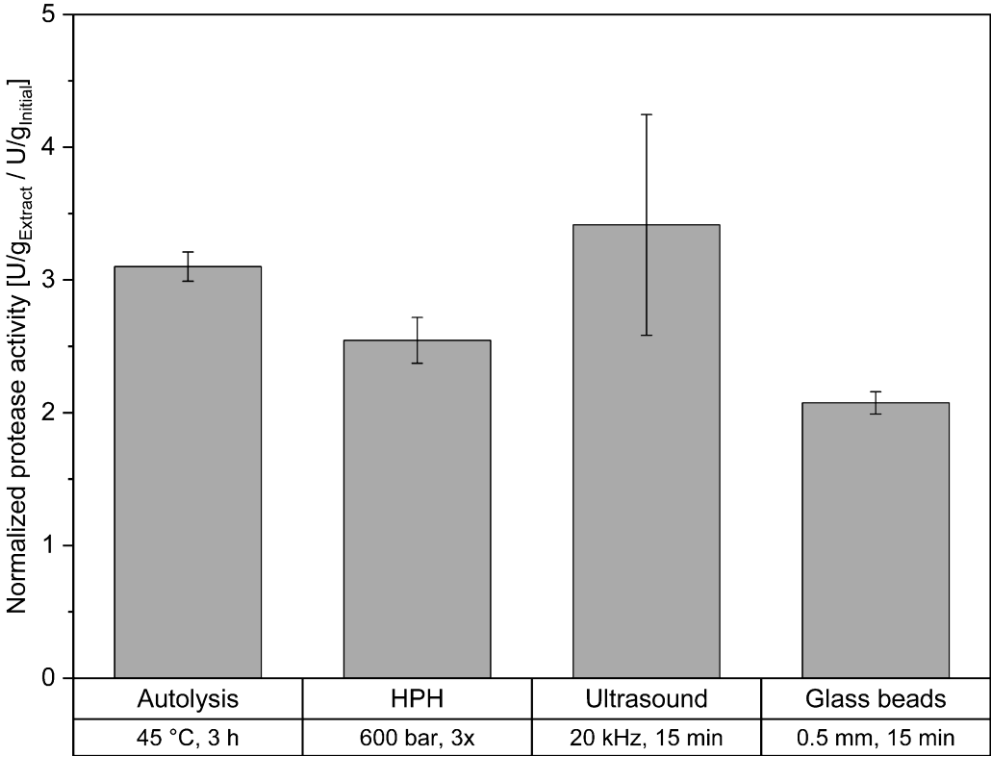

Figure 26: Comparison of highest determined protease activity per cell disruption method. Activity reported as normalized activity to the BSY blank activity of 0.95 ± 0.03 U/g$_{dm}$ for HPH and 0.79 ± 0.46 U/g$_{dm}$ for all other methods. Differences between the groups are significant at a p-value of <0.01 according to a one-way ANOVA.

In contrast to the findings for autolysis, ultrasound treatment exhibited an asymptotic trend toward increased protease activity in the extract with increasing cell disruption time. Given data for the specific yeast strain and brewing process, a first-order kinetic model could be developed to predict the time point at which the highest protease activity occurs. This approach could yield results similar to those already reported by various research groups for protein release in yeast [104–106]. One of the potential challenges with ultrasound treatment is its apparent low reproducibility, as exemplified in Figure 26. The variability in reproducibility may be attributed to the positioning of the ultrasound probe in the BSY suspension, which affects the efficiency of cell disruption. The localized effects of bubble cavitation and the associated temperature gradients may lead to uneven protease inactivation. In contrast, JACOB ET AL. (2019) did not report similarly poor reproducibility when investigating the impact of cell disruption methods on protein release from BSY [118]. This is also observed in the current study for protein content, as shown in Figure 27, which suggests that this technology may be better suited for protein extraction rather than for retrieving intrinsic bioactivities. Ultrasound treatment also faces limitations in upscaling, as the penetration depth of the amplitude and overall energy input have been reported as challenges [66]. However, research groups such as BYSTRYAK ET AL. (2015) are working to address these limitations by developing scalable high-intensity ultrasound systems [114].

High-pressure homogenization (HPH), on the other hand, resulted in a lower normalized protease activity in the extracts compared to autolysis and ultrasound treatment, with a value of 2.55 ± 0.17. Nevertheless, this technology is the most widely used cell disruption method in industrial applications, indicating its potential for the rapid adoption of the proposed production of proteolytic extracts [104,114]. Since no clear trend was observed for protease activity with increasing pass numbers, this technology could potentially be run continuously with just one pass. Additionally, HPH may be relevant for extracting protein from BSY, as it yielded the highest overall protein content in the present study, with a 61.7% yield at 1100 bar after ten passes, as shown in Figure 27. However, the focus of this study was to maximize the extracted

protease activity in BSY extracts, with protein yield being secondary. For protein extraction from BSY, extensive studies already exist that demonstrate the potential of, for example, thermal yeast autolysis to achieve protein extraction yields close to 100% when run for ≥24 h [59,104]. Paragraph adapted from SCHOTTROFF ET AL. (2025) [57].

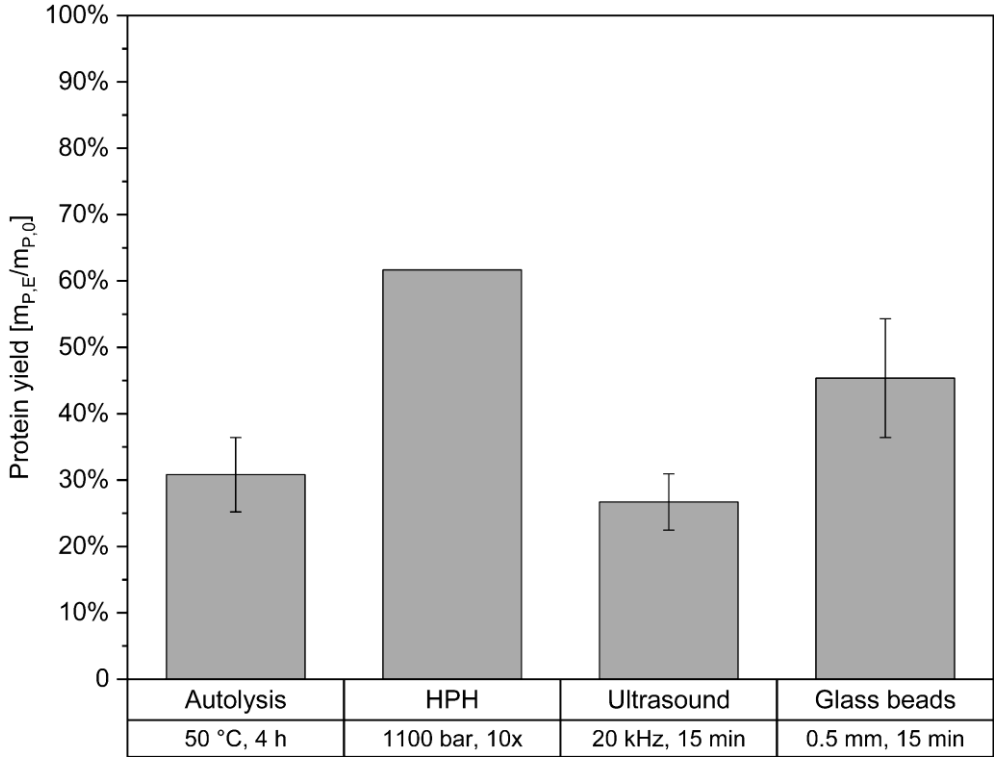

Figure 27: Comparison of highest determined protein yield per cell disruption method. Differences between the groups are significant at a p-value of 0.05 according to a one-way ANOVA.

Glass bead treatment resulted in the lowest relative protease activity with 2.07 ± 0.08. However, since cell mills have been used for decades in industrial applications to disrupt yeast cells and retrieve intracellular components, this method should be studied in more detail [66,125]. In the present study, a commercial cell mill was not available for testing, so a vortex mixer was used instead. The comparability of the obtained results with those from a commercial bead mill is unknown and should be tested experimentally to determine its potential for commercial use.

The overall comparison of qualitative protein size analysis revealed, that for all four investigated cell disruption methods a decrease in protein and peptide size can be observed with increasing cell disruption time in the case of thermal autolysis, glass bead and ultrasound treatment and pass number in the case of high-pressure homogenization. For the three mechanical cell disruption methods, this is hypothesized to be due to the undirected forces of cell disruption, which also act on already extracted proteins in the extracellular medium, thus reducing their size to form peptides over time or pass number, respectively. For thermal yeast autolysis, the increase in peptide and free amino acid content is hypothesized to result from the action of (exo-)peptidases. Previous paragraphs adapted from SCHOTTROFF ET AL. (2025) [57].

In conclusion, all four cell disruption methods investigated—thermal autolysis, ultrasonication, glass bead treatment, and high-pressure homogenization—produced proteolytically active BSY extracts. It was demonstrated that autolysis and ultrasound treatment lead to extracts with comparable levels of protease activity. However, due to challenges in process control, such as the lack of an inline protease activity assay for determining when to stop the thermal

yeast autolysis at the point of highest activity, this method is considered unsuitable for producing proteolytically active BSY extracts. Current technological advancements in ultrasound treatments are attempting to address known scalability issues with this technique [114]. Nevertheless, due to its scalability, widespread industrial application, and the demonstrated potential for continuous operation with just one pass at 1100 bar pressure through the homogenizer, high-pressure homogenization shows great promise for use in the production of BSY extracts.

The release of proteases during high-pressure homogenization, ultrasonication and bead milling is a result of physical disruption of the yeast cell wall. All three cell disruption methods are well established techniques for recovery of intracellular components from yeasts and are described extensively in literature [115,125–127]. However, as every cell disruption method has its drawbacks, new technologies are constantly evaluated for their suitability to release intracellular components [127]. One such new technology in the field of physical cell disruptions might be high-shear mixing (HSM). While to date high-shear mixers are mostly used for dispersion of e.g. immiscible liquids in the food industry, their basic principle of creating high shear forces through a rotor stator type agitator might be suitable for disrupting yeast cell walls [128,129]. To assess the feasibility of using high-shear mixers for this purpose, a 100 L test mixer as described in chapter 3.7.1 was used for disruption of a commercial bottom-fermenting Pilsner yeast strain. As no pilot-scale centrifuge for yeast washing and re-suspension in a buffer was available, the cell disruption was conducted directly in a yeast and beer slurry. A control to account for this deviation to the previous disruptions was run on lab-scale with glass bead treatment for 15 min in both beer and 0.1 M NaPC at pH 6 under the conditions stated in chapter 3.5.3. The resulting cell-free BSY extracts were produced with a lab-scale centrifuge after high-shear mixing as described in chapter 3.5.6. The protease activities in the BSY extracts are summarized in the following Figure 28.

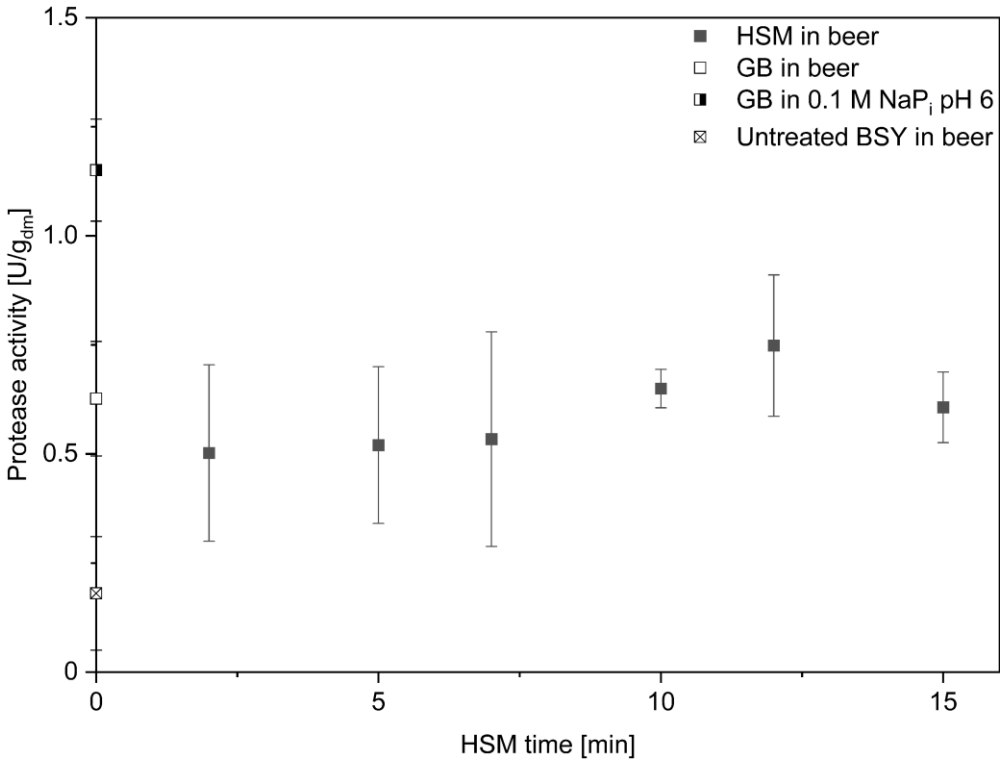

Figure 28: Protease activity in BSY extracts in beer after high-shear mixing (HSM) at 100% power input (7 kW, 2104 rpm) and glass bead (GB) treatment with 0.5 mm beads at 4 °C for 15 min.

As can be clearly seen, all HSM treated samples show a higher proteolytic activity than the untreated blank. However, during the first seven minutes, an increase in high-shear mixing

time did not result in a clear increase in protease activity. In view of the observed high standard deviations, no clear trend can be assumed. This might be attributed to an interfering compound in the beer slurry, that negatively affects reproducibility of the used protease assay or that might have inactivated released proteases prior to analysis. The absolute value of released protease activity is thus likely different from what has been assayed in beer. Further experiments in a controlled environment, e.g. in a 0.1 M NaPC buffer at pH 6, are thus required to assess the order of magnitude of released activity in more detail. What can however be seen is a slight increase in released protease activity after 10 min of HSM. Additionally, the order of magnitude of proteolytic activity is the same as for the glass bead (GB) treated samples in beer. The control run with glass bead treatment in 0.1 M NaPC at pH 6 on the other hand is more than twofold higher than the control in beer. It is thus assumed, that high-shear mixing of BSY in this buffer would also result in higher protease activities than those observed for the disruption in beer. In order to evaluate the efficiency of cell wall disruption over time and to draw conclusions about the observed trends in released protease activity, the resulting protein extraction yields in the cell-free BSY extracts were additionally determined. The corresponding results are summarized in the following Figure 29.

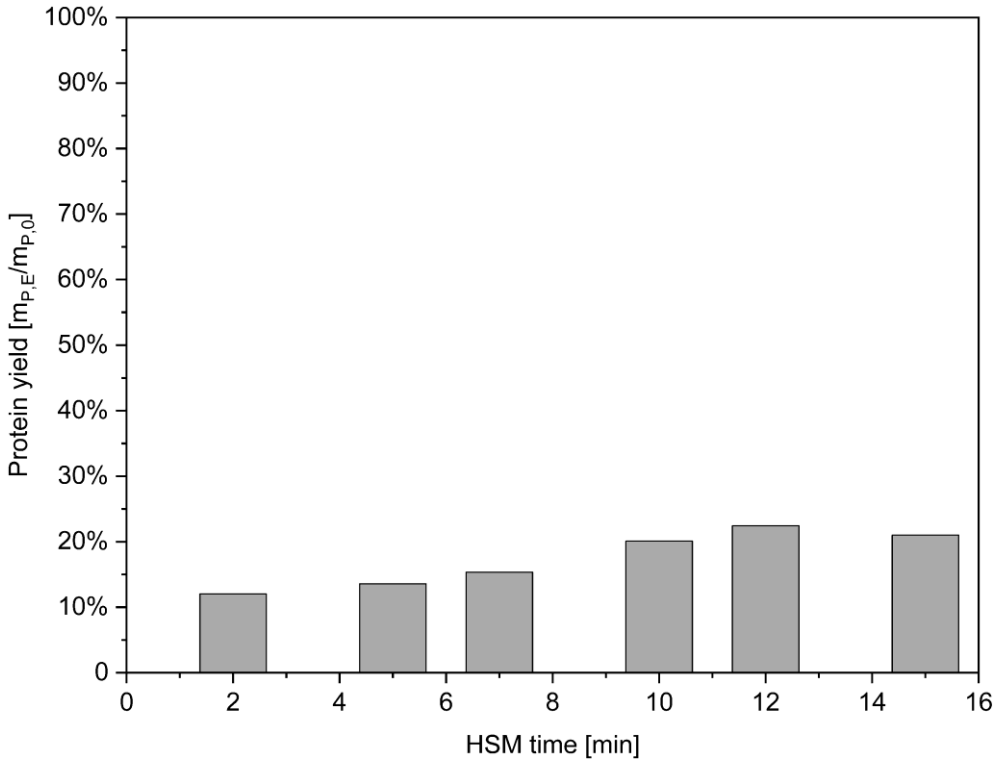

Figure 29: Protein yield in the yeast extract produced via high-shear mixing at 100% power input (7 kW, 2104 rpm) of BSY in beer. Single measurements only.

The protein content increases up until 12 min of high-shear mixing time and seems to reach a plateau thereafter. However, since only a single technical replicate was run, no means of statistical analysis is possible. It might also be, that the evaluated sample at 15 min HSM is an outlier and that in fact the protein content increased further. However, the overall trend of released protein is similar to that observed for the protease activity, where the maximum is observed at 12 min. In the case of proteases, a further increase in HSM time might therefore not be suitable in terms of energy input into the system. Since the protein content did not increase after this time, it is assumed that the limit of possible cell wall disruption with this technique has been reached. If it is assumed, that the protein content at 15 min HSM is an outlier, and that in fact an increase could have been assayed, the lack of an increase in protease activity beyond this HSM time might be similar to what has been described for HPH,

where the rate of released proteolytic activity is in the same order of magnitude than the disruption of already extracted proteases and thus a loss in activity.

What could also have played a role in the fact, that no further increase in activity was observed beyond 12 min, might be the lack of a temperature control during cell disruptions. Due to energy dissipation of the agitators into the suspension during high-shear mixing, the temperature of the slurry rose from 17.8 °C to 44.0 °C after 15 min of HSM. Although it is known, that some yeast proteases are thermally stable until 45 °C, under these conditions, thermal inactivation of some of the proteases cannot be excluded. Especially, considering that brewing yeast strains are optimized for growth in temperatures between 12-20 °C [5,55]. As also no pH control was in place during the experiments, it could also be assumed, that this process parameter was responsible for a loss in activity of the released proteases over time. However, as can be seen in Figure 30, the pH stayed mostly constant during the 15 min of high-shear mixing.

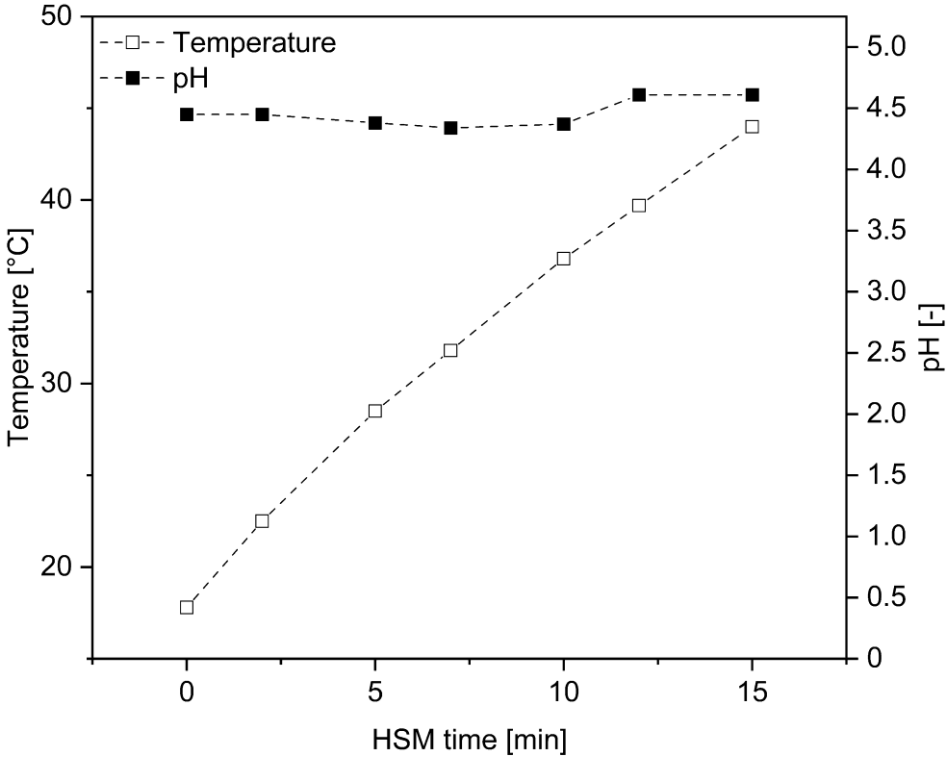

Figure 30: Temperature and pH during high-shear mixing of BSY in beer. Displayed lines serve solely as a visual aid.

In conclusion, high-shear mixing did produce proteolytically active BSY extracts in the same order of magnitude as glass bead treatment. However, due to the missing temperature and pH control as well as the disruptions taking place in beer rather than in a defined buffer medium, further investigations are required to assess and identify optimal disruption conditions.

4.2.2 Characterization of Proteolytic Brewer's Spent Yeast Extracts

During the cell disruption screening described in chapter 4.2.1, the glass bead treatment showed the highest reproducibility, while also releasing protease activity into the produced BSY extracts. 15 min of cell disruption with 0.5 mm beads at 4 °C on a vortex mixer at 100% power input was therefore selected as the standard cell disruption method for further investigations. These investigations focused on the identification of suitable process conditions for the application of the produced BSY extracts, including a pH and temperature screening. The aim was to identify the maximum protease activity at each condition for subsequent selection of process conditions depending on the application. In addition, an identification of

the protease classes present was sought through the application of class specific inhibitors and their effect on the resulting protease activity in the extracts. Among others, the presence of metalloproteases was confirmed, which led to the addition of different inorganic salts to investigate a possible positive effect on the protease activity. The results of these experiments are summarized in the following chapters.

Influence of pH on Proteolytic Activity

The effect of pH on enzymatic activity is well-know, since activity is strongly dependent on the three-dimensional conformational structure of an enzyme. This conformation is a result of the amino acid sequence, posttranslational modifications and the interactions of the enzyme with its surrounding medium as well as substrates and co-factors [98]. The ionization of amino acids due to changes in pH can therefore directly affect enzyme activity. An identification of the pH range of maximum activity was thus conducted. The following Figure 31 summarizes the proteolytic activities determined after standardized glass bead cell disruption. Paragraph and data adapted from SCHOTTROFF ET AL. (2025) [57].

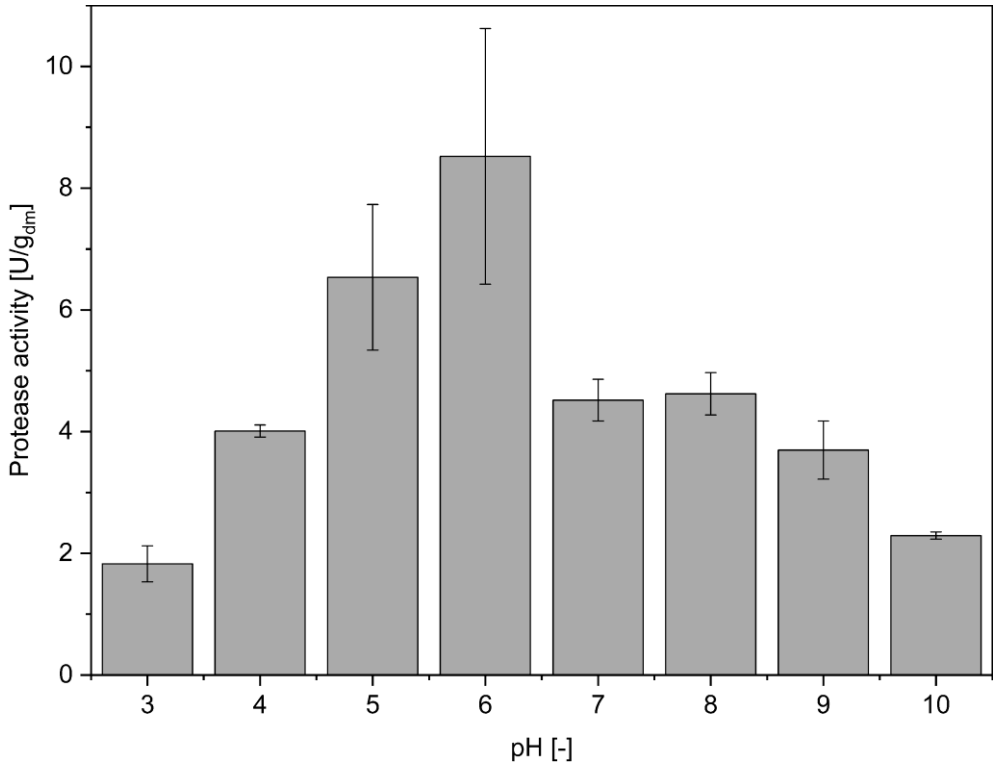

Figure 31: Protease activity in BSY extracts at different pH. All buffers used at 0.1 M concentration. pH 3–7 with NaPC buffer, pH 8–9 with Tris-HCl buffer and pH 10 with sodium carbonate-bicarbonate buffer.

All investigated scenarios resulted in proteolytic activity in the cell-free supernatant. The highest overall activities were found at pH 5 and 6 in 0.1 M NaPC buffer. These pH values correspond to the commonly reported intracellular pH in *S. cerevisiae* as well as in the vacuole compartment itself [130,131]. Therefore, most of the seven known vacuolar proteases are expected to be in their active conformation at these pH values [58]. This assumption is further supported by the found activity at acidic conditions at pH 3–4, which may be linked to protease A, an important exoprotease for the activation of other vacuolar proteases showing high activity at these pH values [55,58,132]. Next to the maximum activity found at pH 6, MADDOX ET AL. (1970) could demonstrate maximum stability of different vacuolar proteases extracted from *S. carlsbergensis*, a common beer yeast strain, at pH values of 6–6.5 [55]. In accordance with these findings and the presented data, pH 6 was chosen as a suitable pH for further studies. Paragraph adapted from SCHOTTROFF ET AL. (2025) [57].

Influence of Temperature on Proteolytic Activity

The effect of temperature on enzyme activity is well known [98]. Activity can be increased with increasing temperature due to faster reaction rates or decreased due to thermal inactivation of the enzyme. The identification of suitable operating conditions for enzymatic processes requires a balance between fast reaction rates and thermal stability of enzymes at elevated temperatures and over time [133]. For the present proteolytic BSY extracts, a study of substrate hydrolysis rates was analyzed photometrically for temperatures between 20-60 °C at pH 6 for up to 4 h. A 1% (w/w) azocasein solution was used as a substrate. The release of azo-groups by proteolytic hydrolysis causes an increase in absorbance at 440 nm. The following Figure 32 summarizes the results obtained relative to a substrate blank.

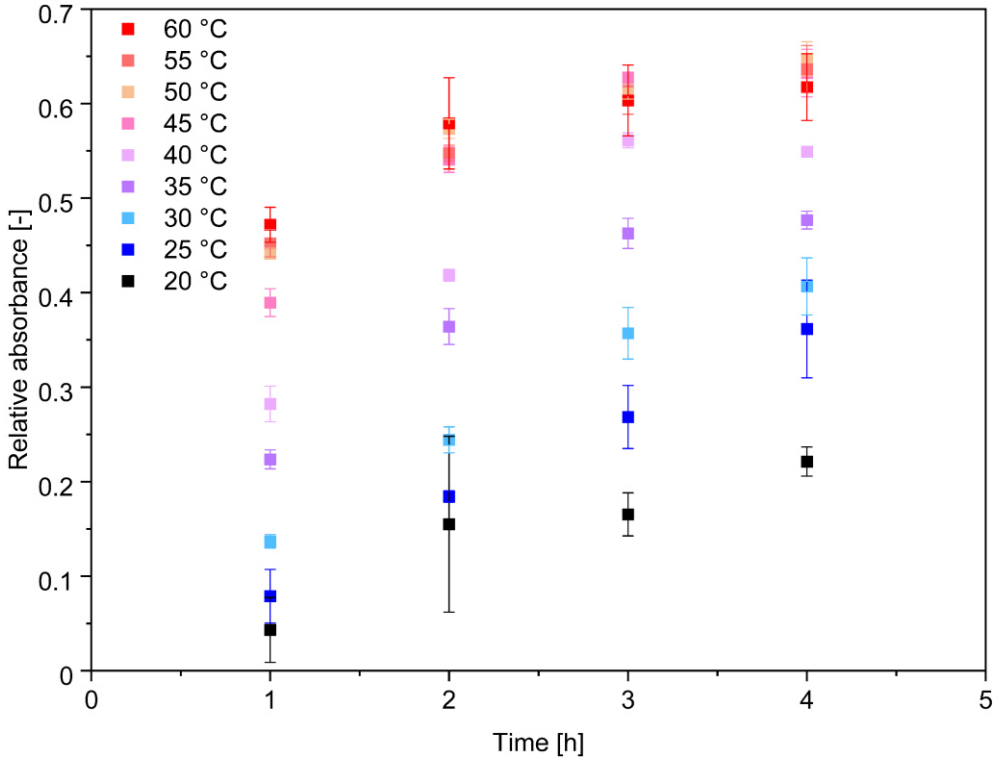

Figure 32: Change in relative absorbance over time for temperatures 20-60 °C in 5 °C steps. All values relative to substrate blank at 0 h. Color change at 440 nm through azo-group release by BSY proteases at pH 6 and 500 rpm on a 2 mL scale.

As can be clearly seen, there is an increase in the release of azo-groups with increasing temperature. This behavior correlates to the quantitative dependance of the reaction rate constant from the temperature via the Arrhenius equation given in equation (28) [134].

$$k = A_R \cdot e^{-\frac{E_A}{RT}} \tag{28}$$

With k representing the reaction rate constant [1/s], A_R the pre-exponential factor [1/s], E_A the activation energy [J/mol], R the universal gas constant [J/mol K] and T the temperature [K].

This equation is applicable for monomolecular reaction kinetics of first order, which can be used to describe the proteolytic degradation of azocasein according to CHARNEY AND TOMARELLI (1947) [92]. Above 45 °C, no further increase in the azocasein release is observed. After 2-3 h at these temperatures, a decrease in the rate of azo group release can be observed. This is assumed to be the point at which thermal enzyme inactivation begins. For temperatures between 35-45 °C, this behavior can be observed at a later time interval of 3-4 h. For temperatures between 20-30 °C, no such inactivation seems to be present. In order to investigate whether thermal inactivation can be observed at these temperatures, a second set

of experiments was carried out for a total of 6 h. The results are summarized in the following Figure 33. For incubation at 55 °C, a thermal inactivation can be observed in between 3-4 h, whereas for incubation at 30 °C this inactivation occurs at a later stage, up to 6 h. At 20 °C, however, no thermal inactivation can be deduced from the recorded data. On the contrary, an increase in azo-group release is observed up to 3 h of incubation, before a linear increase in azo group release follows. This behavior is thought to be related to the natural growth optima of the yeast strains, which are typically in the range of 12-20 °C for brewing yeast strains [5]. The increase in the rate of azo-group release during the first 3 h of incubation may be related to a slow conversion of proteases into their proteolytically active conformations by the action of protease A [58].

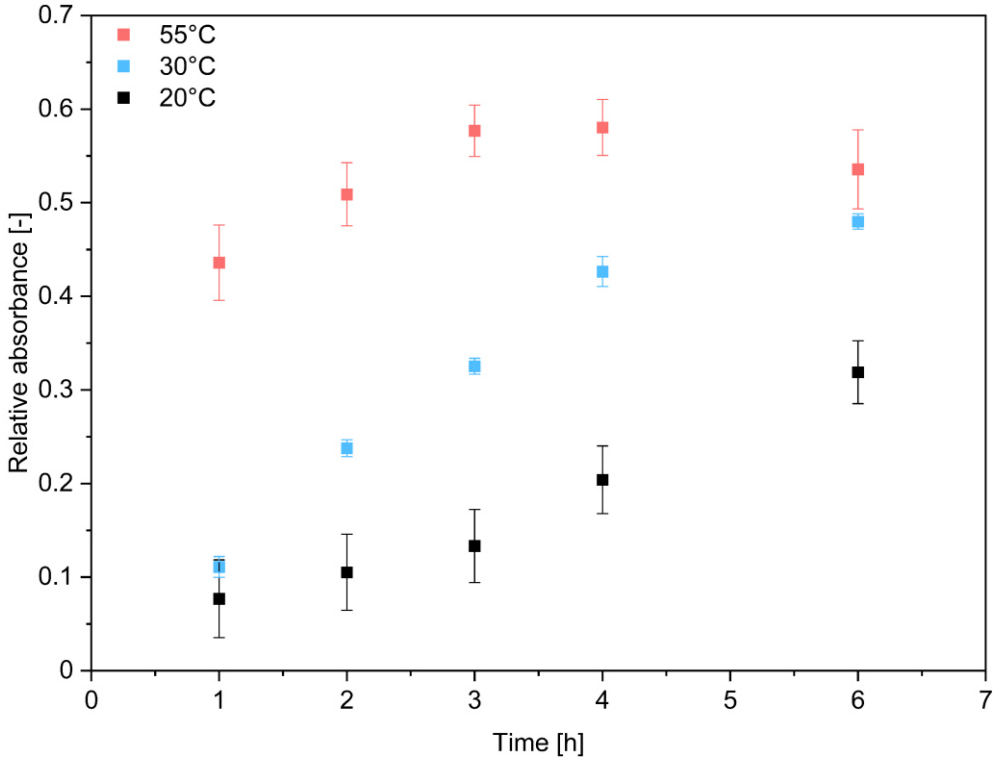

Figure 33: Change in relative absorbance over time for temperatures 20, 30 and 55 °C. All values relative to substrate blank at 0 h. Color change at 440 nm through azo-group release by BSY proteases at pH 6 and 500 rpm on a 2 mL scale.

In a subsequent study, thermal inactivation was found to be present when incubated at 20 °C for 24 h. The results are summarized in Figure 34.

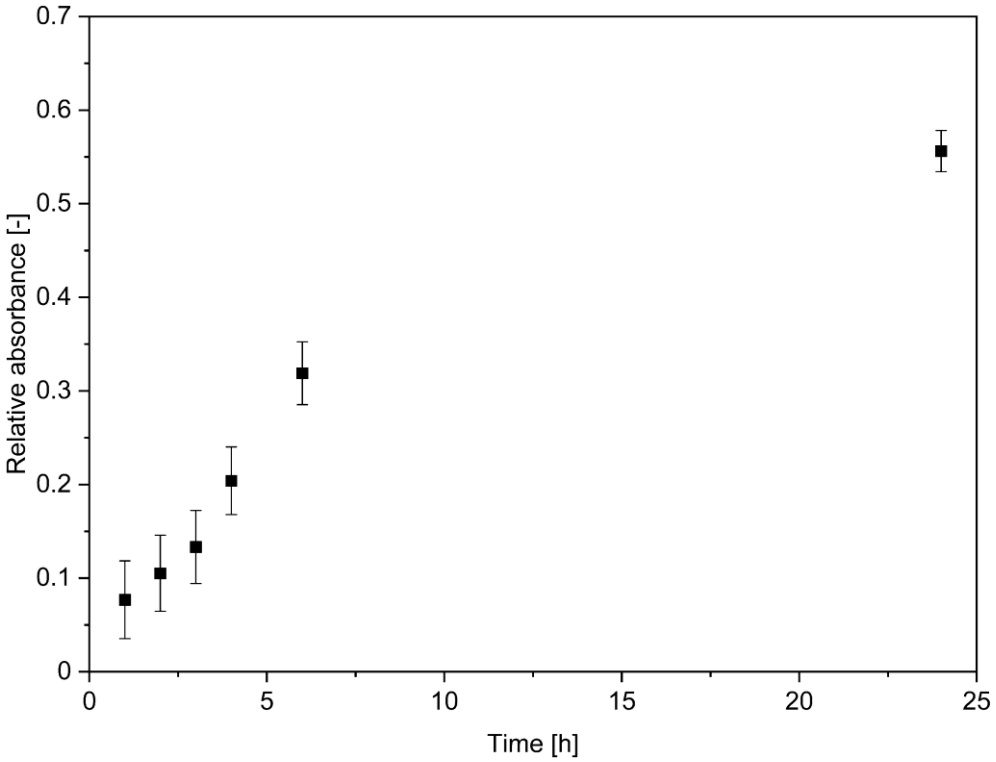

Figure 34: Change in relative absorbance over time for incubation at 20 °C for 24 h. All values relative to substrate blank at 0 h. Color change at 440 nm through azo-group release by BSY proteases at pH 6 and 500 rpm on a 2 mL scale.

In general, the results show a positive influence of temperatures up to 50 °C on the overall hydrolysis rate. No thermal inactivation was observed during the first 2 h of incubation at any of the temperatures studied. It is therefore proposed to use proteolytic BSY extracts for applications where a sufficient degree of hydrolysis can be achieved within this time frame. Alternatively, further dosing of BSY at least every two hours should be considered during process design. As the exact starting point of thermal inactivation will also depend on the yeast strain used, the metabolic state of the cells, the brewing conditions applied and the cell disruption process used, a dosage of BSY extract below this two-hour mark may be beneficial.

Influence of Storage Period and Medium Type

During the present studies, a maximum of around 5 L of BSY slurry could be harvested after each beer fermentation. This slurry was washed and disrupted according to the standardized glass bead treatment described in chapter 3.5.3. To minimize observed effects during the pH and temperature screenings due to the use of different BSY batches, the produced BSY extracts were aliquoted into 15 mL Falcon tubes and frozen at -20 °C until use. To observe, whether freezing and subsequent thawing have an effect on the residual protease activity, produced BSY extracts in four different media were frozen for 24 h at -20 °C and residual protease activity was determined before and after the freezing. Results are summarized in Table 39.

Table 39: Loss of protease activity after freezing for 24 h at -20 °C.

Buffer	Activity loss after freezing
0.2 M KPC pH 7	26.5 ± 3.8%
Tap water pH 7.8	9.6 ± 5.1%
0.1 M NaPC pH 5	6.5 ± 5.3%
Ultrapure water pH 5.9	20.7 ± 6.3%

A maximum activity loss of 26.5 ± 3.8% after freezing was observed for 0.2 M potassium phosphate citrate buffer (KPC) at pH 7. This drastic loss in activity lead to a subsequent

storage stability investigation over the course of six months. BSY extract in 0.1 M NaPC at pH 6 were used. Results are summarized in the following Figure 35. During the first two weeks, an initial loss of activity of approximately 10% was observed, which is thought to be due to the formation of ice crystals and consequent freeze denaturation of the proteases contained [135]. The activity then decreased by a further 5% over the following 1.5 months. Considering the standard deviation, the activity remained more or less constant for the remaining 4 months. This suggests that most of the loss of activity was due to ice crystal formation during the initial freezing, and to a lesser extent to subsequent loss over time. Effects of partial protein unfolding during freezing are associated with the formation of ice crystals during freezing and with localized high solute concentrations due to water crystallization [135]. It is discussed that these effects can be minimized by applying rapid freezing rates, e.g. by freezing in liquid nitrogen [136]. On an industrial level, freezing of the BSY extract is not considered to be an economically feasible route due to the high energy consumption associated with this unit operation. As this process step is therefore not required, it was not investigated further.

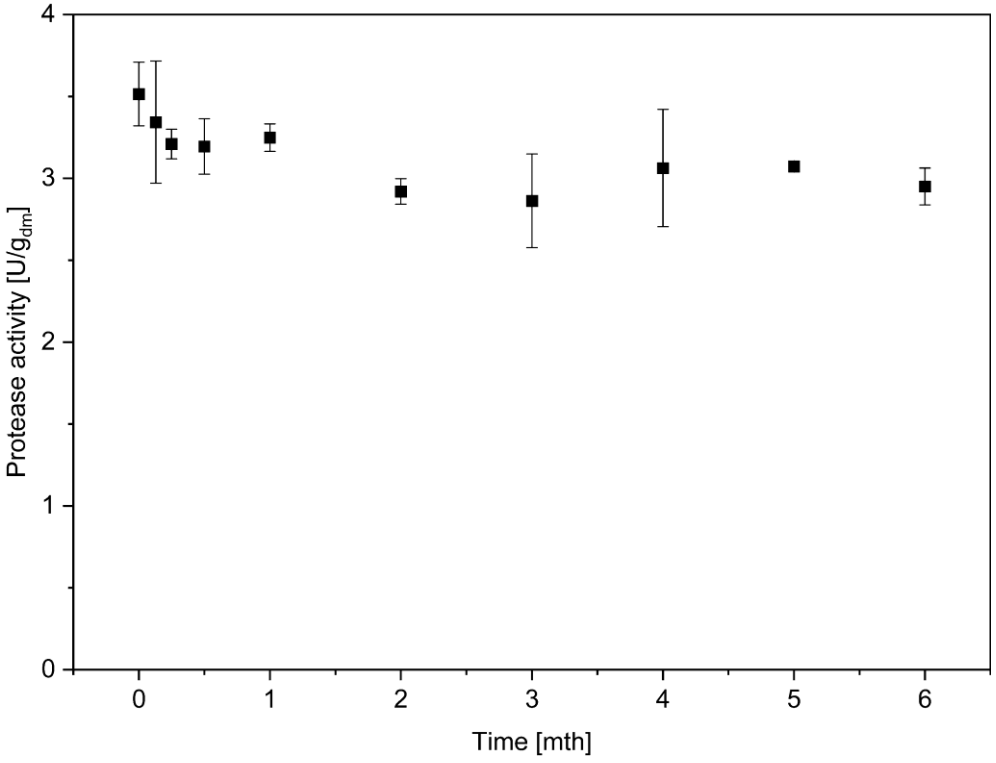

Figure 35: Protease activity over storage time at -20 °C. Cell disruption using 0.5 mm glass beads for 15 min at 4 °C at 100% power input on a vortex mixer.

Instead, it was investigated, if the used 0.1 M NaPC buffer could potentially be replaced with using water, making the process attractive for use in the food industry, where high levels of sodium ions are linked with adverse effects on human health [137]. Two pH levels were chosen for investigation. Results are summarized in Figure 36.

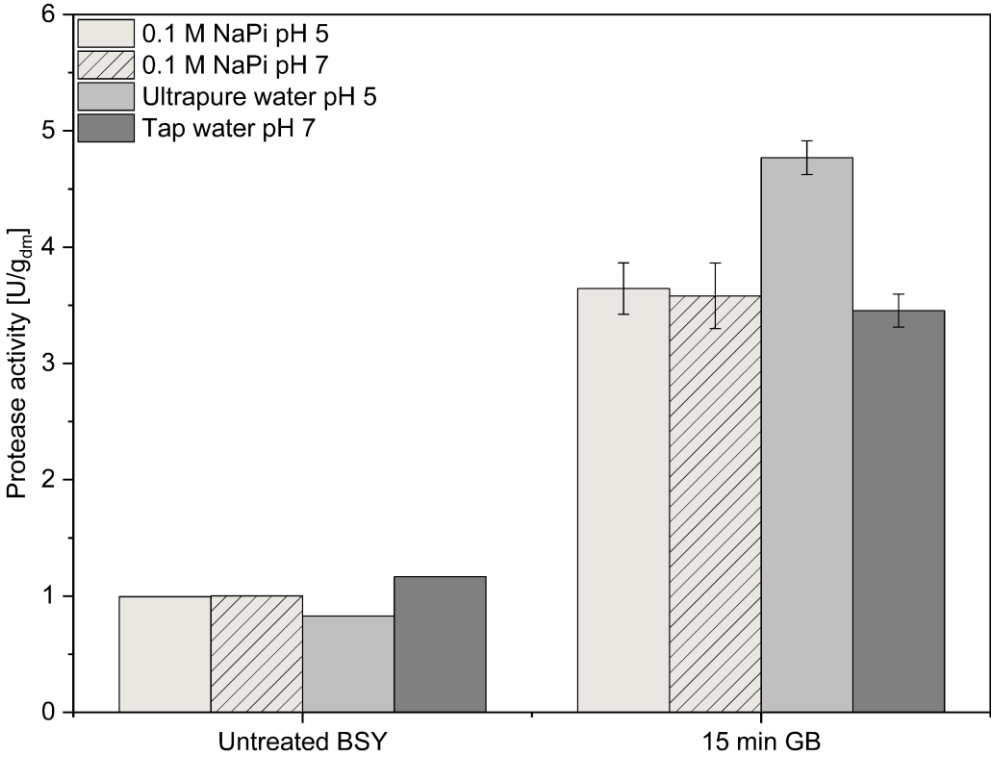

Figure 36: Influence of buffer type on BSY extract activity. Cell disruptions using 0.5 mm glass beads for 15 min at 4 °C at 100% power input on a vortex mixer. The negative control was an untreated BSY supernatant. Activity of the negative control was determined for a single technical replicate only.

Proteolytic activity in all produced BSY extracts is higher than that of the negative control of untreated BSY supernatant. The chosen pH levels of pH 5 and pH 7 did not result in different proteolytic activities for the 0.1 M NaPC buffer. Both tap water and 0.1 M NaPC buffer showed the same order of proteolytic activity in the extracts. However, when ultrapure water was used, the activity increased about 30% compared to the NaPC buffer used. It is thus assumed, that salt concentration and osmotic pressure might be relevant factors influencing protease activities in the BSY extracts. If for example metalloproteases are present, their activity could be increased by the presence of divalent metal ions. Similarly, present mono- and divalent metal ions could lead to inactivation of the same proteases, depending on which ions are relevant for the catalytic mechanism and in which concentrations they are present. The knowledge of contained protease classes and types could thus lead to relevant insights for application of the produced BSY extracts.

Investigation of Protease Classes in BSY Extracts

In order to gain insight into the potential protease classes present in the BSY extracts, an inhibition study was designed. Commercially available protease class specific inhibitors were selected and applied in a standardized assay using 1% (w/w) azocasein as substrate. The hydrolysis of azocasein was monitored photometrically at 440 nm. The exact experimental procedure is described in detail in chapter 3.6.3. The following Figure 37 summarizes the results obtained for an application of the seven inhibitors used. Relative activity describes the ratio of activity of the sample incubated with inhibitor to the activity without inhibitor addition.

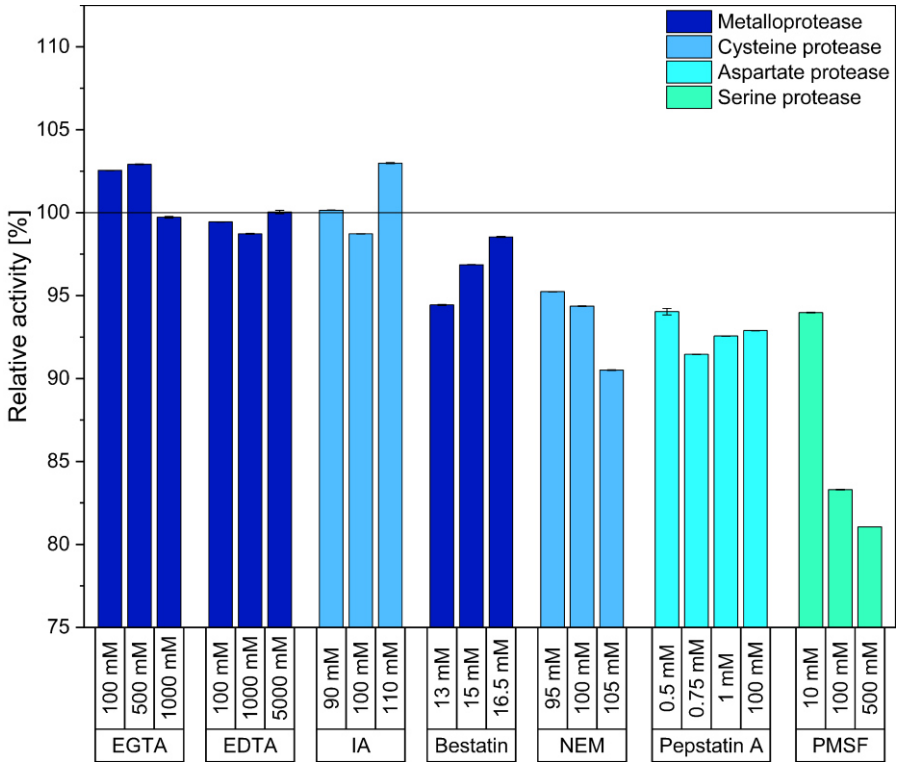

Figure 37: Relative activity of BSY extract per inhibitor used on 1% (w/w) azocasein as a substrate at 37 °C and pH 6 for 60 min with 500 rpm shaking. EGTA = ethylene glycol-bis(β-aminoethyl ether)-*N,N,N',N'*-tetraacetic acid, EDTA = ethylenediaminetetraacetic acid, IA = iodoacetamide, NEM = *n*-ethyl-maleimide, PMSF = phenylmethylsulfonyl fluoride.

The highest overall inhibition was observed for 500 mM PMSF with a value of 81.06 ± 0.01% relative activity and thus an inhibitory effect of almost 20% compared to the hydrolysis of azocasein without the addition of inhibitor. PMSF reacts irreversibly with serine proteases through sulfonation in the catalytic site [54]. Of the seven known vacuolar proteases found in *S. cerevisiae*, three belong to the serine protease class: Proteinase B, Dipeptidylaminopeptidase B and Carboxypeptidase Y [58]. All these proteases are known to present high activity in pH environments around neutrality and slight acidity, which are present in the applied assay. The finding, that serine proteases are a major contributor to BSY extracted proteolytic activity is supported by the findings of VIEIRA ET AL., who found serine and metalloproteases to be the major protease classes responsible for proteolytic activity in BSY extracts [51]. In the present study, the aminopeptidase specific metalloprotease inhibitor Bestatin resulted in a residual activity of 94.44 ± 0.03 mM at 13 mM concentration. This would lead to the assumption, that in fact, metalloproteases of the aminopeptidase type are present in the crude BSY extract. This could be attributed to an inhibition of the aminopeptidase Y and the aminopeptidase I, both belonging to this group of proteases [58]. The decreasing inhibitory effect with increasing Bestatin concentration seems counterintuitive, but may be related to the solvent used, methanol. Bestatin has a maximum solubility in methanol up to 15 mM and only a low solubility in aqueous solutions according to manufacturer data. It might be, that Bestatin precipitated out of the solution and thus an apparent decrease in inhibitory effect is observed at higher concentrations. The effect of methanol itself on BSY extract proteases is not clear. However, brewing yeast strains are optimized for growth in low-molecular-weight alcohol solutions such as beer, which should thus not negatively affect BSY proteases. Additionally, AHMED ET AL. (2024) could prove an activity increase of up to 60% for a fungi-derived metalloendopeptidase when adding methanol at 20% (v/v) at different concentrations to an azocasein activity assay [138]. Another working group around ALIAS ET AL. (2014) found maximum protease activity of a serine protease from an Antarctic yeast *G. antarctica* when expressed at methanol concentrations in the medium of 0.5% (v/v) [139].

The unspecific metalloprotease inhibitors EDTA and EGTA, both inhibiting divalent cation dependent metalloproteases through chelation, did not lead to clear reductions of the assayed residual activity. However, this may not be indicative of the absence of metalloproteases, but may be due to the preparation of the BSY extracts themselves. Before cell wall disruption, the yeast suspension is washed twice with ultrapure water, thus potentially washing out any divalent cations, including calcium, magnesium and zinc, which *S. cerevisiae* derived metalloproteases are known to depend on as co-factors. Thus, it is theorized, that no inhibition through these inhibitors can be observed, as long as these ions are not fed into the extract upfront. This assumption is supported by the results from the addition of inorganic salts given in Figure 38, positively influencing the relative activity.

The cysteine protease specific inhibitor IA also did not result in a relevant reduction of residual activity in the crude extract. This may be due to the fact that no known vacuolar proteases belong to the cysteine protease class. In contrast, the cysteine protease class inhibitor NEM resulted in the third highest overall inhibition with 91.00 ± 0.02% residual activity at 105 mM concentration. The inhibition mechanism of NEM is based on the irreversible reaction with thiol groups in the catalytic site. Thiol groups are found in the active site of cysteine proteases, but are not solely found in this class of proteases. WOODS AND KINSELLA (1980) also found a relevant inhibition through NEM when applied on *S. carlsbergensis* extracted protease fractions [54]. This might be explained either by assuming, that there are yet unknown cysteine proteases present in the BSY extract, potentially not originating from the vacuolar compartment, or that free sulfhydryl groups are relevant for the full proteolytic activity.

Lastly, the proteinase A specific inhibitor Pepstatin A resulted in a residual activity of 91.00 ± 0.01% at 0.75 mM, thus showing the second highest overall observed inhibition. Proteinase A is an important enzyme in yeast metabolism as it catalyzes and activates the first steps of the vacuolar protease activation cascade. A high level of proteinase A may indicate that a high proportion of inactive zymogens in the vacuole are already present in their proteolytically active form, as proteinase A has already cleaved the inhibitory propeptide. [58]

Generally, no individual inhibitor produced observable reductions in the residual activity above 20%. This is mainly attributed to the fact, that a crude enzyme extract has been used for the inhibition studies. Multiple complex substances might interfere with the enzyme's active sites as well as with the inhibitor molecules themselves. Additionally, the individual protease inhibition through specific inhibitors contributes only partially to the overall detected proteolytic activity. As it is theorized, that potentially seven known vacuolar proteases contribute to the overall activity, the (partial) inactivation of one or two of these enzymes will not result in a complete inactivation of the overall proteolytic activity. For more in depth studies of the present proteases, a purification via e.g. a hydroxyapatite chromatography is proposed [54]. Since the results regarding metalloproteases were not clear, but there are three known vacuolar metalloproteases in *S. cerevisiae* strains, a second set of experiments was conducted. Seven different inorganic salts containing mono- and divalent cations and anions were used to test, whether the activity of contained BSY proteases could be enhanced. Results are summarized in the following Figure 38.

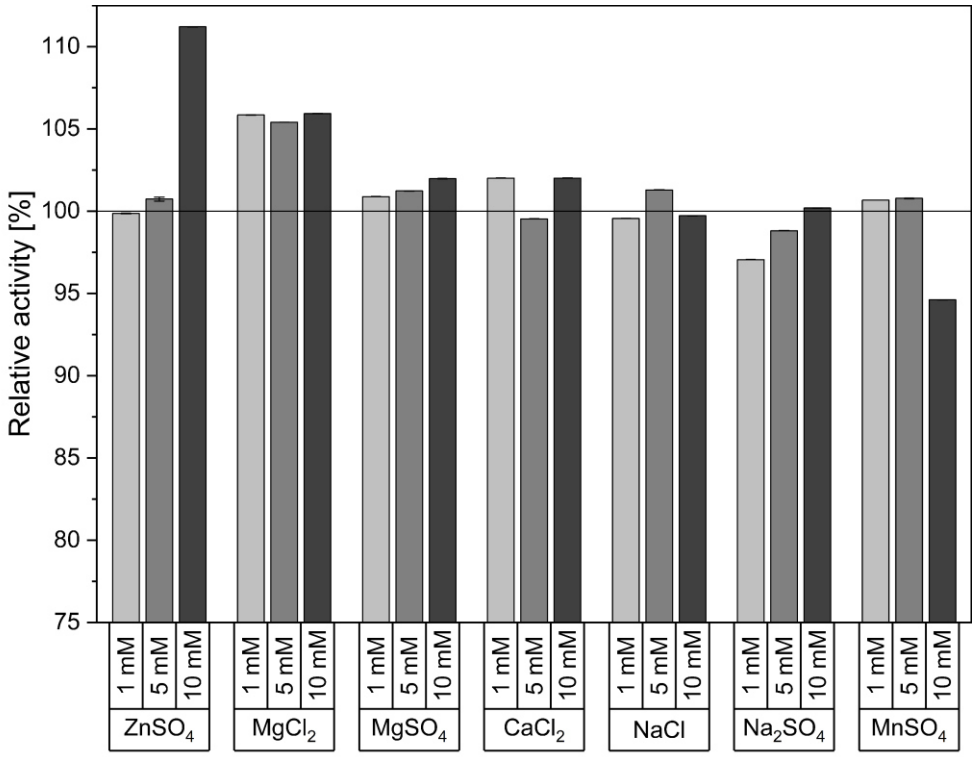

Figure 38: Relative activity of BSY extract per inorganic salt used on 1% (w/w) azocasein as a substrate at 37 °C and pH 6 for 60 min with 500 rpm shaking.

The highest overall determined increase of proteolytic activity resulted from the addition of zinc sulfate with 111.20 ± 0.01% of activity at 10 mM concentration. In the yeast vacuolar compartment, two zinc dependent metalloproteases are known: Carboxypeptidase S and Aminopeptidase I. The activity of these proteases is dependent on divalent zinc ions, which might explain the 11% increase in activity through the addition of these. Both $MgCl_2$ and $MgSO_4$ resulted in an increase in the observable activity of 6% and 2% respectively. This might indicate the presence of magnesium dependent metalloproteases. It can also be an indicator for a higher inhibitory effect of sulfate ions in contrast to the monovalent chloride ions. The divalent sulfate might shield the positive charge in the active site of the metalloprotease required for the nucleophilic attack of the peptide bond for hydrolysis. This theory is supported by the difference in observed proteolytic activity comparing 1 mM NaCl resulting in 101.29 ± 0.01% and 1 mM Na_2SO_4 resulting in 98.81 ± 0.02% residual activity. While NaCl slightly increased the residual activity, Na_2SO_4 acted as a weak inhibitor. Generally, the addition of sodium ions did not enhance or decrease the residual activity of the BSY extract in a relevant order of magnitude. This is in line with findings from other research groups. WOODS AND KINSELLA (1980) detected a decrease in residual activity and thus an inhibitory effect of 2.25 M NaCl of 50% on a neutral *S. carlsbergensis* extract, that had prior been purified via hydroxyapatite chromatography [54]. They theorized this inhibitory effect to be due to a disruption in the electrostatic interactions in the enzyme-inhibitor binding. FELIX AND BROUILLET (1966) observed the opposite behavior for two extracted proteases from BSY after cell disruption via autolysis and subsequent protein purification using chromatography [140]. According to their findings, these two proteases belonged to the group of metalloproteases. Their activity could be maximized at NaCl additions of 0.5 mM. This activation might be explained via the osmotic pressure generated via the NaCl addition, which is in a similar order of magnitude as in the natural vacuolar compartment of BSY. The addition of $MnSO_4$ resulted in an inhibition of 6% of the relative activity. This might be attributed to the high charge density of manganese ions, which shield the catalytic residues required for hydrolyzing peptide bonds in metalloproteases.

Qualtitative Protein Size Analysis

Next to these inhibition and activation studies, a protein size analysis via an SDS-Page has been conducted. The aim was to screen for protein bands in the size region of the seven known vacuolar proteases and to potentially result in an indication of their presence, if clear bands are visible in these regions. The resulting stained SDS-gel is given in the following Figure 39. For an identification of potentially contained proteases, the molecular sizes of the seven known vacuolar yeast proteases are given in Table 36.

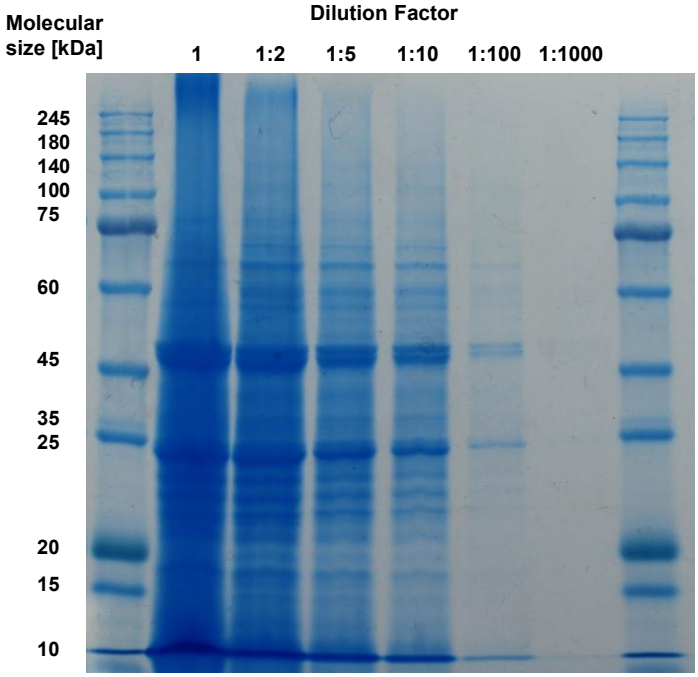

Figure 39: SDS-PAGE of BSY extract for qualitative protein size analysis. Yeast cells disrupted in 0.1 M NaPC at pH 6, 4 °C and 100% power input on a vortex mixer for 15 min using 0.5 mm glass beads.

There are two prominent bands in the region of 25-35 kDa and 45-50 kDa. These two bands match the expected protein size of proteinase B with 31-37 kDa and proteinase A with 42-45 kDa. Proteinase B is a serine dependent protease, which was the protease class with the overall highest inhibition in the inhibition studies. The presence of proteinase A was confirmed through an observed inhibition via the protease specific inhibitor Pepstatin A. It is therefore assumed that these bands are most likely attributed to these two enzymes. Two lighter bands can be identified in the region of 50-60 kDa, which is the expected protease size of both aminopeptidase I and carboxypeptidase Y. Two similarly light bands are found in the region 60-75 kDa, which might be indicative of the proteases aminopeptidase Y and carboxypeptidase S. No clear band is found in the region above 100 kDa, where the dipeptidylaminopeptidase B would be expected. The general trend, that smaller protein and peptide sizes are detected compared to larger ones above 50 kDa might be attributed to the cell wall disruption process during the production of the proteolytic BSY extract. The 0.5 mm glass beads might also disrupt larger proteins and thus lead to non- or only partially functional protein fragments. As no bands above 100 kDa can be clearly identified, it can be assumed, that either the cell wall bound mannoproteins with typical sizes of 100-200 kDa have been successfully separated off from the BSY extract, or have been fragmented to smaller peptides during the cell wall disruption process [141]. In general, it is not possible to distinguish between proteases and non-catalytically active proteins by SDS-PAGE and subsequent staining. It is possible that the observed protein bands associated with known vacuolar protease sizes are only non-catalytically active proteins of the same size as the expected proteases. For further in-depth analysis, protein purification followed by gel chromatography or a western blot is required to obtain results with a higher degree of certainty.

Intermediate Summary

The aim of chapter 4.2 was to investigate the potential of producing proteolytically active yeast extracts from BSY for the application in the food sector. The key take-aways from the production and characterization of these extracts are summarized below.

- Thermal yeast autolysis is not a suitable method to reproducibly produce proteolytically active yeast extracts from BSY due to a missing trend of released protease activity with time and temperature
- All tested mechanical cell disruption methods including ultrasound and glass bead treatment as well as high-pressure homogenization resulted in reproducible proteolytic activities in the produced BSY extracts
- Ultrasound treatment at 20 kHz at 4 °C for up to 30 min followed a first order kinetic for the release of proteolytic activity
- The trend of protease activity release with glass bead treatment using 0.5 mm beads at 100% power input on a vortex mixer at 4 °C for up to 30 min did not reach a clear plateau of maximum activity. Further investigations of this technique on a commercial bead mill are required
- Released protease activity through high-pressure homogenization did not clearly increase with an increasing number of passes through the homogenization chamber and holds the potential to be run continuously with just one pass
- During a pH screening, the highest protease activity after 15 min glass bead treatment with 0.5 mm beads at 4 °C and 100% power input on a vortex mixer was found at pH 6 in 0.1 M sodium phosphate citrate buffer
- Proteolytic activity increased with increasing temperatures from 20-45 °C
- Thermal inactivation was found after 2-4 h incubation with 1% by mass azo-casein as a substrate at temperatures 30-60 °C
- The presence of cysteine, aspartate, serine and metalloproteases could be demonstrated through addition of protease class specific inhibitors
- The addition of zinc, calcium and magnesium containing inorganic salts was able to increase protease activity in the BSY extracts by a maximum of 11%

4.3 Brewer's Spent Grain: Valorization Through Fractionation

Various valorization approaches for BSG have been extensively studied at the laboratory scale. A recent review categorized the focus into four main groups: Biorefinery approaches, material applications, as an energy source and for nutritional use [8]. All efforts are focusing on meeting the UN sustainable development goals (SDG) and making use of a low-cost, widely available substrate [12]. However, despite the widespread knowledge of valorization strategies for BSG, few industrial-scale BSG processing plants have been realized. NAIBAHO ET AL. (2024) concluded in a recent publication, that this might be due to a lack of knowledge on commercialization approaches, consumer acceptance and technological readiness levels [6]. The following chapters thus aim to introduce scalable solutions for the extraction of valuable fractions from BSG, while also focusing on biorefinery approaches for making use of as many BSG constituents as possible.

4.3.1 Protein Extraction from BSG

The extraction of proteins from BSG is well studied on lab-scale [20]. The highest yields are often achieved by an initial particle size reduction of dried BSG, followed by a chemical or enzymatic hydrolysis step for protein extraction, and finally drying of the resulting hydrolysate. For an increased protein extraction yield, further pre-treatment steps are commonly proposed to open up the lignocellulosic structure of BSG including acid pretreatment, steam explosion and solid state fermentations [7,8,20,142]. This basic principle will be followed in the subsequent chapters, however focusing on the needs of large-scale processing plants such as process intensification, wet-processing to avoid energy intensive drying steps, application of the least possible number of additives and enzymes to minimize OPEX and reduce downstream processing efforts, focusing on microbial integrity and using unit operations suitable for scale-up.

High-shear Mixing of BSG

The first step of a protein extraction line from biomass usually consists of pretreatment steps to open up the complex lignocellulosic matrix surrounding the protein. In the course of this study, high-shear mixing was chosen as a pretreatment step to simultaneously reduce BSG particle size, increase available surface area, and potentially open the lignocellulosic matrix through the high shear forces applied. The effect of different high-shear mixing times in the 100 L HSM batch reactor on resulting BSG particle sizes are given in Table 40.

Table 40: Particle size distribution of untreated BSG and after 5 and 10 min of high-shear mixing.

Sample	$d_{x,10}$ [µm]	$d_{x,50}$ [µm]	$d_{x,90}$ [µm]
0 min HSM	1876	3085	4631
5 min HSM	629	1631	3837
10 min HSM	450	1266	3082

Basis for the determined particle size distributions was the diameter of an equivalent circle using the volume density distributions determined via particle image analysis. The diameter of the 50th percentile was reduced by a factor of 2.4. Additionally, the effect of HSM resulted in a relatively even distribution of particle sizes per size class, as can be seen in the volume density distributions given in Figure 40.

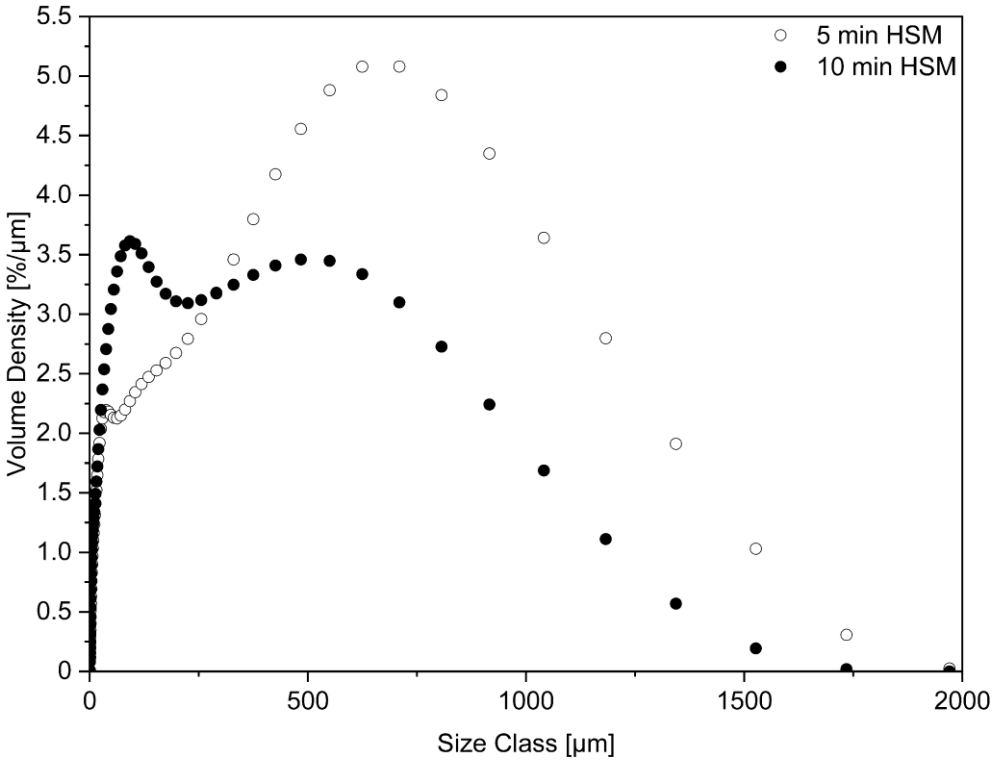

Figure 40: Effect of high-shear mixing time on volume density distribution of BSG particles.

The volume density distribution shows the percentage of total volume occupied per size class. The total sum of the density distributions yields 100%. As can be clearly seen, after 10 min HSM, an even volume density per size class is present for particles below 700 µm. For 5 min HSM, the particles generally present higher volumetric percentages at size classes above 500 µm. The influence of this reduction in average particle size with prolonged HSM times will thus give an indication on the importance of available surface area on protein extraction efficiency.

As a relevant percentage of BSG particles are reduced below 500 µm in diameter, it was investigated whether HSM could be a suitable approach for producing protein-enriched, fine BSG fractions and protein-depleted, coarse BSG particles high in fiber. The theory behind this approach is, that BSG protein mostly originates from the endosperm and aleurone residues of the grain, which are reportedly found in BSG particles below 200 µm in size [143]. The coarser particles are mostly consisting of cellulose, hemicellulose and lignin. To evaluate the potential of high-shear mixing in the 100 L HSM batch reactor for producing protein-enriched BSG fractions, the high-shear mixed samples have been fractionated by size via a 200 µm sieve. The following Table 41 summarizes the determined protein contents in each fraction.

Table 41: Protein contents in fine and coarse BSG fractions determined via amino acid profile.

Sample	Protein content [w/w]	
	Fine fraction [< 200 µm]	Coarse fraction [≥ 200 µm]
BSG 0 min HSM	0.0%	17.2%
BSG 5 min HSM	25.0%	13.5%
BSG 10 min HSM	24.5%	14.6%

It can be seen, that the fractionation did indeed increase the protein content in the fine fraction for every investigated sample. For 5 min high-shear mixing, a concentration factor of 1.37 based on the initial protein content in the BSG raw material was achieved. The approach of

producing a protein enriched BSG fraction is thus principally possible with the high-shear mixing equipment used. However, in view of overall mass balance, the design of the mixer itself would need to be optimized to result in a higher percentage of particles below 200 µm. Potential options are decreasing the size of the mesh inlay from 4 mm down to 2 mm or even below. Additionally, the diameter of the narrowest orifice and thus the point of highest shear forces during mixing could be decreased as well. Both options go in hand with either an increase in required electrical power input during mixing or a decreased dry matter content of the BSG in water to enable the required flow profile for even mixing.

Osborne Fractionation of BSG

After pretreatment, the next step in extracting proteins from biomass is the actual fractionation step. The selection of appropriate extraction techniques as well as the assessment of structural and functional value for subsequent application depend on the protein types present in the biomass. For this, an Osborne fractionation developed for sequentially extracting the four major protein groups of legumes and cereals was used in the course of this study [144]. The detailed procedure is summarized in chapter 3.7.2. In short, water is used to characterize the amount of water-soluble albumins followed by globulins, that are soluble in dilute saline solutions, glutelins soluble in weak acidic or alkaline solutions and lastly prolamins soluble in aqueous ethanol solutions [121,145]. Untreated, wet BSG from the standardized RubyRoast recipe was used for this study. The protein content in BSG prior to extractions was determined as 17.19 ± 0.37%. Additionally, the same BSG subjected to 10 min high-shear mixing for particle size reduction was used as well. The obtained particle size distributions of untreated and high-shear mixed BSG are given in the above Table 40. The results for the Osborne fractionations are summarized in the following Figure 41. Due to an error during the extraction process, the 10 min HSM data are only technical duplicates and the given error bar thus defined as a standard error instead of a standard deviation.

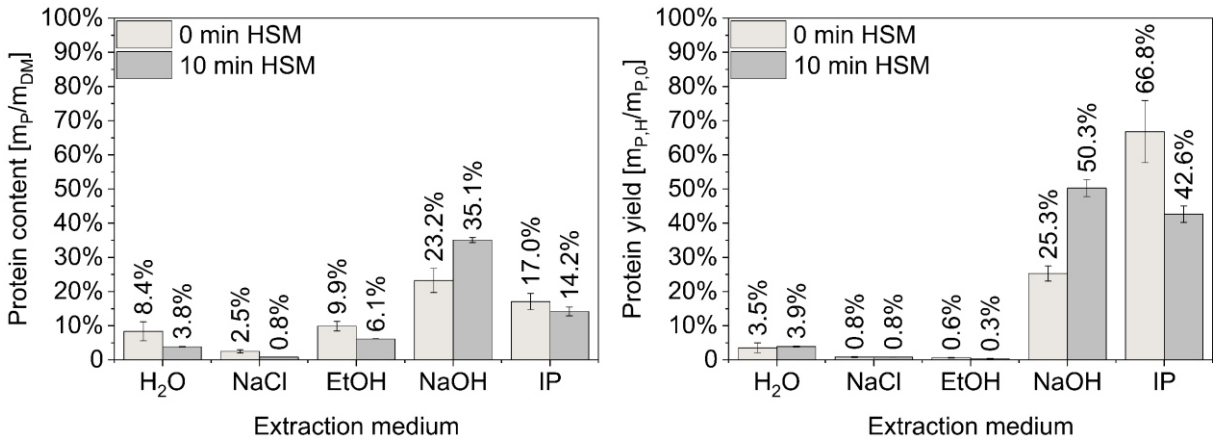

Figure 41: Protein extraction results from Osborne fractionations of BSG. Left: Protein contents of the hydrolysates and insoluble residue. Right: Mass-based protein yields. IP = Insoluble protein. Used concentrations of the solvents: 0.34 mol/L NaCl, 9.6 mol/L EtOH, 0.05 M NaOH.

It can be clearly seen, that most of the extracted protein is soluble in the alkaline medium consisting of 0.05 M NaOH. A total of 25.3 ± 2.2% (w/w) of protein could be extracted from raw BSG using this method. However, the particle size reduction resulted in an almost twofold increase in the mass-based extraction yield to 50.3 ± 2.5 probably due to the increased surface area and hence accessibility to denaturation and hydrolysis by NaOH. The mechanism of protein solubilization by NaOH is primarily based on the disruption of non-covalent interactions such as hydrogen bonds by the addition of OH^- ions, changes in amino acid charges by changes in pH and thus changes in secondary and tertiary protein structure. At high NaOH concentrations, hydrolysis of peptide bonds is also possible due to the strong nucleophilicity of OH^- ions [146,147]. The results led to further studies on the influence of particle size on

protein extraction yields and are discussed in the following chapters. For water, NaCl and EtOH extractions, only low extraction yields are available. Considering that BSG is a residue from the brewing process where it was subjected to mashing and lautering processes, it is expected that most of the water-soluble protein fractions, such as albumins, are already extracted. However, the highest protein yield by mass is obtained from the insoluble fraction with 66.8 ± 9.1% for raw BSG and 42.6 ± 2.4% for 10 min HSM BSG, respectively. It is clear from the data that the available surface area plays an important role in the solubilization of the protein contained in the BSG. An additional factor may be the complex lignocellulosic structure, which may impede access of the medium to the contained protein fraction and thus prevent solubilization. However, it is also possible that the concentration of e.g. NaOH used was too low to effectively solubilize all contained glutelins. Due to the mashing and lautering processes, that take place at temperatures of maximum 78 °C, it is also possible that a denatured and subsequently aggregated portion of the protein is not soluble in either of the four used media. The (partially) denatured protein could form insoluble aggregates through hydrophobic interactions and intermolecular disulfide bridges [93]. To evaluate, whether the fractionation process and coupled analytics are able to close the mass balance, Table 42 summarizes the obtained masses of the total dried solids from all hydrolysates and the final BSG residue as well as for the protein masses of each fraction.

Table 42: Mass balance data for total solid mass and recovered protein mass after Osborne fractionations.

Sample	$m_{DM,0}$ [g]	$m_{DM,SR}$ [g]	Relative difference [-]	$m_{P,0}$ [g]	$m_{P,SR}$ [g]	Relative difference [-]
0 min HSM 1	20	19.85	0.7%	3.44	3.23	6.1%
0 min HSM 2	20	19.99	0.0%	3.44	3.12	9.2%
0 min HSM 3	20	20.28	1.4%	3.44	3.66	6.4%
10 min HSM 1	20	22.65	13.3%	3.44	3.18	7.6%
10 min HSM 2	20	22.535	12.7%	3.44	3.56	3.4%

For the raw BSG, the total solids mass balance can be closed for each run. However, for the 10 min high-shear mixed BSG, the mass balance cannot be completely closed. Around 13% of mass cannot be accounted for. A possible reason for the higher solids weight after extraction could be that salt crystals formed in the hydrolysate after drying, since the NaCl extract could not be effectively separated from the BSG fines and protein solids. For the recovered protein masses, there is a variation in the order of 6% for all samples. Considering that the amino acid content for the initial BSG prior to extractions was determined only once in a technical triplicate, inaccuracies depending on the exact starting material used for each extraction are possible. Additionally, the procedure requires an analytical hydrolysis of the dried residues and thus multiple potential errors in weighing, addition of solutions and preparation of internal and calibration standards. With this in mind, a deviation of 6% is considered sufficiently accurate to continue with this approach for determining protein extraction yields in subsequent studies.

In summary, the predominant protein fraction in BSG after Osborne fractionation consists of both insoluble or inaccessible protein contained in the lignocellulosic matrix as well as alkaline soluble gluetlins. This is consistent with existing literature on BSG protein extractions, which generally use alkaline media to achieve high protein yields [18,93]. However, the maximum yields obtained are always the result of a combination of alkaline media with enzymatic protein hydrolysis, most often with prior particle size reduction [20]. These factors will thus be further investigated in the following chapters.

Influence of High-Shear Mixing on Protein Extractions from BSG

From the results of the Osborne fractionations, it was deduced, that an alkaline medium together with an initial particle size reduction is beneficial for efficient protein extraction. The aim was therefore to investigate the influence of high-shear mixing time on protein extraction yields for different extraction strategies applied. The same BSG was used as for the Osborne fractionations and the particle size diameters given in Table 40 apply.

In a first set of experiments, the influence of ultrapure water as an extraction medium at 60 °C was investigated. Although the Osborne fractionations showed that this medium only extracted less than 4% of the total protein mass present, these experiments were performed at 20 °C. All subsequent extractions in this chapter using NaOH and various enzymes were performed at 60 °C. To establish the baseline protein content extracted using only ultrapure water as the medium, the following results presented in Figure 42 were obtained.

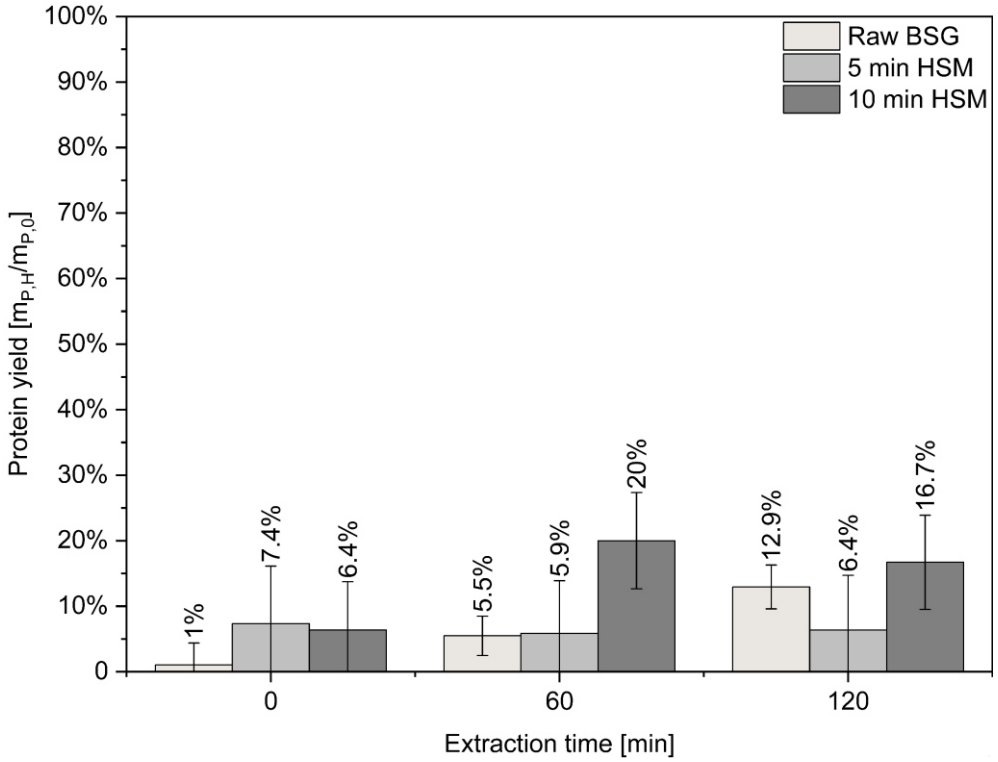

Figure 42: Mass-based protein extraction yield from BSG using ultrapure water at 60 °C. Dry matter content of BSG of 0.1 w/v. Extractions in 50 mL reaction vessels in shaking water bath at 125 rpm.

It is evident, that during water extractions, reproducibility of the results is not given. Slightly higher protein yields may be obtained for extractions with smaller particle sizes after 10 min HSM. However, due to the high standard deviations, no clear trends can be derived from the data. Reasons for the lack of reproducibility could be due to an uneven distribution of water-soluble albumins in the grain and thus different accessibility for extraction. In addition, ultrapure water may not be able to open the lignocellulosic matrix, and thus the amount of protein accessible for solubilization depends on which protein is accessible on the surface of the grain, which may vary for each of the triplicates used. It can be concluded that after 2 h of extraction time, the water-induced protein extraction is below 20% by mass and thus not sufficient for commercialization.

A new strategy was thus applied: Liquid hot water (LHW) treatment. The working principle of this extraction technique is based on using subcritical water to induce autocatalysis of lignocellulosic structures. During LHW, the ion product of water is increased and the pH subsequently reduced. Increased temperatures result additionally in a decrease in the

dielectric constant of water, leading to a polarity similar to that of ethanol and methanol at atmospheric conditions. These property changes might allow for an extraction of the prolamin protein fraction from BSG, as this fraction is known to be soluble in hydroalcoholic solutions. And lastly, with increasing temperature, the overall mass transfer is enhanced through a decrease in viscosity, density and surface tension of water, while the self-diffusivity is enhanced. [148–151] The screening experiments were conducted at 150 °C and 180 °C for 10 min. These temperatures were based on a previous study on BSG by GAIROLA (2014) [152]. Results are summarized in the following Figure 43.

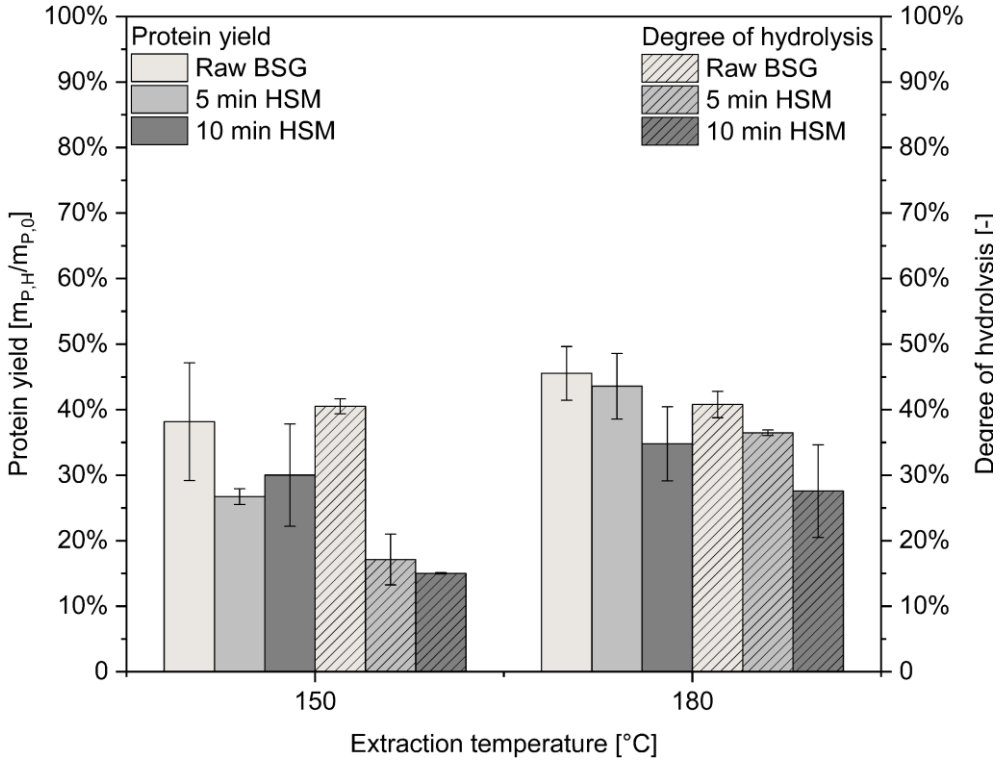

Figure 43: Mass-based protein extraction yield and degree of hydrolysis through LHW treatment of BSG. Dry matter content of 0.1 w/v. Extractions for 10 min in 30 mL reaction vessels with 500 rpm stirring at 50 bar pressure in N_2 atmosphere.

Generally, LHW treatment at 180 °C resulted in a higher protein yield than at 150 °C. The trend regarding the influence of HSM time and thus particle sizes is similar for both investigated temperatures. Opposing to the expectations, the raw, untreated BSG resulted in the highest observed protein extraction yield with 45.5 ± 4.1% for 180 °C. 5 and 10 min HSM resulted in 43.6 ± 5.0% and 34.8 ± 5.7% protein yield, respectively. The lower extraction yield with decreasing particle sizes might be a result of the experimental setup used rather than the actual extraction behavior. It is assumed, that with decreasing particle size, more particles adsorb to the inside of the reactor wall and are thus not homogeneously dispersed via the magnetic stirrer bar set to 500 rpm. The finer particles might be sticking to the wall to a higher extent, as was visible after opening the reactor vessels after the hydrolysis procedure. These particles are then not available to protein hydrolysis, as they are not subjected to the LHW treatment. The degree of hydrolysis (DH), evaluating the amount of cleaved peptide bonds relative to the maximum possible cleaved peptide bonds corresponding to complete protein hydrolysis, shows the same trend as the protein extraction yield [153]. Since all observed yields are below 50% by mass, this approach is not investigated in more detail for protein extractions. An additional factor in this decision was the non-specificity of this method. Next to protein, sugars were co-solubilized, which pose challenges for downstream processing. Additionally, the presence of both proteins and sugars at elevated temperatures always pose the risk of

forming Maillard reaction products, which can be carcinogens [154]. As the intended use of extracted protein is in the food sector, this technique was not investigated further.

The next protein solubilization strategy investigated, focused on the promising results obtained from the Osborne fractionations using NaOH. The aim was to solubilize not only the residual albumin fraction but also the glutelins, one of the two major protein fractions present in BSG. Temperature and concentration ranges were taken from the extensive literature existing for the extraction of BSG proteins via this method [20]. The influence of high-shear mixing on the extraction yields is investigated by analyzing the mass-based protein yields into the hydrolysate fraction as well as the degree of hydrolysis. Results are summarized in Figure 44.

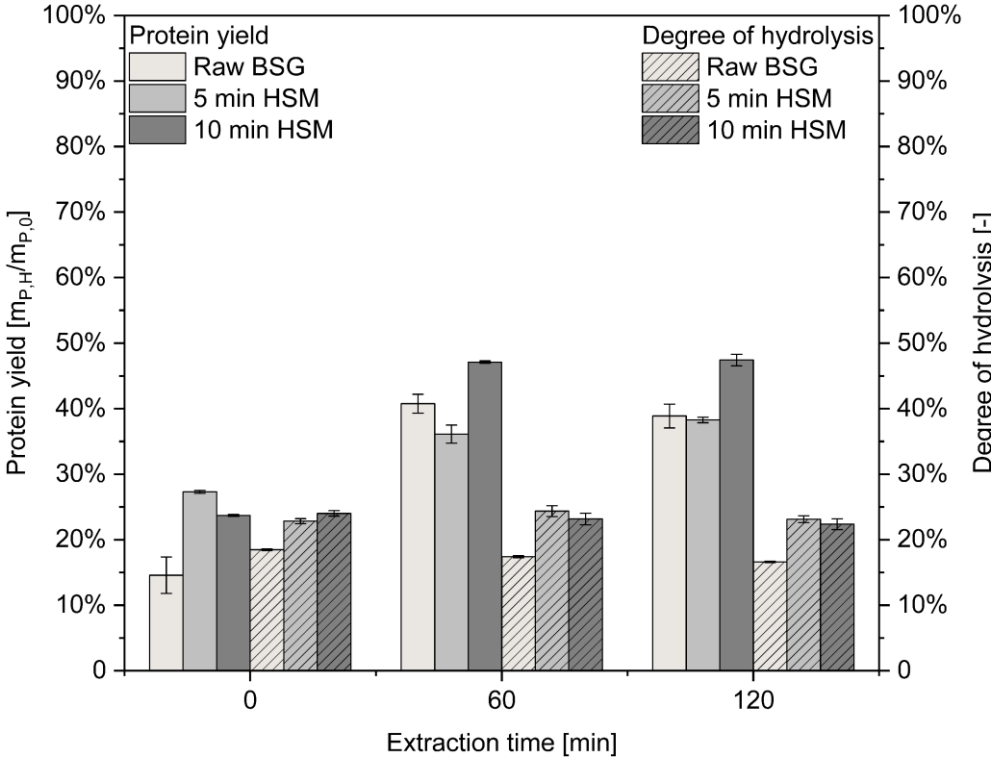

Figure 44: Mass-based protein extraction yield of BSG and degree of hydrolysis through 0.1 M NaOH at pH 11 in ultrapure water as extraction medium. Dry matter content of 0.1 w/v. Extractions in 50 mL reaction vessels in shaking water bath at 60 °C and 125 rpm.

For the alkaline NaOH extractions, a relevant amount of protein is already present in the hydrolysate at the start of the extraction. However, it should be noted that the extraction time was started only after the pH had been adjusted to pH 11, which took about 10 min per sample at room temperature (19-25 °C). Additionally, it is assumed that batch-to-batch variation depending on where the BSG sample was taken from is an important factor in the different trends observed between experimental runs. Further studies are needed to observe the experimental repeatability. This assumption has also prompted an investigation into the impact of BSG type on subsequent extraction results and is discussed in the following chapters. For all three particle size distributions, the majority of protein extraction occurred during the first 60 min of extraction at 60 °C. The protein yield increased for 0 and 5 min HSM time to 40.8 ± 1.4% and 36.1 ± 2.0%, respectively and remained constant during the next hour. This might indicate, that either all of the alkaline soluble protein had already been extracted or that all accessible protein was solubilized. The same behavior could be observed for 10 min HSM time, however resulting in a higher protein yield of 47.1 ± 0.2% after 1 h of extraction. The increased surface area of the BSG particles gave access to further protein extraction by NaOH. The obtained yields remain below 50% by mass, which is not sufficient for commercialization as a protein for human consumption in view of extensive downstream processing efforts

required to remove access sodium ions [137]. Additionally, the achieved protein quality is assumed to be low due to the extraction of denatured protein and peptide fragments as described earlier. The order of magnitude of protein yields is similar to that reported by other research groups [20]. CELUS ET AL. (2007) reported an extraction yield of 41% after extraction from raw BSG at 0.17% w/v with 0.1 M NaOH at 60 °C [155]. However, as the protein content was determined indirectly using a Dumas combustion method for nitrogen content and a conversion factor of 6.25, which is known to regularly overestimate protein content, the reported protein yield is difficult to compare with the present study [122]. In a more recent study, ALONSO-RIAÑO ET AL. (2021) achieved an extraction yield of 50.5 ± 0.2% after extraction for 4 h at 50 °C in 0.1 M NaOH at a dry matter content of 0.05 w/v [156]. Additionally, CONNOLLY ET AL. (2013) reported an extraction yield of 59 ± 5% when running the extraction at 50 °C for 1 h using 0.11 M NaOH at a dry matter content of 0.05 w/v [157]. The latter working group used a particle size reduction in an Ultra Turrax at 24000 rpm for 2 min as a pretreatment strategy, did however not state any resulting particle size distributions. Additionally, both working groups determined the protein contents in the hydrolysate fractions via an indirect nitrogen determination method while applying a protein conversion factor of 6.25, leading to the above-mentioned challenges for comparison. While CONNOLLY ET AL. (2013) stated to have used a pale BSG from an industrial brewery with a starting protein content of 23.10 ± 0.09% by mass, ALONSO-RIAÑO ET AL. (2021) did not report this information. Differences in the obtained results might thus be explained via the different pretreatment steps applied, the varying BSG types used as well as the chosen analytics for protein content determination.

The results for the degree of hydrolysis show similar trends with time compared to the protein yields. For raw BSG, 17.4 ± 0.2% of peptide bonds were hydrolyzed after 2 h. For 5 and 10 min HSM higher DH of 24.3 ± 0.8% and 23.2 ± 0.9% were achieved. Although higher than the values obtained for raw BSG, only a quarter of all peptide bonds were hydrolyzed, leaving potential for further hydrolysis to smaller peptides or single amino acids depending on the target product or an overall higher required extraction yield to obtain a higher DH. A qualitative protein size analysis via an SDS-PAGE presented in Figure 45 confirmed, that a broad protein and peptide size distribution was extracted. The high-shear mixed BSG extractions both resulted in darker blue color in the stained gels, indicating a higher concentration of present protein in line with the findings from the degree of hydrolysis and for the 10 min HSM BSG in terms of protein yield. For both 5 and 10 min HSM BSG, the darkest blue color is present in the column after 10 min extraction, fading to a lighter blue color in the course up to 2 h. This might be an indication for hydrolysis of the extracted protein to smaller peptides over time. For a detailed analysis of protein sizes, a quantitative analysis such as a gel permeation chromatography could be applied.

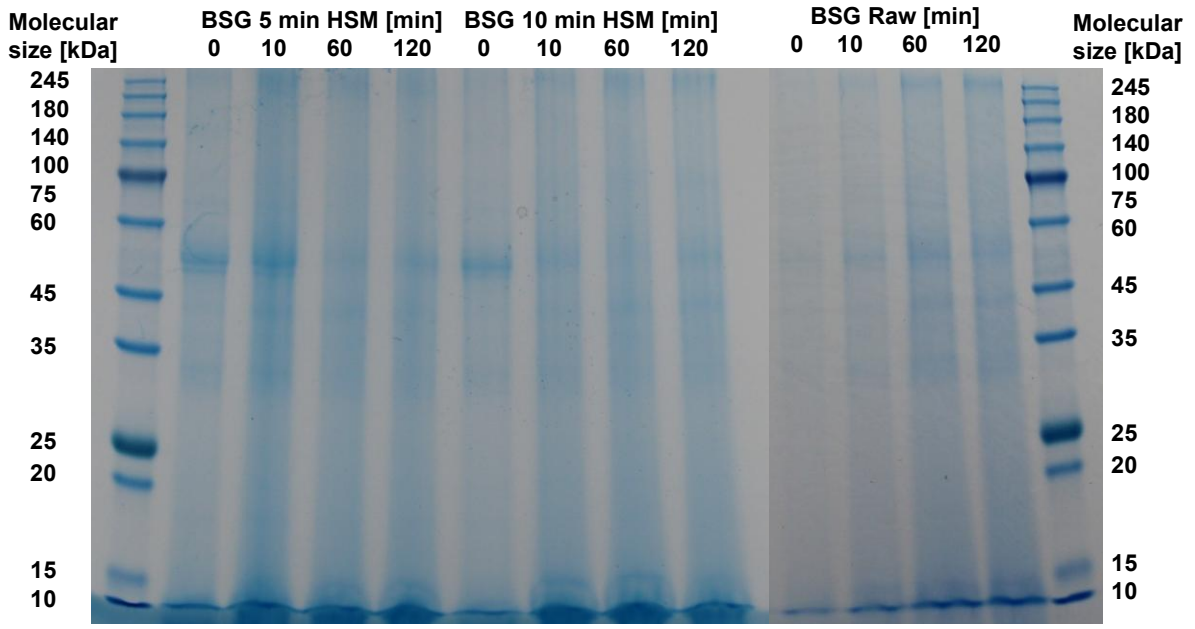

Figure 45: SDS-PAGE of liquid hydrolysates from BSG extractions at 60 °C using 0.1 M NaOH at pH 11.

The NaOH induced extractions presented above showed, that high-shear mixing is able to increase the protein extraction yield by reducing the BSG particle size. It was also shown that the experimental set-up used resulted in protein yields in the same order of magnitude as previously reported by other research groups under similar conditions. However, NaOH as a solvent is not specific for protein extraction, but is also able to solubilize sugars and phenolics from the lignocellulosic matrix of BSG [158,159]. After 2 h of extraction a total degree of solubilization determined as the difference in dry matter weight before and after extractions was determined around 45-50% for all extractions studied. Since only 17.19 ± 0.37% of dry matter of the initial starting material account for protein, other components were co-extracted. In subsequent chapters, this co-solubilization is investigated in more detail. A lack of specificity of this extraction technique does not automatically imply its non-suitability for industrial application. Since the market for plant-based protein is constantly growing, there are applications that might arise. A potential option is the production of a protein- and sugar-rich hydrolysate as a fermentation basis. This could be relevant for the bioethanol industry, but also for emerging industries in the lactic acid fermentation on waste streams [30,160–162]. These approaches will be further investigated in the subsequent chapter 4.3.2. However, for the extraction of protein for direct human consumption, a different approach was chosen for further investigation: Enzymatic extractions with a potentially higher specificity towards protein. As a starting point, the enzyme Alcalase® by Novonesis was used, being the most commonly cited enzyme for extraction of plant proteins [20]. Next to a proteolytic activity, the manufacturer states that an α-amylase activity is present. However, industrial BSG typically contains less than 1-3% of residual starch, making the main activity relevant for BSG the proteolytic activity [7]. Following the procedure described in chapter 3.4.1, a proteolytic activity of 2229.2 ± 46.9 U/mL for the used Alcalase® batch was determined. The manufacturer states that this endo-protease should be used at pH 6.5-10 and temperatures in the range of 60-75°C. The initial screening of enzymatic BSG extractions was carried out at a pH of 8. This pH was chosen, as multiple working groups could show maximum activity of Alcalase® during hydrolysis of BSG proteins at this value [19,155,157,163]. This is in line with the manufacturers application sheet, stating maximum activity in the range of pH 8-8.5 [19,164]. The most commonly cited temperature for BSG protein extraction applying this enzyme is 60 °C, which was thus chosen for all enzymatic protein extractions [20]. The dosage of Alcalase® has also been studied, and is most widely used at 10-20 µL/g BSG [142]. However, as the activity of

the enzyme preparation used is not usually reported together with its dosage, nor are the dry matter content and particle sizes used for BSG extractions, this parameter was investigated in more detail in the present work. Results are summarized in Figure 46.

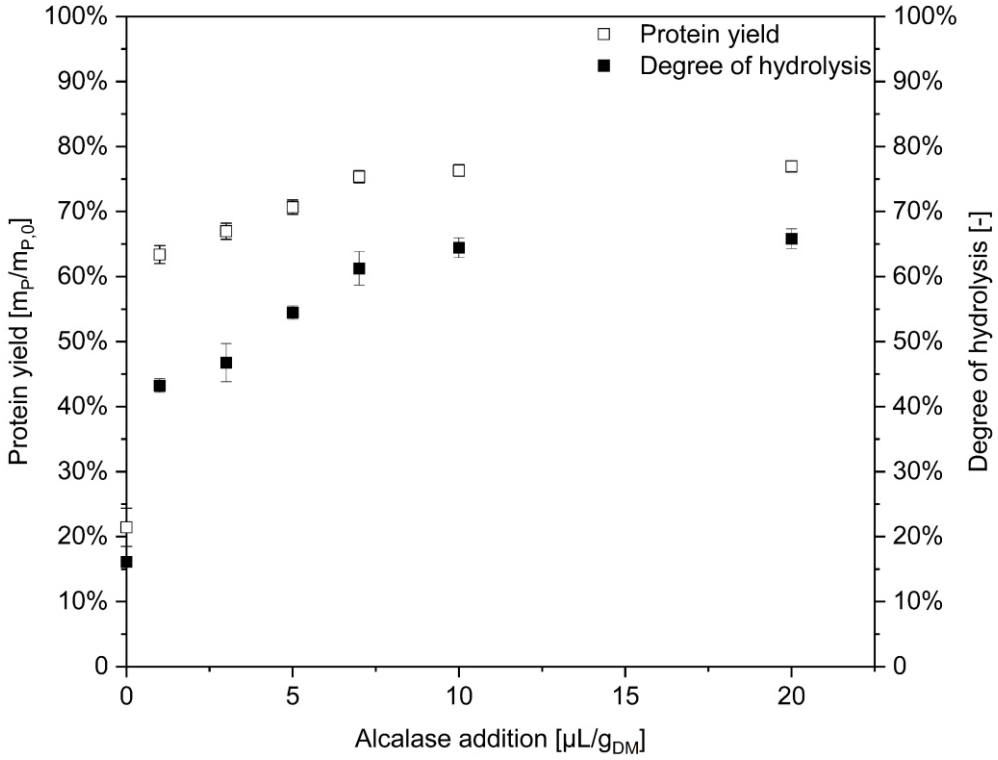

Figure 46: Mass-based protein extraction yield and degree of hydrolysis for 10 min HSM BSG using 0.1 M NaOH until pH 8 in ultrapure water as extraction medium. Dry matter content of BSG of 0.1 w/v. Extractions at 60 °C in 50 mL reaction vessels in shaking water bath at 125 rpm for 2 h. Enzyme activity of 2229.2 ± 46.9 U/mL.

The same trend can be seen for both the protein yield and degree of hydrolysis with enzyme dosage. An increase in yield and degree of hydrolysis can be seen after 2 h of extraction up to an enzyme dosage of 10 µL/g_{dm}. A further increase in enzyme dosage up to 20 µL/g_{dm} did not result in a higher protein yield or degree of hydrolysis. A dosage of 10 µL/g_{dm} at a proteolytic activity of 2229.2 ± 46.9 U/mL was thus chosen as the standard ratio for the present work. To investigate, whether different times or particle sizes change the results obtained during the dosing screening, a second dosage of 20 µL/g_{dm} was run at the same time during the initial screening experiments. The following Figure 47 summarizes the results for protein yield obtained at different extraction times and particle sizes of BSG as a result of high-shear mixing.

For both dosages, the protein yields obtained rise over the complete time observed. Maximum yields were observed after 2 h extraction. For a dosage of 10 µL/g_{dm} a maximum yield of 70.6 ± 0.3% for 10 min HSM BSG and for 20 µL/g_{dm} of 65.2 ± 0.0% for the same BSG sample was achieved. The effect of particle size on protein yield is evident, as for all investigated time points and high-shar mixing times, the smaller particles resulted in higher protein yields. The prominent effect of particle size reduction on the protein yield obtained was to be expected for enzymatic extractions. An external increase in available surface area through particle size reduction thus directly increases the available protein for enzymatic hydrolysis. It can also be assumed, that even smaller particles could lead to a further increased protein yield. However, a trade-off has to be made in terms of energy input required for pretreatment steps and subsequent extraction yields. With the high-shear mixer used, it was shown that increasing the mixing time beyond 10 min did not result in a further decrease in particle size. If smaller particles are desired, the design of the rotor and stator could be adjusted.

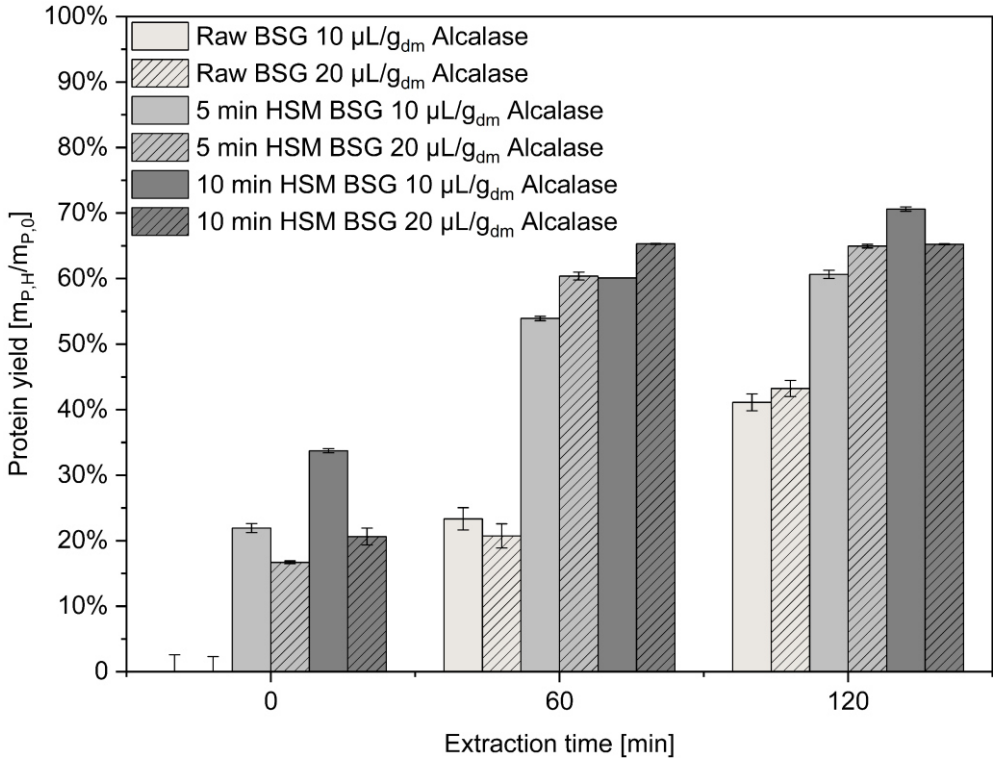

Figure 47: Mass-based protein extraction yield for enzymatic BSG protein extraction. Dry matter content of 0.1 w/v. Extractions in 50 mL reaction vessels in shaking water bath at 60 °C, pH 8 and 125 rpm. Enzyme activity of 2229.2 ± 46.9 U/mL.

For the current study, a 4 mm mesh inlay was used on the rotor. The orifice diameter could be further reduced to potentially decrease the BSG particle sizes obtained. However, as a trial run in this study showed, the decrease in particle size was not substantial enough to account for the non-linearly increasing energy demand during mixing. Additionally, the presence of BSG particles finer than 200 µm might pose challenges for downstream processing options. Instead of focusing on reducing the BSG particle sizes, a subsequent study in a later part of this chapter focused on increasing the extraction time to potentially increase the protein yields obtained. Additionally, the mixing speed was limited to 125 rpm in a water bath due to the experimental setup used. It is highly likely, that mass transfer limitations are present in the system, which will be further investigated in the subsequent chapter of up-scaling the protein extractions.

Comparing the obtained results with literature, similar orders of magnitude were achieved for the extraction yields, however in a shorter amount of time and with a higher solids content favorable for scale-up. YU ET AL. obtained protein yields of 63.3% for extractions of 2 g of BSG at a solids content of 5% after 4 h of extraction at 60 °C, pH 8, 110 rpm shaking and an Alcalase® dosage of 10 µL/g$_{dm}$ [164]. Interestingly, smaller particle sizes with a mean diameter of 331.2 ± 6.4 µm obtained after drying and milling in a hammer mill were used, compared to the median diameter of 1265.7 µm achieved after 10 min HSM in this study. Additionally, a pretreatment step of ultrasonication for opening up the lignocellulosic matrix prior to enzymatic extractions was performed at 20 kHz for 10 min. It is thus theorized, that high-shear mixing might not only reduce the BSG particle sizes, but potentially also alters the lignocellulosic matrix due to the acting high shear forces, thus enhancing accessibility of proteins. The group around CONNOLLY ET AL. (2019) achieved an extraction yield of 63.09% using 1 min wet milled BSG in an Ultra-Turrax at 24000 rpm [165]. Additionally, the BSG was incubated with two carbohydrases, namely Shearzyme® and Ultraflo® by Novonesis, for 4 h at 50 °C at an enzyme dosage of 75 µL/g$_{dm}$ to open up the lignocellulosic matrix of the BSG. The subsequent protease incubation was conducted at 10% dry matter content using the two proteases Alcalase® and

Flavourzyme® by Novonesis. The first enzyme was added at a ratio of 2% by mass and left to incubate for 2 h at 50 °C before the second enzyme was added at a dosage of 1% by mass and left to incubate for another 2 h. And lastly, HE ET AL. (2019) achieved a protein yield of 83.4% after extraction of 2 g of BSG at 60 °C for 4 h at a dry matter content of 5% by mass and an enzyme dosage of 20 µL/g_{dm}. The BSG was pretreated in an Ultra-Turrax mixer at 24000 rpm for 2 min resulting in an average particle size of 161.7 µm [163]. No pH was reported for the extractions. The seemingly high protein yield might be a result of the very fine BSG particles, however are more likely a result of the inaccurate determination of protein yield. Instead of determining the protein content in the hydrolysate or solid BSG residue after extractions, the yield was defined as the total mass of hydrolysate relative to the total mass of hydrolysate plus solid residue. As the hydrolysate does most likely not only contain proteins, the given yield is not comparable to the results of this study. In summary, HSM treated BSG extractions with Alcalase® enzymes resulted in the same order of magnitude of protein yields obtained by other research groups, that optimized different pretreatment strategies and the extractions itself. HSM thus seems to be a suitable pretreatment strategy to not only reduce BSG particle sizes in a wet process, but also to (partly) open up the BSG lignocellulosic structure for enhanced access of proteins by Alcalase® enzymes. Similar to the results obtained for protein yields, the degree of hydrolysis was evaluated and is summarized in the following Figure 48.

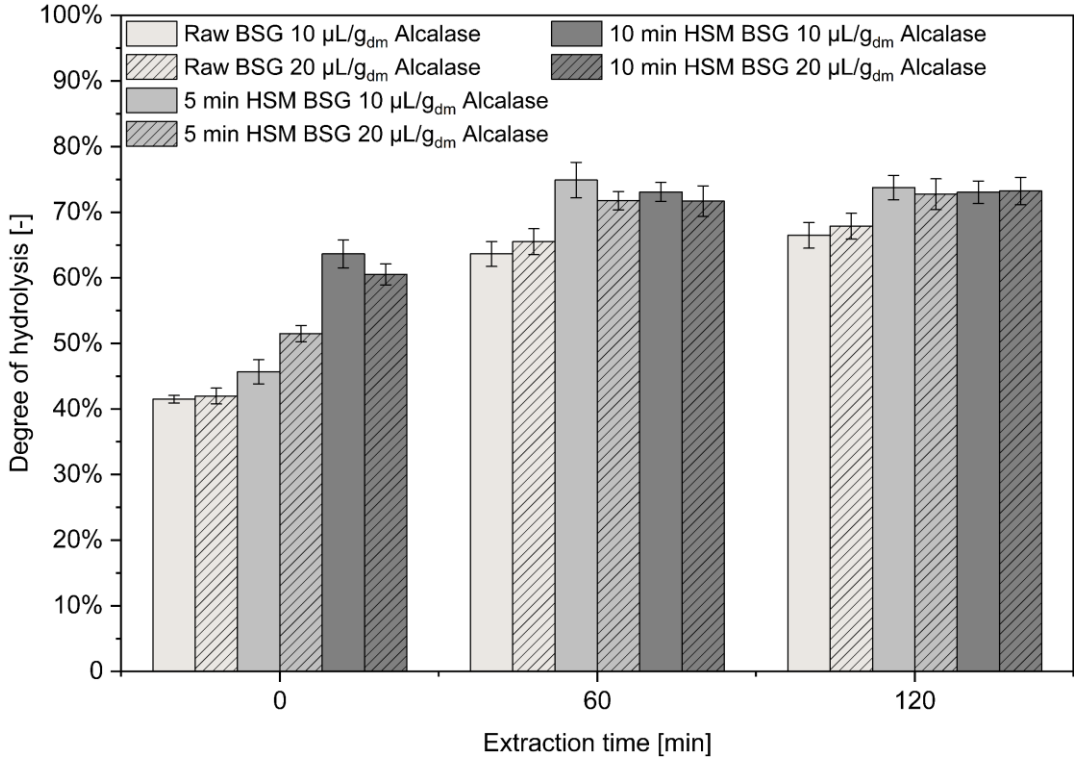

Figure 48: Degree of hydrolysis for enzymatic BSG protein extraction. Dry matter content of 0.1 w/v. Extractions at 60 °C and pH 8 in 50 mL reaction vessels in shaking water bath at 125 rpm. Left: 10 µL/g_{DM} Alcalase dosage. Right: 20 µL/g_{DM} Alcalase® dosage. Enzyme activity at 2229.2 ± 46.9 U/mL.

The same trends can be observed as for the protein yields: The degree of hydrolysis rises with time for every sample investigated. Longer high-shear mixing times resulted in a higher degree of hydrolysis, reaching a maximum of 73% for both 5 and 10 min HSM BSG and both enzyme dosages. Alcalase® is an endo-protease, thus hydrolyzing larger proteins into smaller peptide fragments. It is commonly coupled with an exopeptidase such as Flavourzyme® by Novonesis to produce single amino acids and short chain peptides, while simultaneous enabling a debittering of the proteins [165]. Depending on the desired product properties, an application of an expopeptidase might be useful in the present case, since all investigated scenarios

reached the same degree of hydrolysis, which did not increase further over the last hour of extraction. It might thus be, that a further fragmentation to smaller peptides cannot be effectively hydrolyzed by the endo-protease Alcalase® alone. A qualitative protein size analysis was conducted to verify these findings. The SDS-PAGE is given in Figure 49.

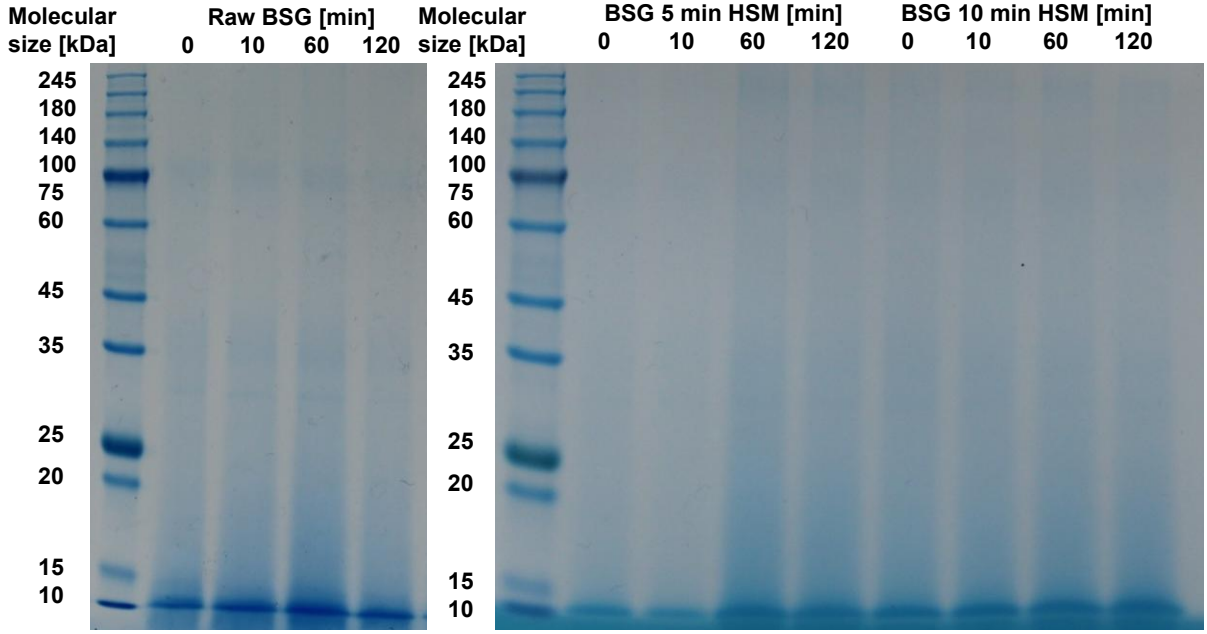

Figure 49: SDS-PAGE of liquid hydrolysates from BSG extractions at 60 °C using 10 µL/g_{dm} Alcalase® enzyme at pH 8.

It can be clearly seen, that mostly peptides below 20 kDa were extracted. Only light blue shades are present at larger protein sizes. There are no clear individual protein bands present, which might indicate, that the majority of peptides hydrolyzed is smaller than the minimum protein size detectable by the used SDS-PAGE.

A maximum of 70.6 ± 0.3% mass-based protein yield was achieved with 10 min HSM BSG and an enzyme dosage of 10 µL/g_{dm}. Even though this yield was already slightly higher than that reported by other research groups, it was investigated, if the application of cellulase and hemicellulase blends in combination with proteases would result in even higher yields. The idea was to investigate the effect of opening up the lignocellulosic matrix of BSG for further access of the protease enzymes to the BSG protein. The enzyme combinations used are summarized in the methods chapter 3.7.3. A new batch of BSG was used for this set of experiments. The protein content of raw BSG was determined as 17.39 ± 0.07% by mass. The particle size distribution of the raw and 10 min HSM BSG is given in the following Table 43.

Table 43: Particle size distribution of untreated BSG for enzymatic extractions and after 10 min of high-shear mixing (HSM).

Sample	$D_{x,10}$ [µm]	$D_{x,50}$ [µm]	$D_{x,90}$ [µm]
0 min HSM	1723.3	3375.0	4974.0
10 min HSM	285.7	775.9	1675.4

The diameter of the 50th percentile was reduced by a factor of 4.3 through the action of 10 min HSM. All subsequent extractions were performed with this pretreated batch of BSG. To investigate the effect of the single enzymes on protein extraction, the following Figure 50 summarizes the results obtained on protein yield and degree of hydrolysis. Details on each of the enzyme blends used can be found in chapter 3.7.3.

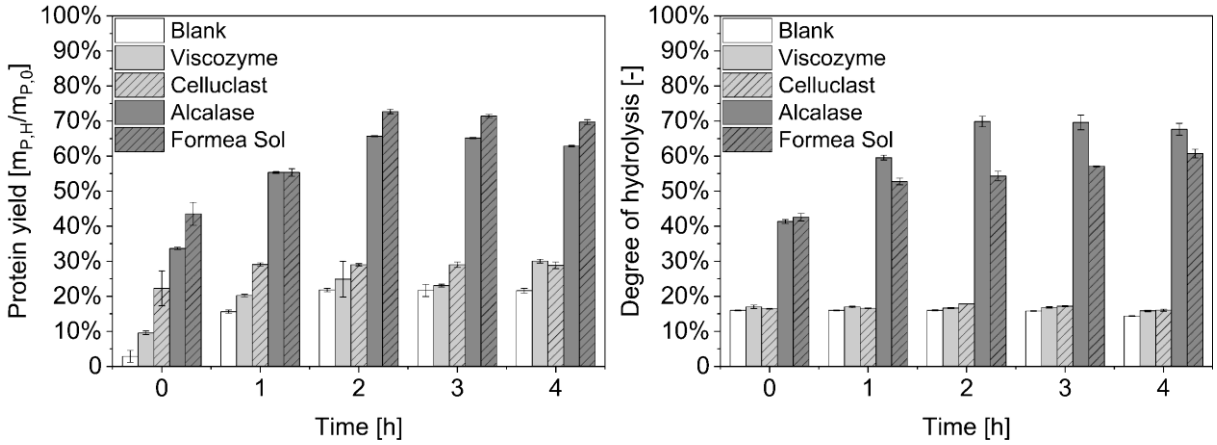

Figure 50: Protein extraction results for single enzymes at 60 °C, pH 6.2 and 125 rpm and an enzyme dosage of 10 µL/g_{dm}. Left: Mass-based protein yield. Right: Degree of hydrolysis.

Over the four-hour extraction period, 21.6 ± 0.7% of protein was extracted from the blank via high-shear mixing and subsequent incubation at 60 °C. The use of the two carbohydrase enzyme blends resulted in only slightly increased yields of 30.0 ± 0.5% for Viscozyme® and 28.8 ± 1.0% for Celluclast®. The slightly higher yield for Viscozyme® was first theorized to be due to the manufacturer stated protease activity of this enzyme blend. However, when assayed with the protease assay described in chapter 3.4.1, an activity of only 6.5 ± 0.2 U/mL was detected, whereas for Celluclast® a proteolytic activity of 8.1 ± 0.9 U/mL was found. Even though not stated by the manufacturer, both enzymes present similar orders of magnitude of proteolytic activity and thus yielded similar amounts of extracted protein. Since the cellulolytic activity determined for Viscozyme® was slightly higher than that of Celluclast®, it might instead be, that this enzyme blend was able to hydrolyze the lignocellulosic matrix of BSG to a slightly higher extent, thus giving access to more hydrolysable protein. However, since the order of magnitude of the extracted protein is similar for both enzyme mixtures, the difference obtained could also be the result of statistical variations in the BSG composition plus measurement errors that accumulate during the experiment and subsequent analysis. This hypothesis is supported by the results of the degree of hydrolysis, for which both enzymes resulted in the same value of 16%. Compared to 14.4 ± 0.0% of DH for the blank, it is evident, that both enzyme blends on their own are not able to hydrolyze BSG contained protein. The two protease enzymes however resulted in protein yields of 65.7 ± 0.2% for Alcalase® and 72.7 ± 9,6% for Formea® Sol after 2 h of extraction. No further increase in extracted protein was detected thereafter. For the degree of hydrolysis, this trend is the same for Alcalase®, resulting in a maximum DH of 69.9 ± 1.5% after 2 h. For Formea® Sol, the DH is at only 54.3 ± 1.4% at this time, increasing up to 60.7 ± 1.2% in the course of the next two hours. From this data it is assumed, that Alcalase® tends to release smaller peptide fractions than Formea® Sol. However, the latter enzyme is able to hydrolyze already extracted peptide fragments to even smaller peptides over time.

For Alcalase®, both the protein yield and the degree of hydrolysis are lower than the results obtained at pH 8. This deviation is assumed to be primarily a result of the change in pH to pH 6.2 to enable the simultaneous application of carbohydrases as described in detail in the methods chapter 3.7.3. The results for protein yield for the combined enzyme runs are presented in the following Figure 51. The data for the protein yield as well as the degree of hydrolysis after 15 min, when the protease enzymes were added, can be found in the appendix in Figure A-4 and Figure A-5.

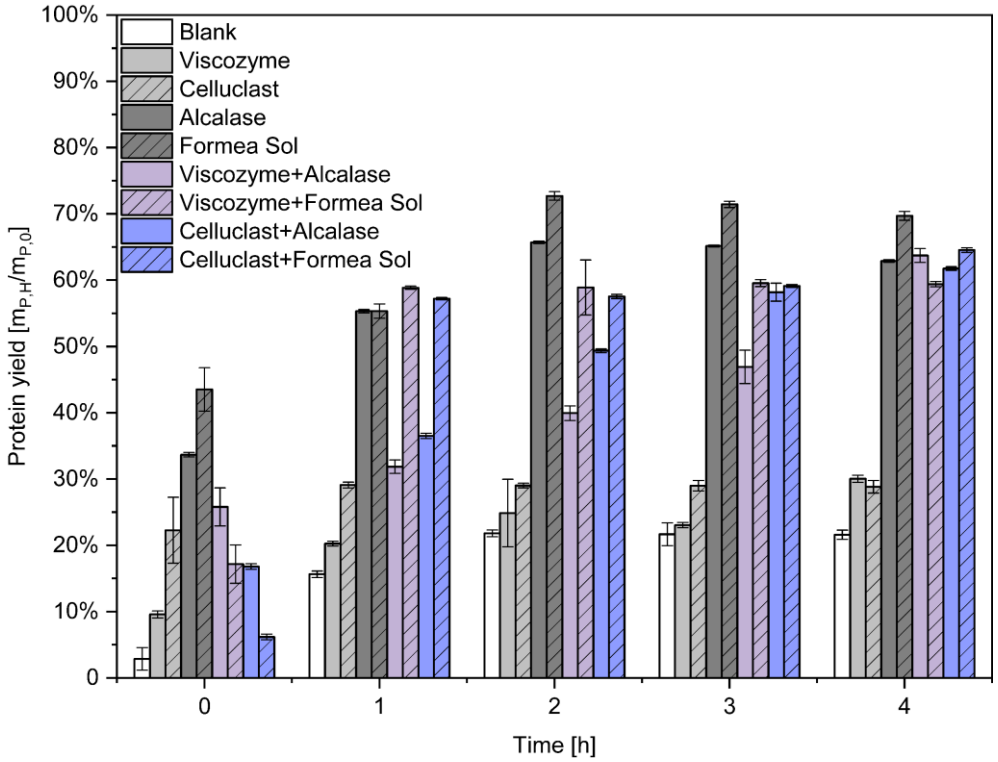

Figure 51: Mass-based protein yield for single enzymes and enzyme combinations at 60 °C, pH 6.2 and 125 rpm and an enzyme dosage of 10 µL/g_{dm}. Protease enzymes were added 15 min after the addition of carbohydrases.

It can be clearly seen, that the addition of both carbohydrases did not result in an increase in the protein extraction yield above that of the single protease enzymes. On the contrary, the obtained extraction yields are even lower than that for Formea® Sol on its own after 4 h. One reason might be, that the 15 min incubation time prior to protease addition did not suffice to result in an additional opening of the lignocellulosic matrix and thus no benefit for the protein hydrolysis. In the case of the combination of Alcalase® and both carbohydrases, a delay in protein hydrolysis seems to have taken place. After 1 h of incubation, the single enzyme resulted in an extraction yield of 55.3 ± 0.3%, whereas the combination with Viscozyme® and Celluclast® resulted in only 31.9 ± 1.0% and 36.5 ± 0.4%, respectively. For both carbohydrases, the same extraction yields as for the single Alcalase® enzyme after 2 h incubation were achieved only after 4 h incubation. This may be due to the fact that instead of hydrolyzing the BSG protein, the proteases first hydrolyzed the carbohydrase enzymes. The research group around CONNOLLY ET AL. (2019) incubated milled BSG with two carbohydrases for 4 h prior to inactivation and subsequent addition of protease enzymes for another 2 h of incubation [165]. This approach resulted in a protein extraction yield of 63.09%, which is in the same order of magnitude than that observed for the single protease enzymes after high-shear mixing as a pretreatment. In view of process costs involved with the additional incubation time as well as the high thermal energy demand for inactivation, this approach was not investigated further. Instead, the two protease enzyme stock solutions were assayed for cellulolytic activity. For Alcalase® an activity of 11531.9 ± 163.4 U/mL was determined via the DNS assays. For Formea® Sol the same assay showed an activity of 11149.9 ± 332.1 U/mL. This is almost half the cellulolytic activity, that the two carbohydrase cocktails Viscozyme® and Celluclast® presented. Thus, it may be, that the carbohydrase activity already present in the two protease enzymes is sufficient to open the lignocellulosic matrix, which is why there was no increase in protein extraction yield when additional carbohydrases were used in advance.

An indication for this could be determined via present sugar and organic acid concentrations in the liquid hydrolysates after the extractions. High released sugar concentrations compared to the blank run without enzyme addition indicate, that sugars from the structural carbohydrates of the BSG were hydrolyzed and thus an opening of the lignocellulosic matrix. For this, all hydrolysates were analyzed for contained monomeric sugars and organic acids as described in chapter 3.3.4. In the blank run without enzyme addition, a maximum of 7 g/L of cellobiose, 3 g/L of glucose and 0.6 g/L of xylose were present in the hydrolysate. No arabinose, formic acid and acetic acid were found. Results for all blank hydrolysates and enzymatic extractions can be found in the appendix in Figure A-6 to Figure A-14.

For the two protease enzymes, the three cellulose- and hemicellulose-derived sugars glucose, xylose and arabinose were present in the hydrolysates in similar orders of magnitude of 8 g/L, 2.5-3 g/L and 0.5 g/L, respectively. In addition, high amounts of formic acid with a maximum of 27.1 g/L were present during the Alcalase® extractions. This maximum concentration was found after 2 h of incubation in the single enzyme run. The formation of formic acid as a side product of Alcalase® during incubation with a lignocellulosic matrix is not well described in literature. An error in the measurement or an incorrect interpretation of the results could be present. This error could be caused by the overlapping peak times of formic acid and an unidentified component, released through one of Alcalase®'s known carbohydrase activities. Alternatively, the formation of organic acid could be linked to a yet unknown side activity of this enzyme. This could indicate a different mechanism of hydrolysis than for all other used enzymes and combinations thereof. For a further investigation of this behavior, the sum of the released sugars cellobiose, glucose, arabinose and xylose is compared to the sum of released acetic and formic acid. Results are summarized in the following Figure 52.

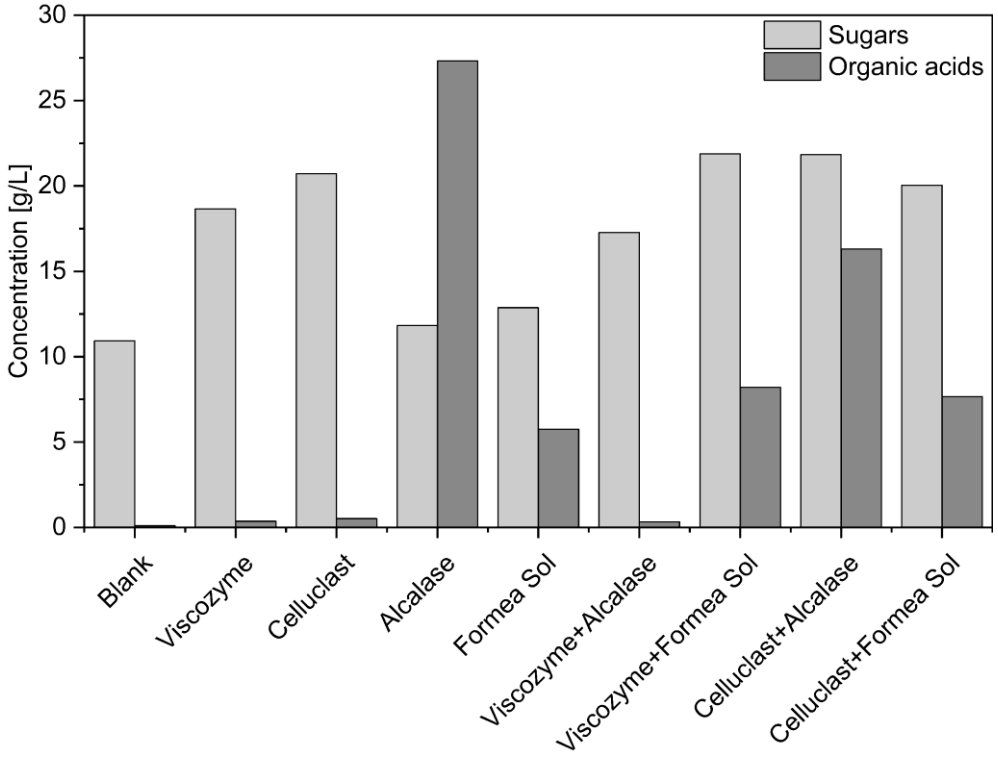

Figure 52: Sum of sugar and organic acid concentrations co-extracted after incubation for 2 h at 60 °C, pH 6.2 and 125 rpm and an enzyme dosage of 10 µL/g_{dm} with different enzymes and enzyme combinations. Sugars include concentrations of cellobiose, glucose, arabinose and xylose. Sum of organic acids include acetic and formic acid.

It is evident, that the blank and single carbohydrase incubations did not release relevant amounts of organic acids. The single enzyme runs of Alcalase® and Formea® Sol are differentiated clearly by their ability to release organic acids. While the former released 27.1 g/L

of formic acid, the maximum concentration found in the Formea® Sol runs was only at 5 g/L. As expected, the two carbohydrases resulted in higher sugar contents in the hydrolysates and a lower formation of organic acids than the two protease enyzmes. However, the concentrations with a maximum of 9-12 g/L of released glucose and 2-5 g/L for both xylose and arabinose are not orders of magnitude higher than those released by the two protease enzymes. And lastly, the enzyme combinations show even higher released sugar concentrations, either due to the overall higher carbohydrase activity added through the addition of two times 10 µL/g_{dm} of first the carbohydrase and second the protease enzymes or through synergistic effects between the different enzymes. For a differentiation of these effects, a principal component analysis was conducted and is summarized in Figure 53.

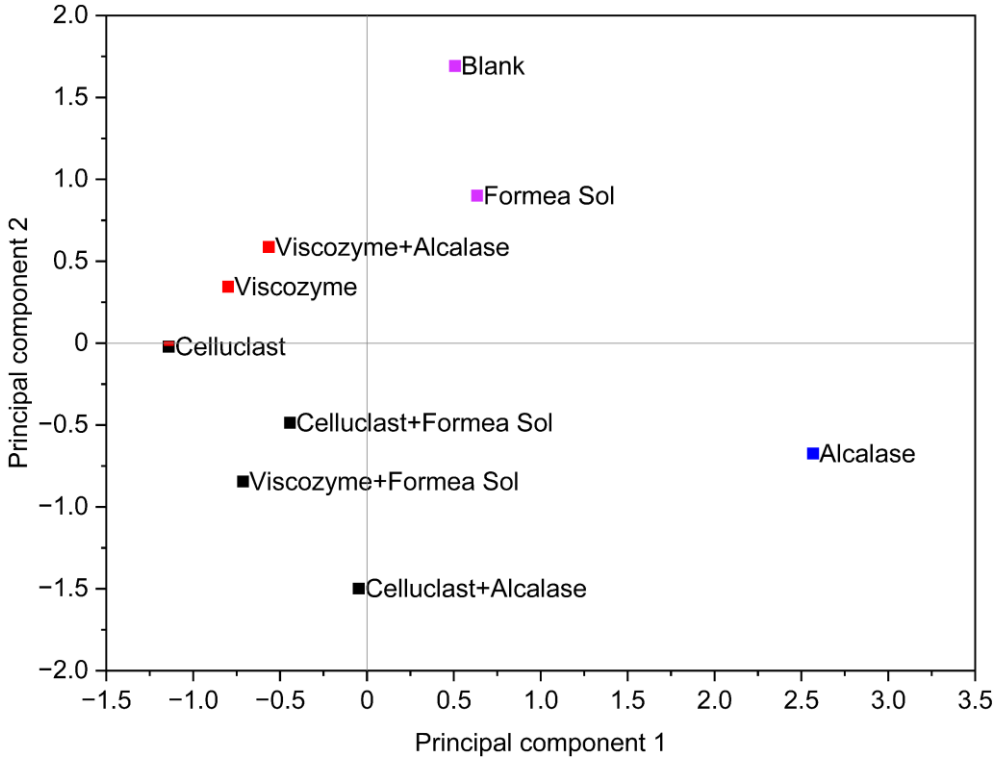

Figure 53: Principal component analysis of the co-extraction of sugars and organic acids from BSG with different enzymes and enzyme combinations. Principal component 1 = differences in organic acid release. Principal component 2 = differences in sugar release.

Overall, the proteases are separated from the cellulases by their differences in organic acid release. Especially Alcalase® is clearly separated from all other enzymes by its ability to release organic acids. This supports the assumption that a different mechanism of extraction is present. The incubation of BSG with the single carbohydrases resulted in the lowest effect on organic acid release. The co-incubation together with the proteases resulted in more balanced contents of organic acids compared to the released sugars. Viscozyme® in combination with the proteases resulted in slightly lower organic acid releases than the co-incubation of Celluclast® with them. Overall, the results from the principle component analysis suggest that the co-incubation caused synergistic or differentiated effects on sugar and organic acid extraction that differ from the effects of applying single enzymes individually.

For the overall purpose of extracting maximum levels of protein it can be concluded that high-shear mixing in combination with one of the two proteases Alcalase® and Formea® Sol is a promising approach for extracting protein from BSG. Since no additional benefit in terms of maximizing the protein yield was present when using carbohydrases as a pretreatment prior to protease addition, the next strategy for optimizing the process was increasing the power input for mixing and focusing on investigating the transferability of the results to a larger scale.

Scale-up of Protein Extractions to 35 kg scale

As high-shear mixing combined with enzymatic extraction proved to be a promising approach for BSG protein extraction, the focus was on scaling up the process to the 35 kg scale and investigating relevant process parameters for industrial operation. The scale-up relates to a factor of 700 compared to the 50 g lab-scale extractions of the previous chapters. For this purpose, the 100 L HSM batch reactor was used. Details regarding the design of the device are given in chapter 3.7.1. The main idea was to investigate the transferability of the results obtained at laboratory scale and to identify the influence of power input and scale on the protein yields achieved. The use of the high-shear mixer also allows for a process intensification approach as the unit operations of particle size reduction, sterilization, protein hydrolysis and inactivation could be performed in a single unit. If successful, this new approach would enable both a reduction in the CAPEX for the BSG valorization line and a dramatic reduction in the footprint of the overall plant.

The first step in investigating this approach was to characterize the mixing time and behavior when using the top-mounted agitator at different power inputs. 100% power relate to 53 rpm. The following Table 44 summarizes the obtained mixing times for tap water.

Table 44: Mixing time of 1 L 0.01 M NaCl solution in 34 L tap water using top-mounted agitator at varying power inputs.

Power input [%]	Mixing time [s]
50	69.0 ± 10.6
75	43.0 ± 2.0
100	34.7 ± 6.0

In addition, the Newton number was calculated and plotted against the Reynolds number to investigate the efficiency of power input in relation to fluid flow behavior in the system. The following Figure 54 summarizes the results obtained.

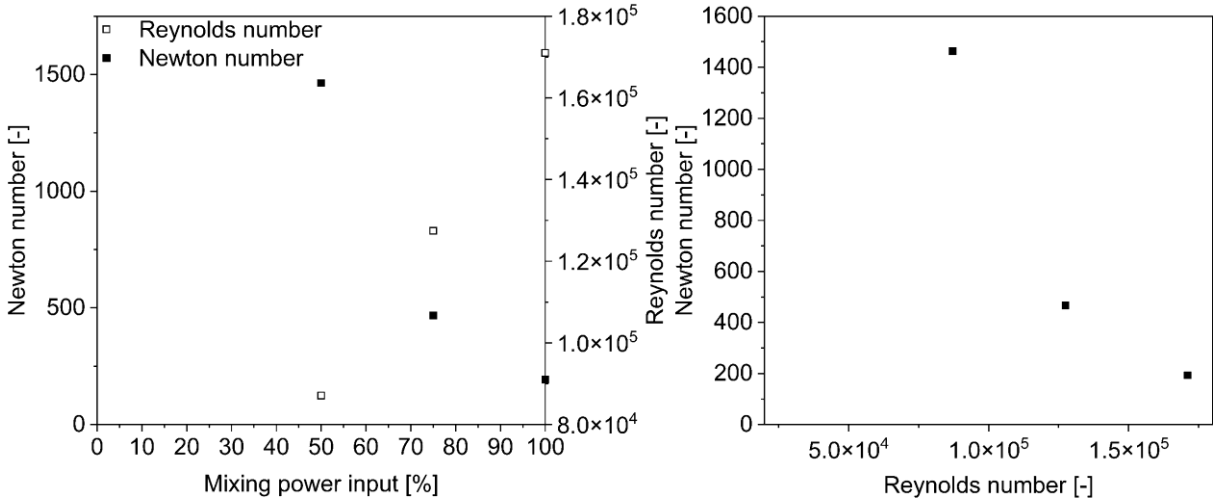

Figure 54: Left: Newton and Reynolds number over mixing power input. Right: Power characteristic of the top-mounted agitator in the 100 L HSM batch reactor.

The obtained Reynolds numbers are all below 20000. For a stirred tank reactor, this indicates a transitional flow regime in between laminar and turbulent flow [70]. This finding is supported by the fact, that the Newton number decreases with increasing Reynolds number. In a laminar flow regime, the Newton number would decrease linearly with increasing Reynolds numbers while in the turbulent regime, the Newton number would be constant due to the dominating inertia forces [71]. Generally, low Newton numbers in a turbulent flow regime are desirable for high mass transfer rates at low OPEX. For the use of a BSG and water suspension instead of

the pure tap water used for the above data, a higher viscosity and density are expected. This will most likely affect the mixing time and with it the overall mass transfer negatively. It is thus highly likely, that mass transfer limitations will occur during the subsequent protein extractions from BSG. From an equipment design perspective, a higher power input for the top-mounted agitator is desirable. The currently installed 2.2 kW are not sufficient to result in a turbulent flow regime. Although mass transfer was expected to be limited, the potential of using the high-shear mixer for BSG protein extractions was still evaluated. For this, a new batch of BSG folowing the recipe RubyRoast was produced in the Campus Perle brewery. Its compositional profile is given in Figure 55.

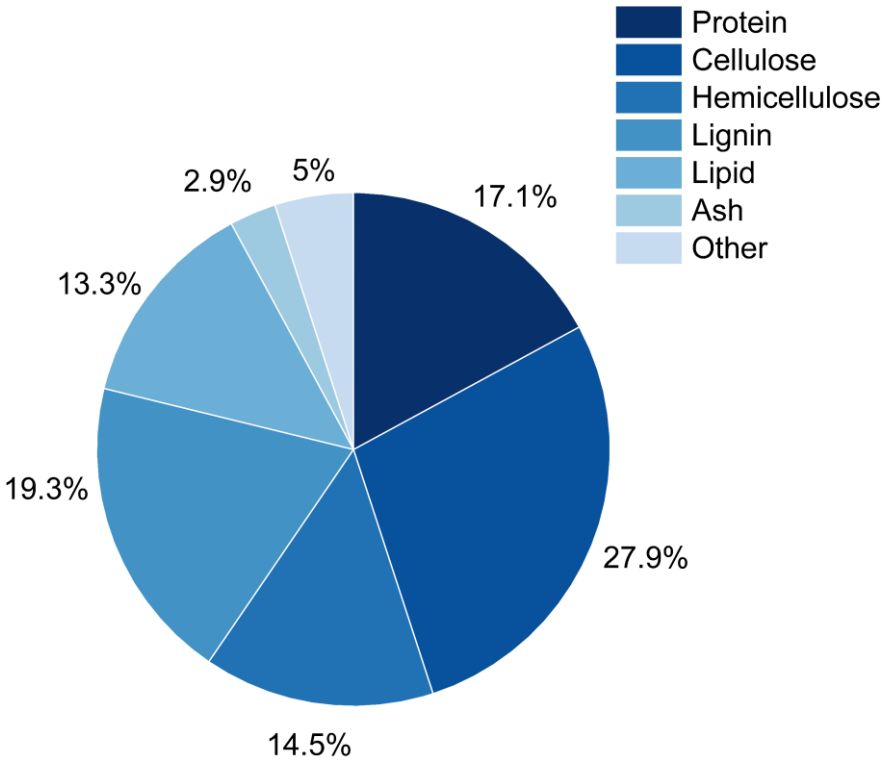

Figure 55: Compositional profile of BSG used for screening trials in 100 L HSM batch reactor.

The protein, cellulose, hemicellulose, lignin and ash contents for the BSG are in the same order of magnitude as for all other BSG batches brewed with the recipe RubyRoast at the Campus Perle brewery. The lipid content is slightly higher with 13.3 ± 1.5% compared to 8.1 ± 0.4% for a representative BSG batch. This might be a result of a different harvest of the barley malts used, which fluctuate depending on the season [166]. As the focus of the screening study was on protein extraction, and the main factors influencing enzymatic extractions are assumed to be the accessibility of the protein through the lignocellulosic matrix and the protein content itself, the lipid content is assumed to be less critical and comparability to previous results still given. The particle sizes obtained for untreated and 5 min as well as 10 min HSM BSG are given in Table 45. The particle size of the 50th percentile decreased about 2.3-fold, being comparable to the previously stated particle size reductions during HSM for BSG.

Table 45: Particle size distribution of untreated BSG and after 5 and 10 min of high-shear mixing (HSM) for screening trials in 100 L HSM batch reactor.

Sample	$d_{x,10}$ [µm]	$d_{x,50}$ [µm]	$d_{x,90}$ [µm]
0 min HSM	366.0	1107.3	2564.9
5 min HSM	180.3	492.0	1354.3
10 min HSM	143.2	488.9	1480.6

With this basic characterization being comparable to the results obtained on lab-scale, a total of four extraction runs were conducted with the experimental conditions described in chapter 4.3.1. For the NaOH extractions, the first trial run was conducted at 20% dry matter content w/v, while the second run was conducted at the lab-scale dry matter content of 10% w/v. For both tested enzyme-assisted extractions, Alcalase® was used at the two previously investigated dosings of 10 µL/g_{dm} and 20 µL/g_{dm} and a dry matter content of 10% (w/v). The same Alcalase® batch was used as for the lab-scale extractions. The activity remained at 2229.2 ± 46.9 U/m. Since no pH control was done during the extractions, the following Figure 56 shows the decrease of pH over time during protein hydrolysis.

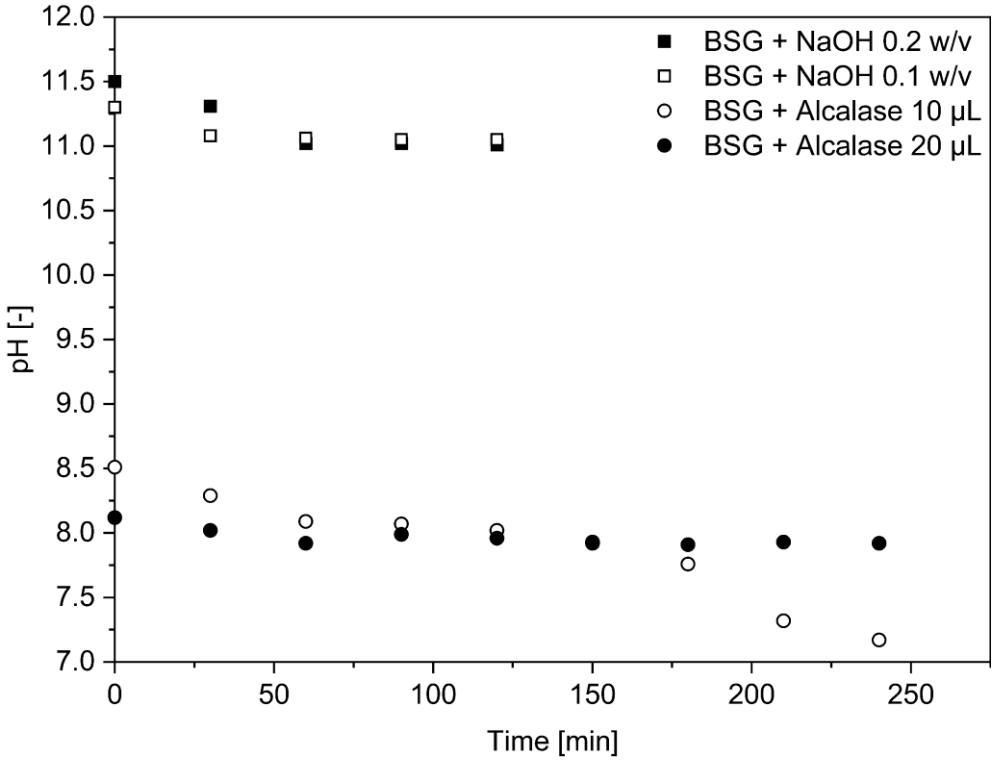

Figure 56: pH over time for protein extraction in 100 L HSM batch reactor at 50 °C and 50% stirring power.

A slight drop in pH can be seen during all extractions. This drop could be an indication of progressive protein hydrolysis, where peptide bonds are hydrolyzed to release carboxylic acid groups on the C-terminal amino acid [167]. Another explanation could be the partial hydrolysis of cellulose and hemicellulose, either directly releasing organic acids or indirectly as a sugar degradation product [149]. The main quality parameter for the extractions is the protein yield. The obtained yields after 2 h of extraction are given in the following Table 46. For the alkaline extraction, the solid to liquid ratio shows to be of great importance for the overall protein extraction efficiency. The extraction yield for a 20% dry matter content (w/v) is half of what was achieved at 10% BSG dry matter to tap water ratio. This might indicate a mass transfer limitation due to the high viscosity of the suspension and the limited power input into the system. Furthermore, it was not possible to separate a liquid hydrolysate fraction directly from the 0.2 w/v samples via centrifugation, which implies downstream processing challenges on larger scales. Compared to the lab-scale results, a similar order of magnitude for protein yield was achieved with 47.4 ± 0.9% on 50 g lab-scale compared to 42.8 ± 8.3% on the 35 kg scale. The slightly lower extraction yield for the larger scale trial runs might be a result of difficulties in maintaining the required extraction temperature over the 2 h extraction period. No active heating was available on-site, which resulted in an average temperature of only 50 °C during the extractions. This deviation could also be the reason for the higher standard deviation compared to the lab-scale results.

Table 46: Mass-based protein yields after protein extractions in 100 L HSM batch reactor at 50 °C and 50% power input for top-mounted agitator. NaOH extractions at pH 11 with 0.1 M NaOH. Enzyme-assisted extractions at pH 8.

Sample	Protein Yield [w/w]
BSG+NaOH 0.2 w/v 120 min	21.4 ± 9.7%
BSG+NaOH 0.1 w/v 120 min	42.8 ± 8.3%
BSG+Alcalase® 20 µL/g_{DM} 0.1 w/v 120 min	60.2 ± 8.2%
BSG+Alcalase® 10 µL/g_{DM} 0.1 w/v 120 min	60.1 ± 5.5%

*Alcalase® activity of 2229.2 ± 46.9 U/mL

For the enzyme-assisted extractions, both dosages of 10 and 20 µL/g_{dm} resulted in the same protein extraction yields of around 60%. Lab-scale extractions were slightly higher with 70.6 ± 0.3% for 10 µL/g_{dm} Alcalase® dosage and 65.2 ± 0.0% for 20 µL/g_{dm}. However, in view of the obtained standard deviation for the larger scale extractions, it is evident, that limitations in terms of reproducibility occurred. One reason might be the sampling size of 0.2 g dry matter required for HPLC analysis of contained amino acids relative to the overall batch size of 35 kg. Additional equipment limitations for drying the remaining solid residue prohibited the direct determination of the total dry weight of remaining solids required for determining the protein yields in the hydrolysate as per equation (7). Instead, the dry matter content of three different samples of each batch was determined and used as a basis for the mass balance calculations. And lastly, the above-mentioned challenges in maintaining a constant hydrolysis temperature could have influenced each extraction run differently.

Next to the protein yield, the specific energy input required per kilogram of extracted protein is a relevant parameter for comparing results obtained with different unit operations. With the installed power on the 100 L HSM batch reactor given in Table 12 and the achieved protein extraction yields, a specific electrical power consumption was calculated. Results are given in Table 47.

Table 47: Specific electrical energy input of BSG protein extraction on 35 kg scale.

Extraction parameter	Power consumption [kWh/$kg_{Protein}$]		
	5 min HSM	120 min agitation	Total
NaOH, 0.1 w/v	1.21	2.91	4.12
Alcalase®, 10 µL/g_{dm}	0.86	2.07	2.94

Due to the overall higher yield obtained for the enzymatic runs, the specific power consumption per mass of protein extracted is lower than for the chemical extraction using 0.1 M NaOH. Most of the power is required for stirring during the 2 h extraction period, especially considering the expected mass transfer limitations mentioned above due to the limited power supply. For an optimized process, a higher electrical power consumption is expected to be required during this period. In addition, the thermal energy demand was not considered as it is highly specific to each on-site condition. During 5 min of high-shear mixing, a temperature increase of about 20 °C was observed for each experiment. Depending on the initial temperature of the BSG water slurry, the thermal energy demand will vary. In addition, the heating medium used could be compressed steam or water at different temperature levels, either supplied by heat-coupled systems using the excess heat typically available on site in breweries. However, if the valorization line is a stand-alone system in an external facility, the heating demand would have to be calculated differently. With this in mind, no estimation of the heating demand has been made, as the variability does not allow for generalized assumptions.

Influence of Brewing Type Variations on BSG Protein Extractions

One of the major challenges in designing valorization processes for biomass feedstocks is the varying composition of the feedstock itself. In the case of BSG, this is not only due to seasonal and regional differences, but can also be a consequence of the recipe and brewing style used. To understand the influence of these variabilities on the proposed process at the 35 kg scale, BSG particle size distributions and protein extraction yields were evaluated for the different recipes and brewing styles summarized in Table 19. Resulting particle size distributions are given in the following Figure 57.

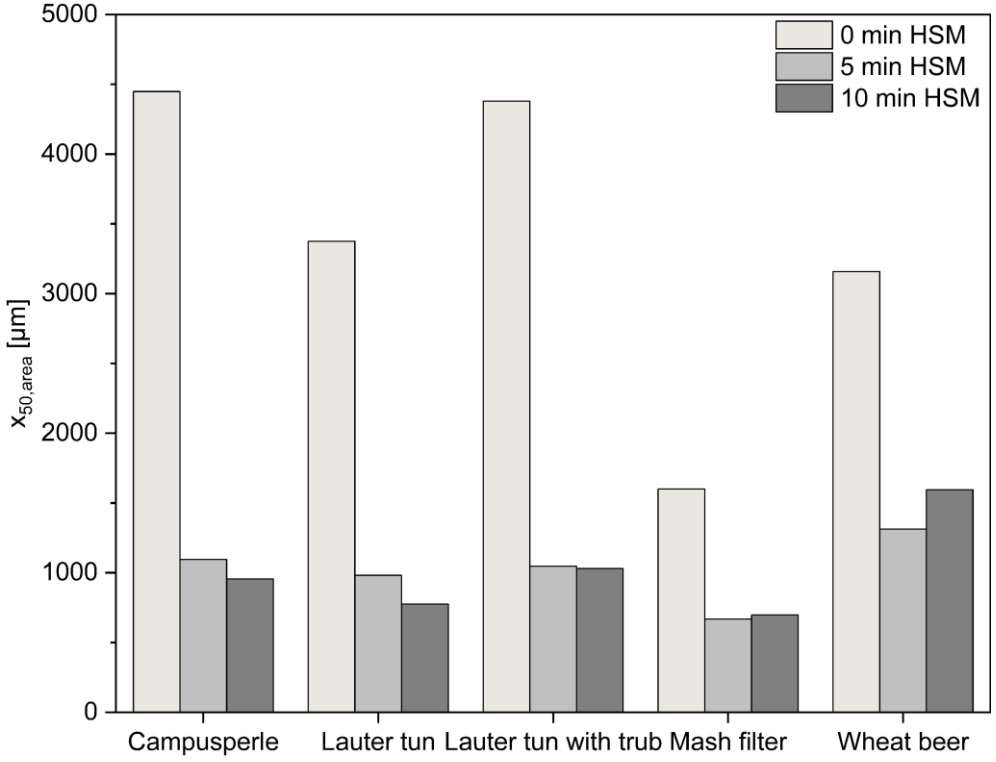

Figure 57: Diameter of equivalent circle of 50th percentile for 0, 5 and 10 min high-shear mixing of different BSG types used.

It is evident, that high-shear mixing resulted in a reduction of the particle size for all investigated scenarios. In general, the same order of magnitude of ≤1000 µm for all types of BSG after 5 min HSM is achieved, with the exception of BSG from wheat beer production. For this BSG type, a median diameter of 1594 µm resulted. With a wheat malt content of > 50 this cereal type might be more resistant to the shear forces acting on the lignocellulosic matrix during high-shear mixing. Therefore, it may be necessary to increase the shear forces applied when wheat malt is present in high proportions. In addition, the mash filter malt has the overall smallest particle sizes before and after high-shear mixing. Wet milling prior to mashing typically reduces malt particle sizes below those possible in lauter tun processes. This type of solid-liquid separation requires intact husk structures and thus larger particle sizes to form the desired filter bed [5]. Finally, it is evident that most of the particle size reduction occurs in the first 5 min of high-shear mixing. If smaller particle sizes are desired, it may be advantageous to adjust the mixer design rather than extend the energy-intensive high-shear mixing time. In the case of wheat beer BSG, 10 min HSM resulted in a higher apparent particle size than after 5 min HSM. This is most likely due to agglomeration of smaller particles during the prior drying step or during measurement of the particle size distribution. Following the particle size reductions, the obtained protein extraction yields for the alkaline and enzyme-assisted processes used in the previous chapter were investigated. The following Figure 58 summarizes the yields obtained. The Alcalase® activity of the used batch was determined as 3620.8 ± 52.9 U/mL.

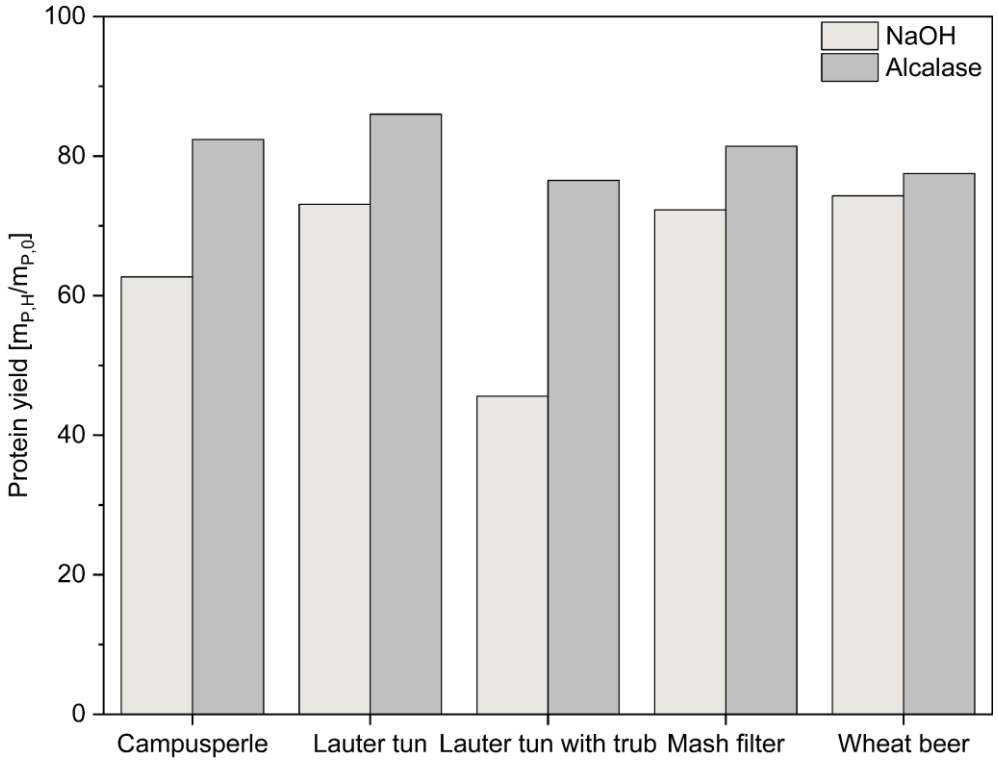

Figure 58: Mass-based protein yields for different BSG types at 10% dry matter content, 60 °C and 50% agitation power (27 rpm). Alkaline extractions at pH 11 using 0.1 M NaOH. Alcalase® extractions at pH 8 and a dosage of 10 µL/g_{dm}.

Due to the required BSG mass per batch, only a single technical replicate was conducted per BSG type and extraction method. A statistical analysis is thus not possible and discussed results only to be taken as an indication for the potential order of magnitude. For the alkaline extractions, the order of magnitude of all protein extraction yields is at 60-70%. This is higher than for previous extraction runs conducted during this work. However, for the present extraction runs, a temperature control was implemented to maintain the 60 °C extraction temperature over the whole 2 h period. It might be, that this increase in temperature resulted in the increase in obtained yields. The order of magnitude is also in line with results reported by other research groups. CONNOLLY ET AL. (2013) reported an extraction yield of 59 ± 5% when running the extraction at 50 °C for 1 h using 0.11 M NaOH at a dry matter content of 0.05 w/v on a 5 L scale [157]. The outlier of the obtained results is the lauter tun BSG, where hot trub was added during lautering. A protein extraction yield of only 45.6% was achieved. This might be a direct result of the hot trubs composition, which is around 50% by mass of protein. Hot trub is the insoluble, denatured protein separated from the wort in the whirlpool after boiling. The once water-soluble proteins extracted from the malt and hops used are denatured during boiling and might thus not be soluble in an alkaline medium such as 0.1 M NaOH. The same BSG without the addition of hot trub did not show this low protein extraction yield under the extraction conditions, further supporting the above assumption. The alkaline extraction method is thus not deemed suitable for protein extraction of hot trub containing BSG. The enzyme-assisted extractions however showed no such outlier for the trub added BSG. Instead, all investigated types of BSG resulted in the same order of magnitude for protein yields: 76-86% by mass. These values are again higher than those reported by other research groups and also higher than for the previous screening extractions of this work. Since only a single extraction run for each experimental condition could be conducted, these values are to be repeated and validated before implementation on a larger scale. Especially, since limits in available equipment on site did not allow for a gravimetric determination of the solids mass after extractions. This implies, that the overall mass balance could not be closed accurately.

The general takeaways from the investigation of brewing type influences on BSG protein extractions are, that both alkaline and enzyme-assisted extractions each resulted in the same order of magnitude for all investigated types of BSG. The only exception being Pilsner BSG from a lauter tun, where hot trub was added as a lautering aid. This BSG is not suitable for extraction with 0.1 M NaOH at pH 11, as only low extraction yields were observed.

Next to the protein yield, the co-extraction of sugars and organic acids was analyzed for the Campus Perle BSG used during the scale-up experiments. The hydrolysates of both the alkaline and enzyme-assisted protein extractions after 120 min were analyzed. In addition, the sugar and organic acid concentrations of the hydrolysates obtained after 10 min high-shear mixing are given in Figure 59. For both high-shear mixed BSG batches, starting concentrations of cellobiose are well above 60 g/L. These high values might be a result of the origin of this BSG from a microbrewery. In contrast to industrial scale applications, mashing is not fully automated and thus heating and holding times for starch solubilization can vary for each brew. It is thus assumed, that the cellobiose concentrations present are a result of incomplete starch and sugar solubilization from the grains during mashing and lautering. It is also evident, that the alkaline extraction reduced the cellobiose concentration to 5.2 g/L, whereas during the Alcalase® extraction, 42.4 g/L remained in the hydrolysate. The mechanism of cellobiose degradation is assumed to be due to a retro-aldol condensation to glucose and subsequent degradation products such as furfural and organic acids [168]. This could then also explain the presence of formic acid and acetic acid in the hydrolysate after 120 min of extraction. In addition, a xylose concentration of 16.7 g/L was found. Xylose is assumed to originate from the hemicellulose backbone of BSG through direct hydrolysis of the glycosidic bonds. While all monosaccharide sugar concentrations remained in the same order of magnitude before the extraction for the Alcalase® process, both formic acid and acetic acid were formed. This is assumed to be a result of the carbohydrase activities detected via the DNS-assay as described in the previous chapter. Generally, the enzyme-assisted extractions led to a lower concentration of degradation products than the alkaline extractions using 0.1 M NaOH.

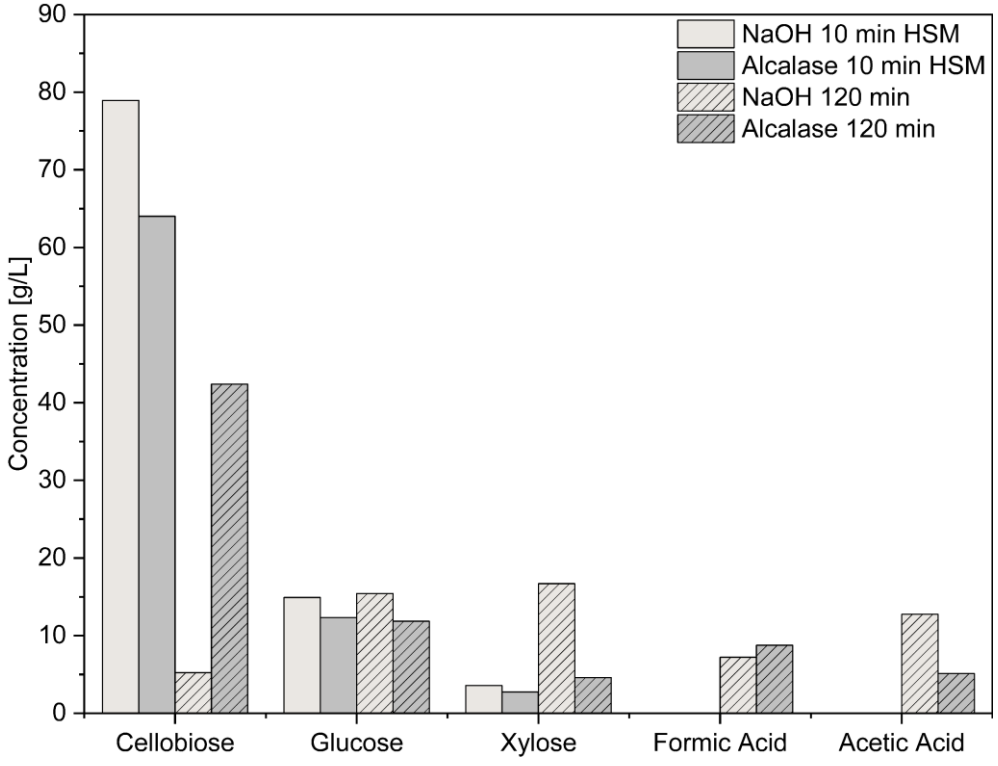

Figure 59: Concentrations of sugars and organic acids in hydrolysates after BSG protein extractions on 35 kg scale. BSG from Campus Perle microbrewery.

Application of BSY Cells on BSG under Autolysis Conditions for Protein Extraction

Next to the use of commercial enzymes, the use of BSY for the hydrolysis of BSG protein was investigated. This co-valorization of BSG and BSY could potentially facilitate to make use of the different by-products in a single valorization process, thus minimizing the overall footprint of the plant. The first approach investigated is the application of whole BSY cells on BSG for protein extraction under autolysis conditions. This endogenous process of yeasts results in the partial degradation of the yeast cell wall by the action of protease and carbohydrase enzymes, which subsequently leads to the release of the inner cell wall components [169]. The release of protease enzymes in their active form would allow the process of cell disruption and protein hydrolysis of BSG to occur in a single step. The following results summarize the findings from a feasibility study using this approach.

Autolysis can be triggered by external stress conditions such as increased temperature and pH changes [170]. On an industrial level, temperatures above 45 °C are commonly used for *S. cerevisiae* autolysis processes [65,170]. Optimized conditions for BSY autolysis reported by other working groups were applied [104,170]. The following Figure 60 summarizes the obtained protein recoveries and protein contents in the supernatants.

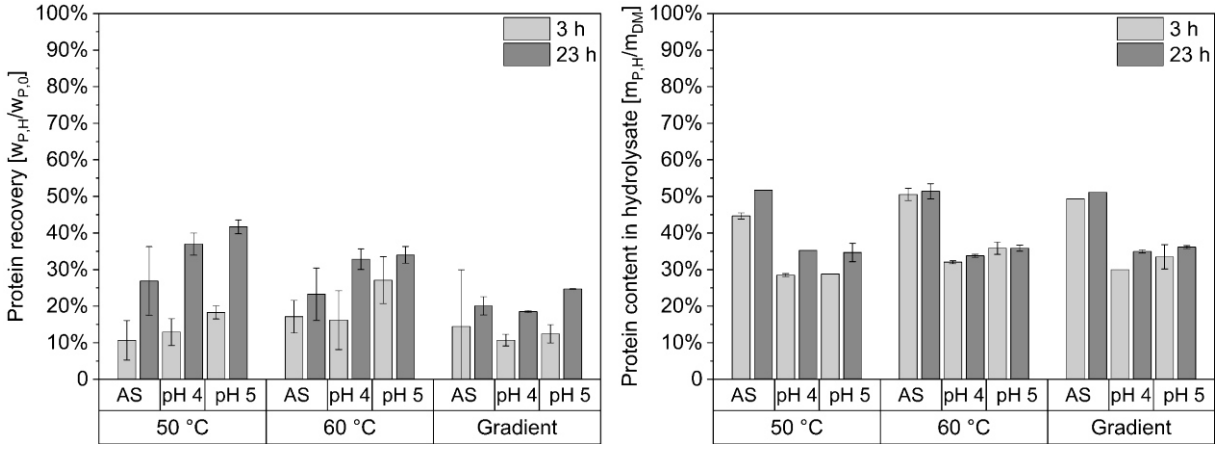

Figure 60: Results from incubation of BSG with BSY at a ratio of 1:1 w/w under autolysis conditions. Left: Protein recovery. Right: Protein content in the hydrolysate. AS = acid shock using 96% H_2SO_4 at 0.01% v/v of BSY suspension. Gradient = Hourly increase of temperature from 45 °C to 60 °C in 5 °C steps.

The first effect observed is the influence of autolysis temperature on the protein recovery. At 50 °C the highest overall protein recoveries were found after 23 h of autolysis with a maximum of 41.7 ± 1.9% at pH 5. This is in line with findings of other research groups for pure BSY autolysis [104,113,170]. The acid shock seems to have a negative effect on protein recoveries observed. However, when taking the protein content into account, this technique led to the highest overall protein contents in the range of 50% based on dry mass. A potential reason, why this is not reflected in the protein recoveries might be due to the definition of this parameter itself, which only takes the protein contents before and after the process based on dry mass into account. Any co-solubilization, which leads to a change in the dry mass is not considered. This is especially prevalent, if the BSG control runs without the addition of BSY are considered, represented in Figure 61. Negative protein recoveries were found due to the high degree of non-protein dry matter solubilized, which could be a result of the solubilization of residual starch or sugars from the lignocellulosic matrix of BSG. As the BSG used came from the Campus Perle microbrewery, where mashing is not automatically controlled by residual starch analyses, but instead based purely on experience values, residual starch-originating sugars could be one of the major components that were solubilized. This is especially the case given that around 10% by mass of the BSG could not be accounted for in the analysis of its compositional profile (see chapter 4.1.1). This effect does not seem to be as pronounced for BSY, where higher protein recoveries than for the combined BSG and BSY autolysis runs were found. It can thus

be assumed, that the reported protein recoveries for the combined runs are underestimating efficiency of protein solubilized due to the dry matter changes associated with BSG.

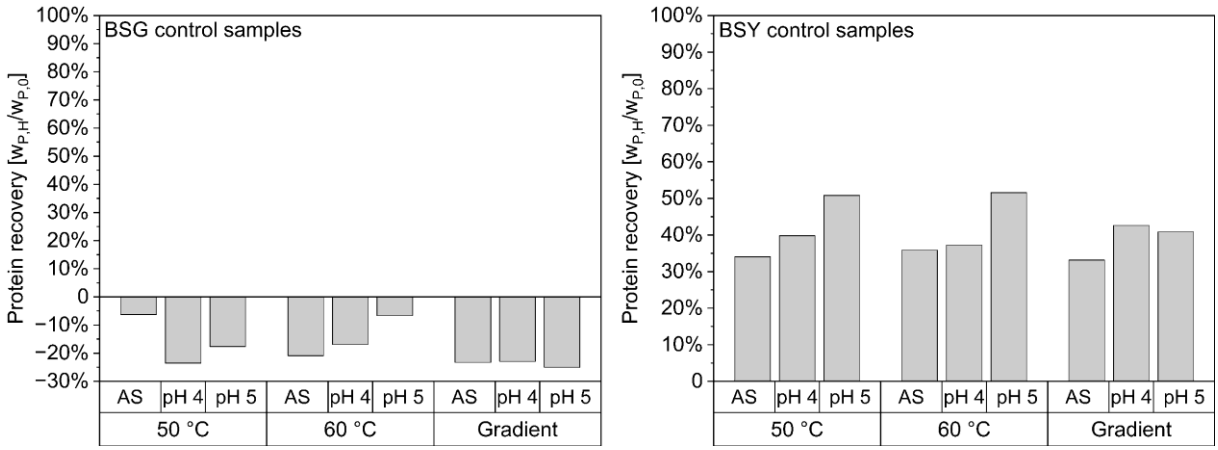

Figure 61: Protein recovery of the control samples from 23 h incubation under autolysis conditions. Left: BSG control samples. Right: BSY control samples. AS = acid shock using 96% H_2SO_4 at 0.01% v/v of BSY suspension. Gradient = Hourly increase of temperature from 45 °C to 60 °C in 5 °C steps.

However, due to the experimental set up, a determination of the dry mass after the autolysis runs was not possible, omitting the possibility of determining the mass-based protein yields. Instead, the protein contents in the hydrolysate were analyzed and used as a basis for comparison. The protein contents of the control samples are given in Figure 62.

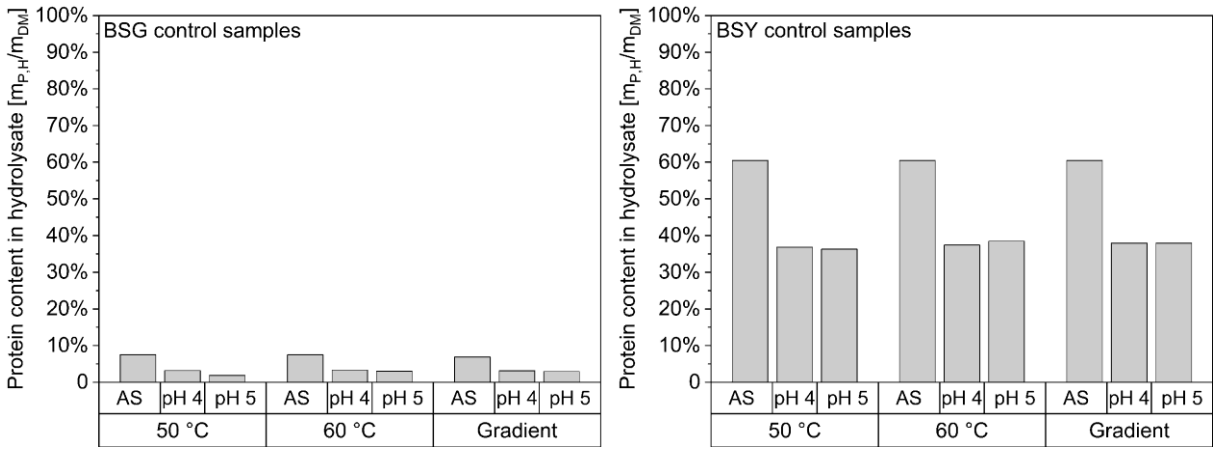

Figure 62: Protein content in the hydrolysates of the control samples from 23 h incubation under autolysis conditions. Left: BSG control samples. Right: BSY control samples. AS = acid shock using 96% H_2SO_4 at 0.01% v/v of BSY suspension. Gradient = Hourly increase of temperature from 45 °C to 60 °C in 5 °C steps.

As can be clearly seen, the autolysis process of pure BSY yielded protein contents above 30% based on dry mass for all investigated scenarios. For BSG, protein contents below 10% based on dry mass were found, in line with the low number of water- and salt-soluble proteins determined during Osborne fractionations. The acid shock aided the pure BSY autolysis to a greater extent than in the case of BSG. For BSY, this is in line with results from other working groups, reporting an addition of 98% H_2SO_4 at 10 µL/g dry BSY at 60 °C to result in a 36.84% protein yield in the produced yeast extract after 2 h [170]. For BSG, it is known that contained protein fractions such as glutelins are soluble in weak acidic solutions [13]. As can be seen in Figure 62, there is a protein content after the acid shock of 7.5% based on dry mass in the hydrolysate, which is in line with these findings. The effect of the acid shock does however also solubilize other components such as sugars from the lignocellulosic backbone of the BSG.

Overall, evaluating the effect of incubating BSG with BSY under autolysis conditions is challenging with the limited data present. Generally, the protein contents found in the hydrolysates were around 10% lower than those obtained for pure BSY hydrolysis in the control runs. However, due to the increased solubilization of non-protein substances from BSG, this value alone does not allow for an evaluation, whether the released BSY proteases were able to hydrolyze BSG protein. Instead, two runs were chosen, where the overall protein mass balance was taken into account. For the two runs specified in Table 48, the protein contents for both the BSG and BSY co-solubilization run as well as the BSY control run resulted in the same order of magnitude of protein content in the hydrolysate.

Table 48: Actual and theoretical yield considering only BSY protein and resulting BSG mass fractions required to close the mass balance for BSG incubations with BSY under autolysis conditions.

Sample	Y_{Actual} $[m_{P,H}/m_{P,0}]$	$Y_{Theoretical,OnlyBSYProtein}$ $[m_{P,H}/m_{P,0}]$	$w_{BSG,Protein}$ $[m_P/m_{dm}]$
50 °C, pH 4, 23 h	37.0 ± 3.0%	32%	22%
60 °C, pH 4, 23 h	32.8 ± 2.8%	29%	18%

Under the assumption, that the protein recovery equals the mass-based yield, around 20% by mass of the protein present in the hydrolysate have to be of BSG origin, when 100% of the present BSY protein is already solubilized. This may indicate that BSY proteases are in principle capable of hydrolyzing BSG protein, in line with the results presented in the following chapter. However, for a definitive conclusion, further experiments are required to investigate the mass-based protein yields as well as optimizing the set up used in terms of particle size reduction of the BSG, varying the BSY content in the slurry and potentially using plasmolysis agents such as ethyl acetate or sodium chloride to aid the autolysis efficiency. Another important factor to consider is the overall resulting complex component mixture. The separation of BSY cell wall originating β-glucans from the remaining solid BSG residue should be investigated to understand the potential of valorizing these two fractions individually after protein extractions.

Application of Proteolytic BSY Extract on BSG Protein

Next to the use of whole BSY cells on BSG for protein extraction, another strategy of co-valorization could be the use of a proteolytic BSY extract on BSG protein for peptide hydrolysis. Most crude protein hydrolysates from plant-based sources do not present the desired flavor profile required for direct human consumption. It is well known, that peptides and amino acids are the most important factors in determining specific tastes of a protein hydrolysate [171–173]. This flavor can be achieved by producing small peptides and free amino acids through a secondary enzymatic hydrolysis step [19,174]. Instead of using commercially available enzymes, the use of a proteolytically active BSY extract is proposed. To evaluate, whether the yeast derived enzymes are able to hydrolyze BSG protein, a crude protein extract thereof was concentrated. Two different protein extraction methods were used as described in chapter 3.7.3 resulting in different protein sizes as shown in chapter 4.3.1. The chosen method of concentration was an isoelectric point (IEP) precipitation. Results from the identification experiments of the isoelectric points for both extraction methods are given in Figure 63. A lower Pierce protein content indicates, that more protein has precipitated.

For the alkaline protein extraction, the lowest protein content in the liquid phase was found at pH 3.5, which is assumed to be the isoelectric point of most of the contained proteins. The precipitated protein pellet had a protein content of 22.6 ± 1.4% based on dry matter. For the enzyme assisted extraction, no clear isoelectric point was found. The region of pH 3-4 yielded the lowest Pierce protein content in the liquid phase. The highest protein content in the protein precipitate was found at pH 4 with 29.2 ± 2.4% based on dry matter, whereas the highest overall mass of the precipitate was found at pH 3.

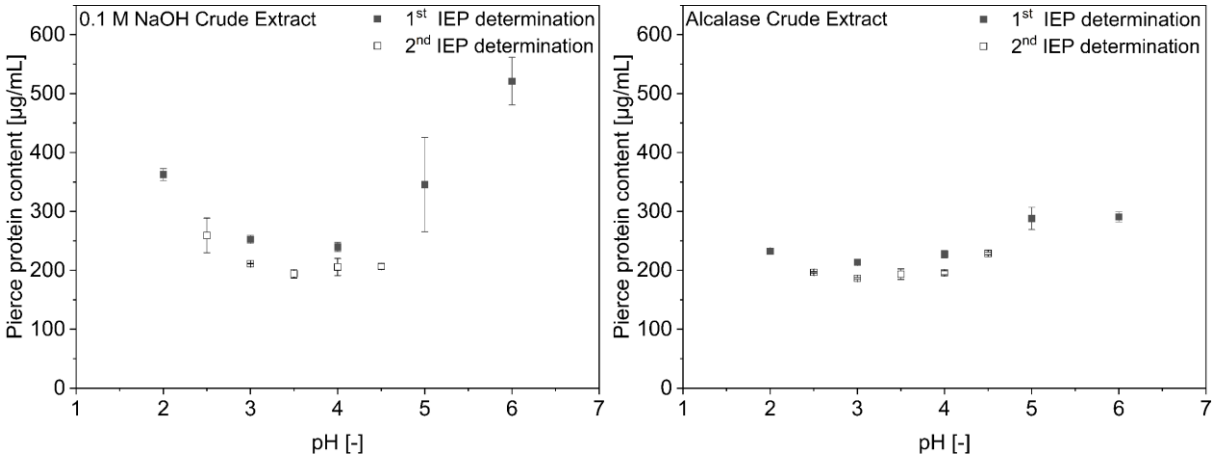

Figure 63: Pierce protein contents in hydrolysates after isoelectric point precipitations at different pH. Left: Crude extract from alkaline treatment. Right: Crude extract from Alcalase® treatment.

Since the aim of the precipitation was a protein concentration for subsequent hydrolysis using BSY proteases, pH 4 was chosen for concentration in the course of this study. The protein precipitate was redissolved in 0.1 M NaPC buffer with the required pH for a first set of screening experiments. For all experiments of the screening phase, the substrate used was from an alkaline BSG protein extraction. Figure 64 summarizes the results from the first experiments at 50 °C, pH 6 and 500 rpm mixing at different enzyme to substrate (E/S) ratios. The activity of the BSY extract used was 1 U/mL.

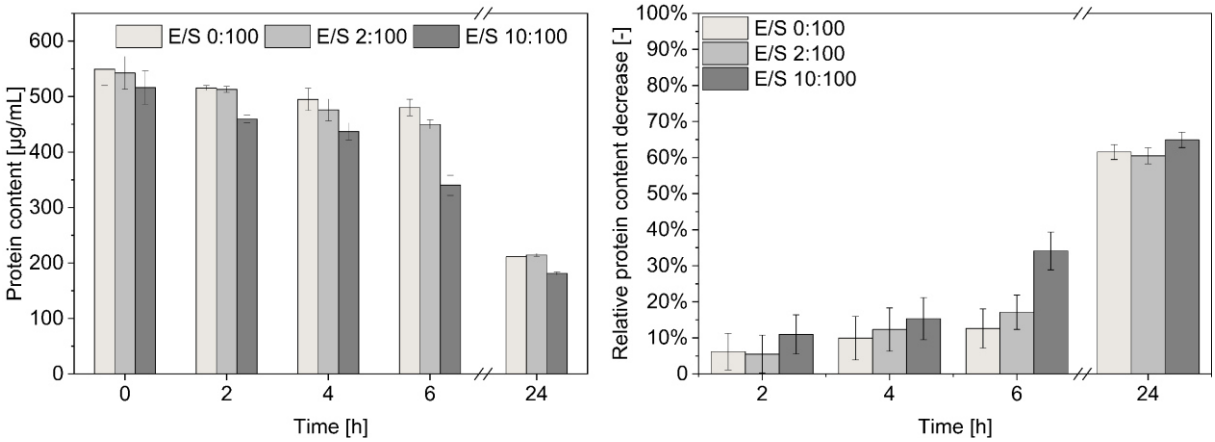

Figure 64: Hydrolysis of BSG protein using a proteolytic BSY extract at 50 °C, pH 6, 500 rpm shaking and E/S of 0-10:100 v/v. Left: Pierce protein content. Right: Relative protein content decrease.

As can be clearly seen, the higher E/S ratio of 10:100 v/v resulted in a visible effect of Pierce protein content reduction, indicating hydrolysis of proteins and peptides to smaller peptides or free amino acids outside of the detection limit of the Pierce reagent. In view of the standard deviation present, no significant effect compared to the control without enzyme addition is present for the enzyme dosage of 2:100 v/v. This is also the case for the relative protein content decrease based on the protein content prior to enzyme addition. However, after 24 h of incubation, the protein content of the control is reduced at the same order of magnitude as the enzyme samples. This might be a result of a contamination, as the hydrolysis runs were conducted under non-sterile conditions. It could also be, that during prolonged hydrolysis times, a complex of interfering compounds for the Pierce reagent was formed. To avoid these interfering effects and since the hydrolysis effect was already present during the first 6 h of incubation, shorter hydrolysis times were investigated during the later optimization phase.

During the ongoing screening experiments, the next factor investigated was the influence of mixing speed on the resulting hydrolysis effects. Results are summarized in Figure 65.

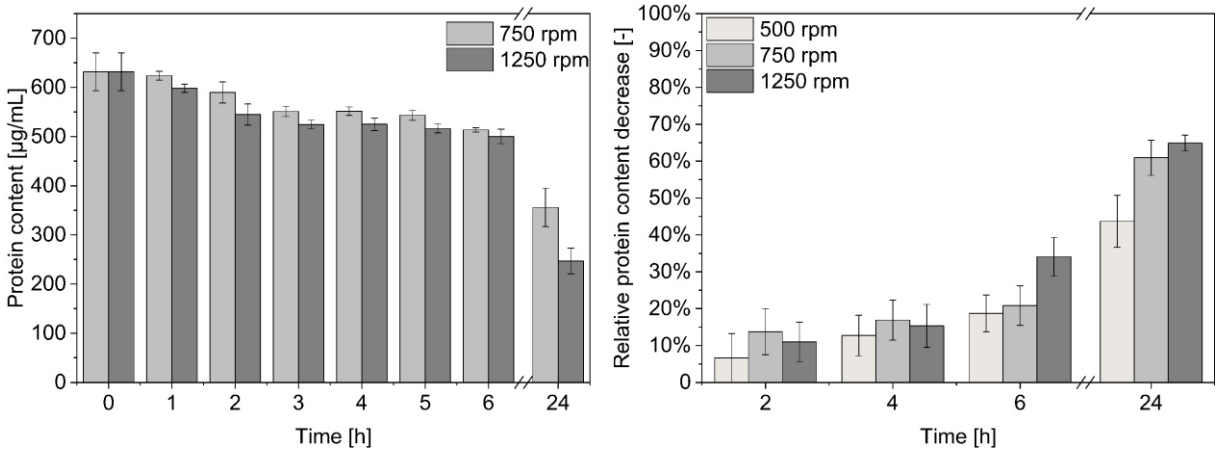

Figure 65: Hydrolysis of BSG protein using a proteolytic BSY extract at 50 °C, pH 6 and E/S of 15:100 v/v. Left: Pierce protein content. Right: Relative protein content decrease.

For a comparison to the results obtained at 500 rpm, only the data points for 2, 4, 6 and 24 h were evaluated for the relative protein content decrease. It can be clearly seen, that higher mixing rates positively affect the resulting relative protein content decrease. In the experimental setup, a thermoshaker was used for mixing. This type of rotational mixing is not comparable to industrial mixing equipment. The mixing rate was thus not considered as an optimization parameter on the small scale, but used as an important factor to consider during scale-up. The last experiment of the screening phase investigated, whether pH influenced the obtained hydrolysis results. For this, the pH was increased from pH 6 to pH 8. All other parameters were held constant. Results are summarized in the following Figure 66.

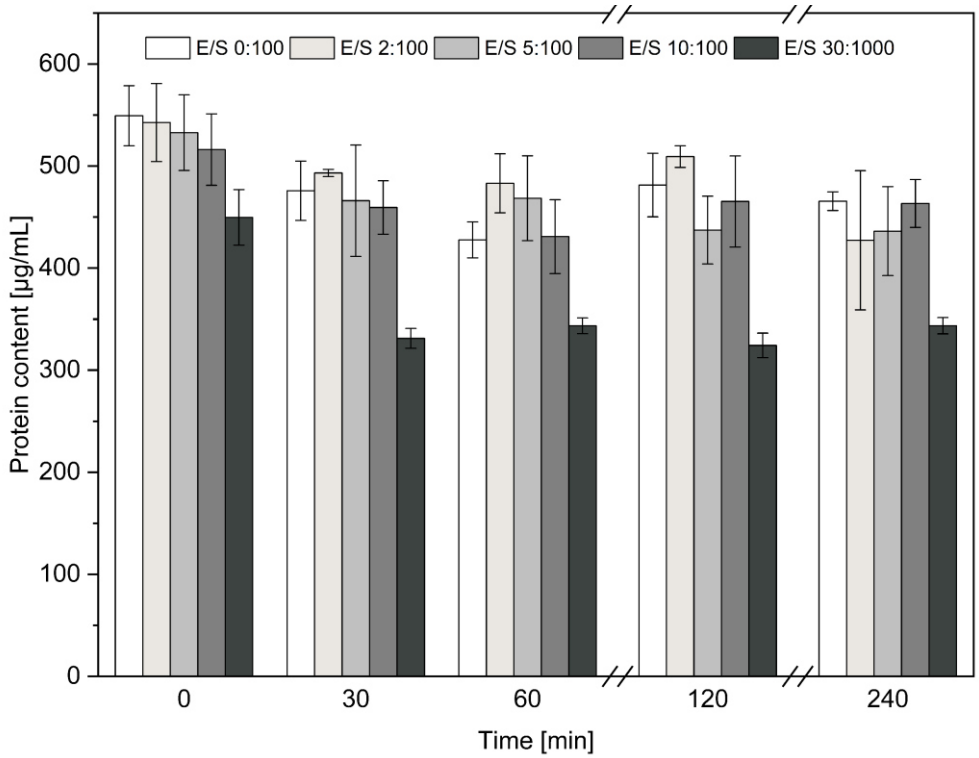

Figure 66: Pierce protein content for hydrolysis of BSG protein using a proteolytic BSY extract at 50 °C, pH 8, 500 rpm shaking and E/S of 0-30:100 v/v.

As can be clearly seen, only E/S ratios above 10:100 v/v were able to reduce the Pierce protein content during the first 30 min, equaling 26.3 ± 5.0% of protein hydrolyzed to peptides smaller than the detection limit of the assay. After this time point, no further reduction is present. It is

assumed, that the proteases are inactivated by pH-driven effects after this time. These findings are in line with the results presented in chapter 4.2.2, where a pH above pH 7 resulted in a drastic decrease in BSY protease activity during 10 min of incubation. Together with the results from the temperature screening presented in chapter 3.6.2, the following Table 49 summarizes the parameters identified for an optimization study.

Table 49: Identified parameters for optimization study of BSG protein hydrolysis by BSY proteases.

Parameter	Value
Temperature [°C]	30 – 60
pH [-]	5.5 – 7
Time [h]	2 – 8
E/S [v/v]	10-30:100

With these parameters, an optimization design of experiments (DoE) was set up, to identify process conditions for maximum protein hydrolysis through BSY proteases. Factors temperature, time, pH and enzyme to substrate ratio were varied and their influence on the relative protein concentration decrease evaluated. The substrate concentration was set to 2.4 mg/mL in pH adjusted 0.1 M NaPC buffer. The BSY extract used had a protease activity of 1 U/mL. The model used as well as experimental conditions applied are summarized in the methods chapter 3.7.3. The full table of experimental results can be found in the appendix in Table A-2.

During DoE evaluations, a quadratic model showed the best fit to the data of the relative protein content decrease. The quadratic model was selected due to the highest polynomial order where the sequential p-value was significant. No transformation was performed. The sequential p-value of the model with <0.0001 was lower than the defined threshold of 0.05 and the model thus considered significant. The resulting regression equation is given in the following equation (29).

$$x_P = 0.7977 + 0.0543A - 0.2119B - 0.014C + 0.0208D + 0.0852AB + 0.0111AC - 0.0834\mathrm{AD} - 0.0354\mathrm{BC} - 0.0124\mathrm{BD} + 0.0388\mathrm{CD} - 0.0988\mathrm{A}^2 - 0.2093\mathrm{B}^2 + 0.0962\mathrm{C}^2 - 0.0175D^2 \quad (29)$$

With x_P representing the relative protein content decrease [-] and the factors *A*, *B*, *C* and *D* representing temperature [°C], pH [-], time [h] and enzyme to substrate ratio [v/v], respectively. It is important to note that this is a black-box model, which means that recognizing the physical and chemical reasons behind the model's behavior is difficult, as it is based on a purely empirical approach. The statistical significance of equation (29) was tested by an F test analysis and an analysis of variance (ANOVA) using the software Design Expert 12. The following Table 50 summarizes the obtained results. The p-value of the obtained model was significant (p=<0.0001), while the Lack of Fit term was not significant (p=0.0553), indicating that the regression equation has a good fit and describes the relationship between the factors and the resulting protein content decrease well. The factors temperature and time showed a significant effect on the output variable, whereas the effect of time and pH were not identified as significant. A potential reason could be, that the investigated design space was not in an ideal range to observe effects. From the model graphs it could be seen, that the maximum protein hydrolysis did not increase with time.

Table 50: Regression coefficients and their significance on the relative protein content decrease in the central composite design model.

Source	Sum of Squares	df	Mean Square	F-value	p-value	
Model	1.08	14	0.0771	35.50	< 0.0001	significant
A-Temperature	0.0360	1	0.0360	16.57	0.0022	significant
B-pH	0.5987	1	0.5987	275.63	< 0.0001	significant
C-Time	0.0023	1	0.0023	1.05	0.3307	
D-E/S	0.0064	1	0.0064	2.92	0.1180	
AB	0.0530	1	0.0530	24.39	0.0006	significant
AC	0.0009	1	0.0009	0.4310	0.5263	
AD	0.0590	1	0.0590	27.16	0.0004	significant
BC	0.0084	1	0.0084	3.85	0.0780	
BD	0.0012	1	0.0012	0.5601	0.4715	
CD	0.0117	1	0.0117	5.38	0.0429	significant
A^2	0.0354	1	0.0354	16.30	0.0024	significant
B^2	0.1998	1	0.1998	91.99	< 0.0001	significant
C^2	0.0380	1	0.0380	17.48	0.0019	significant
D^2	0.0015	1	0.0015	0.6684	0.4327	
Residual	0.0217	10	0.0022			
Lack of Fit	0.0180	5	0.0036	4.79	0.0553	not significant
Pure Error	0.0038	5	0.0008			
Cor Total	1.10	24				

An example of this is given in Figure 67, where the obtained percentage of relative protein content decrease is not depending on the incubation time. This could indicate, that the hydrolysis took place in the first 2 h of the incubation period and was thus out of the chosen design space. Another potential explanation arises due to the two maxima identified at temperatures above 40 °C. One of these maxima occurred at low incubation times supporting the previous assumption. The other is visible around an 8 h incubation period. A potential reason could be the coupled processes of precipitation or agglomeration of already hydrolyzed proteins with heat-activated enzymes. These enzymes could hydrolyze the precipitated or agglomerated proteins to smaller peptides once they are present in their heat-activated form. To validate this assumption, the crude enzyme extract would need be purified into individual proteolytic fractions containing only one enzyme type. Then, subsequent incubation experiments must be conducted under the same conditions as the present trials.

Regarding the enzyme to substrate ratio, it may be that the ratios used were too small to make a significant difference in the relative decrease in protein content. It may be necessary to either increase the dosage of BSY to observe significant effects or to perform a concentration or purification of the proteolytic extract.

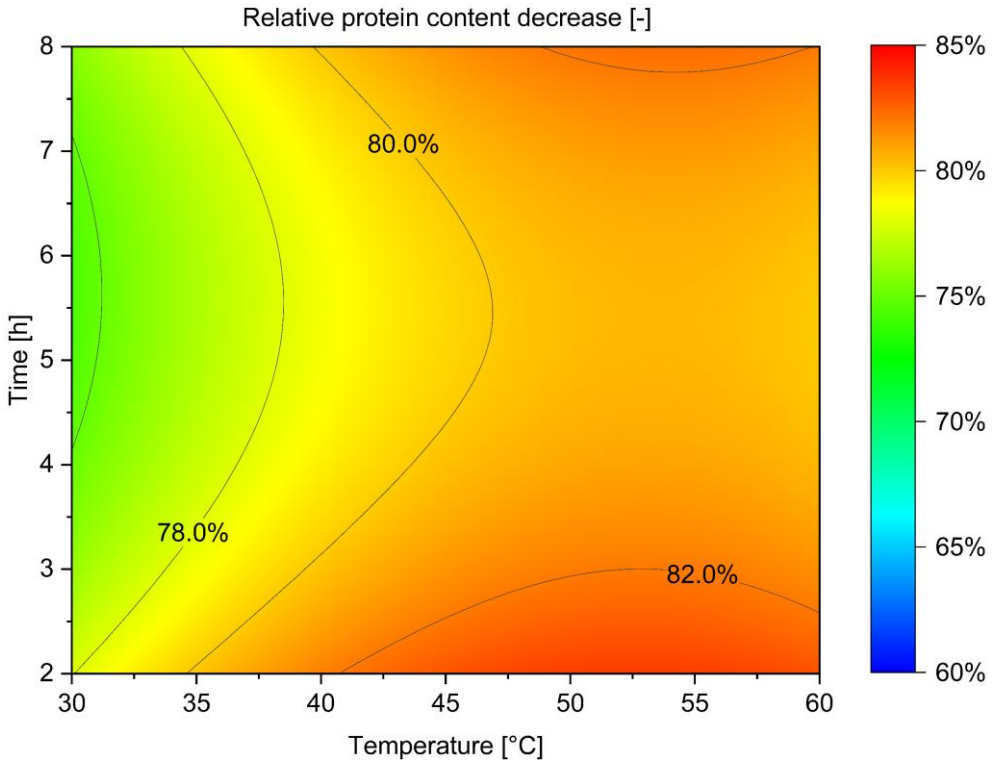

Figure 67: Dependance of the relative protein content decrease on time and temperature. Incubation at pH 6.25 and an E/S ratio of 20:100 v/v.

For the two significant factors, temperature and pH, a clear optimum was identified by the DoE model. At an incubation time of 5 h and an enzyme to substrate ratio of 20:100 v/v, the maximum protein hydrolysis was found at temperatures 36-54 °C and pH 5.5-6.3, as represented in Figure 68.

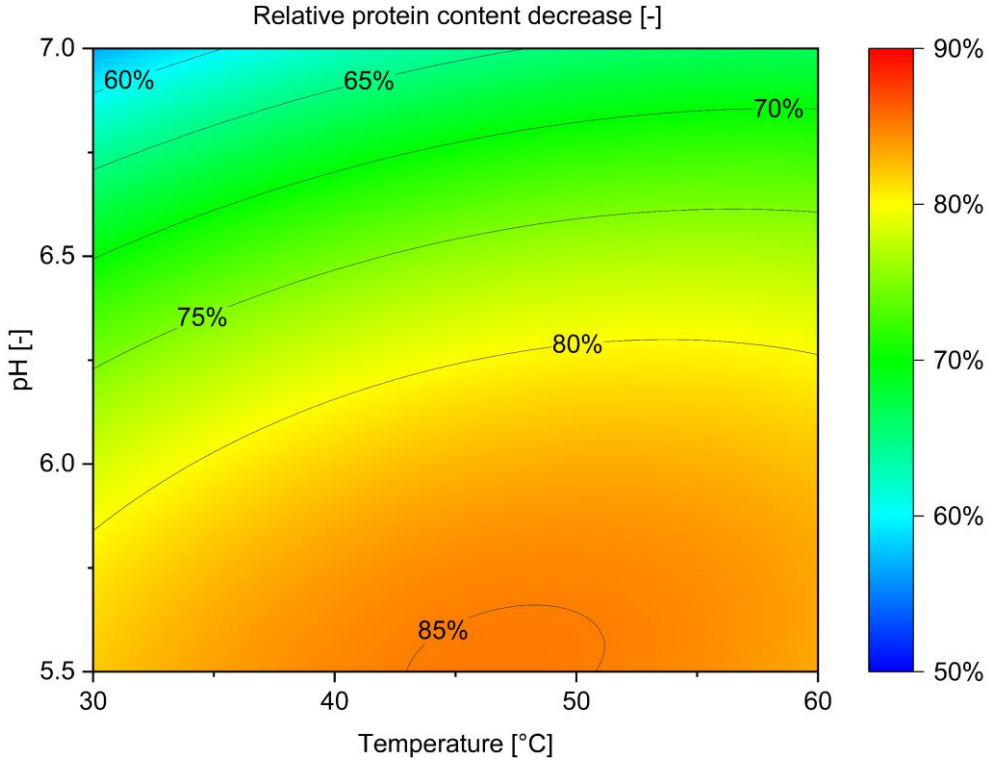

Figure 68: Dependance of the relative protein content decrease on pH and temperature at 5 h incubation time and an E/S ratio of 20:100 v/v.

The identified pH range is in line with the findings from the pH screening in chapter 4.2.2 as well as with intracellular pH values found in the yeast vacuole compartment, where most of the proteolytic activity in the BSY extract is assumed to originate from [130,131]. In the temperature screening of chapter 4.2.2, it could be shown that the BSY extract shows the highest activity on the chosen model substrate azocasein at temperatures 50-60 °C. The linked inactivation of the enzymes at these temperatures was present after 2-4 h, which could be another explanation for the present non-significant effect of temperature on the protein hydrolysis. It may be, that the maximum hydrolysis took place until 2-3 h of incubation time at elevated temperatures and subsequently no further hydrolysis was visible due to most of the BSY proteases already being inactivated.

The model identified the overall optimum for an incubation at 42 °C and pH 5.7 with an E/S ratio of 30:100 for 8 h. With the limitations for the incubation time and E/S ratio as discussed above, the model chose the highest values for these factors in the design space. Since the incubation time is assumed to be a dependent variable on the enzyme inactivation, this parameter should be re-evaluated at times below 2 h.

With these findings and limitations of the DoE study in mind, an exemplary experimental run was used to scale the process up from 2 mL to 50 mL to evaluate the transferability of the results obtained among scale. Results are summarized in Figure 69. For both scales, the same order of magnitude of relative protein content decrease was found for the protein content decrease relative to the negative control at the same time ($x_{P,Rel}$). For the protein content decrease relative to the starting protein concentration (x_P), a value of 75.4 ± 0.6% was found for the 2 mL scale, while the 50 mL yielded a decrease of 66.2 ± 6.6%. The decrease in efficiency is likely due to lower mixing rates at the larger scale, which were limited to 200 rpm in contrast to the 500 rpm on the 2 mL scale due to the experimental setup used.

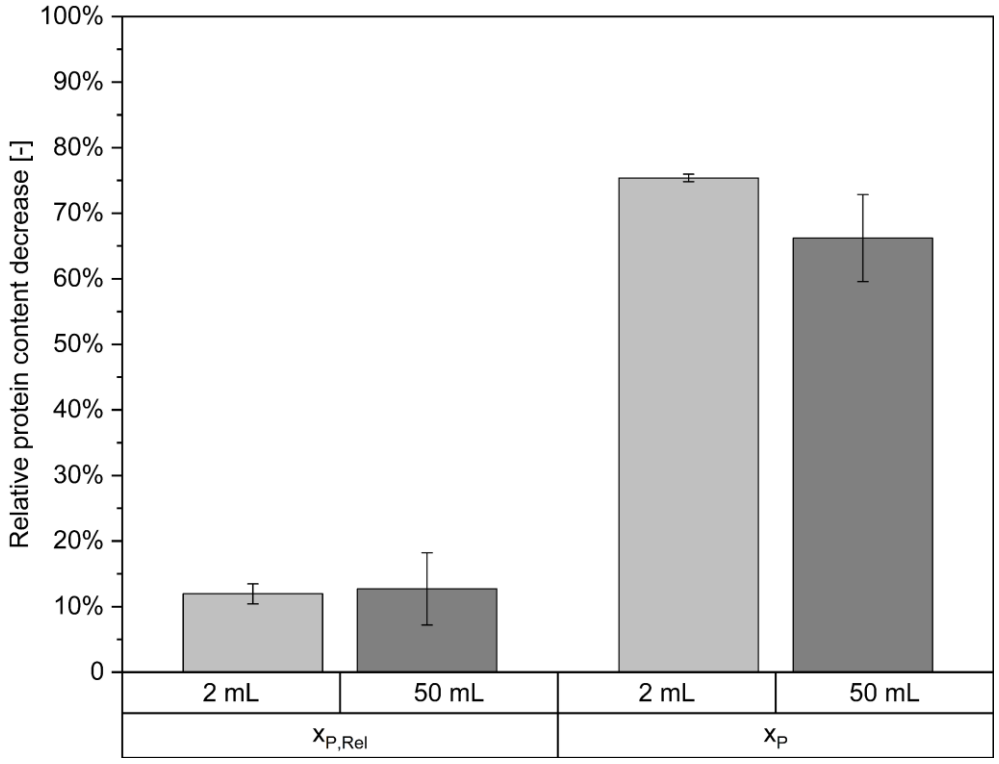

Figure 69: Influence of reaction scale during BSG protein hydrolysis with BSY proteases at 30 °C, pH 6, E/S 30:100 (v/v) for 2 h. $x_{P,Rel}$ = Protein content decrease relative to the negative control at the same time. x_P = Protein content decrease relative to the starting protein content.

Next to the protein content decrease, the degree of hydrolysis was evaluated for the 50 mL scale. In addition, a second experiment with a BSG protein substrate originating from an enzyme-assisted extraction was conducted to enable a comparison to the alkaline extracted protein results. The obtained degrees of hydrolysis are summarized in Table 51.

Table 51: Relative protein content decrease and relative degree of hydrolysis increase for BSG protein hydrolyzed with BSY proteases.

Substrate	x_P [%]	DH_{Rel} [%]
Alkaline extracted BSG protein	66.2 ± 6.6	71.4 ± 1.5
Enzymatically extracted BSG protein	29.3 ± 7.7	24.4 ± 2.3

As expected from the results of the SDS-PAGE given in chapter 4.3.1 for both BSG protein extraction methods, the alkaline extracts contain larger proteins and fragments thereof, which can be hydrolyzed to a higher degree than the already peptized extracts produced via Alcalase® hydrolysis. Since from the seven know vacuolar BSY proteases only two are classified as exoproteases, it was to be expected to see a lower protein content decrease as well as a lower degree of hydrolysis increase for the Alcalase® supported extract. However, since the decisive factor in this feasibility study was to assess, whether BSY proteases are able to hydrolyze BSG proteins, the results are to be considered as promising. Further insights into the protein extracts produced are required to investigate the suitability for use as a food ingredient from a flavor point of view. Additionally, the extracts could be analyzed on bioactivities, which are known to be common in protein extracts with high degrees of hydrolysis [48,49,165].

4.3.2 Sugar Extraction from BSG

In addition to protein extraction, another potential valorization route for BSG is the extraction of valuable components from its fiber fraction. Two different approaches to fractionate the structural carbohydrates were investigated. The first approach focused on the extraction of xylo- and arabino-oligosaccharides for food and nutraceutical applications. If successful, this approach could be coupled with an upfront protein extraction to further valorize BSG-contained components for human consumption. The second approach focused on a non-food application where monomeric C5 and C6 sugars were extracted for subsequent fermentation applications. This approach could also be coupled with an upfront protein extraction process, utilizing most of the remaining structural carbohydrates. The following chapters summarize the results obtained.

Extraction of Xylo- and Arabino-oligosaccharides

New sources of short-chain xylo-oligosaccharides (XOS) and arabino-oligosaccharides (AOS) are highly sought-after in the food sector due to their prebiotic health-benefits in human digestion [175]. In addition, their low caloric value in combination with a mild sweet flavor make them interesting for functional foods [176]. In the case of BSG, the hemicellulose backbone is mostly comprised of xylan and arabinan, making it an interesting substrate for XOS and AOS production [24]. For the current study, a new batch of BSG from the standardized RubyRoast recipe was used, containing 12.4% by mass of hemicellulose. The full compositional profile is given in Figure 70.

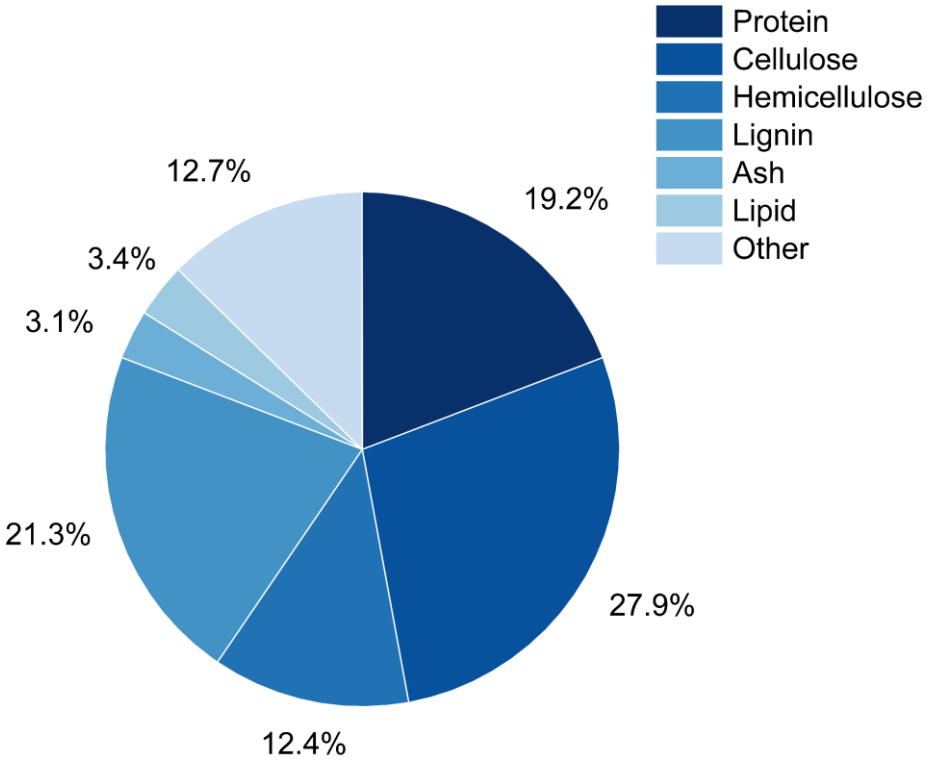

Figure 70: Compositional profile of RubyRoast BSG used for xylo- and arabino-oligosaccharide extractions.

The chosen method for extraction of XOS and AOS is liquid hot water (LHW) treatment with no additional chemicals. This method is known to be able to selectively extract hemicellulose components, when run at biomass specific temperature ranges [148]. Especially with an upfront protein extraction to avoid Maillard reactions and thus undesired side-products, this approach holds high potential for XOS and AOS production. A first set of screening experiments as described in chapter 3.7.4 were conducted on a 30 mL scale. Obtained results for XOS and AOS concentrations are given qualitatively in the following Figure 71.

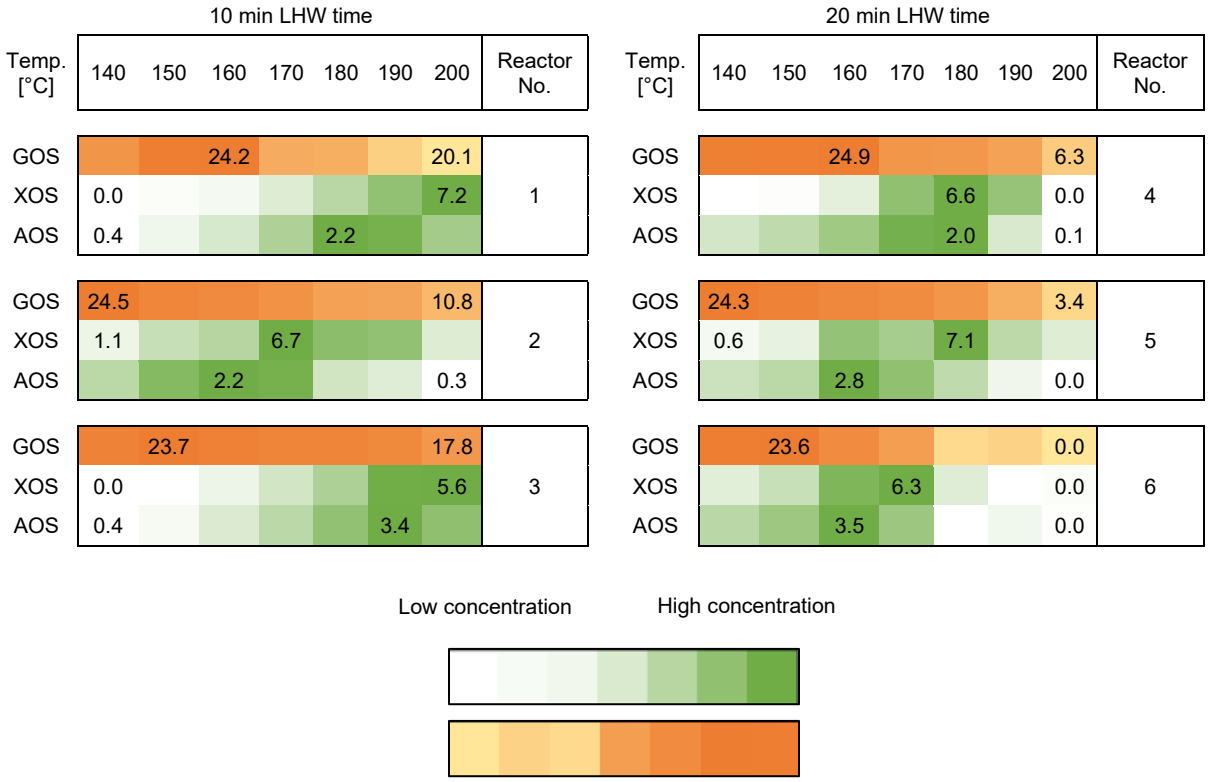

Figure 71: Qualitative oligosaccharide concentrations in hydrolysate after screening experiments on 30 mL liquid hot water reactors. GOS = gluco-oligosaccharide. XOS = xylo-oligosaccharide. AOS = arabino-oligosaccharide.

For each set of conditions, three reactors were run in parallel. For 10 min extraction time, maximum XOS and AOS concentrations were achieved at temperatures 180-200 °C. Reactor 2 showed a deviating trend, where the maximum was found at 160-180 °C. However, during the experiments, a poor temperature control loop was found for this reactor, resulting in an overshooting of the setpoint value and thus irreproducible results. Due to this behavior, results from reactor 2 were not considered for further discussions. For the 20 min LHW treatment time, maximum XOS and AOS concentrations were found at lower temperatures in the range of 160-180 °C. For both treatment times, the order of magnitude for maximum XOS concentrations was in the range of 7 g/L and for AOS in the range of 3.5 g/L. This correlates to overall extraction yields of up to 75.1 ± 2.4% by mass for 10 min LHW treatment at 200 °C and to 74.8 ± 1.5% by mass for 20 min LHW treatment at 180 °C as can be seen in the following Figure 72. The yield is given as a sum parameter for both AOS and XOS masses per mass of hemicellulose in the feedstock. The values for the yields are in line with existing literature on hydrothermal treatments for hemicellulose solubilization. ZETZL ET AL. (2011) reported common solubilization yields of 60-70% by mass [149]. For BSG, a XOS extraction yield of 73% was reported by SWART ET AL. (2022) during steam explosion at 180 °C for 10 min, which is another common hydrothermal treatment used for biomass fractionation [177].

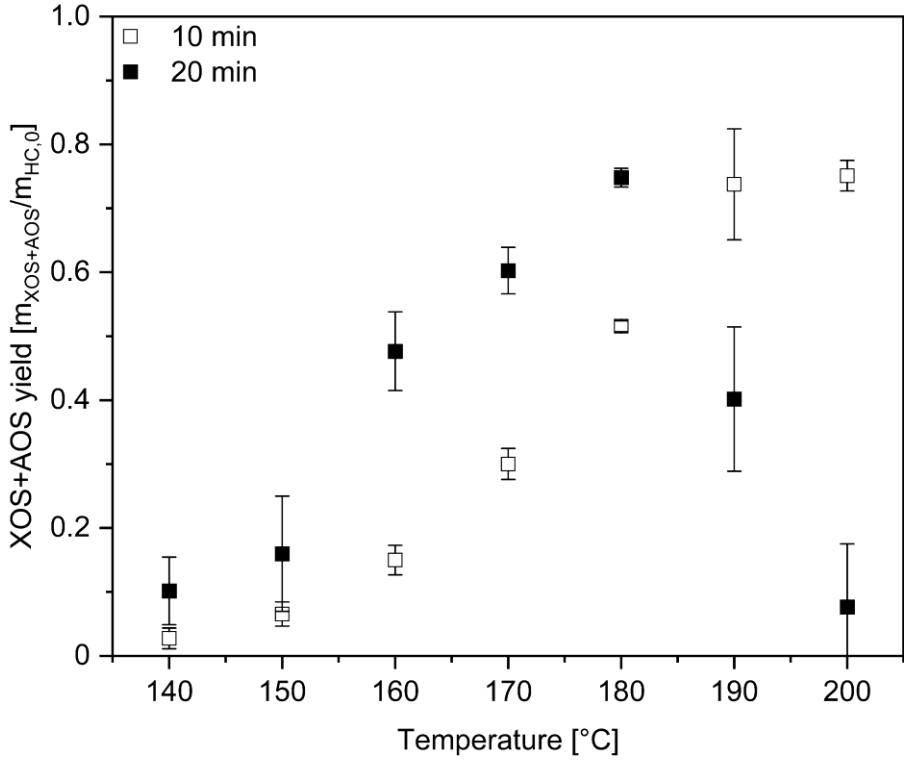

Figure 72: XOS and AOS extraction yield over temperature for LHW treatment at 30 mL scale.

As can be clearly seen, temperatures above 180 °C reduce the achieved XOS and AOS yield for 20 min of treatment time. This is assumed to be a consequence of thermal degradation of the oligomers to monomeric sugars or to degradation products such as organic acids. This theory is supported by the following Figure 73, summarizing the monomeric sugar concentrations over time.

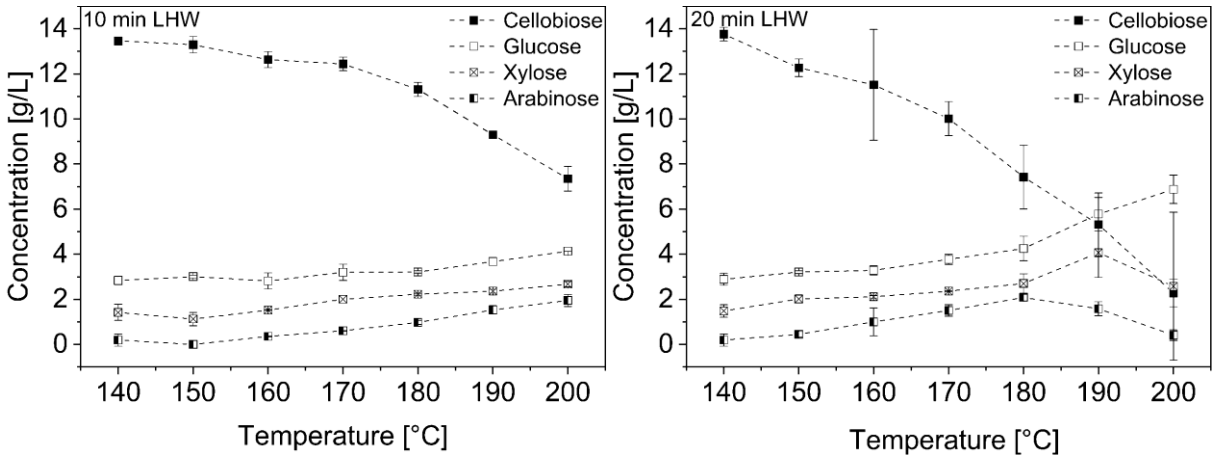

Figure 73: Cellobiose and monosaccharide concentrations for LHW screening experiments at 30 mL scale. Left: 10 min LHW. Right: 20 min LHW. Displayed lines serve solely as a visual aid.

It can be clearly seen, that for 20 min treatment time the C5 sugar concentrations increase with increasing temperature. For xylose, a sharp concentration increase above 180 °C is present, before a decline above 190 °C, most likely indicating a further hydrolysis to organic acids or furfural. Arabino-oligosaccharides seem to be more temperature sensitive and begin to degrade to monomers at lower temperatures until 180 °C. Above this temperature, the rate of arabinose degradation to organic acids or furfural increases above the oligosaccharide hydrolysis to monomeric sugar. This is in line with the AOS concentrations presented in Figure 71, where the AOS concentrations decrease above 180 °C and thus earlier than AOS. In

addition, both Figure 71 and Figure 73 indicate the presence of residual starch in the BSG used. At temperatures below 160 °C, the highest gluco-oligosaccharide (GOS) concentrations were found. Additionally, concentrations of 14 g/L cellobiose were detected at 140 °C, decreasing at higher temperatures. However, it is known in existing literature on LHW treatment for lignocellulosic matrices, that cellulose is not extracted in relevant amounts at temperatures below 200 °C [148,178,179]. With cellulose most likely not being the source of detected GOS and cellobiose, starch is left as the only C6 sugar containing component present in BSG. Starch quantities were not determined in the compositional profile of BSG. However, when closing the mass balance of the compositional profile, a fraction of 12.7% by mass of unidentified components was present. A major part of this fraction is assumed to be starch left in the BSG due to incomplete solubilization during the brewing process. For an industrial BSG this is assumed to be of lower concentration, due to more effective starch solubilization during mashing and lautering. Typically only 1-3% of starch remain in BSG [7]. The results obtained for C6 sugars are thus not considered representative for large scale applications.

With the obtained results from the screening phase, an optimization design of experiments (DoE) was set up, to identify process conditions for maximum XOS and AOS extraction. Factors solid to liquid ratio, temperature and time were varied and their influence on XOS and AOS concentrations as well as corresponding yields and monomeric arabinose and xylose concentrations evaluated. The model used as well as experimental conditions applied are summarized in chapter 3.7.4. The full table of experimental results is summarized in the appendix in Table A-3.

During DoE evaluations, a quadratic model showed the best fit to the data for the mass-based XOS and AOS yields. No transformation was performed. The sequential p-value with 0.013 was lower than the defined threshold of 0.05 and the model thus considered significant. The fit summary is given in the following Table 52.

Table 52: Fit summary of model used for evaluating the combined XOS and AOS yield.

Model	Sequential p-value	Lack of fit p-value	Adjusted R^2	Predicted R^2
Quadratic	0.0130	0.4879	0.7531	0.0026

The quadratic model was selected due to the highest polynomial order where the sequential p-value was significant. The lack of fit p-value was not significant and the model was not aliased. However, a discrepancy exists between the predicted R^2, at 0.0026, and the adjusted R^2, at 0.7531, a difference greater than the commonly acceptable margin of 0.2. This could suggest a large block effect or issues with the model or data. To address this, a total of four confirmation experiments were conducted as described in chapter 3.7.4. The results matched the model predictions within the given confidence intervals as summarized in the appendix in Table A-4 to Table A-7. The model is thus deemed sufficiently accurate to predict XOS and AOS yields within the given experimental set-up and ranges investigated. The resulting regression equation from the model is given in the following equation (30).

$$Y_H = 0.4412 + 0.0161A - 0.0789B - 0.0255C - 0.551AB - 0.1871AC + 0.0655\mathrm{BC} - 0.2215\mathrm{A}^2 + 0.0776\mathrm{B}^2 - 0.0113\mathrm{C}^2 \quad (30)$$

With Y_H representing the XOS and AOS yield in the hydrolysate [-], and *A*, *B* and *C* the factors temperature [°C], solid to liquid ratio [w/v] and time [min], respectively. The statistical significance of equation (30) was tested by an F test analysis and an analysis of variance (ANOVA) using the software Design Expert 12. The following Table 53 summarizes the obtained results.

Table 53: Regression coefficients and their significance on XOS and AOS yield in the central composite design model.

Source	Sum of Squares	df	Mean Square	F-value	p-value	
Model	0.5863	9	0.0651	7.10	0.0037	significant
A-Temperature	0.0026	1	0.0026	0.2829	0.6077	
B-Solid-liquid ratio	0.0622	1	0.0622	6.78	0.0286	significant
C-Time	0.0065	1	0.0065	0.7096	0.4214	
AB	0.0243	1	0.0243	2.65	0.1380	
AC	0.2801	1	0.2801	30.53	0.0004	significant
BC	0.0343	1	0.0343	3.74	0.0851	
A^2	0.1340	1	0.1340	14.61	0.0041	significant
B^2	0.0164	1	0.0164	1.79	0.2134	
C^2	0.0003	1	0.0003	0.0379	0.8500	
Residual	0.0826	9	0.0092			
Lack of Fit	0.0472	5	0.0094	1.07	0.4879	not significant
Pure Error	0.0353	4	0.0088			
Cor Total	0.6689	18				

The p-value of the obtained model was significant (p=0.0037), while the Lack of Fit term was not significant (p=0.4879), indicating that the regression equation has a good fit and describes the relationship between the factors and resulting yields well. Based on the F-values given in Table 53 the order of influence of the three factors on the combined yield is: solid-liquid ratio (B) > time (C) > temperature (A), in which the primary terms B and AC reach a significant level ($p<0.05$). Therefore, the solid to liquid ratio significantly affects the combined yield. However, the solid to liquid ratio is not an independent factor in the observed experimental system. It could also be, that this factor is influenced strongly by the mixing efficiency in the system. On the lab-scale, a magnetic stirrer bar was used to stir the BSG and water slurry at 500 rpm. It could be overserved, that at solid loadings above 10% by mass, part of the solid residue adhered to the inside wall of the reactor cartridge after LHW treatment. Since the experimental set-up using magnetic stirrer bars is hardly comparable to industrial sized stirrer dimensions and power inputs used, this parameter needs to be considered during scale-up of the process. For this, the heat and mass transfer regime in the larger reactor was analyzed. The following Table 54 summarizes the dimensionless numbers obtained.

Table 54: Dimensionless numbers for water under subcritical conditions of 185 °C and 50 °bar in the 3 L stirred tank reactor.

Parameter	Value [-]
Reynolds number	$5.18 \cdot 10^5$
Prandtl number	0.97
Nusselt number	4219.75

The Reynolds number is above 10^5, which indicates a turbulent flow regime for a stirred tank reactor under the given conditions [70]. The Prandtl number with a value of 0.97 is characteristic for water under subcritical conditions and indicates favorable conditions for heat transfer in fluid systems, as the thermal diffusivity dominates the impulse transport [69]. The Nusselt number with a value of 4219.75 represents a system with active convection and turbulence [180]. Overall, a system with turbulent flow and good heat transfer properties is present. However, the given dimensionless numbers were developed for single-phase flow systems. Limitations may arise in the applicability of the used correlations. For suspensions with low solid loadings, small particle diameters and a turbulent flow regime, the given system can, however, be considered as quasi-homogeneous in a stirred tank vessel [69]. However, an additional challenge arises due to the subcritical conditions present in the system. The given

fluid properties resulting in a Prandtl number below 840 are outside of the valid range for the used Nusselt number correlation due to missing data on correlations for subcritical fluid systems. The given data can thus only be taken as estimates for the heat transfer properties of the system. To minimize the risk of potential mass transfer limitations during the scale-up experiments, the lowest solid to liquid ratio from the DoE experiments was chosen, which is in line with highest XOS and AOS yields obtained. The following Table 55 summarizes the conditions identified as optimal under the given experimental setup. These conditions were the basis for the scale-up experiments.

Table 55: Identified optimal conditions from the DoE for XOS and AOS extractions on 30 mL LHW scale.

Parameter	Optimum 1	Optimum 2
Temperature [°C]	185	180
Time [min]	5	10
Solid to liquid ratio [w/v]	0.05	0.05

Next to these identified optimal conditions two further conditions with similar severity factors were tested on the 3 L scale to investigate potential deviations from the lab-scale results. Results for XOS and AOS yields and concentrations obtained are summarized in the following Table 56. Obtained monomeric sugar yields can be found in the appendix in Table A-8.

Table 56: XOS and AOS extraction yields and concentrations on 3 L LHW scale.

Temperature [°C]	Reaction time [min]	XOS+AOS yield [w/w]	XOS concentration [g/L]	AOS concentration [g/L]
185	5	88.3 ± 5%	5.33 ± 0.25	1.57 ± 0.63
180	5	79.3 ± 2%	4.64 ± 0.02	1.55 ± 0.12
180	10	89.9 ± 3%	5.76 ± 0.21	1.26 ± 0.01
170	20	79.1 ± 0.4%	4.74 ± 0.07	1.44 ± 0.04

As can be seen, the highest overall concentrations were achieved for the two optima obtained from the DoE model. Both conditions resulted in the same order of magnitude of XOS and AOS yield of 89% by mass. This value is higher than what has been previously reported for hydrothermal extractions from BSG. ALONSO-RIAÑO ET AL. (2023) reported an oligomeric pentose yield for BSG of 63.96% from a 25 L LHW treatment with a solids content of 5% by mass at 170 °C for 22 min [181]. SWART ET AL. (2021) reported a XOS yield on lab-scale for LHW of BSG at 180 °C for 5 min with a XOS yield of 78% by mass at 15.3% solids loading and 40 rpm stirring [182]. And lastly MICHELIN AND TEIXEIRA (2016) reported a hemicellulose extraction yield of 64.1% for LHW in a 50 mL reactor at 190 °C for 30 min and 10% solids loading resulting in a XOS concentration of 10.1 g/L in the hydrolysate [179]. Potential reasons for the higher XOS+AOS yields might lie in the efficient heat and mass transfer in the pilot-scale reactor of the present work. No dimensionless numbers were stated in the studies of ALONSO-RIAÑO ET AL. (2023) and SWART ET AL. (2021), who were working groups that scaled-up BSG hydrothermal treatments to pilot-scales. Additionally, the applied pre-treatments differed from the present work, that used untreated BSG only. Overall, liquid hot water treatment has been shown to be a promising technique for XOS and AOS extraction from BSG. However, as ALONSO-RIAÑO ET AL. (2023) reported a high amount of proteins and peptides co-extracted during the LHW treatment, this technology is only suitable for food production with an upfront protein extraction process or a sophisticated downstream process removing Maillard reaction products.

Extraction of C5 and C6 Monosaccharides

One of the most important valorization strategies for BSG next to its application in the food sector is its use as a fermentation medium [160]. Recent publications focused on the use of BSG in solid state fermentations to improve its nutritional value or to produce target compounds of interest [27,183,184]. The use of BSG extracts as a medium for submerged fermentations has received increasing attention [15]. A special interest was set on the extraction of C6 sugars for the bioethanol industry [178]. However, most studies focusing on monosaccharide extractions from BSG apply chemical pretreatments with concentrated sulfuric acid, sodium sulfite or energy intensive disruptions like steam explosion [178]. In view of life cycle assessments and especially costs related to the production of fermentation media, new pretreatment and extraction techniques are required to achieve a broad application on an industrial level [178,185]. In line with these objectives, the extraction of C5 and C6 sugar monosaccharides from high-shear mixed BSG by enzymatic hydrolysis was investigated. The BSG originated from a new batch of RubyRoast brewed in the Campus Perle and had the compositional profile given in Figure 74.

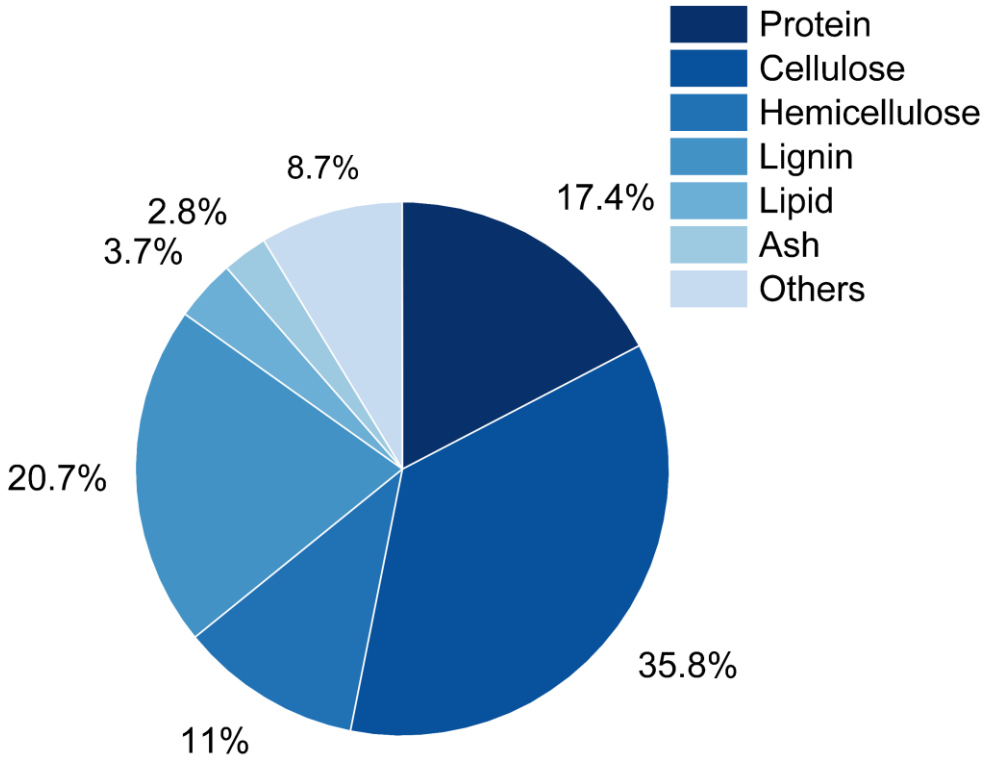

Figure 74: Compositional profile of RubyRoast BSG used for C5 and C6 monosaccharide extractions.

The compositional profile presented a higher cellulose fraction compared to other RubyRoast BSG obtained in this study. This could be a result of a different harvest of the malt used in the brew. To account for this deviation from other RubyRoast BSG used, the mass-based extraction yields will be given wherever possible. The BSG obtained was subjected to high-shear mixing for 0, 2, 5 and 10 min and the resulting particle size distributions are given in Table 57.

Table 57: Particle size distribution of untreated BSG and after 2, 5 and 10 min of high-shear mixing (HSM) in 100 L HSM batch reactor.

Sample	$d_{x,10}$ [µm]	$d_{x,50}$ [µm]	$d_{x,90}$ [µm]
BSG 0 min HSM	2090	4422	6828
BSG 2 min HSM	1274	4530	5233
BSG 5 min HSM	668	1570	4018
BSG 10 min HSM	415	1203	2768

From the data obtained it is evident that the major portion of the particle size reduction takes place during the first 5 min of HSM, specifically between 2 and 5 min. The influence of the different HSM times on the sugar extraction yields obtained after enzymatic hydrolysis were under investigation. In a first set of screening experiments, four different enzyme cocktails were used for monosaccharide extractions. Details on the enzymes used and the experimental design of the screening experiments are given in chapter 3.7.4. The highest obtained monosaccharide sugar yields per enzyme are given in the following Figure 75.

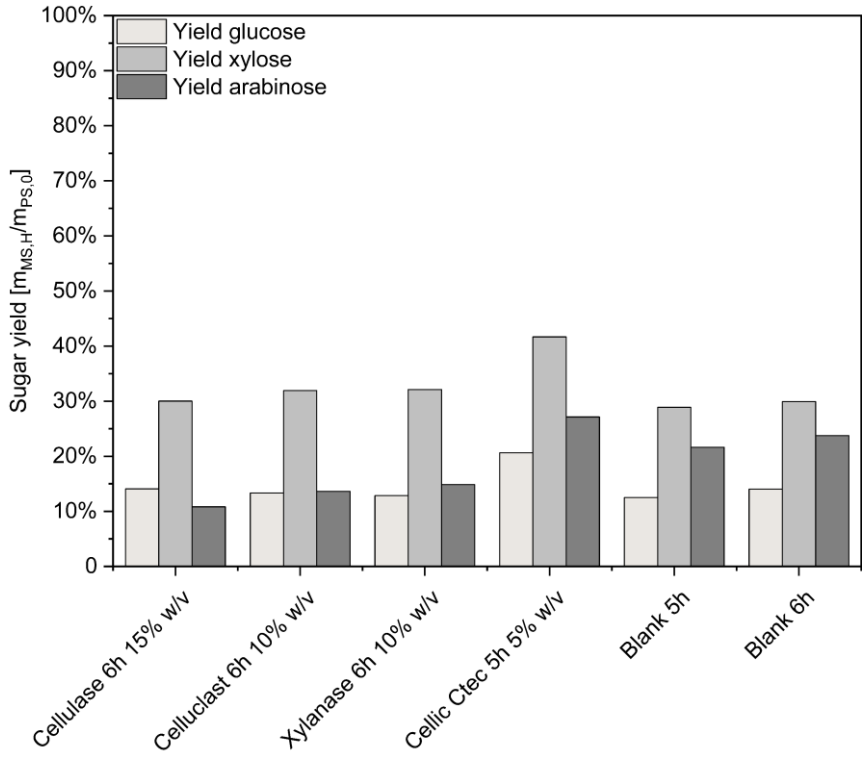

Figure 75: Highest obtained sugar yields per enzyme during screening phase of C5 and C6 monosaccharide extractions. Activity of stock solutions: 10 U/mL. Extractions performed with 5 min HSM BSG at 50 °C, pH 5 and 120 rpm.

As can be clearly seen, only the enzyme cocktail Cellic® Ctec produced extraction yields higher than the blanks without enzyme addition. The relatively high yields in the blanks are assumed to be a result of the high-shear mixing, whereby the lignocellulosic structure is opened up. Additionally, the presence of residual starch after the brewing process degraded by endogenous BSG amylases could potentially lead to the glucose yields of 12-14% in the blanks. For cellulase and xylanase, lower C5 sugar yields than for the blank runs were detected. At the same time, the concentration of organic acids increased by a factor of three for both enzymes. It is thus assumed, that extracted C5 sugars were further hydrolyzed to these by-products, which lowers the apparent C5 sugar yields. All achieved concentrations for the screening phase are given in the appendix in Figure A-16 to Figure A-19.

The overall lack of observed effects of incubation with the enzymes is thought to be due to low enzyme activity in the stock solutions of only 10 U/mL. For subsequent optimization experiments, the activity in the stock solutions was increased to 100 U/mL. Cellic® Ctec as the best performing enzyme under the non-optimized screening conditions produced 5.84 g/L glucose, 2.20 g/L xylose, 0.87 g/L arabinose and notably 40 g/L cellobiose after 5 h incubation at an enzyme dosage of 5% w/v of the stock solution, 50 °C, pH 5 and 120 rpm mixing. To evaluate transferability of the results obtained to a larger scale, the best performing case from the screening phase was scaled-up from 5 g to 35 kg in the 100 L HSM batch reactor. The following Figure 76 summarizes the results obtained for Cellic® Ctec.

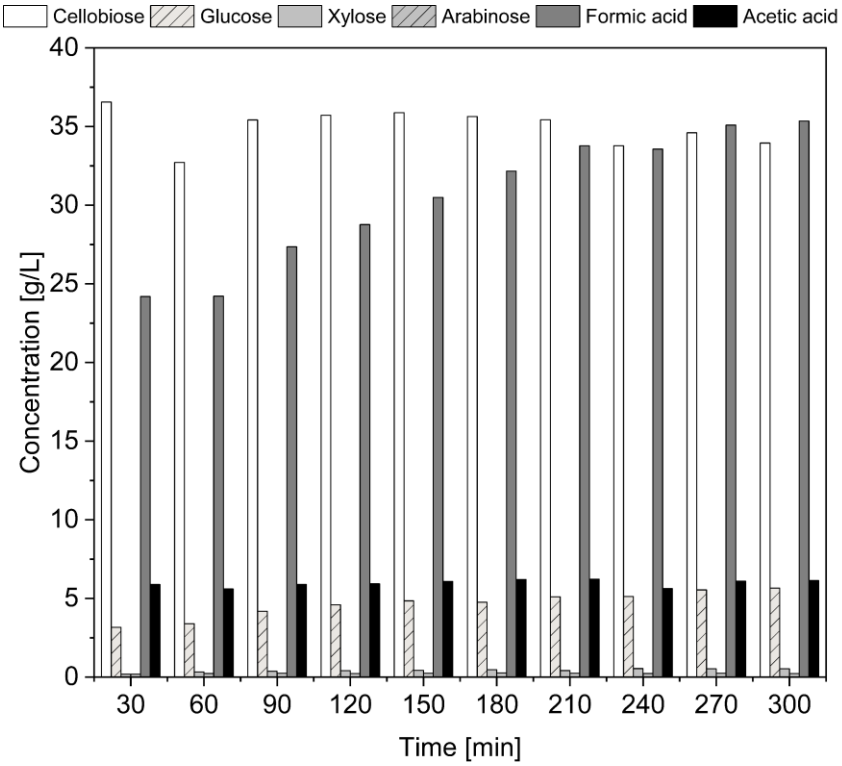

Figure 76: Monosaccharide and organic acid concentrations for scale-up experiment using Cellic® Ctec at 5% w/v enzyme dosage. Activity of stock solution: 10 U/mL. Extractions performed with 5 min HSM BSG at 50 °C, pH 5 and 50% power input of top-mounted agitator (27 rpm).

Over the 5 h extraction time the monomeric sugar concentrations for glucose and xylose increased with every 30 min interval resulting in a maximum concentration of 5.66 g/L glucose and 0.53 g/L xylose. The arabinose concentration however only increased in the course of the first 90 min and subsequently remained constant at 0.23 g/L. The concentration of formic acid increased over the complete extraction period and reached a value of 35.35 g/L. Organic acids can act as fermentation inhibitors depending on the microorganism used. Since the formic acid content is already above 20 g/L at the beginning of the extraction, this is assumed to be due to microbial contamination of the BSG prior to use. The direct sterilization of BSG after lautering is crucial for microbial integrity as well as for all valorization approaches applied as BSG is known to be microbially stable for <24 h under room temperature conditions [14]. In the present study, the BSG was produced during a brew two days prior to the extractions and was stored at 4 °C until use. However, this time might have been sufficient for microbial contamination. Due to missing large-scale equipment and steam on-site, no sterilization of the feedstock was conducted prior to extractions. In a subsequent extraction run, fresh BSG directly from the microbrewery was used, which showed no presence of organic acids at the beginning of the extraction runs as can be seen in the appendix in Figure A-20.

Overall, the achieved concentrations for glucose on the larger scale are within the same order of magnitude as obtained on the 5 g lab-scale. However, both the xylose and arabinose

concentrations from lab-scale experiments are not met. Potential reasons might be limits in the mass transfer efficiency during larger scale extractions, as the viscosity increased over the course of the process and BSG sedimentation occurred. Therefore, it may be necessary to increase the power input to the system over the course of the extraction.

Additionally, it is highly likely, that the assumed microbial contamination led to a decrease in available polysaccharides for hydrolysis. This also implies, that the obtained low monosaccharide yields given in Figure 77 are a result thereof. Especially, since the yields are considerably lower than those obtained for the lab-scale experiments.

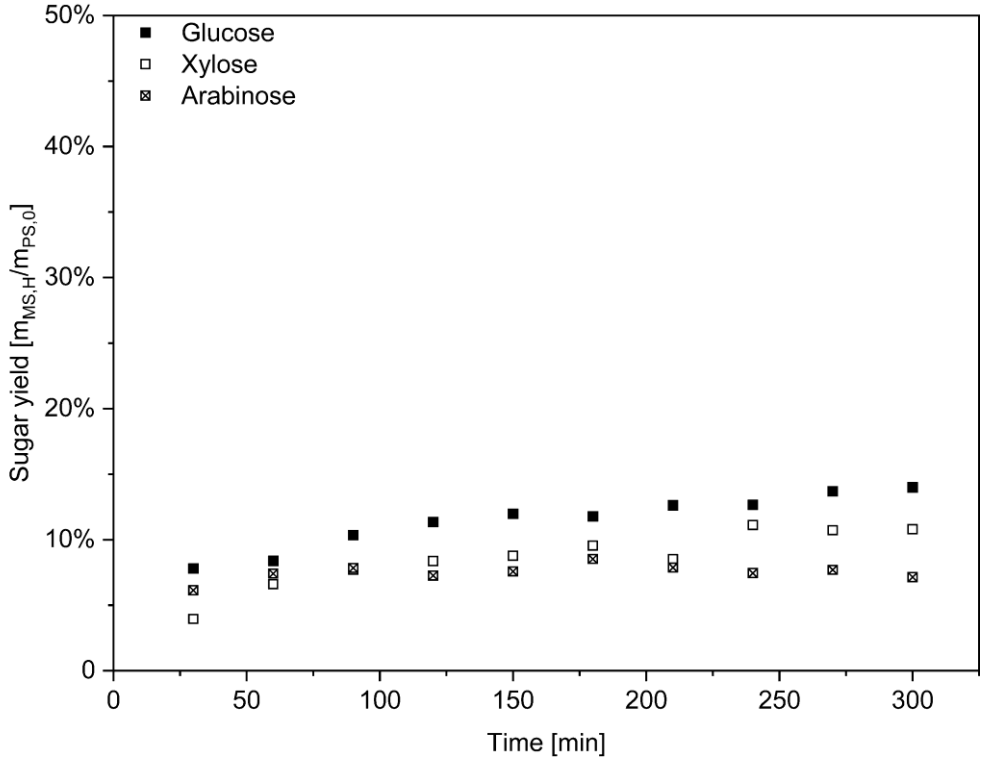

Figure 77: Monosaccharide yields for scale-up experiment using Cellic® Ctec at 5% w/v enzyme dosage. Activity of stock solution: 10 U/mL. Extractions performed with 5 min HSM BSG at 50 °C, pH 5 and 50% power input of top-mounted agitator (27 rpm).

For the optimization study of the monosaccharide extraction from BSG, two enzymes were chosen. Cellic® Ctec due to its performance during the screening experiments on lab-scale and Celluclast® due to its frequent mention in existing literature for saccharification in the bioethanol industry [186]. Before designing the optimization study, these two enzymes were tested on stability under extraction conditions due to the low obtained yields and no yield increase above 2 h during the screening phase experiments. The first test was a stability over time analysis at 50 °C, pH 5 and 120 rpm in 0.1 M acetic acid sodium acetate buffer. Results are summarized in Figure 78.

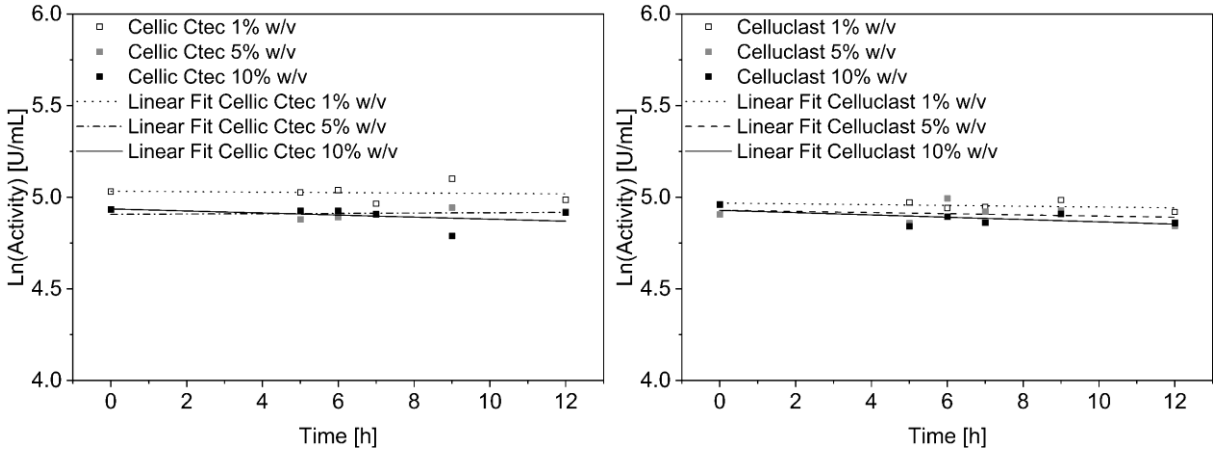

Figure 78: Logarithmic enzyme inactivation of Cellic® Ctec and Celluclast over time. Incubation of enzymes at 50 °C, pH 5 and 120 rpm in 0.1 M acetic acid sodium acetate buffer.

No substantial decrease in activity was observed for either enzyme and enzyme dosage over the 12 h period studied. Since no pH control was performed during the screening experiments and the pH decreased from pH 5 at the beginning of each extraction to around pH 4.5 over the course of 6 h due to the progressing hydrolysis, the influence of pH on the enzyme activity was investigated. Results are presented in Figure 79.

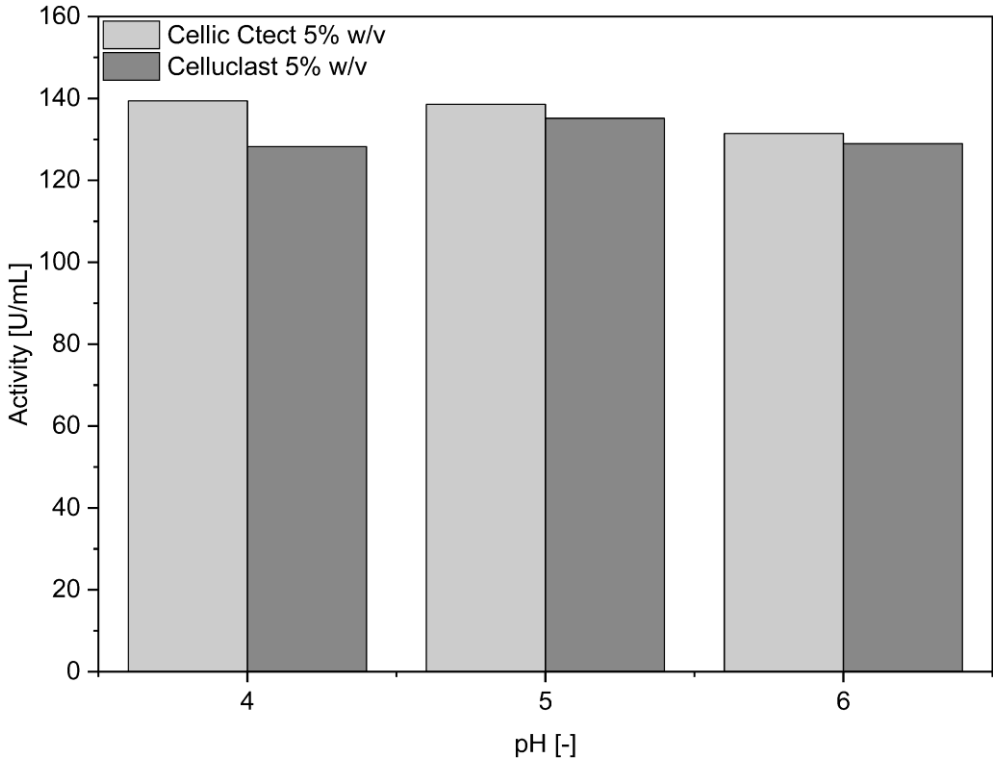

Figure 79: Effect of pH on Cellic® Ctec and Celluclast® activity after 5 h incubation at 50 °C and 120 rpm in 0.1 M acetic acid sodium acetate buffer.

No drastic difference in activity was observed at any of the pH levels studied. This is consistent with the manufacturer's recommended working pH for both enzyme cocktails. The last parameter investigated was mixing speed on resulting sugar concentrations due to the viscosity challenges during the scale-up experiment. Results can be found in Figure A-21 in the appendix. A mixing speed of 170 rpm was chosen for the optimization experiments.

With the results obtained from the screening phase, an optimization design of experiments (DoE) was set up to identify process conditions for maximum monosaccharide sugar

extraction. Factors temperature, time, enzyme dosage per dry matter of BSG and pH were varied and their influence on monosaccharide concentrations in the hydrolysates as well as on corresponding yields evaluated. All experiments were conducted with Celluclast® and Cellic® Ctec. The model used as well as experimental conditions applied are summarized in chapter 3.7.4. The full table of experimental results can be found in the appendix in Table A-9 and Table A-10.

For both Cellic® Ctec and Celluclast®, quadratic models showed the best fit to the data for the mass-based C5 and C6 sugar yields. No transformation was performed. All sequential p-values were lower than the defined threshold of 0.05 and the models thus considered significant. The quadratic models were selected due to the highest polynomial order where the sequential p-value was significant. The lack of fit p-values were not significant and the models were not aliased. The resulting regression parameters as well as a detailed summary of the significance analysis via an F-test and an ANOVA are given in the appendix in Table A-11 to Table A-14.

For the C5 sugar yield using Celluclast®, key factors and interactions that significantly influence yield were highlighted in the DoE. The model itself is statistically significant, with an F-value of 5.54, indicating a very low probability of 0.40%, that this result is due to random noise. Among the tested factors, temperature emerged as the most influential variable, with a p-value of 0.00495, showing a significant effect on C5 yield. The enzyme to substrate ratio (E/S) was also determined as a significant factor for C5 sugar yield, with a p-value of 0.0042, while reaction time showed no significance with 0.0842. The interaction between temperature and E/S ratio, with a p-value of 0.0253, is particularly notable, indicating that their combined influence on C5 yield exceeds the effect of each factor individually. Additionally, the interactions between temperature and time, with a p-value of 0.0009, and between E/S ratio and pH, with a p-value of 0.0222, are significant. This further underscores the impact of these paired factors on the C5 sugar yield obtained with Celluclast®. The model's predictive accuracy is supported by an R-squared value of 0.9209, which indicates, that 92% of the variability in C5 yield is explained by the model, though the adjusted R-squared, 0.7547, reflects a more conservative estimate, accounting for model complexity. Furthermore, an adequate precision ratio of 8.923, well above the desired threshold of 4, indicates a strong signal-to-noise ratio. Maximum C5 sugar yields close to 100% were found in temperature rages from 46-53 °C at reaction times of 5-7 h at pH 5 with an enzyme dosage of 1% w/v based on BSG dry matter, as representatively shown in Figure 80. Yields above 100% bear no physical meaning and are indicated in red color. These values are assumed to be due to the different HPLC systems used for the determination of the monosaccharides and hemicellulose contents as well as due to the indirect determination of hemicellulose based on solely xylose and arabinose contents from the analytical acid hydrolysis procedure described in chapter 3.3.4.

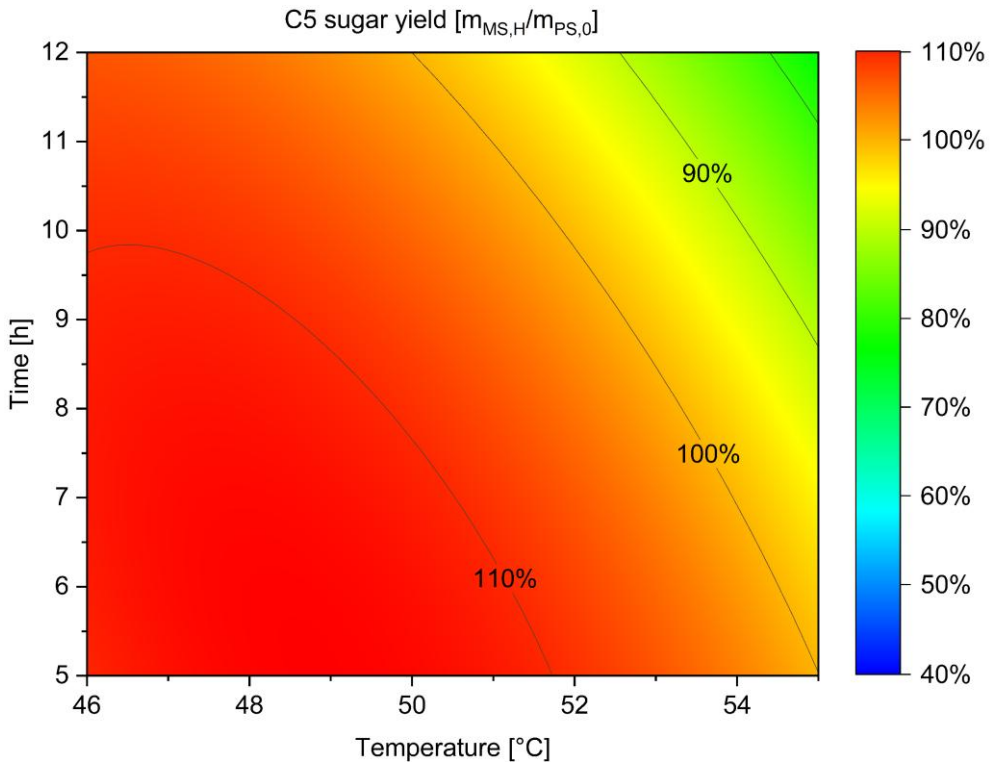

Figure 80: Dependance of C5 sugar yield from 5 min HSM BSG on temperature and time. Celluclast® used at 1% w/v based on BSG dry matter at pH 5.

For the C5 sugar yield using Cellic® Ctec, E/S ratio and pH were the most influential factors with p-values of 0.0002 and 0.0447, respectively. A significant quadratic relationship for temperature with a p-value of 0.0019 suggests that there is a temperature range beyond which yield may decrease, emphasizing the need for precise temperature control.

While reaction time did not significantly impact C5 yield having a p-value equal to 0.8319, a moderate interaction between reaction time and pH, with 0.0621, indicates that the combined influence of these factors is relevant, though secondary to the reaction time alone. The same is valid for the combination of the temperature and the reaction time, with a p-value of 0.0578. The model explains 92.6% of the variability in C5 yield, with the R-squared of 0.9258, and demonstrates robust predictive capability with an adequate precision ratio of 10.273, well above the threshold of 4. Maximum C5 sugar yields of 100% were found over a broad range of conditions tested. At pH 5 and an enzyme dosage of 1% w/v based on BSG dry matter, these yields were achieved for extraction temperatures of 45-53 °C for times in between 5-10 h as can be seen in the following Figure 81.

For both enzymes, the obtained process conditions for maximum C5 sugar yields are in line with existing literature on saccharification of lignocellulosic biomass [26,187–189]. However, the observed reaction times are significantly lower than the commonly stated extractions performed >24 h. This might be a result of the particle size reduction through HSM upfront of the extractions, enabling an enhanced mass transfer to the hemicellulose for hydrolysis. Steric hindrance through lignin as well as limited adsorption of carbohydrases to cellulose and hemicellulose are known to be a limiting step during saccharification of lignocellulosic biomass [190]. The steric hindrance through lignin may be reduced through HSM pretreatment of BSG, while temperatures of 50 °C and below have been demonstrated to enhance Langmuir-type adsorption kinetics of cellulases to BSG [188]. In addition, diffusion of carbohydrases to the available cellulose or hemicellulose surface limits the rate of monosaccharide release.

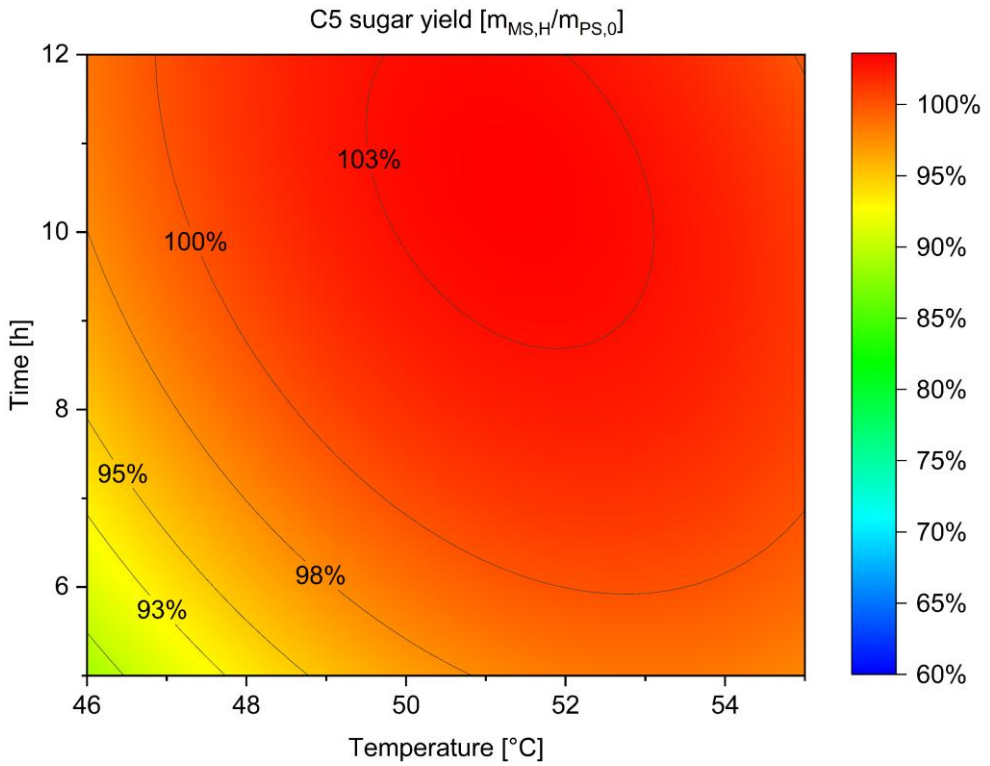

Figure 81: Dependance of C5 sugar yield from 5 min HSM BSG on temperature and time. Cellic® Ctec used at 1% w/v based on BSG dry matter at pH 5.

For lignocellulosic particles above 1000 µm in size, increasing enzyme dosages have been shown to positively influence these limits by improving enzyme penetration via a high concentration gradient within the particle. [191] This is in line with the results obtained during DoE experiments for both enzymes, where BSG with a particle size of the 50th percentile of 1569.5 µm was used and highest yields were observed for the highest enzyme dosages. Both enzymes showed to be suitable to release C5 sugars from the BSG hemicellulose fraction. Cellic® Ctec showed to have a broader working range were sugar yields of 100% were reached and thus a higher flexibility for the process design.

For the C6 sugar yields on the other hand, drastic differences in extraction efficiencies between the two enzymes were found. For Celluclast®, reaction time and substrate to enzyme stock solution ratio were identified as the most influential factors, both showing significant impacts on yield with a p-value of 0.0415 for reaction time and 0.0118 for E/S. A notable quadratic effect for reaction time with a p-value of 0.0082 suggests a non-linear relationship, where yield increases with time up to an optimal point before leveling off or decreasing, highlighting the need for precise control of reaction duration. While temperature did not individually impact C6 yield significantly, its interactions with reaction time and E/S ratio indicate that these combinations might have subtle effects when these factors are optimized together. The model explains 93.2% of the variability in C6 yield with an R-squared value of 0.9321 and shows strong predictive capability with an adequate precision ratio of 10.334, affirming its reliability. These findings emphasize reaction time and substrate per enzyme ratio as key parameters for maximizing C6 sugar yield with Celluclast®. A maximum C6 sugar yield of 39% was found in the temperature range of 46-50 °C during 6-11 h of extraction at pH 5 and an enzyme dosage of 1% based on BSG dry matter as can be seen in Figure 82. The working group of FENILA ET AL. (2016) achieved a glucose yield of 38% by mass after 24 h hydrolysis with a cellulase at a temperature of 45 °C through application of an optimization algorithm [188]. The order of magnitude for this type of enzyme is the same, however achieved only after 24 h. The shorter time required to achieve the same order of magnitude of sugar yields is potentially due to the pretreatment of HSM in this study and previously described positive effects on the hydrolysis.

Additionally, the DoE model extrapolated missing data points for extraction times above 10 h without considering the physical implications. At a constant temperature, the model predicts a decrease in C6 sugar extraction yield over time. This could be due to co-extracted organic acids reacting with the released sugars or the yield could remain constant in reality. Further experiments are required to confirm the model's validity.

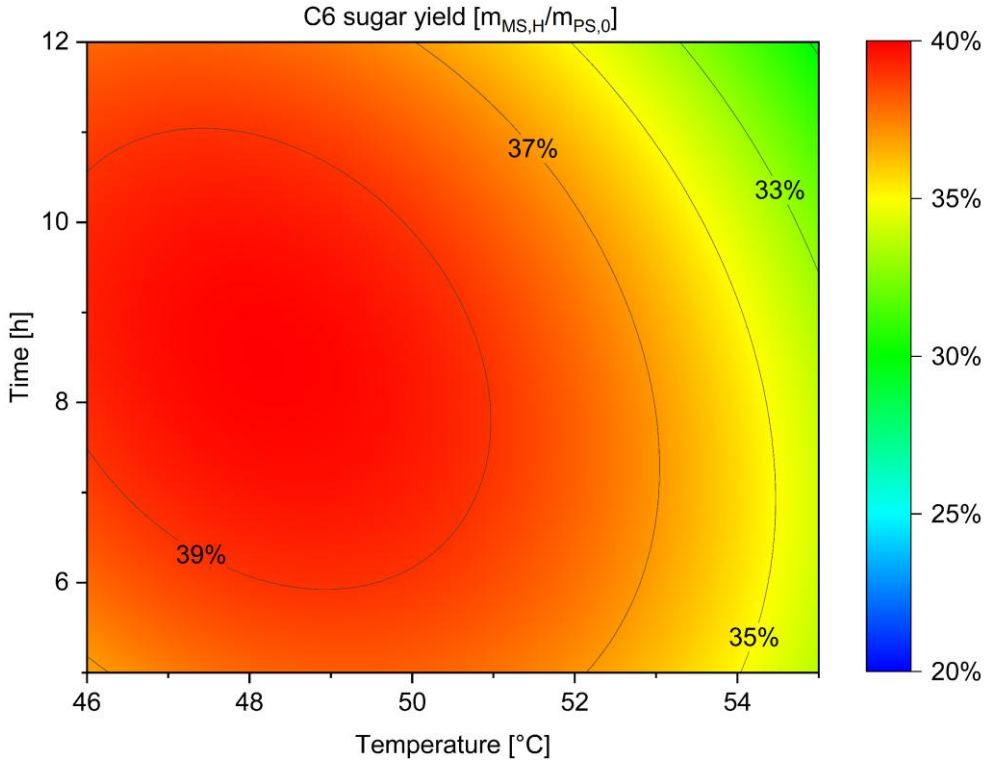

Figure 82: Dependance of C6 sugar yield from 5 min HSM BSG on temperature and time. Celluclast® used at 1% w/v based on BSG dry matter at pH 5.

For C6 sugar yields obtained with Cellic® Ctec, a highly significant model with an F-value of 74.56 and a p-value of less than 0.0001 was achieved, confirming that the tested factors and their interactions strongly influence the C6 yield. Among the individual factors, the enzyme to substrate ratio and pH were the most impactful, both with a p-value of less than 0.0001, underscoring their critical role in optimizing C6 sugar extraction. The significant quadratic effect for the reaction time and the temperature with a p-value of less than 0.0001 and 0.0002 respectively, suggests a non-linear relationship, indicating that beyond a certain point, increasing the reaction time and temperature may not proportionally improve yield and could even reduce extraction efficiency. Additionally, the interaction between the temperature and pH, with a p-value of less than 0.0001, highlights the importance of balancing these two factors to maximize yields. The model demonstrates a good fit, with an R-squared value of 0.9937 and an adjusted R- squared of 0.9803, indicating that nearly all the variability in C6 sugar yield is explained by the factors and interactions included in the model. Furthermore, the adequate precision ratio of 29.77 far exceeds the threshold of 4, confirming a strong signal-to-noise ratio and supporting the model's robustness and predictive capability. Maximum yields are in the range of 65% by mass for extraction temperatures of 54-55 °C in 8-10 h experiments at pH 5 and an enzyme dosage of 1% w/v by mass of BSG dry matter as can be seen in Figure 83. The higher extraction yield compared to Celluclast® may be linked to the low β-glucosidase activity of Celluclast®, which is required to obtain monomeric glucose from the dimer cellobiose released through its β-1,4-endoglucan hydrolase, exoglucanase and 1,4-β-cellobiosidase activities from cellulose [192]. This could also explain, why prolonging the hydrolysis time did not result in a higher glucose yield during Celluclast® extractions, as potentially a product

inhibition of cellobiose was present. Cellic® Ctec on the other hand is known to present a higher β-glucosidase activity, which could explain the observed differences.

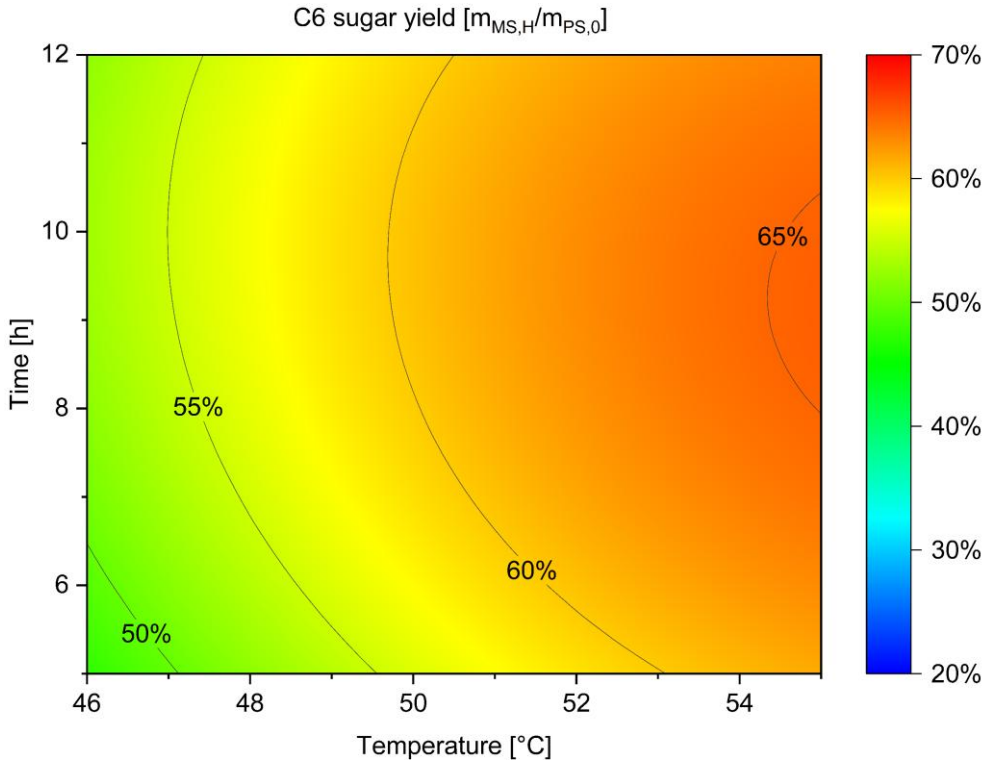

Figure 83: Dependance of C6 sugar yield from 5 min HSM BSG on temperature and time. Cellic® Ctec used at 1% w/v based on BSG dry matter at pH 5.

Based on the DoE model predictions, the optimal conditions for maximizing glucose and xylose extraction withtin the used experimental setup have been identified for both Celluclast® and Cellic® Ctec. For a maximum glucose concentration in the hydrolysate, the following Table 58 summarizes the obtained process parameters per enzyme.

Table 58: Optimal glucose extraction conditions identified by the DoE study for Celluclast® and Cellic® Ctec.

Enzyme	Glucose concentration [g/L]	Temperature range [°C]	Incubation time [h]	pH [-]	S/E [% v/w]
Celluclast®	8	48 – 50	7 – 10	4.5	1
Celluclast®	8	47 – 50	6 – 9	5.5	1
Cellic® Ctec	16	45 – 53	5 – 11	5.5	1
Cellic® Ctec	14	53 – 55	8 – 10	5	5

For a maximum xylose concentration in the hydrolysate, the following Table 59 summarizes the obtained process parameters per enzyme.

Table 59: Optimal xylose extraction conditions identified by the DoE study for Celluclast® and Cellic® Ctec.

Enzyme	Xylose concentration [g/L]	Temperature range [°C]	Incubation time [h]	pH [-]	S/E [% v/w]
Celluclast®	4	47 – 52	6 – 10	4.4	1
Celluclast®	4	47 – 52	4.5 – 10	5.5	1
Cellic® Ctec	5 – 6	45 – 49	9 – 11	5.5	1
Cellic® Ctec	5 – 6	52 – 55	7 – 10	5	5

The DoE optimization study was conducted with 5 min HSM BSG. To investigate, whether different HSM times and thus particle size distributions influence the results obtained, the following Figure 84 summarizes the released sugar concentrations and yields for both Celluclast® and Cellic® Ctec with 2 min and 10 min HSM BSG.

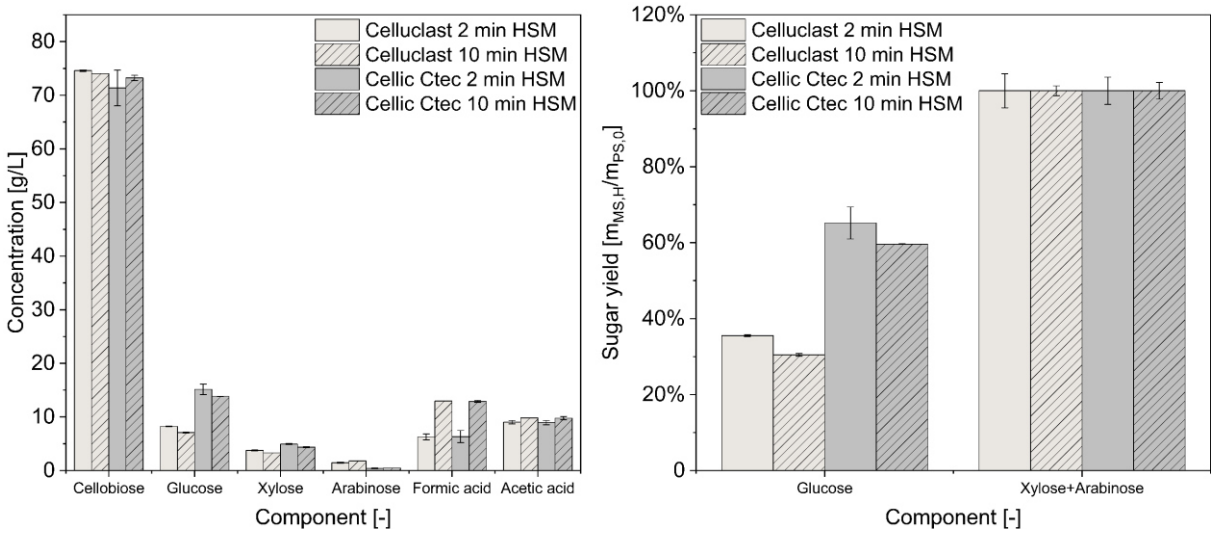

Figure 84: Influence of high-shear mixing time on sugar concentrations and yields for optimized extractions with 1% w/v Cellic® Ctec and Celluclast® at 100 U/mL stock solution activity. Extractions at 49 °C, pH 5.5 and 170 rpm mixing for 6 h. Left: Sugar and organic acid concentrations. Right: Sugar yields.

It can be clearly seen, that for both HSM times, the same trend as in the DoE study was found for both enzymes. Celluclast® and Cellic® Ctec released on average 100% of the available xylose and arabinose contents. In regards to the C6 sugar yields, Cellic® Ctec released 65.2 ± 4.2% by mass of total glucose for 2 min HSM BSG and 59.6 ± 0.0% by mass of glucose for 10 min HSM BSG. Celluclast® on the other hand released only 35.5 ± 0.3% by mass of glucose for 2 min HSM BSG and 30.5 ± 0.4% by mass of glucose for 10 min HSM BSG, showing the same trend as observed during the optimization DoE. Notably, the experimental runs with the smaller particle size distribution after 10 min HSM resulted in lower glucose yields than for the extractions with the 2 min HSM BSG. The lower glucose concentrations go however hand in hand with an increased formic acid content of 12 g/L in comparison to 6 g/L for the 2 min HSM BSG. It is thus theorized, that the formic acid is a degradation product of previously released glucose, thus reducing the overall glucose yield. To test this assumption, shorter extraction times should be tested and both glucose and formic acid concentrations evaluated. However, the reaction mechanism remains unclear. Formic acid production from glucose is well known under hydrothermal conditions as well as under milder conditions at 70 °C through an oxidative C-C bond cleavage [182,193]. However, these reactions require the presence of an oxidizing agent such as hydrogen peroxide or alternatively the presence of a base catalyst for an aldose-ketose isomerization followed by a retro-aldol reaction [193].

In summary, the enzymatic extraction of 60% by mass of glucose and close to 100% by mass of xylose and arabinose from BSG cellulose and hemicellulose fractions was achieved for 2 min, 5 min and 10 min HSM BSG, opening a pathway for the production of fermentable sugars for subsequent bioconversions into higher value chemicals.

4.3.3 Application of BSG-residue in a 3D-printable Filament

After the protein and sugar fractionations proposed in this study, a lignin-rich residue with reduced protein and structural carbohydrate content remains. Valorization of this residue as a whole would close the loop and allow for a complete valorization of all BSG components. This work proposes to use the remaining residue in materials applications, more specifically as an additive in a 3D-printable filament. The thermoplastic of choice is polylactic acid (PLA) due to its widespread use in additive manufacturing, its biodegradability under industrial conditions and the potential to be produced from lactic acid fermentation using renewable resources. The main application area of a BSG-PLA filament for fused deposition modelling (FDM) is assumed to be in prototyping and for applications with a limited life-time, such as in food packaging, ideally enabling a fully biobased approach in line with current trends in additive manufacturing [194]. The results from the experiments can additionally be used as a basis for injection molding processes using BSG and PLA composites, enabling a way to an industrially relevant technology for materials applications.

In this study, a BSG residue from an Alcalase®-assisted protein extraction process was used. To avoid clogging of the nozzle during 3D-printing, BSG particles were milled in a centrifugal mill with an 80 µm mesh size. The resulting median diameter based on the diameter of an equivalent circle was determined as 67.9 µm. Additionally, a mean sphericity of the particles of 80.4% was present. Previous studies focused on the production of 3D printable bio-composites using PLA and lignin particles, cellulose fibers, or wood pulp remnants and have reported particle sizes well below 100 µm as suitable for FDM 3D printing [195–197].

In a first set of screening experiments, the BSG particles were mixed at 5, 10 and 15% by mass with PLA pellets and subsequently extruded in the 3devo filament maker ONE type Composer 350. However, the extrusion process was not successful as the extrusion was either aborted due to internal clogging by the BSG particles or through an uneven distribution of the BSG particles in the extruded filament. To avoid clogging of the extruder and to allow for a homogenous distribution of BSG particles inside of the BSG, a pretreatment process was implemented. The first step consisted of producing a masterbatch with a 50% w/w BSG content in PLA. The particulate mixture was dissolved in dichloromethane under constant stirring to achieve a homogenous mixture and was subsequently dried. An exemplary filament strand is presented in Figure 85.

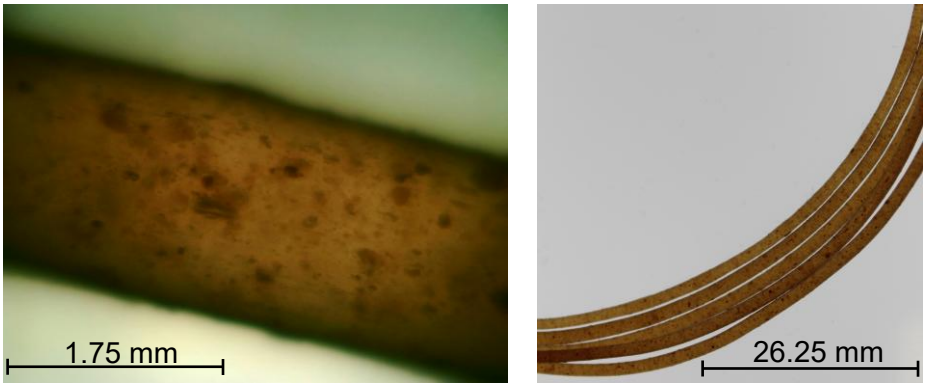

Figure 85: 5% by weight pre-compounded BSG in PLA filament extruded at 195 °C, 5.5 rpm and 65% fan speed. Left: BSG particle distribution in 5x magnification through light microscope. Right: Full view of extruded filament strand.

To analyze, whether the dissolution of BSG and PLA in DCM resulted in any structural changes of their surfaces, FTIR spectra were recorded. A representative spectrum of BSG and BSG previously dissolved in DCM is given in Figure 86. The FTIR spectrum for PLA can be found in the appendix in Figure A-23.

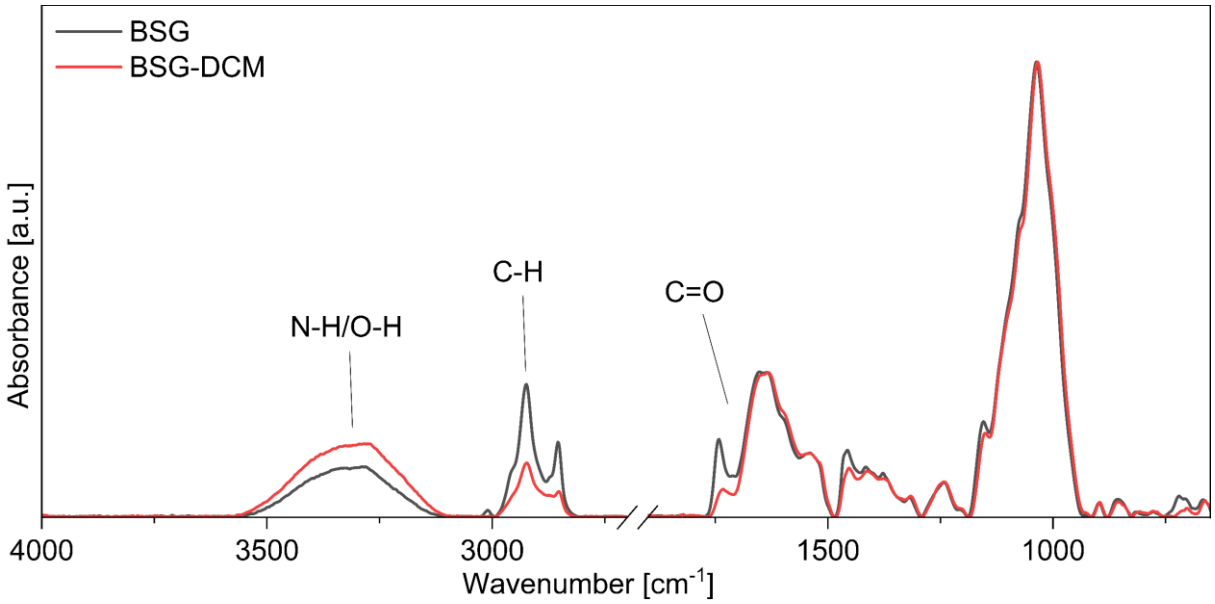

Figure 86: FTIR spectrum of untreated BSG and of BSG treated with DCM.

The main difference observed is the carbonyl group peak decrease around 1700 cm^{-1}. This is assumed to be related to fatty acids dissolved in DCM. The overall lipid content in the RubyRoast BSG used in this work is ranging from 3-8% by mass. Existing literature reports, that only 18-30% by mass of these lipids are present in the form of unbound fatty acids [198]. With this small mass fraction potentially dissolved during DCM treatment, the general BSG structural changes due to this treatment are assumed to be negligible.

The produced masterbatch was subsequently milled and mixed with virgin PLA pellets to result in a 5% by weight BSG content. The next step consisted of a pre-compounding procedure to avoid separation of the masterbatch and virgin PLA pellets during filament extrusion. The details of the extrusion in a Haake Polylabsystem twin screw extruder followed by pelletizing in an Axon ab plastics machinery pelletizer are summarized in chapter 3.7.5. With this pretreatment process, a homogenous filament was produced in the Filament maker One extruder as shown in Figure 85. With these adjustments of the starting material, the extrusion parameters were investigated in more detail.

Initially extruded filaments could not be used successfully for 3D-printing in the Bambulab P1S FDM printer as a result of the varying filament thickness during pulling towards the melting zone. The maximum allowed diameter for an even pulling of the filament was identified as 2 mm. During filament extrusion, this diameter was periodically overshot, resulting in the aforementioned printing challenges. To overcome this challenge, the setpoint for filament thickness in the extruder was decreased from 1.75 mm to 1.65 mm, resulting in a printable thickness of the final product, as shown in Figure 87.

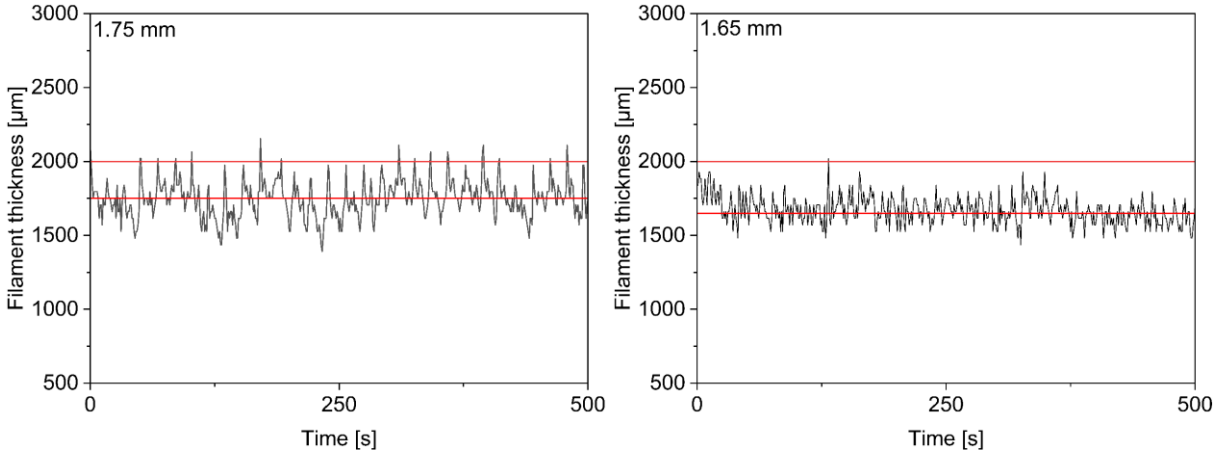

Figure 87: Filament thickness over time during extrusion at 195 °C, 5.5 rpm and 65% fan speed of 5% by weight BSG + PLA composite. Left: Filament thickness setpoint of 1.75 mm. Right: Filament thickness setpoint of 1.65 mm.

Another general finding was, that the addition of BSG particles to PLA increased variations in extruded filament thickness, as shown in Figure 88.

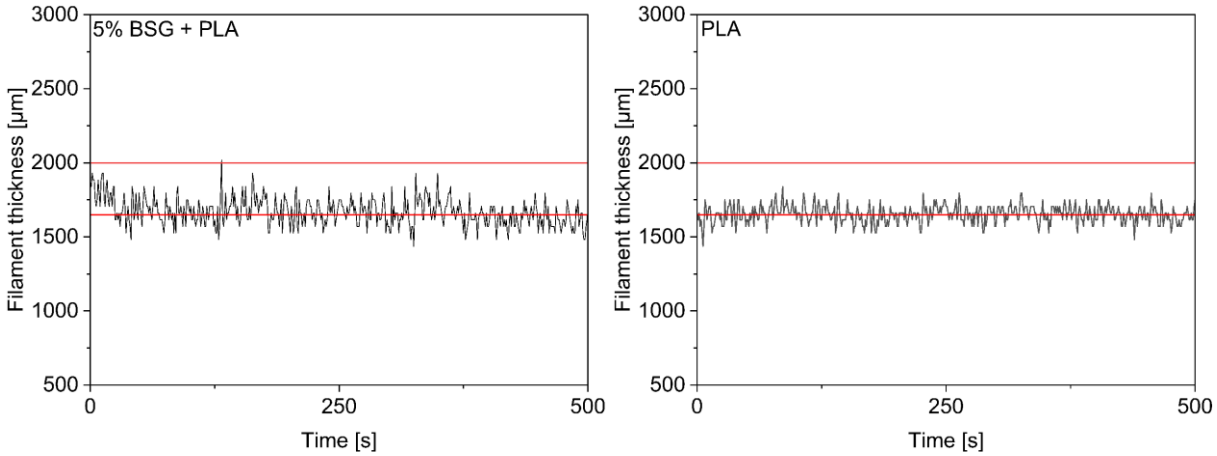

Figure 88: Filament thickness over time during extrusion at 195 °C, 5.5 rpm and 65% fan speed. Left: 5% by weight BSG + PLA composite. Right: PLA.

This could be a result of a not completely homogenous BSG-PLA mixture in the feed of the extrusion process. To avoid partial demixing, a twin-srew extruder could be used. In addition, the use of plasticizers may be beneficial during extrusion or even pre-compounding to increase the miscibility of BSG and PLA. It could be possible, that BSG particles aggregate due to their hydrophilicity and the PLAs hydrophobic nature, resulting in the uneven filament thickness. To avoid this behavior, a pretreatment in the form of a surface modification of the BSG particles may be useful.

Next to the filament thickness itself, optimal printing results were found for the extrusion parameters summarized in the following Table 60.

Table 60: Identified optimal extrusion parameters on 3Devo extruder using 5% (w/w) BSG to PLA ratio.

Parameter	Value
Extrusion temperature [°C]	190-195
Extruder speed [rpm]	5.5
Filament thickness setpoint [mm]	1.65
Fan speed [-]	65%

Within these parameter ranges, good flow behavior inside of the extruder was achieved. Above 200 °C, degradation of the BSG particles was present. Existing literature on BSG confirms these finding through thermogravimetric analyses, where hemicellulose degradation occurred at temperatures of 200-250 °C [199]. In addition, it was not possible to extrude a virgin PLA filament as a reference material at 190 °C. The melting temperature of PLA used in 3D printing ranges from 145-175 °C depending on the PLA quality used [200,201]. For the PLA used in the present study, melting temperatures are in the range of 145-160 °C based on the information provided by the manufacturer in an oral technical discussion. Extrusion temperatures are thus required to be above this melting temperature to result in a suitable melt flow index. Based on the extruder manufacturer's recommendations, melt flow indices in the range of 10 g/min are optimal for homogenous filament properties, which are present at 200 °C for the used extruder model. It is thus assumed, that the flow properties of the PLA used are not sufficient at 190 °C to result in an even filament flow. This implies on the other hand, that the incorporation of BSG particles changes the melt flow behavior of the composite material to allow for extrusion at lower temperatures. This is consistent with previous studies that incorporated lignin particles into PLA to form bio-composites and also found a reduction in glass transition and melting temperatures compared to virgin PLA. [202].

The produced BSG-PLA filament was used to print test specimen for investigation of the mechanical properties of the composite material to virgin PLA. The tests were conducted in accordance with ISO 527-2 for two different printing directions as shown in Figure 89.

Figure 89: 3D printed test specimen according to ISO 527-2. Left: Printed in x-y direction. Right: Printed in z direction.

The test specimens were used for investigating the tensile strength and derive parameters from a stress strain curve. The resulting curves for virgin PLA and a 5% by weight BSG in PLA composite both extruded at 195 °C are presented in Figure 90.

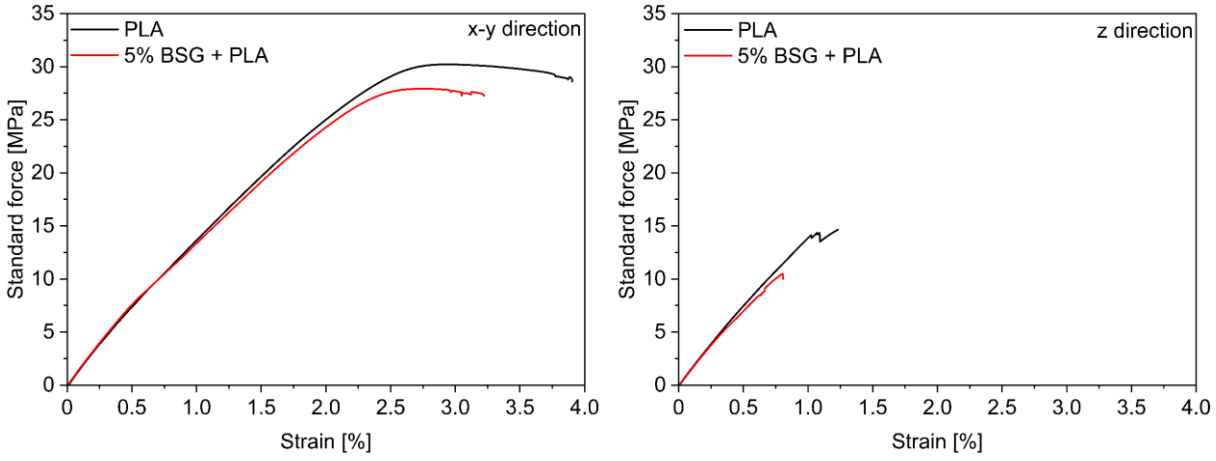

Figure 90: Stress-strain curves for virgin PLA and a 5% by weight BSG in PLA composite extruded at 195 °C. Left: Testing bodies printed in x-y direction. Right: Testing bodies printed in z direction.

As can be clearly seen, there are no great differences for the PLA and the BSG+PLA composite printed in the x-y direction in the linear region of the stress strain curve. This indicates, that the elastic deformation behavior according to Hooke's law does not differ. The yield strength is however lower for the BSG-PLA composite, indicating that the point of plastic deformation starts at a lower force per unit area compared to PLA. The overall relative deformation in the plastic deformation region is also lower before the fracture of the specimen occurred. The

incorporation of BSG makes the PLA overall more brittle. A similar behavior is found for the specimen printed in the z direction. PLA shows a higher strain and resistance to the standard force before the fracture point. Generally, the specimen printed in z-direction show a lower tensile strength, which was to be expected due to the lower surface area between printed layers. This printing style is thus used to characterize the interlayer adhesion behavior of virgin PLA compared to the BSG-PLA composite. It is evident, that the addition of BSG particles reduces this interlayer adhesion. Reasons might be in the opposite surface wettability of BSG and PLA, with the former being mostly hydrophilic while the latter is characterized mostly as hydrophobic. For an acrylonitrile butadiene styrene (ABS) and lignin-graphene filler composite material it could be shown, that the interlayer adhesion after 3D printing increased through the hydrophobic interactions of all materials involved [196]. It might thus be beneficial for interlayer adhesion in the present case, to use a plasticizer during extrusion or to modify the surface properties of BSG prior to extrusion. A potential effect on plasticity by the addition of BSY protein may be an interesting aspect for further development.

The effect of BSG-PLA filaments extruded at different temperatures of 190 °C and 195 °C on the stress strain curves are shown in Figure 91.

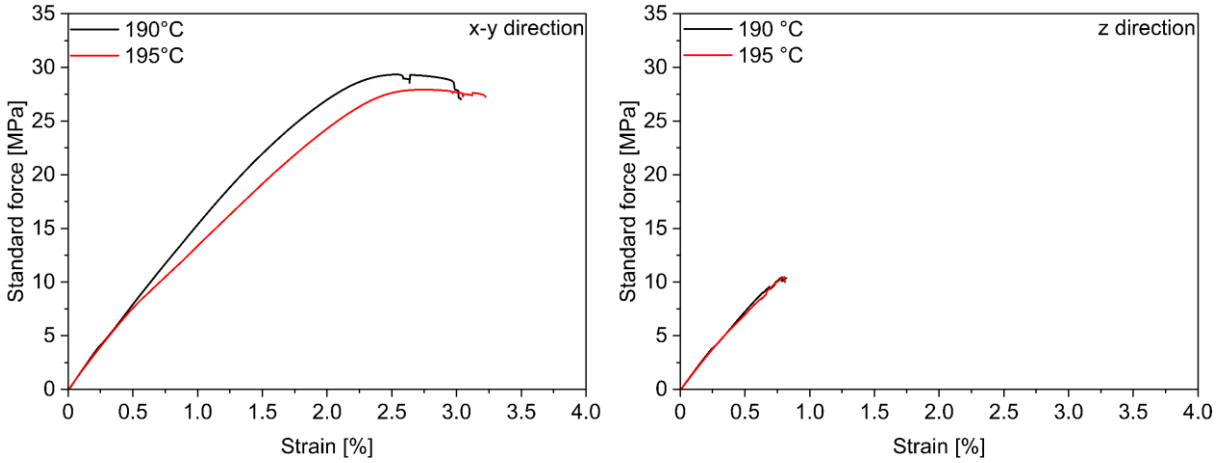

Figure 91: Stress-strain curves for a 5% by weight BSG in PLA composite extruded at 190 °C and 195 °C. Left: Testing bodies printed in x-y direction. Right: Testing bodies printed in z direction.

It can be clearly seen, that there are no visible differences in the interlayer adhesion as observed for the results of the z direction printed samples. For the specimen printed in x-y direction, a slightly higher maximum tensile strength for the specimen extruded at 190 °C is present, while the specimen extruded at 195 °C show a higher breakage strain. For the investigation of a real trend, further investigations at more temperatures are required.

The following Table 61 summarizes the parameters Young's modulus, tangent modulus as well as the maximum tensile strength and breakage strain for virgin PLA and the BSG-PLA composites extruded at 190 °C and 195 °C in the x-y and z direction. Results were derived from the stress strain curves presented above.

Table 61: Young's modulus, Tangent modulus of elasticity, maximum tensile strength and breakage strain for 3D printed PLA and 5% by weight BSG-PLA composites.

Sample	E_Y [MPa]	E_t [MPa]	σ_m [MPa]	ε_b [%]
PLA 195 °C xy	1347.3 ± 58.8	1576.3 ± 77.4	30.2 ± 0.7	3.9 ± 0.1
PLA 195 °C z	1538.0 ± 172.7	1552.8 ± 126.7	14.9 ± 0.4	1.1 ± 0.1
BSG+PLA 195 °C xy	1335.8 ± 29.2	1593.6 ± 50.3	27.9 ± 0.7	2.7 ± 0.1
BSG+PLA 195 °C z	1535.4 ± 86.0	1526.4 ± 90.6	9.4 ± 0.9	0.7 ± 0.1
BSG+PLA 190 °C xy	1537.8 ± 130.5	1702.5 ± 95.8	29.4 ± 1.4	2.6 ± 0.1
BSG+PLA 190 °C z	1553.0 ± 55.4	1575.0 ± 63.9	10.1 ± 0.6	0.7 ± 0.1

The Young's modulus results show clearly, that the printing direction is the deciding factor on the printed specimens stiffness. The specimens printed in the z direction show a higher Young's modulus compared to all specimens printed in the x-y direction. This means, that these specimens present a higher stiffness and thus a lower deformation at the same force per area applied. There are no great differences in between pure PLA and BSG-PLA composites. This is in line with findings from other research groups on FDM 3D printed PLA-wood and PLA-lignin composites [194,202]. For both composites, no major differences in Young's modulus were found at low percentages of particulate additive. At solid loadings above 10% by mass, a decrease thereof was found. MATHEW ET AL. (2005) reported the same behavior for a PLA and microcrystalline cellulose (MCC) composite material, linking it to a poor stress transfer behavior between the fiber and the polymer matrix, resulting in poor adhesion between the two [195]. This is most likely also the case for the present BSG-PLA composites, as described earlier and visible in the more than 50% decreased maximum tensile strength for all specimen printed in z direction when compared to the x-y direction specimen. The elongation at break shows the greatest difference for the BSG-PLA composites when compared to virgin PLA. The overall brittleness seems to be increased as a result of the BSG addition. This is in line with findings for PLA-lignin filaments investigated by GKARTOUZ ET AL. (2017) [197].

Overall, the feasibility of producing a BSG-PLA filament for 3D printing has been demonstrated. However, there is a need to fine-tune the interlayer adhesion of BSG and PLA to potentially improve the mechanical properties of the material. This becomes particularly important as the mass fraction of BSG is increased to increase the overall feasibility of the proposed application. In addition, the degradability of the produced material should be investigated to enable a full life cycle assessment thereof.

Intermediate Summary

The aim of chapter 4.3 was the investigation of scalable solutions for the extraction of valuable fractions from BSG. The key take-aways from the extraction of proteins, xylo- and arabino-oligosaccharides, C5 and C6 sugars as well as the production of a 3D-printable filament from BSG are summarized below.

- High-shear mixing on a 35 kg scale was shown to be a suitable wet-milling technique to reduce the particle sizes of BSG
- Osborne fractionations as well as subsequent in-depth investigations of alkaline extractions revealed, that no single solvent is able to extract more than 50% by mass of present BSG protein
- Enzymatic extractions with Alcalase® and FormeaSol® protease enzymes resulted in promising protein yields of around 70% by mass
- Protein extraction yields could not be increased further through a co-incubation with different cellulase and hemicellulase blends
- During scale-up experiments, protein extraction yields of 80% by mass were achieved for different BSG types on a 35 kg scale
- An application of a proteolytically active BSY extract on BSG protein resulted in >80% hydrolysis rates under optimized conditions on a 2 mL scale
- Liquid hot water extractions on a 30 mL and 3 L scale showed xylo- and arabino-oligosaccharide extraction yields above 85% under optimized conditions
- Cellic® Ctec was identified as a suitable enzyme blend for the extraction of C5 and C6 sugars from BSG. A yield of 100% by mass for C5 sugars and 60% by mass for C6 sugars was achieved on a 5 g scale.
- An application of a BSG residue from previous protein extraction studies was successfully used to produce a 5% by mass BSG in PLA filament suitable for 3D printing

5 Overall Discussion and Outlook

Valorization approaches for brewer's spent grain and brewer's spent yeast have been intensely studied in the scientific community [7,12,42]. These valuable by-products of the brewing industry offer promising compositional profiles for subsequent industries such as the food, energy, materials and biotechnology sectors [8,42,74]. Utilization of BSG and BSY would not only be a step towards zero-emission brewery concepts, but would also be in line with the broader UN Sustainable Development Goals (SDG). In specific, SDG 2 – Zero Hunger, SDG 9 – Industry, Innovation and Infrastructure and lastly SDG 12 – Responsible Consumption and Production. To achieve these goals, valorization strategies for BSG and BSY must meet industrial-level acceptance criteria. However, there is a gap in knowledge and expectations between lab-scale valorization approaches and industrial needs. To bridge this gap, this work aimed to identify scalable solutions for BSG and BSY valorization processes. The following chapters will give an in-depth discussion of the results obtained and the work still required to realize industrial sized valorization plants.

5.1 Brewer's Spent Yeast: Valorization as Hydrolytic Extract

The valorization strategy for BSY focused on the production of a yeast extract with intrinsic proteolytic activity. The results for achieved normalized protease activity as well as the corresponding protein yields in the extracts are given in the following Figure 92. The normalized activity is based on the blank activity in the untreated BSY supernatant. Overall, the mechanical cell disruption methods high-pressure homogenization, glass bead treatment, and ultrasound treatment have been shown to result in reproducible proteolytic activities.

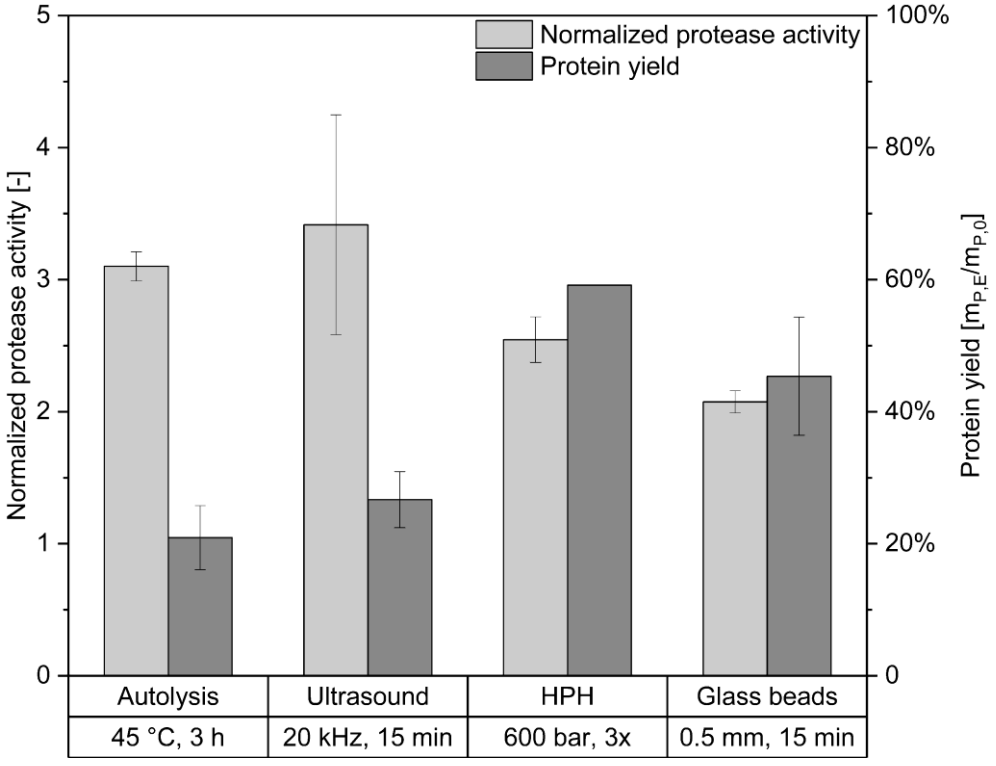

Figure 92: Comparison of highest determined protease activity at pH 6 in 0.1 M NaPC and corresponding protein yield per cell disruption method. Activity reported as normalized activity to the BSY blank activity of 0.95 ± 0.03 U/g_{dm} for HPH and 0.79 ± 0.46 U/g_{dm} for all other methods. Single technical replicate used for HPH protein yield determination after 10 passes through the homogenizer. HPH = High-pressure homogenization.

Ultrasound treatment at 20 kHz for 15 min at pH 6 resulted in the highest overall activities, while currently still posing challenges for scale-up due to limited power-inputs into the system. There are however first solutions on the market aiming at overcoming these limitations through high-intensity ultrasound probe designs [114] or through flow cell approaches from e.g. Hielscher Ultrasonics GmbH (Teltow, Germany) or IncBio's ultrasonic reactor (Maia, Portugal). These solutions could enable the first step towards an industrial sized application. An additional benefit for this cell disruption technology was identified when investigating the release of protease activity over time. It could be shown, that this release follows first order kinetics, similar to what other research groups had previously shown for protein release over time [105]. For an industrial application, this behavior could be used to automate optimal process durations per valorized BSY type, minimizing the risk of activity loss and keeping the required energy input to a minimum. The co-extraction of proteins was lower than with all the other mechanical cell disruption methods that were investigated. This could indicate that a more selective extraction toward proteases was achieved, or that the cell disruption was incomplete. Further investigation is required to understand this behavior.

High pressure homogenization at 600 bar for 3 passes through the homogenization chamber released proteolytic activity of a similar order of magnitude as that released by ultrasonic treatment. This technology has long been accepted in the industry for large-scale applications and is easily scalable [203]. Next to the released protease activity, HPH at 1100 bar and 10 passes through the homogenization valve released 60% by mass of all protein from the BSY cells. This would give the manufacturer process flexibility in terms of the final product, depending on the final application and current market demand. In contrast to the ultrasound treatment, no trend in released protease activity was observed over the number of passes. The magnitude of the released activity was the same for each pass, opening the way to a single pass and thus continuous process.

The third mechanical cell disruption technology investigated was glass bead treatment, which resulted in the lowest protease activity achieved in the produced extract. This technology is however also accepted on an industrial level, especially in the field of yeast applications [203,204]. In addition, the low achieved activities are assumed to be a result of the low energy input into the system due to the experimental set up used compared to industrial cell mills, where the rotating speed has been identified as a crucial factor for enzyme extraction from *S. cerevisiae* [205,206]. Due to its wide acceptance and potential for continuous operation, further insight into the disruption of BSY with the aim of producing a proteolytic extract on an industrial bead mill is required to draw more precise conclusions on its suitability.

Thermal yeast autolysis was the last investigated cell disruption method leading to high released protease activities in the same order of magnitude as the ultrasound treatment. This technology is additionally widely accepted in the industry for yeast extract production and has been identified as a suitable technology for production of peptide-rich yeast extracts from BSY [104]. However, there are some limitations in terms of automation of the process due to missing inline protease activity assays. The time point and temperature at which the highest protease activity in the extracts were found varied greatly in between brews from 3-4 h and 45-55 °C. In addition, no trend was found between autolysis time and the highest protease activity measured, omitting the possibility of using this correlation as a stop criterion for the process. Compared to the mechanical cell disruption methods, this technology poses additional challenges in terms of process duration. While ultrasound and glass bead treatment were conducted for 15 min each, the autolysis processes were run for multiple hours in a batch set up. This technology was thus deemed unsuitable for the production of proteolytic BSY extracts.

Aiming at overcoming these limitations, a feasibility study of using whole BSY cells on BSG under autolysis conditions showed, that the presence of BSG reduces the autolysis efficiency. No substantial amount of BSG protein was solubilized, which led to the final conclusion, that thermal yeast autolysis was not a suitable technology for the aim of scaling up the proposed valorization processes for BSG and BSY.

The produced BSY extracts were characterized to identify suitable process parameters for subsequent application. Maximum proteolytic activity was found at pH 6. In addition, the BSY extracts showed proteolytic activity over the complete investigated temperature range of 20-60 °C on azocasein as a substrate. For an application, the starting point of thermal inactivation was identified as late as 6 h at temperatures below 30 °C and at 2-4 h at temperatures above. The rate of azocasein hydrolysis increased with increasing temperature. Depending on the desired application, a trade-off has to be made between fast conversion of the substrate and fast inactivation. Due to the mass of available BSY and its low cost, it might be worthwhile to investigate the addition of fresh enzyme during hydrolysis to counteract the progressing thermal inactivation over time. When using the BSY extract on BSG protein, it could be shown, that temperatures of 35-45 °C at pH 5.7 resulted in maximum protein hydrolysis. Experimental results could show a maximum protein content decrease due to hydrolysis of 87.1 ± 0.3% after incubation of 2.4 mg/mL BSG protein at 55 °C and pH 5.5 for 8 h with 30:100 v/v BSY extract to substrate dosage. With this, the basic feasibility of using a hydrolytic BSY extract on a model protein substrate could be demonstrated. Since metalloproteases were identified as one of the present protease classes in the BSY extracts, the hydrolysis process could benefit from the addition of 10 mM $ZnSO_4$ or 1 mM $MgCl_2$ to increase the proteolytic activity.

Challenges in this valorization approach still remain, especially in the logistics of the overall process. It could be shown, that the BSY extract activity decreases with freezing and over storage time. A use of the extract directly after cell disruption is thus recommended. This is a critical parameter for the location of the valorization plant. If the plant is not located directly at the brewery location, a cooled yeast slurry would have to be transported to the valorization location. Additional challenges arise due to the different metabolic states of the yeast cells after each harvest and with storage time. The determined yeast vitality parameters varied for each brewing cycle and influenced the resulting proteolytic activity. Since no means of an inline protease activity measurement exists, the adjustment of the process depending on the achieved protease activity implies offline analytics and potentially concentration or dilution steps, depending on the resulting activity. The development of a fast and reliable protease assay, or the development of an empirical correlation between yeast vitality and resulting protease activity should be prioritized. One approach in developing such a correlation might be the use of an inline flow cytometry approach for analyzing the BSY intracellular pH prior to cell disruption [102,103]. And lastly, challenges in terms of final application of the hydrolysis product remain due to the addition of a complex BSY extract influencing final product properties such as taste. BSY extracts are known to have a bitter taste due to contained hop flavor compounds from the brewing process. A debittering step for application in the food sector might thus be required.

Overall, the valorization of BSY has great potential. Scalable solutions such as high-pressure homogenization and cell milling could enable a fast application on an industrial level. Both technologies allow for flexible process conditions to adjust the process to maximum protease release or maximum protein recovery. The location of the valorization plant has been identified as a critical parameter for the overall feasibility of the process due to metabolic changes in the yeast during storage and associated costs with cooling and transportation. An in-house valorization inside of the brewery into a stable intermediate such as a protein-rich, but still bitter yeast extract or the direct use of a produced proteolytic BSY extract for the hydrolysis of BSG protein are proposed as scalable valorization processes.

5.2 Brewer's Spent Grain: Valorization Through Fractionation

The valorization strategy for BSG focused on the use of industrially applicable processing equipment for the extraction of protein and sugars. Minimizing the required amount of different unit operations reduce the overall footprint of the valorization plant and with it the overall CAPEX correlated with it. In addition, many breweries are located near or in densely populated areas, where in the case of an in-house valorization the available space is limited. To cater to these challenges, the use of a high-shear mixer for both particle size reductions of BSG and subsequent protein or sugar extractions in the same device were proposed in this work. It could be shown, that 10 min high-shear mixing reduces the median particle sizes below 50% of the starting value. The added value in using this technology is the use of a wet-milling technique, thus omitting the energy intensive drying step of BSG after lautering compared to commonly cited lab-scale processes in scientific literature [20]. In addition, the temperature inside of the mixing vessel rises about 20 °C during 10 min high-shear mixing of a 10% dry matter BSG-water mixture. This can be directly used for subsequent hydrolysis processes at elevated temperatures, minimizing the overall heating demand.

It could be shown, that most contained BSG protein is soluble in alkaline media, corresponding to a large glutelin content according to Osborne fractions [93,144]. For the extraction of denatured protein from BSG via a classical chemical process, 0.1 M NaOH at a pH of 11 and 60 °C was thus used. For a 50 g lab-scale experiment using 10 min HSM BSG, an extraction yield of 47.1 ± 0.2% was achieved. Scaling this process up to 35 kg in the high-shear mixer, a protein extraction yield of 62.7% was achieved as can be seen in Figure 93.

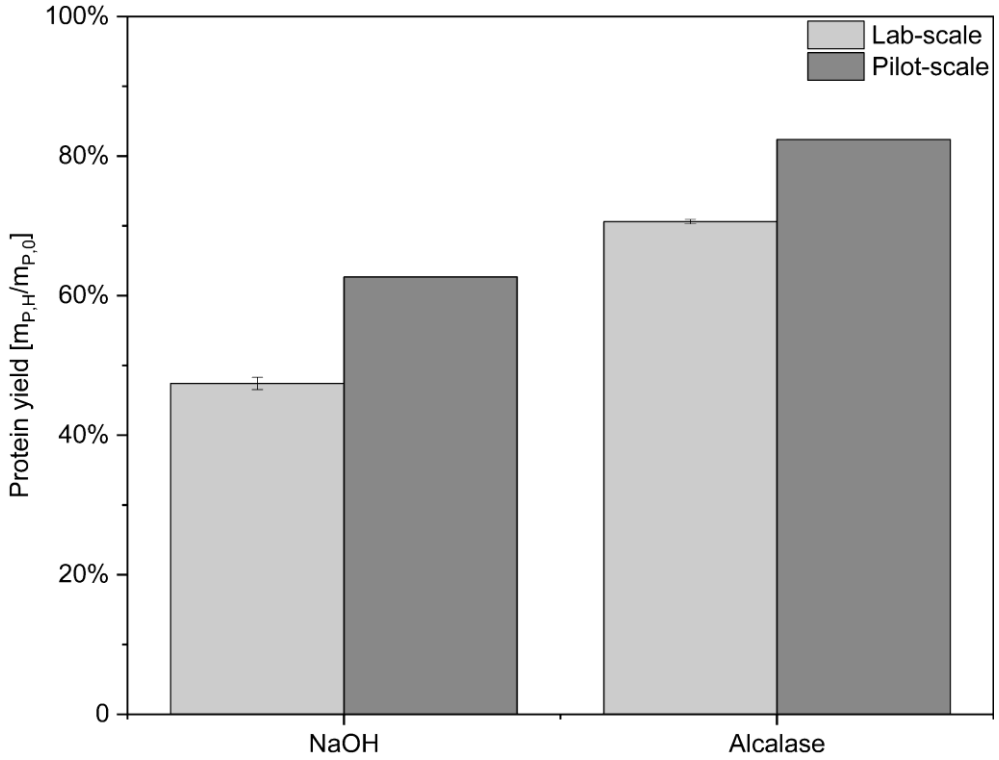

Figure 93: Comparison of lab- and pilot-scale protein yields for 10 min HSM RubyRoast BSG. Extractions performed at 60 °C for 120 min. 0.1 M NaOH used to set pH 11 for alkaline extractions "NaOH" and pH 8 for enzyme-assissted extractions "Alcalase". 10 µL/g_{dm} Alcalase® dosed at an activity of 3620.8 ± 52.9 U/mL.

The higher yield on the larger scale is assumed to be due to an enhanced mass transfer through the used top-mounted anchor-type impeller as compared to the linear shaking in a water bath on lab-scale. The order of magnitude for the pilot-scale experiment is also in line with results reported by other research groups, e.g. by CONNOLLY ET AL. (2013) who reported

an extraction yield of 59 ± 5% when running the extraction at 50 °C for 1 h using 0.11 M NaOH at a dry matter content of 0.05 w/v on a 5 L scale [157]. The mentioned working group used wet-milling in an Ultra Turrax at 24000 rpm for 2 min as a pretreatment strategy, which might further highlight the transferability of results among scale. However, the use of a purely chemical approach for BSG protein extraction has its limits in terms of protein soluble in alkaline media. Especially if adjuncts or lautering aids such as hot trub from the brewing process are used, it could be shown that the NaOH extraction method is not suitable for achieving high protein yields above 50% by mass. Since the brewing process is a recipe dependent process that changes based on brewery size, location, and company, a more flexible extraction method was found that could accommodate the different BSG compositions present: Enzyme-assisted protein extractions. On the 50 g lab-scale, the use of both Alcalase® and Formea® Sol, two commercially available endo-proteases, were able to hydrolyze 65.7 ± 0.2% and 72.7 ± 0.6% of all protein contained inside of BSG. Both endo-proteases were found to contain intrinsic carbohydrase activities, making them suitable to hydrolyze lignocellulosic matrices and thus enhancing access to BSG protein. Together with the effect of high-shear mixing on BSG particles and the lignocellulosic structure, the protein extraction yields could not be further increased by co-incubation with the carbohydrases Viscozyme® and Celluclast®. The commonly used pre-incubation with carbohydrases prior to protein extraction is thus not required to achieve extraction yields above 65% when both high-shear mixing and Alcalase® or Formea® Sol are used. This finding is especially relevant in terms of reducing processing times for BSG protein extractions due to the sheer mass of BSG produced in every brew. Per 100 L of beer produced, around 20 kg of BSG are generated, indicating the need for a fast valorization process to be able to minimize the required footprint of the valorization plant [7]. Additionally, omitting the need for a pretreatment with carbohydrase enzymes reduces the overall OPEX related to the process. Transferring the results from the 50 g lab-scale to a 35 kg pilot-scale was proven to be successful as shown in Figure 93. A mass-based protein extraction yield of 82.4% was obtained for an Alcalase® extraction run at 60 °C, pH 8 and an enzyme dosage of 10 $\mu L/g_{dm}$ with a protease activity of 3620.8 ± 52.9 U/mL. The achieved yield was at the same level or higher than that reported by other research groups for lab-scale extractions [20].

Overall, the feasibility of using high-shear mixing and a subsequent enzymatic protein hydrolysis was shown to be a successful strategy for further scale-up. However, there remain limitations, that need to be addressed. An analysis of the dimensionless Reynolds and Newton numbers for the high-shear mixing device used revealed, that even 100% agitation power (53 rpm) is not sufficient to result in a turbulent flow regime. A higher installed power is thus required to enhance heat and mass transfer during BSG protein extractions. This might enable shorter extraction times as well as even higher yields, as BSG sedimentation occurred over the course of the 2 h extraction period. Additionally, sterilization is currently only possible via direct steam injection. It would be beneficial to add an indirect heating loop for sterilization of the biomass prior to protein extractions.

Next to the extraction of protein, two different approaches for valorization of the BSG fiber fraction were evaluated. The extraction of arabino- and xylo-oligosaccharides through liquid hot water treatment was successfully scaled-up to a 3 L batch system. Extraction yields of 89.9 ± 3.0% were achieved at 180 °C for 10 min at a solid to liquid ratio of 0.05 based on BSG dry matter. The application of this approach after BSG protein extraction would allow the production of higher value food-ingredients from the low-value fiber fraction. However, limitations to this approach lie in the non-specificity of this process. A high amount of monosaccharide sugars as well as remaining proteins were co-extracted, posing challenges for downstream processing. Additionally, the high temperatures in combination with residual protein contents pose the risk of Maillard reactions, leading to carcinogenic and mutagenic chemicals [154]. To avoid a potentially cost-intensive downstream processing, the overall

mass-balance and techno-economic analysis of the processes need to be considered carefully. The overall mass of hemicellulose was determined to be low compared to cellulose and lignin fractions. It may thus be beneficial to valorize more than just the individual hemicellulose fraction to result in 6-7 g/L of XOS and 2.5 g/L of AOS. To investigate this further, the enzyme-assisted extraction of monosaccharide sugars from high-shear mixed BSG was evaluated. The carbohydrase enzyme cocktail Cellic® Ctec was identified as the best performing enzyme for this purpose, resulting in 14-16 g/L glucose and 5-6 g/L xylose monomers. Additionally, the presence of >40 g/L cellobiose was found. Using enzymes with a higher β-glucosidase activity could allow the glucose content to drastically increase. It has to be noted however, that the majority of this cellobiose is assumed to be a result of residual starch present in the BSG from the microbrewery Campus Perle. In an industrial brewery, the residual starch content is expected to be lower than 3% by mass, which might drastically limit the present cellobiose content [7]. Further experiments using industrially sourced BSG are required to confirm these assumptions. In addition to these investigations, the sterilization of BSG prior to extractions has been shown to be crucial to avoid microbial contamination during sugar hydrolysis. A high presence of formic acid of 20 g/L was present right from the start of one of the scale-up experiments for the sugar extractions, indicating microbial contamination.

Additionally, the order of the extractions should be investigated in more detail. It might be beneficial for protein extractions, if the carbohydrase extractions are carried out upfront. This could potentially open up the lignocellulosic matrix for a faster protein extraction. On the other hand, the co-solubilization of water-soluble proteins or proteins soluble in weak acidic environments during sugar extractions might reduce the overall protein yield for the subsequent process. Optimum process conditions need to be identified specifically for the final application according to market demands and techno-economic feasibility. The aim of this work was not to design a single process for a specified end-product, but rather to show the potential of using scalable processing options for fast adoption on an industrial level. It could be shown, that wet-milling in the form of high-shear mixing is a promising technology for reducing particle sizes and potentially opening up the lignocellulosic matrix of BSG. In addition, the same device could be used for successfully extracting protein and monosaccharides from BSG, demonstrating the potential for process intensification using a single device for the particle size reduction, hydrolysis, inactivation and sterilization processes.

Lastly, the potential suitability of using the remaining BSG residue in the field of materials application has been demonstrated by producing a 3D printable PLA filament with 5% by mass BSG content. The composite possessed similar, but slightly earlier plastic deformation properties compared to virgin PLA filaments. The produced filaments may be used in the private consumer market, in prototyping applications inside of the brewery or on a broader scale as packaging material. For this approach however, technologies like injection molding might be better suited to be able to increase the BSG content above 5%. Using BSG-PLA composites may be used for any application with a limited life-cycle time, such as in food packaging. The BSG particles could theoretically enhance the biodegradability of the material through a higher porosity and brittleness compared to virgin PLA or other thermoplastics. The biodegradability should thus be investigated with priority for a fast application on an industrial level.

Overall, the valorization of BSG holds great potential due to its shear mass and global availability [7,12,160]. To enable the adoption of the vast valorization processes proposed in the scientific literature, scalable solutions need to be identified for industrial application. This work identified high-shear mixing as a suitable technology for different BSG valorization processes. Next steps should focus on the overall techno-economic feasibility depending on the targeted end-product and market, taking into account the logistics of the process as well as CAPEX and OPEX of the overall production plant.

5.3 Brewer's Co-Products: Feedstocks of the Present and Future

Overall, this work identified and evaluated different valorization strategies for the two-most abundant by-products of the brewing process: Brewer's spent yeast and brewer's spent grain. Transforming these by-products into co-products requires the adoption of new processes on an industrial level. The results of this work indicate, that the most promising approach for BSG valorization is the sequential extraction of valuable components as proposed in the following Figure 94.

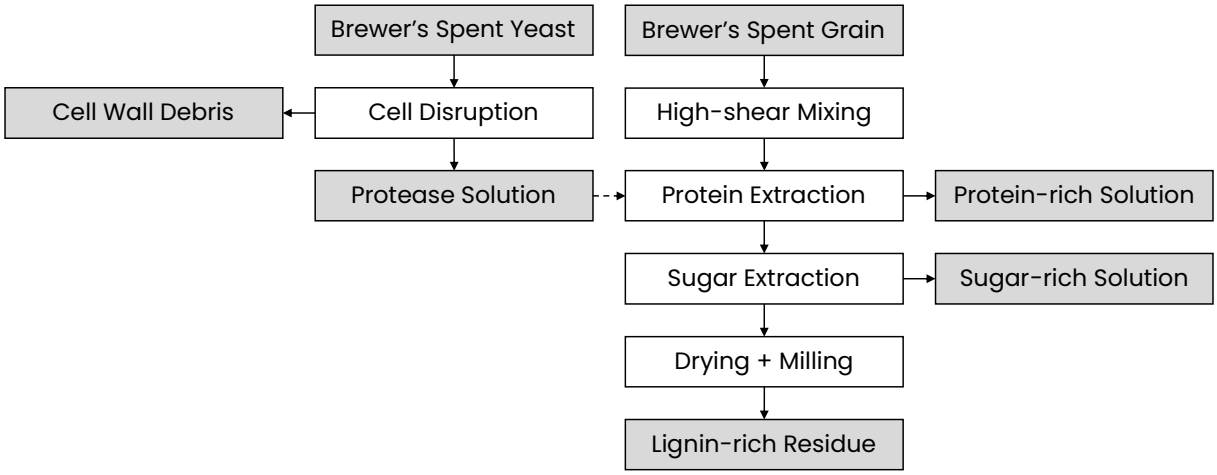

Figure 94: Proposed valorization process for BSG and BSY.

The use of a single high-shear mixing device for the pretreatment as well as the hydrolysis steps enables a way towards scalable, low-footprint valorization pathways. These processes include the steps particle size reduction, sterilization, pH and temperature adjustment, enzymatic extractions as well as inactivation in a single device. This drastically reduces setup and cleaning times compared to processes with individual, sequential units.

The proposed process first yields a protein-rich solution through enzymatic hydrolysis. Depending on the enzymes used and the product's intended use, a second hydrolysis of the extracted protein fraction may be necessary to increase the degree of hydrolysis. One option for this is the use of a proteolytically active BSY extract. This study demonstrates that hydrolysis rates of over 80% are possible with this approach. Further studies are required to identify the exact product properties like flavor profile and bioactivities present. Overall, a technological readiness level (TRL) of 5 can be assumed for the process. The second hydrolysis step of the remaining BSG residue yields a sugar-rich solution suitable for microbial or fungal fermentations. Challenges remain in the microbial stability of the process, which requires further sterilization and aseptic filling processes. Overall, a TRL of 4 is assumed for this part of the overall valorization process.

The remaining solid residue is primarily lignin-rich and has high potential in the materials sector. Simple processes such as pressing and drying could enable direct use as a packaging material within the brewery. Within the scope of this study, the incorporation of a dried BSG fraction into a 3D-printable PLA filament was successfully demonstrated. Further work is required, including the use of plasticizers to increase the percentage of added BSG and improve the mechanical stability of the produced material. This material could be used for prototyping within the brewery or marketed as a food-grade packaging material. For the latter application, injection molding might be a suitable alternative process to investigate. Overall, a TRL of 3 is assumed for this part of the proposed process.

6 Conclusion

This work aimed at identifying suitable valorization strategies for BSG and BSY, that could enable a fast adoption on the industrial scale. For BSY it could be shown, that different industrially relevant cell disruption technologies such as high-pressure homogenization and cell milling are capable of producing proteolytically active yeast extracts. In addition, these technologies were shown to effectively release protein, which could be a process alternative depending on the local market requirements. Ultrasonication was also shown to be a suitable technology for cell disruption of BSY. However, this technology is still in the process of gaining industrial acceptance through first continuous ultrasound reactor systems available on a commercial scale. The proteolytic BSY extract itself was shown to contain cysteine, aspartate, serine and metalloproteases. In a pH screening, a maximum proteolytic activity was found at pH 6. At this pH, the proteolytic activity could be increased by 10% via the addition of 10 mM zinc sulfate, presumably due to the presence of zinc dependent metalloproteases. The yeast extract could be successfully applied for hydrolysis of two model substrates: Azocasein and BSG protein. Activity was present in the temperature range 20-60 °C, with the highest hydrolysis rates at temperatures above 45 °C. Thermal inactivation in this temperature range occurred in the time between 2-4 h of incubation. With this, BSY extracts could be used as an inhouse hydrolysis feedstock for the production of food-grade peptide products.

For the valorization of BSG, high-shear mixing has been shown to be an effective technology for particle size reduction, that potentially already opens up the lignocellulosic matrix for subsequent enzymatic extractions. 10 min high-shear mixing of a 10% BSG dry mass in water suspension at 100% power input (2104 rpm) with a 4 mm stator mesh inlet were identified as suitable process conditions. Subsequent protein hydrolysis on a 50 g lab-scale was shown to release up to 65% of all protein applying the commercial enzyme Alcalase® at 60 °C for 2 h. The enzyme Formea® Sol could release up to 73% of all protein present in 10 min high-shear mixed BSG. The Alcalase® process was scaled-up to a 35 kg scale in the high-shear mixing device and resulted in above 80% protein extraction yields for different types of BSG. An analysis of the mixing regime in the high-shear mixer when using the top-mounted agitator revealed a transitional flow regime, indicating that higher power inputs could result in increased mixing efficiencies. This could be a suitable parameter for further optimization to potentially reduce the overall extraction time required. Sugar extractions from the BSG fiber fraction were conducted successfully in the high-shear mixing device. The importance of the microbial integrity of the starting biomass was demonstrated by the high levels of organic acids present from the start of the enzymatic hydrolysis. This highlights the importance of either sterilizing BSG prior to extraction or, in the case of later food grade applications, directly processing BSG in the brewery to avoid upfront accumulation of mycotoxins.

Overall, it could be shown, that the valorization of both BSY and BSG can be realized in industrially relevant processing equipment, achieving promising extraction yields for further scale-up. Critical parameters for industrial adoption were identified as the microbial integrity of the starting biomass and thus the location of the valorization plant. Depending on the desired application, BSG and BSY can be preprocessed in the brewery to a stable intermediate and transported to different valorization sites of industrial partners. In line with this approach, a one-pot system is proposed for the sequential protein and sugar hydrolysis of BSG. With this knowledge generated for the upstream and extraction processes, breweries and their industrial partners are enabled to choose relevant downstream processing options for their desired used case.

References

[1] A. Hejna, M. Barczewski, P. Kosmela, J. Aniśko, A. Piasecki, M. R. Saeb, *Cellulose*. **2025**. DOI: 10.1007/s10570-025-06605-9.

[2] G. V. Marson, M. T. D. C. Machado, R. J. S. De Castro, M. D. Hubinger, *Process Biochemistry*. **2019**, *84*, 91–102. DOI: 10.1016/j.procbio.2019.06.018.

[3] P. Hintermeier, H. Meier, *BarthHaas GmbH & Co. KG*. **2024**, 40.

[4] I. Cabras, D. Higgins, D. Preece, Eds. , *Brewing, Beer and Pubs: A Global Perspective*, 1st ed., Palgrave Macmillan, London **2016**.

[5] L. Narziß, W. Back, M. Gastl, M. Zarnkow, *Abriss der Bierbrauerei*, 1st ed., Wiley, Weinheim **2017**.

[6] J. Naibaho, M. Korzeniowska, A. B. Sitanggang, Y. Lu, E. Julianti, *Trends in Food Science & Technology*. **2024**, *152*, 104685. DOI: 10.1016/j.tifs.2024.104685.

[7] K. M. Lynch, E. J. Steffen, E. K. Arendt, *Journal of the Institute of Brewing*. **2016**, *122* (4), 553–568. DOI: 10.1002/jib.363.

[8] P. Dancker, K. Glas, M. Gastl, *International Journal of Food Science and Technology*. **2025**, *60* (1). DOI: 10.1093/ijfood/vvae022.

[9] W. Kunze, *Technologie Brauer & Mälzer*, 10., überarb. Aufl. ed., VLB Versuchs- Und Lehranstalt Für Brauerei, Berlin **2011**.

[10] S. I. Mussatto, G. Dragone, I. C. Roberto, *Journal of Cereal Science*. **2006**, *43* (1), 1–14. DOI: 10.1016/j.jcs.2005.06.001.

[11] L. E. N. Castro, L. M. S. Colpini, *European Food Research and Technology*. **2021**, *247* (12), 3013–3021. DOI: 10.1007/s00217-021-03860-5.

[12] S. I. Mussatto, *Journal of the science of food and agriculture*. **2014**, *94* (7), 1264–1275. DOI: 10.1002/jsfa.6486.

[13] S. Ikram, L. Huang, H. Zhang, J. Wang, M. Yin, *Journal of food science*. **2017**, *82* (10), 2232–2242. DOI: 10.1111/1750-3841.13794.

[14] A. Bianco, M. Budroni, S. Zara, I. Mannazzu, F. Fancello, G. Zara, *Applied microbiology and biotechnology*. **2020**, *104* (20), 8661–8678. DOI: 10.1007/s00253-020-10843-1.

[15] S. Mitri, S.-J. Salameh, A. Khelfa, E. Leonard, R. G. Maroun, N. Louka, M. Koubaa, *Fermentation*. **2022**, *8* (2), 50. DOI: 10.3390/fermentation8020050.

[16] European Union, *Farm to Fork Strategy*, European Commission, Brussels **2020**.

[17] “UN Sustainable Development Goals,” available at https://sdgs.un.org/goals (27.03.2025), **2015**.

[18] I. Celus, K. Brijs, J. A. Delcour, *Journal of Cereal Science*. **2006**, *44* (2), 203–211. DOI: 10.1016/j.jcs.2006.06.003.

[19] J. Treimo, S. I. Aspmo, V. G. H. Eijsink, S. J. Horn, *Journal of agricultural and food chemistry*. **2008**, *56* (13), 5359–5365. DOI: 10.1021/jf073317s.

[20] B. Devnani, G. C. Moran, L. Grossmann, *Foods (Basel, Switzerland)*. **2023**, *12* (7). DOI: 10.3390/foods12071543.

[21] Y. L. Chin, J. K. Keppler, S. T. Dinani, W. N. Chen, R. Boom, *Innovative Food Science & Emerging Technologies*. **2024**, *94*, 103666. DOI: 10.1016/j.ifset.2024.103666.

[22] K. M. Lynch, C. R. Strain, C. Johnson, D. Patangia, C. Stanton, F. Koc, J. Gil-Martinez, P. O’Riordan, A. W. Sahin, R. P. Ross, et al., *European journal of nutrition*. **2021**, *60* (8), 4393–4411. DOI: 10.1007/s00394-021-02570-8.

[23] L. Barbosa-Pereira, A. Bilbao, P. Vilches, I. Angulo, J. LLuis, B. Fité, P. Paseiro-Losada, J. M. Cruz, *Food chemistry*. **2014**, *145*, 191–197. DOI: 10.1016/j.foodchem.2013.08.033.

[24] L. J. Swart, A. M. Petersen, O. K. K. Bedzo, J. F. Görgens, *Journal of Chemical Technology & Biotechnology*. **2021**, *96* (6), 1632–1644. DOI: 10.1002/jctb.6683.

[25] M. Mechelke, Enzymatische Hydrolyse von Hemicellulose Zu Oligosacchariden, Dissertation, Technische Universität München, München **2017**.

[26] R. Ravindran, S. Jaiswal, N. Abu-Ghannam, A. K. Jaiswal, *Bioresource technology*. **2018**, *248* (Pt A), 272–279. DOI: 10.1016/j.biortech.2017.06.039.
[27] J. Ibarruri, M. Cebrián, I. Hernández, *Waste and Biomass Valorization*. **2019**, *10* (12), 3687–3700. DOI: 10.1007/s12649-019-00654-5.
[28] R. Wang, R. Chau Sing Law, C. Webb, *Process Biochemistry*. **2005**, *40* (1), 217–227. DOI: 10.1016/j.procbio.2003.12.008.
[29] S. I. Mussatto, M. Fernandes, I. M. Mancilha, I. C. Roberto, *Biochemical Engineering Journal*. **2008**, *40* (3), 437–444. DOI: 10.1016/j.bej.2008.01.013.
[30] S. Bedő, M. Rozbach, L. Nagy, A. Fehér, C. Fehér, *Processes*. **2021**, *9* (2), 366. DOI: 10.3390/pr9020366.
[31] Z. Qazanfarzadeh, A. R. Ganesan, L. Mariniello, L. Conterno, V. Kumaravel, *Journal of Cleaner Production*. **2023**, *385*, 135726. DOI: 10.1016/j.jclepro.2022.135726.
[32] A. M. Ferreira, J. Martins, L. H. Carvalho, F. D. Magalhães, *Polymers*. **2019**, *11* (5). DOI: 10.3390/polym11050923.
[33] L. Rossi, L. Wechsler, M. A. Peltzer, E. M. Ciannamea, R. A. Ruseckaite, P. M. Stefani, *Polymers*. **2023**, *16* (1). DOI: 10.3390/polym16010059.
[34] E. J. Lodolo, J. L. F. Kock, B. C. Axcell, M. Brooks, *FEMS Yeast Research*. **2008**, *8* (7), 1018–1036. DOI: 10.1111/j.1567-1364.2008.00433.x.
[35] G. M. Walker, *Yeast Physiology and Biotechnology*, Wiley, Chichester **1998**.
[36] E. Vieira, S. C. Cunha, I. M. P. L. V. O. Ferreira, *Waste and Biomass Valorization*. **2019**, *10* (11), 3235–3242. DOI: 10.1007/s12649-018-0368-9.
[37] A. Jaeger, E. K. Arendt, E. Zannini, A. W. Sahin, *Fermentation*. **2020**, *6* (4), 123. DOI: 10.3390/fermentation6040123.
[38] I. Bleoanca, G. Bahrim, *Romanian Biotechnological Letters*. **2013**, *2013* (18), 8551–8572.
[39] F. F. Jacob, L. Striegel, M. Rychlik, M. Hutzler, F.-J. Methner, *Fermentation*. **2019**, *5* (2), 51. DOI: 10.3390/fermentation5020051.
[40] G. V. Marson, R. J. S. de Castro, M.-P. Belleville, M. D. Hubinger, *World journal of microbiology & biotechnology*. **2020**, *36* (7), 95. DOI: 10.1007/s11274-020-02866-7.
[41] F. G. Priest, *Handbook of Brewing*, 2. ed. ed., Vol. 157, CRC/Taylor & Francis, Boca Raton **2005**.
[42] P. Puligundla, C. Mok, S. Park, *Innovative Food Science & Emerging Technologies*. **2020**, *62*, 102350. DOI: 10.1016/j.ifset.2020.102350.
[43] D. San Martin, J. Ibarruri, B. Iñarra, N. Luengo, J. Ferrer, C. Alvarez-Ossorio, C. Bald, M. Gutierrez, J. Zufía, *Sustainability*. **2021**, *13* (12), 6520. DOI: 10.3390/su13126520.
[44] A. Jaeger, N. Ahern, A. W. Sahin, L. Nyhan, J. J. Mes, C. van der Aa, I. Vrasidas, E. K. Arendt, *Innovative Food Science & Emerging Technologies*. **2024**, *92*, 103571. DOI: 10.1016/j.ifset.2024.103571.
[45] M. Łukaszewicz, P. Leszczyński, S. J. Jabłoński, J. Kawa-Rygielska, *Applied Sciences*. **2024**, *14* (6), 2529. DOI: 10.3390/app14062529.
[46] O. P. Ward, in *Comprehensive Biotechnology*, Elsevier **2011**.
[47] F. L. Garcia-Carreon, *Biochemical Education*. **1997**, *25* (3), 161–167. DOI: 10.1016/S0307-4412(97)00005-8.
[48] C. C. Udenigwe, R. E. Aluko, *J Food Sci*. **2012**, *77* (1), 11–24. DOI: 10.1111/j.1750-3841.2011.02455.x.
[49] B. P. Singh, S. P. Bangar, M. Alblooshi, F. F. Ajayi, P. Mudgil, S. Maqsood, *Critical Reviews in Food Science and Nutrition*. **2023**, *63* (28), 9539–9560. DOI: 10.1080/10408398.2022.2067120.
[50] F. Rivero-Pino, M. J. Leon, M. C. Millan-Linares, S. La Montserrat-de Paz, *Trends in Food Science & Technology*. **2023**, *135*, 32–42. DOI: 10.1016/j.tifs.2023.03.005.
[51] E. Vieira, J. Teixeira, I. M. P. L. V. O. Ferreira, *European Food Research and Technology*. **2016**, *242* (11), 1975–1984. DOI: 10.1007/s00217-016-2696-y.
[52] E. F. Vieira, I. M. P. L. V. O. Ferreira, *International Journal of Food Properties*. **2017**, *20* (3), 662–673. DOI: 10.1080/10942912.2016.1176036.
[53] O. Martínez-Alvarez, L. Guimas, C. Delannoy, M. Fouchereau-Peron, *J Agric Food Chem*. **2008**, *56* (17), 7853–9. DOI: 10.1021/jf801393r.

[54] F. C. . Woods, J. Kinsella, *Journal of Food Biochemistry*. **1980**, *4* (2), 79–98. DOI: 10.1111/j.1745-4514.1980.tb00647.x.
[55] I. S. Maddox, J. S. Hough, *The Biochemical journal*. **1970**, *117* (5), 843–852. DOI: 10.1042/bj1170843.
[56] E. Kominami, H. Hoffschulte, L. Leuschel, K. Maier, H. Holzer, *Biochimica et Biophysica Acta (BBA) - Enzymology*. **1981**, *661* (1), 136–141. DOI: 10.1016/0005-2744(81)90092-9.
[57] M. Schottroff, K.-M. Jaeger, A. Malvis Romero, M. Schneeberger, A. Liese, *Foods*. **2025**, *14* (3), 503. DOI: 10.3390/foods14030503.
[58] K. A. Hecht, A. F. O'Donnell, J. L. Brodsky, *Cellular logistics*. **2014**, *4* (1), e28023. DOI: 10.4161/cl.28023.
[59] H. Tanguler, H. Erten, *Food and Bioproducts Processing*. **2008**, *86* (4), 317–321. DOI: 10.1016/j.fbp.2007.10.015.
[60] A. J. Barrett, N. D. Rawlings, Eds. , *Handbook of Proteolytic Enzymes*, 2. ed. ed., Elsevier Acad. Press, Amsterdam **2004**.
[61] T. Dreyer, *Carlsberg research communications*. **1989**, *54* (3), 85–97. DOI: 10.1007/BF02908301.
[62] T. Bolumar, Y. Sanz, M.-C. Aristoy, F. Toldrá, *International journal of food microbiology*. **2005**, *98* (2), 167–177. DOI: 10.1016/j.ijfoodmicro.2004.05.021.
[63] H. Kondo, Y. Shibano, T. Amachi, N. Cronin, K. Oda, B. M. Dunn, *Journal of biochemistry*. **1998**, *124* (1), 141–147. DOI: 10.1093/oxfordjournals.jbchem.a022072.
[64] F. L. Garcia-Carreno, *Biotechnology Education*. **1992**, (4), 145–150.
[65] A. K. Athnasios, M. Quantz, in *Ullmann's Encyclopedia of Industrial Chemistry*, Wiley **2003**.
[66] A. S. Oliveira, C. Ferreira, J. O. Pereira, M. E. Pintado, A. P. Carvalho, *Biomass Conversion and Biorefinery*. **2022**. DOI: 10.1007/s13399-022-02636-5.
[67] *Nature Chemical Engineering*. **2024**, *1* (6), 387–388. DOI: 10.1038/s44286-024-00086-6.
[68] M. Zlokarnik, *Scale-up: Modellübertragung in Der Verfahrenstechnik*, WILEY-VCH, Weinheim; New York **2005**.
[69] VDI e. V., Ed. , *VDI-Wärmeatlas*, Springer Berlin Heidelberg, Berlin, Heidelberg **2013**.
[70] M. B. Machado, K. J. Bittorf, V. T. Roussinova, S. M. Kresta, *Chemical Engineering Science*. **2013**, *98*, 218–230. DOI: 10.1016/j.ces.2013.04.039.
[71] W. Reschetilowski, Ed. , *Handbuch Chemische Reaktoren: Theoretische und praktische Grundlagen, Chemische Reaktionsapparate in Theorie und Praxis*, Springer Berlin Heidelberg, Berlin, Heidelberg **2020**.
[72] Y. He, D. D. Kuhn, S. F. O'Keefe, J. A. Ogejo, C. F. Fraguas, H. Wang, H. Huang, *Food and Bioproducts Processing*. **2021**, *126*, 234–244. DOI: 10.1016/j.fbp.2021.01.005.
[73] S. I. Mussatto, J. Moncada, I. C. Roberto, C. A. Cardona, *Bioresource technology*. **2013**, *148*, 302–310. DOI: 10.1016/j.biortech.2013.08.046.
[74] I. M. P. L. V. O. Ferreira, O. Pinho, E. Vieira, J. G. Tavarela, *Trends in Food Science & Technology*. **2010**, *21* (2), 77–84. DOI: 10.1016/j.tifs.2009.10.008.
[75] Fermentis by Lesaffre, "SAFLAGER (TM) W-34/70," available at https://fermentis.com/en/product/saflager-w-34-70/ (01.11.2024), **2025**.
[76] P. K. Smith, R. I. Krohn, G. T. Hermanson, A. K. Mallia, F. H. Gartner, M. D. Provenzano, E. K. Fujimoto, N. M. Goeke, B. J. Olson, D. C. Klenk, *Analytical Biochemistry*. **1985**, *150* (1), 76–85. DOI: 10.1016/0003-2697(85)90442-7.
[77] A. Lamp, M. Kaltschmitt, O. Lüdtke, *Analytical Biochemistry*. **2018**, *543*, 140–145. DOI: 10.1016/j.ab.2017.12.009.
[78] G. M. Caballero-Cordoba, V. C. Sgarbieri, *Journal of the Science of Food and Agriculture*. **2000**, *80* (3), 341–351. DOI: 10.1002/1097-0010(200002)80:3\textless341::AID-JSFA533\textgreater3.0.CO;2-M.
[79] M. B. Gutiérrez-Barrutia, M. D. Del Castillo, P. Arcia, S. Cozzano, *Foods (Basel, Switzerland)*. **2022**, *11* (10). DOI: 10.3390/foods11101403.
[80] David Breese Jones, **1931**, (138).

[81] G. Reed, T. W. Nagodawithana, *Yeast Technology*, 2nd ed., Springer Netherlands, Dordrecht **1990**.
[82] J. Adler-Nissen, *Journal of Agricultural and Food Chemistry*. **1979**, (27), 1256–1262.
[83] S. Benjakul, M. T. Morrissey, *Journal of Agricultural and Food Chemistry*. **1997**, *45* (9), 3423–3430. DOI: 10.1021/jf970294g.
[84] A. Sluiter, B. Hames, R. Ruiz, C. Scarlata, J. Sluiter, D. Templeton, *National Renewable Energy Laboratory*. **2006**, (NREL/TP-510-42623).
[85] A. Sluiter, B. Hames, R. Ruiz, C. Scarlata, J. Sluiter, D. Templeton, and D. Crocker, *National Renewable Energy Laboratory*. **2012**, (NREL/TP-510-42618).
[86] M. Rut, *Research Institute of Brewing and Malting, Plc.* **1973**, *19* (6), 131–133. DOI: 10.18832/kp1973011.
[87] P. Gabriel, M. Dienstbier, D. Matoulková, K. Kosař, K. Sigler, *Journal of the Institute of Brewing*. **2008**, *114* (3), 270–276. DOI: 10.1002/j.2050-0416.2008.tb00338.x.
[88] F. Thiele, Einfluss Der Hefevitalität Und Der Gärparameter Auf Die Stoffwechselprodukte Der Hefe Und Auf Die Geschmacksstabilität, Dissertation, München **2006**.
[89] T. Imai, I. Nakajima, T. Ohno, *Journal of the American Society of Brewing Chemists*. **1994**, *52* (1), 5–8. DOI: 10.1094/ASBCJ-52-0005.
[90] C. Cupp-Enyard, *Journal of Visualized Experiments*. **2008**, (19), 899–901. DOI: 10.3791/899.
[91] A. V. Gusakov, E. G. Kondratyeva, A. P. Sinitsyn, *International Journal of Analytical Chemistry*. **2011**, *2011*, 1–4. DOI: 10.1155/2011/283658.
[92] J. Charney, R. M. Tomarelli, *Journal of Biological Chemistry*. **1947**, (5), 501–505.
[93] A. Lamp, Proteingewinnung aus Bioethanolschlempe, Dissertation, Technische Universität Hamburg, Hamburg **2021**.
[94] RP. Overend, E. Chornet, JA. Gascoigne, *Philosophical Transactions of the Royal Society of London. Series A, Mathematical and Physical Sciences*. **1987**, *321* (1561), 523–536. DOI: 10.1098/rsta.1987.0029.
[95] DIN EN ISO 527-2, *DIN Media GmbH*. **2012**. DOI: 10.31030/1860304.
[96] A. Böge, W. Böge, *Technische Mechanik: Statik – Reibung – Dynamik – Festigkeitslehre – Fluidmechanik*, Springer Fachmedien Wiesbaden, Wiesbaden **2024**.
[97] J. Zhang, W. Hou, J. Bao, *Advances in Biochemical Engineering/Biotechnology*. **2016**, *152*, 75–90. DOI: 10.1007/10_2015_307.
[98] K.-E. Jaeger, A. Liese, C. Syldatk, Eds. , *Introduction to Enzyme Technology*, Springer International Publishing, Cham **2024**.
[99] M. Li, D. Wilkinson, K. Patchigolla, *Particulate Science and Technology*. **2005**, *23* (3), 265–284. DOI: 10.1080/02726350590955912.
[100] *Protein and Amino Acid Requirements in Human Nutrition: Report of a Joint WHO/FAO/UNU Expert Consultation*, Vol. 935, WHO, Geneva **2007**.
[101] *Energy and Protein Requirements: Report of a Joint FAO/WHO/UNU Expert Consultation*, Repr ed., Vol. 724, WHO, Geneva **1991**.
[102] C. Weigert, F. Steffler, T. Kurz, T. H. Shellhammer, F.-J. Methner, *Applied and Environmental Microbiology*. **2009**, *75* (17), 5615–20. DOI: 10.1128/AEM.00650-09.
[103] M. Eigenfeld, L. Wittmann, R. Kerpes, S. Schwaminger, T. Becker, *Analytical and bioanalytical chemistry*. **2023**, *415* (16), 3201–3213. DOI: 10.1007/s00216-023-04676-w.
[104] F. F. Jacob, M. Hutzler, F.-J. Methner, *European Food Research and Technology*. **2019**, *245* (1), 95–109. DOI: 10.1007/s00217-018-3143-z.
[105] Dilek Kilic Apar, Belma Ozmek, *Chemical and Biochemical Engineering Quarterly*. **2008**, (22), 113–118.
[106] C. J. James, W. T. Coakley, D. E. Hughes, *Biotech & Bioengineering*. **1972**, *14* (1), 33–42. DOI: 10.1002/bit.260140105.
[107] D. Liu, X.-A. Zeng, D.-W. Sun, Z. Han, *Innovative Food Science & Emerging Technologies*. **2013**, *18*, 132–137. DOI: 10.1016/j.ifset.2013.02.006.
[108] J. A. Currie, P. Dunnill, M. D. Lilly, *Biotech & Bioengineering*. **1972**, *14* (5), 725–736. DOI: 10.1002/bit.260140504.

[109] A. Demirdöven, T. Baysal, *Food Reviews International*. **2008**, *25* (1), 1–11. DOI: 10.1080/87559120802306157.
[110] L. Zhang, Y. Jin, Y. Xie, X. Wu, T. Wu, *Ultrasonics Sonochemistry*. **2014**, *21* (2), 576–581. DOI: 10.1016/j.ultsonch.2013.10.016.
[111] D. Van Gaver, A. Huyghebaert, *Enzyme and Microbial Technology*. **1991**, *13* (8), 665–671. DOI: 10.1016/0141-0229(91)90082-L.
[112] H. B. van den Hazel, M. C. Kielland-Brandt, J. R. Winther, *Yeast*. **1996**, *12* (1), 1–16. DOI: 10.1002/(SICI)1097-0061(199601)12:1%3C1::AID-YEA902%3E3.0.CO;2-N.
[113] B. Podpora, F. Swiderski, *Journal of Food Processing & Technology*. **2015**, *6* (12). DOI: 10.4172/2157-7110.1000526.
[114] S. Bystryak, R. Santockyte, A. S. Peshkovsky, *Biochemical Engineering Journal*. **2015**, *99*, 99–106. DOI: 10.1016/j.bej.2015.03.014.
[115] T. A. Gomes, C. M. Zanette, M. R. Spier, *Preparative Biochemistry & Biotechnology*. **2020**, *50* (7), 635–654. DOI: 10.1080/10826068.2020.1728696.
[116] M. Kula, H. Schütte, *Biotechnology Progress*. **1987**, *3* (1), 31–42. DOI: 10.1002/btpr.5420030107.
[117] E. K. Moore, M. Hoare, P. Dunnill, *Enzyme and Microbial Technology*. **1990**, *12* (10), 764–770. DOI: 10.1016/0141-0229(90)90149-K.
[118] F. F. Jacob, L. Striegel, M. Rychlik, M. Hutzler, F.-J. Methner, *European Food Research and Technology*. **2019**, *245* (6), 1169–1182. DOI: 10.1007/s00217-019-03237-9.
[119] S. Lee, E. Kim, M. Jo, Y. J. Choi, *Journal of Food Science*. **2024**, *89* (2), 900–912. DOI: 10.1111/1750-3841.16918.
[120] C. Verduyn, A. Suksomcheep, M. Suphantharika, *World Journal of Microbiology and Biotechnology*. **1999**, *15* (1), 57–63. DOI: 10.1023/A:1008818511497.
[121] H. K. Mæhre, L. Dalheim, G. K. Edvinsen, E. O. Elvevoll, I.-J. Jensen, *Foods (Basel, Switzerland)*. **2018**, *7* (1). DOI: 10.3390/foods7010005.
[122] F. Mariotti, D. Tomé, P. P. Mirand, *Critical Reviews in Food Science and Nutrition*. **2008**, *48* (2), 177–84. DOI: 10.1080/10408390701279749.
[123] David Breese Jones, United States Department of Agriculture Washington, D.C., *Factors for Converting Percentages of Nitrogen in Foods and Feeds Into Percentages of Proteins*, 1st ed., Washington, D.C. **1931**.
[124] M. V. Shynkaryk, N. I. Lebovka, J.-L. Lanoisellé, M. Nonus, C. Bedel-Clotour, E. Vorobiev, *Journal of Food Engineering*. **2009**, *92* (2), 189–195. DOI: 10.1016/j.jfoodeng.2008.10.041.
[125] D. Liu, L. Ding, J. Sun, N. Boussetta, E. Vorobiev, *Innovative Food Science & Emerging Technologies*. **2016**, *36*, 181–192. DOI: 10.1016/j.ifset.2016.06.017.
[126] R. Agrawal, *Textbook of Industrial Microbiology*, 1st ed. 2024 ed., Springer Nature Singapore, Singapore **2024**.
[127] E. D'Hondt, J. Martín-Juárez, S. Bolado, J. Kasperoviciene, J. Koreiviene, S. Sulcius, K. Elst, L. Bastiaens, in *Microalgae-Based Biofuels and Bioproducts*, Elsevier **2017**.
[128] L. L. A. Koh, J. Chandrapala, B. Zisu, G. J. O. Martin, S. E. Kentish, M. Ashokkumar, *Food and Bioprocess Technology*. **2014**, *7* (2), 556–566. DOI: 10.1007/s11947-013-1072-1.
[129] V. Vashisth, K. D. P. Nigam, V. Kumar, *Chemical Engineering Science*. **2021**, *232*, 116296. DOI: 10.1016/j.ces.2020.116296.
[130] R. A. Preston, R. F. Murphy, E. W. Jones, *Proceedings of the National Academy of Sciences of the United States of America*. **1989**, *86* (18), 7027–31. DOI: 10.1073/pnas.86.18.7027.
[131] C. L. Brett, L. Kallay, Z. Hua, R. Green, A. Chyou, Y. Zhang, T. R. Graham, M. Donowitz, R. Rao, *PLoS ONE*. **2011**, *6* (3), e17619. DOI: 10.1371/journal.pone.0017619.
[132] C. L. Parr, R. A. B. Keates, B. C. Bryksa, M. Ogawa, R. Y. Yada, *Yeast (Chichester, England)*. **2007**, *24* (6), 467–480. DOI: 10.1002/yea.1485.
[133] A. Illanes, L. Wilson, *Critical Reviews in Biotechnology*. **2003**, *23* (1), 61–93. DOI: 10.1080/713609298.
[134] S. Arrhenius, *Zeitschrift für Physikalische Chemie*. **1889**, *4U* (1), 226–248. DOI: 10.1515/zpch-1889-0416.

[135] E. Cao, Y. Chen, Z. Cui, P. R. Foster, *Biotech & Bioengineering*. **2003**, *82* (6), 684–690. DOI: 10.1002/bit.10612.
[136] V. S. Waravdekar, P. J. Goldblatt, B. F. Trump, C. C. Griffin, R. E. Stowell, *Journal of Histochemistry & Cytochemistry*. **1964**, *12* (7), 498–503. DOI: 10.1177/12.7.498.
[137] M. E. Doyle, K. A. Glass, *Comprehensive Reviews in Food Science and Food Safety*. **2010**, *9* (1), 44–56. DOI: 10.1111/j.1541-4337.2009.00096.x.
[138] U. Ahmed, T. Stadelmann, D. Heid, B. Würtz, J. Pfannstiel, K. Ochsenreither, T. Eisele, *Applied Microbiology and Biotechnology*. **2024**, *108* (1), 103. DOI: 10.1007/s00253-023-12986-3.
[139] N. Alias, M. Ahmad Mazian, A. B. Salleh, M. Basri, R. N. Z. R. Abd. Rahman, *Enzyme Research*. **2014**, *2014*, 1–20. DOI: 10.1155/2014/197938.
[140] F. Félix, N. Brouillet, *Biochimica et Biophysica Acta (BBA) - Enzymology and Biological Oxidation*. **1966**, *122* (1), 127–144. DOI: 10.1016/0926-6593(66)90096-8.
[141] Peter N. Lipke, Rafael Ovalle, *Journal of Bacteriology*. **1998**, (180), 3735–3740. DOI: 10.1128/JB.180.15.3735-3740.1998.
[142] A. Jaeger, E. Zannini, A. W. Sahin, E. K. Arendt, *Foods (Basel, Switzerland)*. **2021**, *10* (6). DOI: 10.3390/foods10061389.
[143] R. Ibbett, R. White, G. Tucker, T. Foster, *Innovative Food Science & Emerging Technologies*. **2019**, *56*, 102184. DOI: 10.1016/j.ifset.2019.102184.
[144] T. B. Osborne, *The Proteins of the Wheat Kernel*, Carnegie Institution Of Washington, Washington, D.C. **1907**.
[145] G. Chen, M. Stump, Y. Li, in *Plant-Based Proteins* (Ed: Y. Li), Springer US, New York, NY **2025**.
[146] S. K. Sathe, V. D. Zaffran, S. Gupta, T. Li, *Journal of the American Oil Chemists' Society*. **2018**, *95* (8), 883–901. DOI: 10.1002/aocs.12058.
[147] J. S. Hamada, *Cereal Chemistry*. **1997**, *74* (5), 662–668. DOI: 10.1094/CCHEM.1997.74.5.662.
[148] C. Zetzl, K. Gairola, C. Kirsch, L. Perez-Cantu, I. Smirnova, *Chemie Ingenieur Technik*. **2012**, *84* (1–2), 27–35. DOI: 10.1002/cite.201100161.
[149] C. Zetzl, K. Gairola, C. Kirsch, L. Perez-Cantu, I. Smirnova, *Chemie Ingenieur Technik*. **2011**, *83* (7), 1016–1025. DOI: 10.1002/cite.201100025.
[150] T. R. Sarker, F. Pattnaik, S. Nanda, A. K. Dalai, V. Meda, S. Naik, *Chemosphere*. **2021**, *284*, 131372. DOI: 10.1016/j.chemosphere.2021.131372.
[151] A. Lamp, M. Kaltschmitt, O. Lüdtke, *The Journal of Supercritical Fluids*. **2020**, *155*, 104624. DOI: 10.1016/j.supflu.2019.104624.
[152] K. Gairola, I. Smirnova, A. Liese, Prozessintegrierte Wertstoffgewinnung Aus Protein-Und Lignocellulosereichen Reststoffen, Dissertation, Technische Universität Hamburg **2014**.
[153] S. M. Rutherfurd, *Journal of AOAC International*. **2010**, *93* (5), 1515–1522. DOI: 10.1093/JAOAC%2F93.5.1515.
[154] J. H. Weisburger, in *Maillard Reactions in Chemistry, Food and Health*, Elsevier **2005**.
[155] I. Celus, K. Brijs, J. A. Delcour, *Journal of Agricultural and Food Chemistry*. **2007**, *55* (21), 8703–10. DOI: 10.1021/jf071793c.
[156] P. Alonso-Riaño, M. T. Sanz, O. Benito-Román, S. Beltrán, E. Trigueros, *Food Chemistry*. **2021**, *351*, 129264. DOI: 10.1016/j.foodchem.2021.129264.
[157] A. Connolly, C. O. Piggott, R. J. FitzGerald, *International Journal of Food Science & Technology*. **2013**, *48* (8), 1670–1681. DOI: 10.1111/ijfs.12137.
[158] E. Vieira, M. A. M. Rocha, E. Coelho, O. Pinho, J. A. Saraiva, I. M. P. L. V. O. Ferreira, M. A. Coimbra, *Industrial Crops and Products*. **2014**, *52*, 136–143. DOI: 10.1016/j.indcrop.2013.10.012.
[159] S. Wilkinson, K. A. Smart, D. J. Cook, *Industrial Crops and Products*. **2014**, *62*, 219–227. DOI: 10.1016/j.indcrop.2014.08.036.
[160] W. G. Sganzerla, L. C. Ampese, S. I. Mussatto, T. Forster–Carneiro, *Biofuels, Bioproducts and Biorefining*. **2021**, *15* (6), 1965–1988. DOI: 10.1002/bbb.2290.
[161] S. Shindo, T. Tachibana, *Journal of the Institute of Brewing*. **2004**, *110* (4), 347–351. DOI: 10.1002/j.2050-0416.2004.tb00631.x.

[162] M. Radosavljević, J. Pejin, M. Pribić, S. Kocić-Tanackov, R. Romanić, D. Mladenović, A. Djukić-Vuković, L. Mojović, *Applied Microbiology and Biotechnology*. **2019**, *103* (7), 3001–3013. DOI: 10.1007/s00253-019-09683-5.
[163] Y. He, D. D. Kuhn, J. A. Ogejo, S. F. O'Keefe, C. F. Fraguas, B. D. Wiersema, Q. Jin, D. Yu, H. Huang, *Food and Bioproducts Processing*. **2019**, *117*, 266–274. DOI: 10.1016/j.fbp.2019.07.011.
[164] D. Yu, Y. Sun, W. Wang, S. F. O'Keefe, A. P. Neilson, H. Feng, Z. Wang, H. Huang, *International Journal of Food Science & Technology*. **2020**, *55* (1), 357–368. DOI: 10.1111/ijfs.14314.
[165] A. Connolly, M. Cermeño, D. Crowley, Y. O'Callaghan, N. M. O'Brien, R. J. FitzGerald, *Food Research International*. **2019**, *121*, 524–532. DOI: 10.1016/j.foodres.2018.12.008.
[166] N. Przulj, V. Momcilovic, J. Simic, M. Mirosavljevic, *Genetika*. **2014**, *46* (1), 59–73. DOI: 10.2298/GENSR1401059P.
[167] H.-D. Belitz, W. Grosch, P. Schieberle, *Food Chemistry*, 4th ed., Springer Berlin Heidelberg, Berlin, Heidelberg **2009**.
[168] M. Sasaki, M. Furukawa, K. Minami, T. Adschiri, K. Arai, *Industrial & Engineering Chemistry Research*. **2002**, *41* (26), 6642–6649. DOI: 10.1021/ie020326b.
[169] Z. Takalloo, M. Nikkhah, R. Nemati, N. Jalilian, R. H. Sajedi, *World Journal of Microbiology and Biotechnology*. **2020**, *36* (5), 68. DOI: 10.1007/s11274-020-02840-3.
[170] E. M. Alves, J. F. de Souza, P. de Oliva Neto, *Brazilian Journal of Food Technology*. **2021**, *24*. DOI: 10.1590/1981-6723.24920.
[171] J. Solms, *Journal of Agricultural and Food Chemistry*. **1969**, *17* (4), 686–688. DOI: 10.1021/jf60164a016.
[172] K. Maehashi, M. Matsuzaki, Y. Yamamoto, S. Udaka, *Bioscience, Biotechnology, and Biochemistry*. **1999**, *63* (3), 555–559. DOI: 10.1271/bbb.63.555.
[173] P. A. Temussi, *Journal of Peptide Science*. **2012**, *18* (2), 73–82. DOI: 10.1002/psc.1428.
[174] M. Kriisa, A. Taivosalo, M. Föste, M.-L. Kütt, M. Viirma, R. Priidik, M. Korzeniowska, Y. Tian, O. Laaksonen, B. Yang, et al., *Applied Food Research*. **2022**, *2* (1), 100108. DOI: 10.1016/j.afres.2022.100108.
[175] N. Mhetras, V. Mapre, D. Gokhale, *Advances in Microbiology*. **2019**, *09* (01), 14–20. DOI: 10.4236/aim.2019.91002.
[176] L. Santibáñez, C. Henríquez, R. Corro-Tejeda, S. Bernal, B. Armijo, O. Salazar, *Carbohydrate Polymers*. **2021**, *251*, 117118. DOI: 10.1016/j.carbpol.2020.117118.
[177] L. J. Swart, O. K. K. Bedzo, E. van Rensburg, J. F. Görgens, *Biomass Conversion and Biorefinery*. **2022**, *12* (4), 1295–1309. DOI: 10.1007/s13399-020-01099-w.
[178] J. A. Quintero, L. E. Rincón, C. A. Cardona, in *Biofuels*, Elsevier **2011**.
[179] M. Michelin, J. A. Teixeira, *Bioresource Technology*. **2016**, *216*, 862–9. DOI: 10.1016/j.biortech.2016.06.018.
[180] S. A. Daza, R. J. Prada, J. R. Nunhez, G. J. Castilho, *The Canadian Journal of Chemical Engineering*. **2019**, *97* (2), 586–593. DOI: 10.1002/cjce.23385.
[181] P. Alonso-Riaño, C. Ramos, E. Trigueros, S. Beltrán, M. T. Sanz, *Industrial Crops and Products*. **2023**, *191*, 115927. DOI: 10.1016/j.indcrop.2022.115927.
[182] L. J. Swart, O. K. K. Bedzo, E. Van Rensburg, J. F. Görgens, *Applied Biochemistry and Biotechnology*. **2021**, *193* (6), 1979–2003. DOI: 10.1007/s12010-021-03525-9.
[183] C. Eliopoulos, D. Arapoglou, N. Chorianopoulos, G. Markou, S. A. Haroutounian, *Environ Sci Pollut Res*. **2022**, *29* (20), 29562–29569. DOI: 10.1007/s11356-021-15495-w.
[184] J. Chutmanop, S. Chuichulcherm, Y. Chisti, P. Srinophakun, *Journal of Chemical Technology & Biotechnology*. **2008**, *83* (7), 1012–1018. DOI: 10.1002/jctb.1907.
[185] M. Kennedy, D. Krouse, *Journal of Industrial Microbiology and Biotechnology*. **1999**, *23* (6), 456–475. DOI: 10.1038/sj.jim.2900755.
[186] A. C. Rodrigues, M. Ø. Haven, J. Lindedam, C. Felby, M. Gama, *Enzyme and Microbial Technology*. **2015**, *79–80*, 70–77. DOI: 10.1016/j.enzmictec.2015.06.019.
[187] S. I. Mussatto, M. Fernandes, A. M. F. Milagres, I. C. Roberto, *Enzyme and Microbial Technology*. **2008**, *43* (2), 124–129. DOI: 10.1016/j.enzmictec.2007.11.006.

[188] F. F., Y. Shastri, *Resource-Efficient Technologies*. **2016**, *2*, S96–S104. DOI: 10.1016/j.reffit.2016.11.006.
[189] P. Forssell, H. Kontkanen, H. A. Schols, S. Hinz, V. G. H. Eijsink, J. Treimo, J. A. Robertson, K. W. Waldron, C. B. Faulds, J. Buchert, *Journal of the Institute of Brewing*. **2008**, *114* (4), 306–314. DOI: 10.1002/j.2050-0416.2008.tb00774.x.
[190] Y. Zheng, S. Zhang, S. Miao, Z. Su, P. Wang, *Journal of Biotechnology*. **2013**, *166* (3), 135–143. DOI: 10.1016/j.jbiotec.2013.04.018.
[191] J. C. Rohrbach, J. S. Luterbacher, *Biotechnology for Biofuels*. **2021**, *14* (1), 103. DOI: 10.1186/s13068-021-01920-2.
[192] M. Grubišić, M. Galić Perečinec, I. Peremin, K. Mihajlovski, S. Beluhan, B. Šantek, M. Ivančić Šantek, *Energies*. **2022**, *15* (9), 3208. DOI: 10.3390/en15093208.
[193] A. Takagaki, W. Obata, T. Ishihara, *ChemistryOpen*. **2021**, *10* (10), 954–959. DOI: 10.1002/open.202100074.
[194] M. Kariz, M. Sernek, M. Obućina, M. K. Kuzman, *Materials Today Communications*. **2018**, *14*, 135–140. DOI: 10.1016/j.mtcomm.2017.12.016.
[195] A. P. Mathew, K. Oksman, M. Sain, *Journal of Applied Polymer Science*. **2005**, *97* (5), 2014–2025. DOI: 10.1002/app.21779.
[196] D. Mohan, A. N. Bakir, M. S. Sajab, S. B. Bakarudin, N. N. Mansor, R. Roslan, H. Kaco, *Polymer Composites*. **2021**, *42* (5), 2408–2421. DOI: 10.1002/pc.25987.
[197] E. Gkartzou, E. P. Koumoulos, C. A. Charitidis, *Manufacturing Review*. **2017**, *4*, 1. DOI: 10.1051/mfreview/2016020.
[198] A. C. Fărcaş, S. A. Socaci, F. V. Dulf, M. Tofană, E. Mudura, Z. Diaconeasa, *Journal of Cereal Science*. **2015**, *64*, 34–42. DOI: 10.1016/j.jcs.2015.04.003.
[199] O. P. Gbenebor, O. A. Olanrewaju, M. A. Usman, S. O. Adeosun, *Polymers*. **2023**, *15* (10), 2346. DOI: 10.3390/polym15102346.
[200] B. D. M. Matos, V. Rocha, E. J. Da Silva, F. H. Moro, A. C. Bottene, C. A. Ribeiro, D. Dos Santos Dias, S. G. Antonio, A. C. Do Amaral, S. A. Cruz, et al., *Journal of Thermal Analysis and Calorimetry*. **2019**, *137* (2), 555–562. DOI: 10.1007/s10973-018-7967-3.
[201] S. Solarski, M. Ferreira, E. Devaux, *Polymer*. **2005**, *46* (25), 11187–11192. DOI: 10.1016/j.polymer.2005.10.027.
[202] Z. Ren, X. Zhou, K. Ding, T. Ji, H. Sun, X. Chi, Y. Wei, M. Xu, L. Cai, C. Xia, *International Journal of Biological Macromolecules*. **2023**, *253*, 127264. DOI: 10.1016/j.ijbiomac.2023.127264.
[203] F. Zhao, Z. Wang, H. Huang, *Processes*. **2024**, *12* (10), 2059. DOI: 10.3390/pr12102059.
[204] D. Spickermann, Ohly GmbH, *Functional Yeast Protein Concentrate: International Patent*, WO2020127951A2, **2019**.
[205] M. E. Ricci-Silva, M. Vitolo, J. Abrahão-Neto, *Process Biochemistry*. **2000**, *35* (8), 831–835. DOI: 10.1016/S0032-9592(99)00151-X.
[206] C. Y. Mei, T. B. Ti, M. N. Ibrahim, A. Ariff, L. T. Chuan, *Biotechnology and Bioprocess Engineering*. **2005**, *10* (3), 284–288. DOI: 10.1007/BF02932027.

Appendix

A.1 Brewer's Spent Yeast: Valorization as Hydrolytic Extract

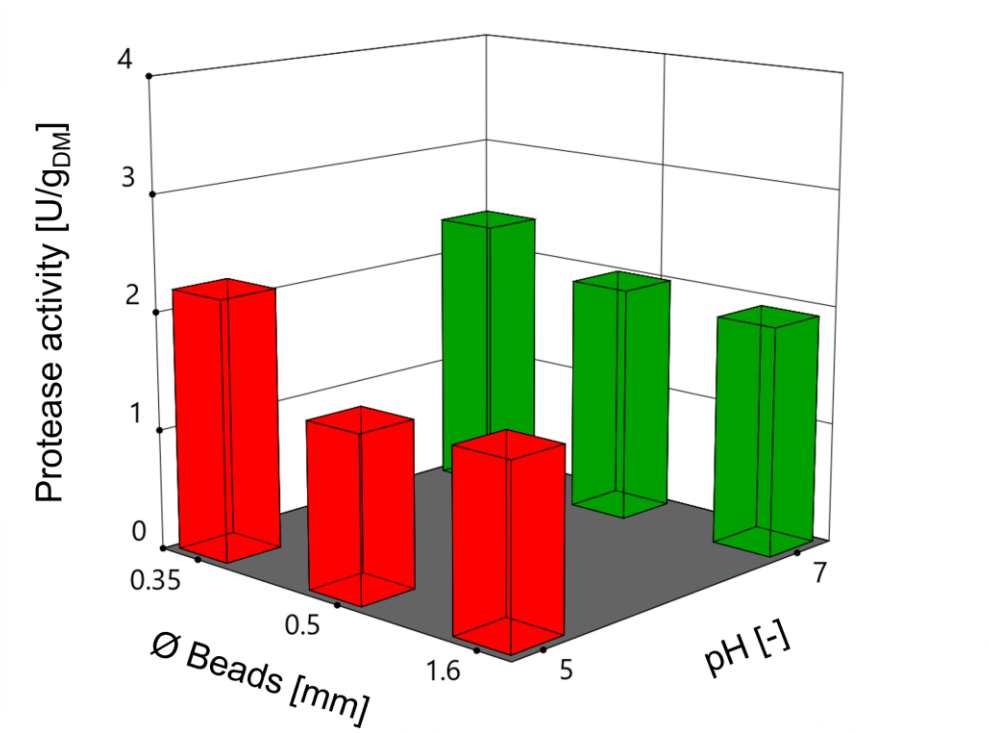

Figure A-1: Effect of glass bead size and pH on protease activity in BSY extracts in 0.2 M KPC at pH 7.

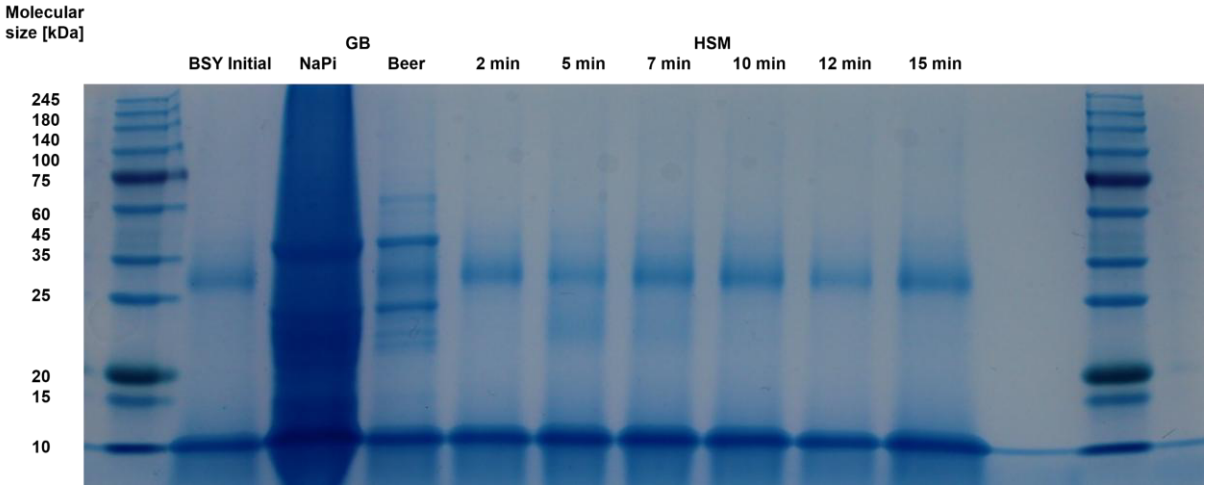

Figure A-2: SDS-PAGE for high-shear mixed BSY extracts in beer. Control with untreated BSY and standardized glass bead treatment in 0.1 M NaPC at pH 6 and in beer.

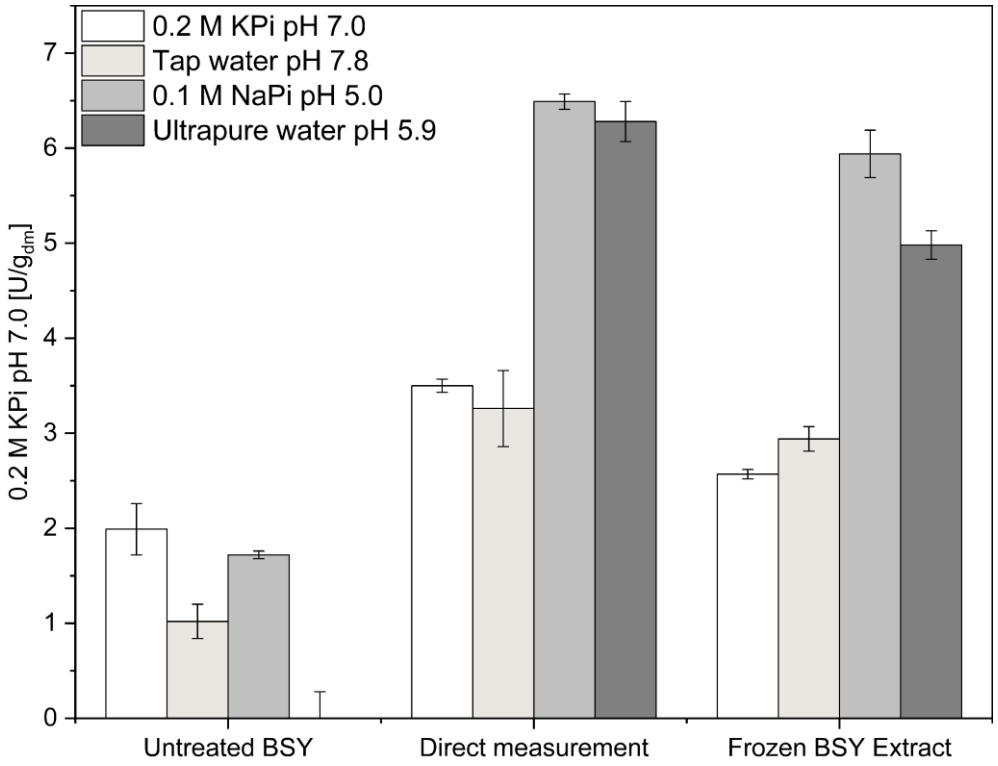

Figure A-3: Protease activity before and after freezing in different media. Cell disruptions using 0.5 mm glass beads for 15 min at 4 °C at 100% power input on a vortex mixer.

Table A-1: Summary of ion content in water qualities used.

Property	Tap Water	Ultrapure Water
pH [-]	7.8	5.85
Electrical conductivity at 25 °C [µS/cm]	240	0.05
Total hardness [°dH]	5.9	-
Hydrogencarbonate [mg/L]	-	< 5.0
Carbonate [mg/L]	-	< 3.0
Calcium [mg/L]	39	< 0.2
Magnesium [mg/L]	2	< 0.1
Sodium [mg/L]	8	< 1.4
Potassium [mg/L]	1	< 0.3
Chloride [mg/L]	10	< 1
Sulfate [mg/L]	12	< 1

*Measurements for water quality from TUHH central lab in 2011.

A.2 Brewer's Spent Grain: Valorization Through Fractionation

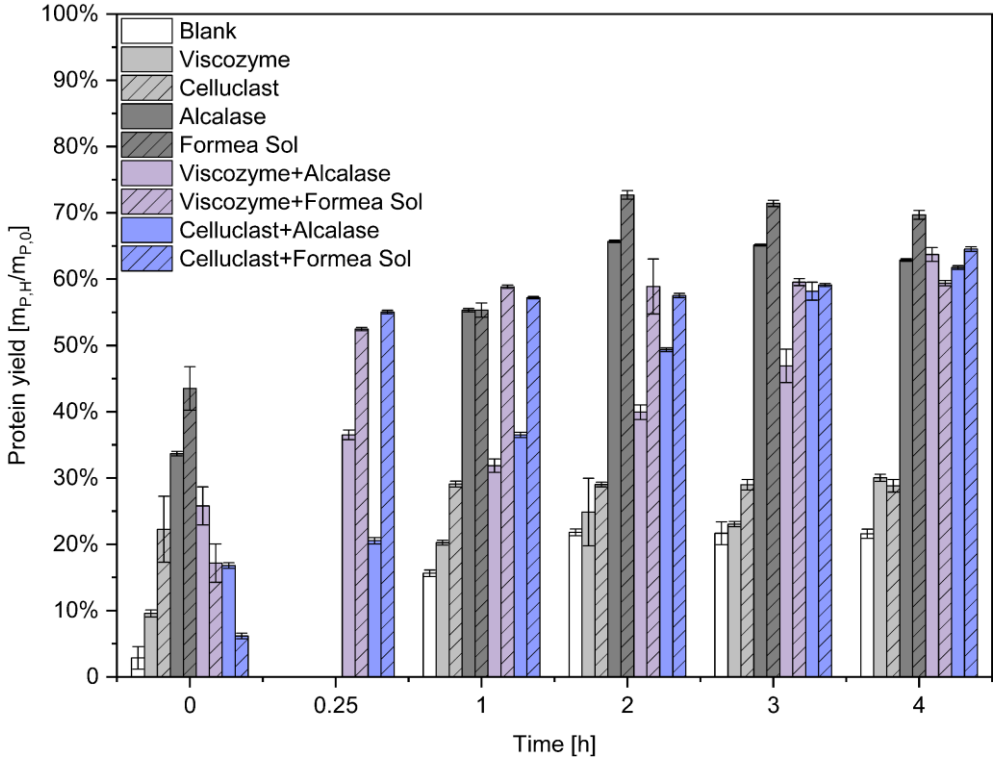

Figure A-4: Mass-based protein yield for single enzymes and enzyme combinations at 60 °C, pH 6.2 and 125 rpm and an enzyme dosage of 10 µL/g_{dm}. Protease enzymes were added 15 min after addition of carbohydrases.

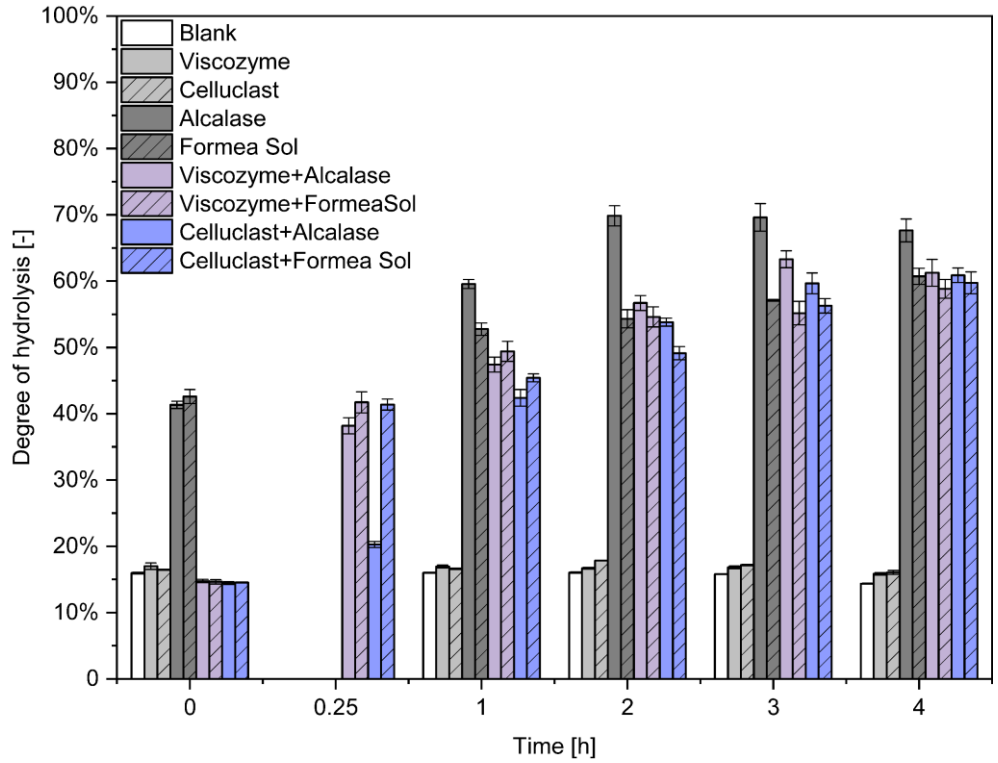

Figure A-5: Degree of hydrolysis for single enzymes and enzyme combinations at 60 °C, pH 6.2 and 125 rpm and an enzyme dosage of 10 µL/g_{dm}. Protease enzymes were added 15 min after addition of carbohydrases.

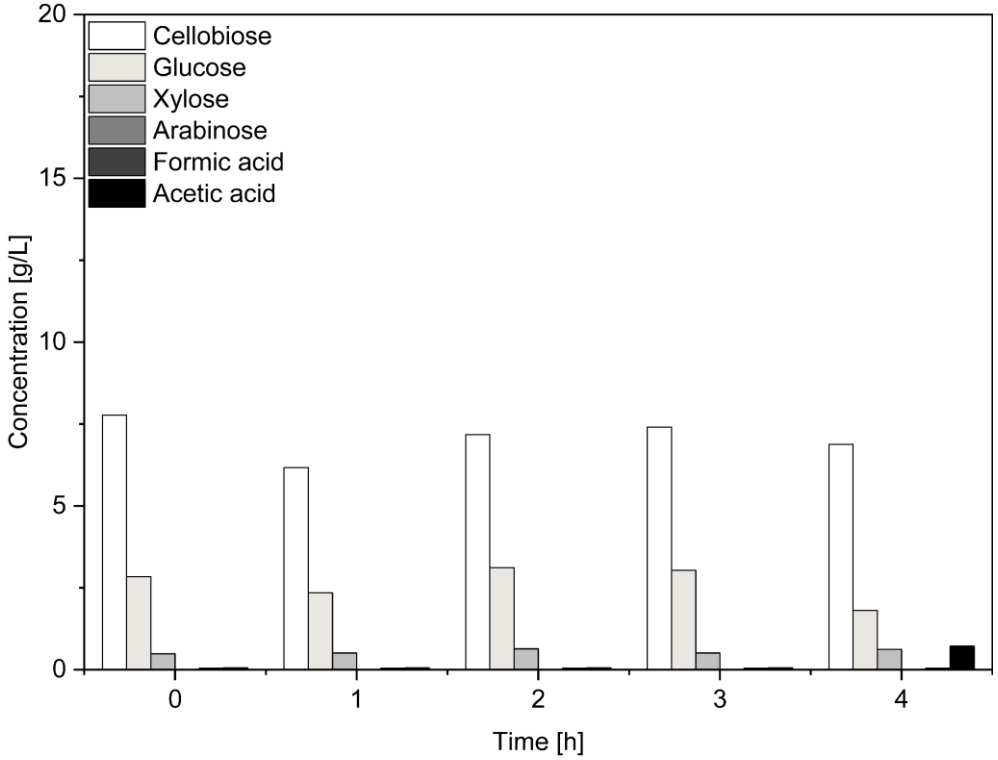

Figure A-6: Sugar and organic acid contents in BSG extraction with ultrapure water without the addition of enzyme. Extractions performed at 60 °C, 0.1 w/v BSG dry matter content and 125 rpm mixing.

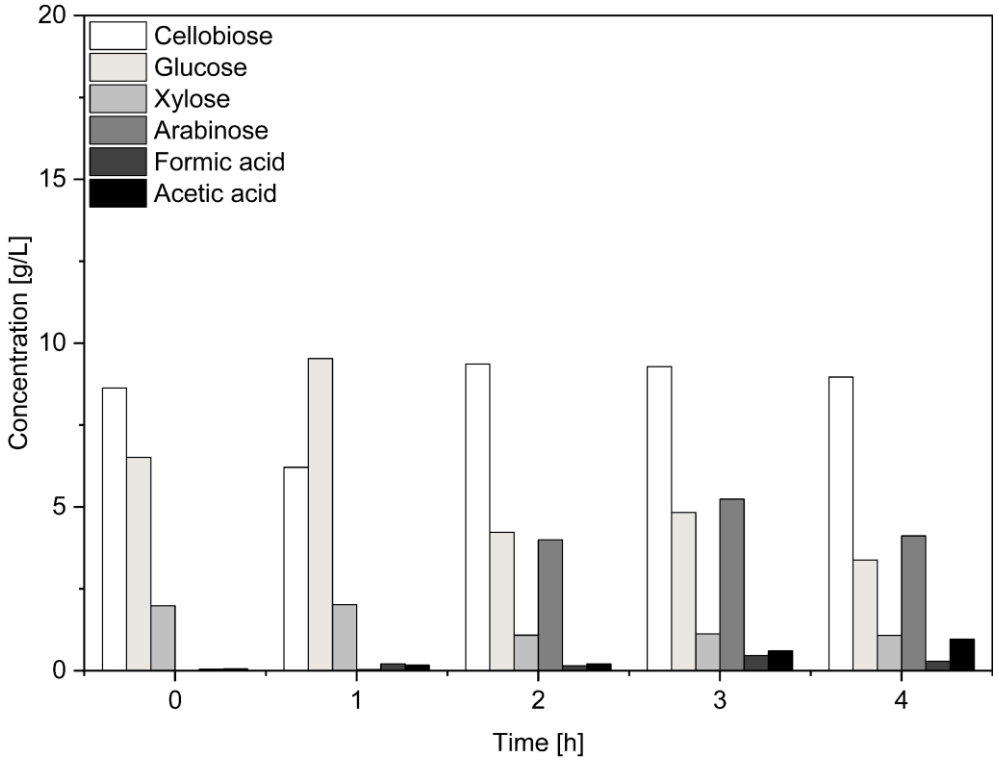

Figure A-7: Sugar and organic acid contents over time of 10 min HSM BSG after treatment with Viscozyme®. Extraction performed at 60 °C for 4 h at 0.1 w/v BSG dry matter content and 125 rpm mixing.

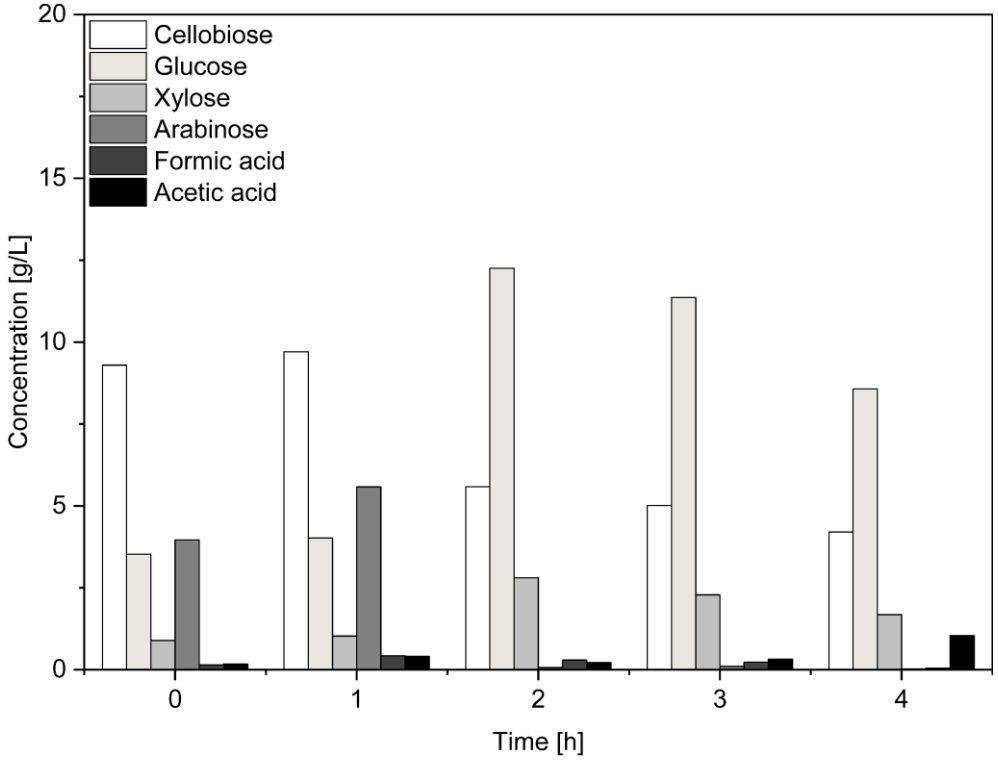

Figure A-8: Sugar and organic acid contents over time of 10 min HSM BSG after treatment with Celluclast®. Extraction performed at 60 °C for 4 h at 0.1 w/v BSG dry matter content and 125 rpm mixing.

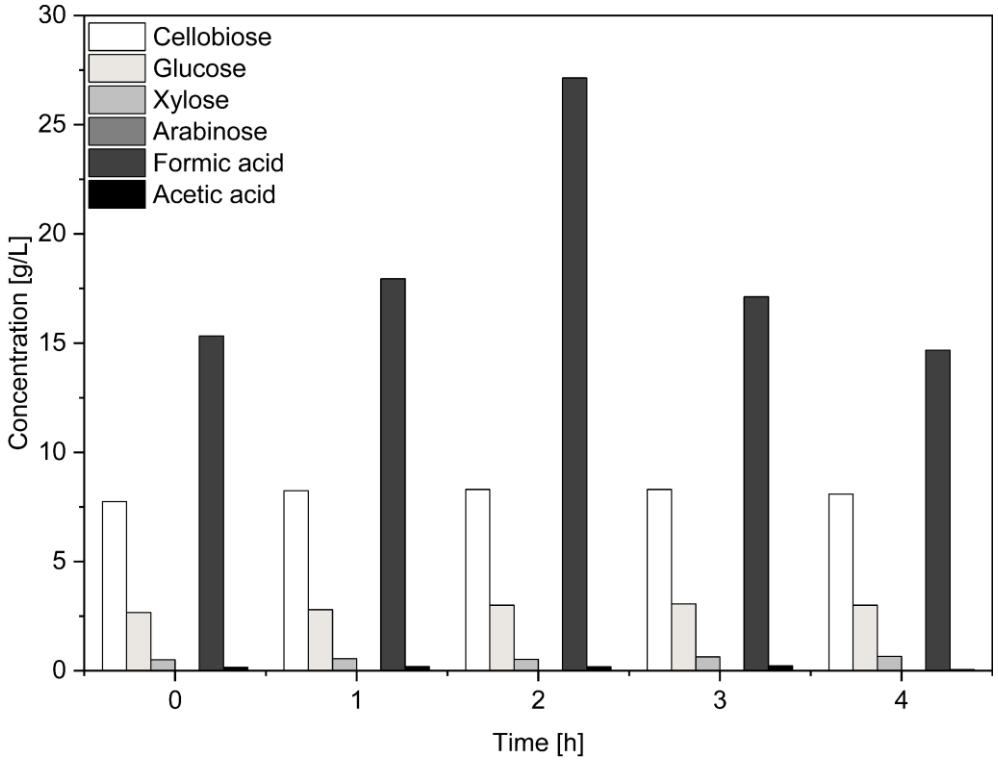

Figure A-9: Sugar and organic acid contents over time of 10 min HSM BSG after treatment with Alcalase®. Extraction performed at 60 °C for 4 h at 0.1 w/v BSG dry matter content and 125 rpm mixing.

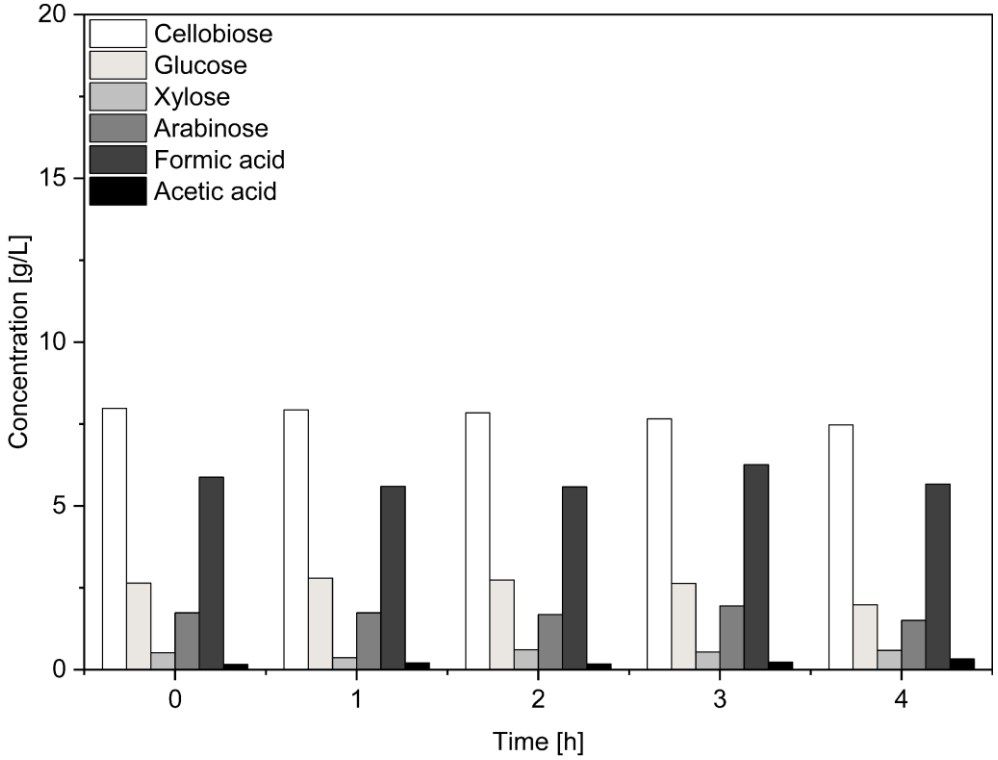

Figure A-10: Sugar and organic acid contents over time of 10 min HSM BSG after treatment with Formea® Sol. Extraction performed at 60 °C for 4 h at 0.1 w/v BSG dry matter content and 125 rpm mixing.

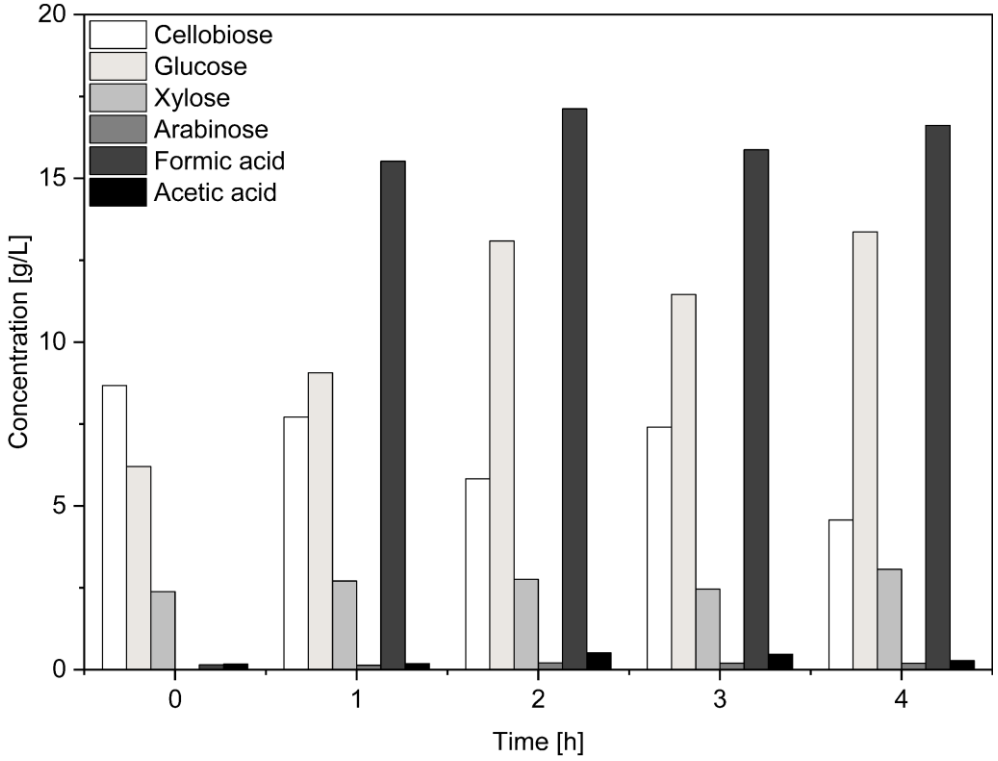

Figure A-11: Sugar and organic acid contents over time of 10 min HSM BSG after treatment with Viscozyme® and Alcalase®. Extraction performed at 60 °C for 4 h at 0.1 w/v BSG dry matter content and 125 rpm mixing.

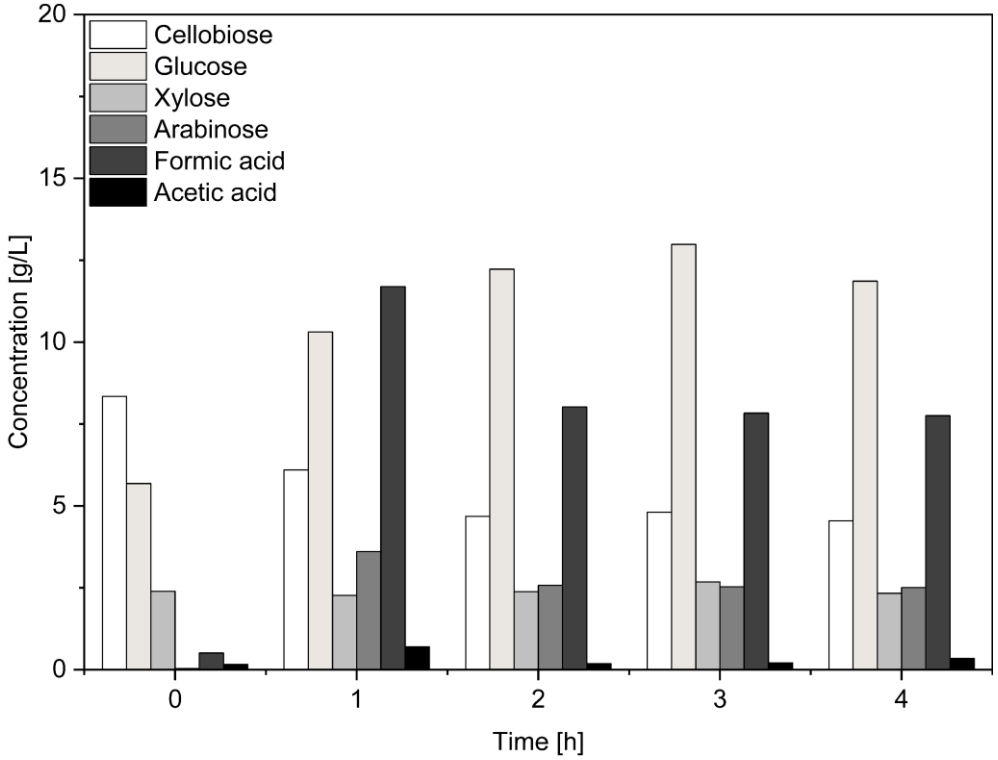

Figure A- 12: Sugar and organic acid contents over time of 10 min HSM BSG after treatment with Viscozyme® and Formea® Sol. Extraction performed at 60 °C for 4 h at 0.1 w/v BSG dry matter content and 125 rpm mixing.

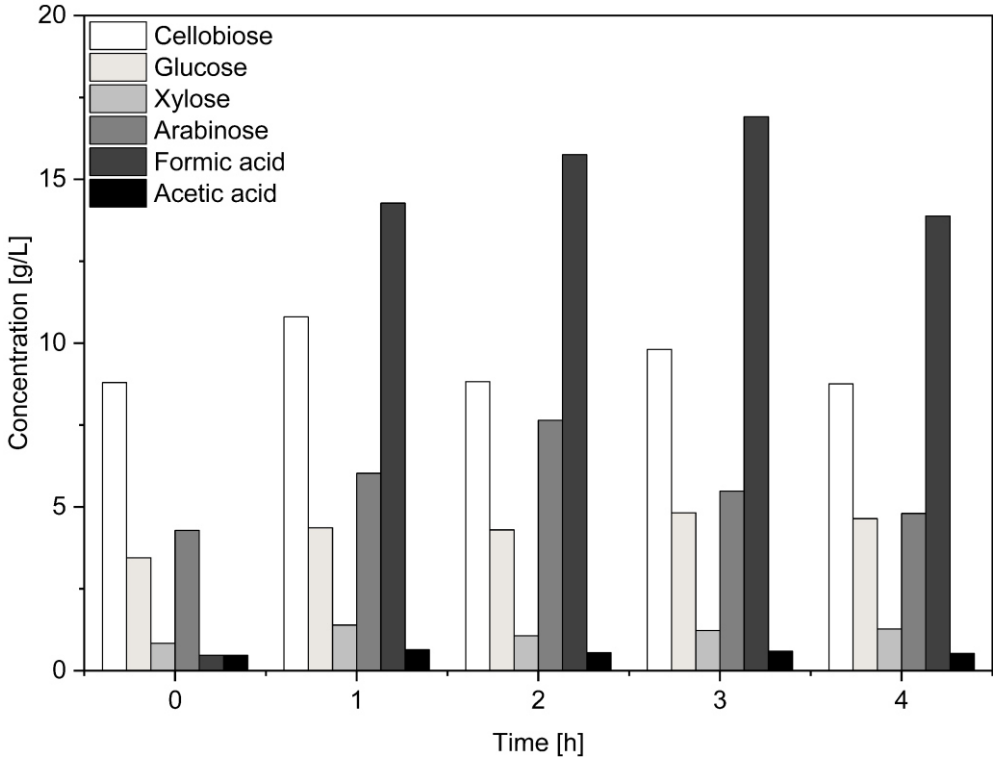

Figure A-13: Sugar and organic acid contents over time of 10 min HSM BSG after treatment with Celluclast® and Alcalase®. Extraction performed at 60 °C for 4 h at 0.1 w/v BSG dry matter content and 125 rpm mixing.

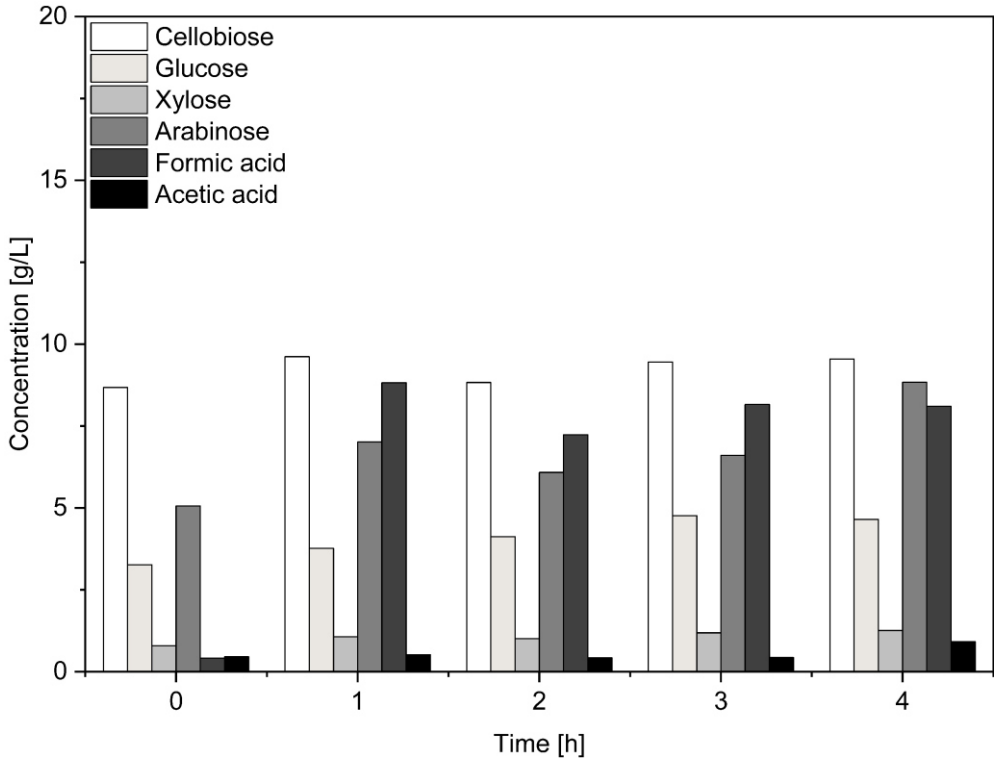

Figure A-14: Sugar and organic acid contents over time of 10 min HSM BSG after treatment with Celluclast® Formea® Sol. Extraction performed at 60 °C for 4 h at 0.1 w/v BSG dry matter content and 125 rpm mixing.

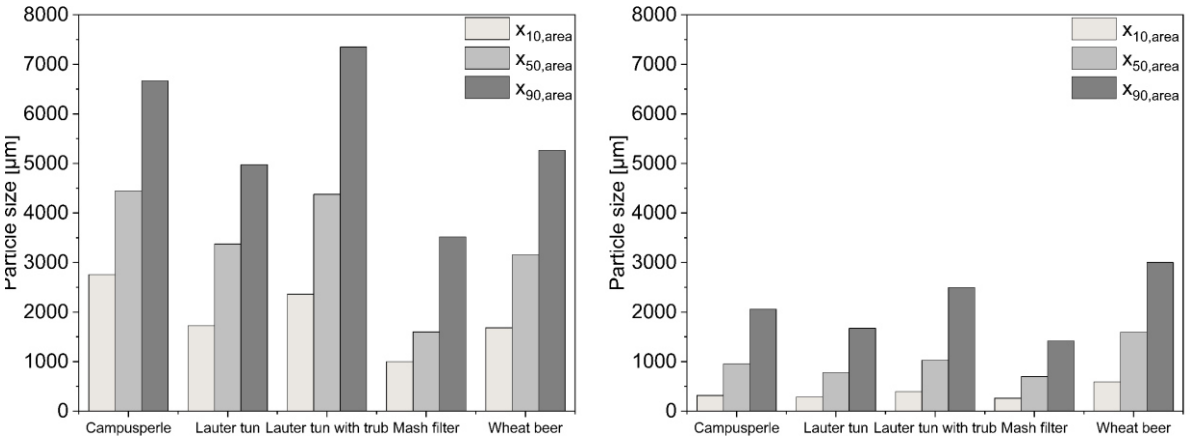

Figure A-15: Particle size distributions of different BSG types used. Left: 0 min HSM. Right: 10 min HSM.

Table A-2: Results obtained during DoE optimization study of BSG protein hydrolysis by BSY proteases.

Run	Temperature [°C]	pH [-]	Time [h]	E/S [v/v]	$x_{P,ABS}$ [-]	StDev [-]
1	30	6	6	30	82.5%	0.4%
2	30	5.5	2	30	83.8%	0.3%
3	30	6	6	30	83.3%	1.8%
4	30	6	2	10	75.4%	0.6%
5	30	7	6	10	0.0%	3.8%
6	60	5.5	2	10	81.8%	0.4%
7	60	7	2	20	53.9%	3.2%
8	60	7	8	10	54.9%	2.6%
9	60	6	6	20	78.3%	2.6%
10	60	6	6	20	81.6%	0.5%
11	41	5.5	4	20	83.2%	0.3%
12	41	5.5	4	20	81.5%	0.6%
13	41	6.5	8	20	76.3%	1.6%
14	41	6.5	8	20	71.0%	2.8%
15	55	7	6	30	33.0%	8.7%
16	55	5.5	8	30	87.1%	0.3%
17	55	6	2	30	81.8%	1.4%
18	47	6.5	4	10	68.8%	5.7%
19	47	6.5	4	10	74.5%	1.5%
20	34	7	2	30	41.7%	7.9%
21	44	6.5	4	30	77.3%	0.8%
22	39	7	4	20	30.1%	8.3%
23	32	5.5	8	10	72.4%	0.8%
24	59	6	8	10	83.1%	0.3%
25	48	5.5	6	10	73.8%	0.7%

Table A-3: Experimental results for optimization DoE for XOS and AOS extraction using LHW treatment on 30 mL scale. V = verification run for DoE. S = scale-up run in 3 L reactor.

Run	Temprature	Solid Liquid ratio	Time	XOS Concentration	AOS Concentration	Combined Yield	Xylose Concentration	Arabinose Concentration	Severity Factor
	°C	-	min	g/L	g/L		[g/L]	[g/L]	-
1	160	0.05	5	0.42	0.54	0.15	0.85	0.40	2.47
2	180	0.05	15	3.27	1.20	0.68	1.49	1.01	3.53
3	200	0.15	5	6.72	1.76	0.31	8.36	1.78	3.64
4	200	0.05	25	0.50	0.49	0.08	3.50	0.54	4.34
5	160	0.15	25	6.68	2.76	0.43	4.21	2.04	3.16
6	160	0.15	5	0.89	1.47	0.10	2.17	0.36	2.47
7	180	0.1	15	4.13	2.26	0.46	2.14	1.13	3.53
8	180	0.1	15	5.55	2.30	0.57	2.80	1.69	3.53
9	180	0.1	15	3.35	1.41	0.32	1.60	0.86	3.53
10	180	0.1	5	3.33	2.01	0.39	2.01	1.02	3.05
11	160	0.1	15	1.41	1.54	0.21	1.77	0.54	2.94
12	200	0.1	15	2.55	0.87	0.22	3.99	1.13	4.12
13	200	0.05	5	3.75	1.56	0.76	1.04	0.98	3.64
14	180	0.1	25	5.50	1.00	0.47	2.76	1.86	3.75
15	180	0.1	15	4.79	1.69	0.47	2.79	1.59	3.53
16	200	0.15	25	1.21	1.04	0.07	5.10	0.95	4.34
17	180	0.1	15	3.36	2.33	0.39	1.95	1.04	3.53
18	180	0.15	15	5.95	1.73	0.35	4.49	2.07	3.53
19	160	0.05	25	1.45	1.11	0.39	0.82	0.50	3.16
V1	160	0.1	10	0.88	1.28	0.17	1.71	0.54	2.77
V2	170	0.1	10	0.63	1.29	0.16	1.83	0.55	3.06
V3	180	0.125	15	7.38	2.00	0.61	2.80	2.29	3.53
V4	190	0.05	20	3.59	0.47	0.65	1.57	1.11	3.95
S1	170	0.05	20	4.74	1.44	0.79	0.78	1.04	3.36
S2	180	0.05	10	5.76	1.26	0.90	0.91	1.19	3.36
S3	180	0.05	5	4.64	1.55	0.79	0.78	0.98	3.05
S4	185	0.05	5	5.33	1.57	0.88	1.06	1.19	3.20

Table A-4: Results and predicted values for DoE verification experiment at 190 °C for 20 min and a solid to liquid ratio of 0.05.

Response	Predicted Mean	Predicted Median	Std Dev	SE Pred	95% PI low	Data Mean	95% PI high
XOS Concentration [g/L]	2.64072	2.64072	1.18929	1.43734	-0.61076	3.59052	5.8922
AOS Concentration [g/L]	0.94884	0.94884	0.487113	0.549584	-0.24860	0.46813	2.14628
Combined Yield	0.482781	0.482781	0.0957778	0.115754	0.220927	0.65453	0.744636

Table A-5: Results and predicted values for DoE verification experiment at 180 °C for 15 min and a solid to liquid ratio of 0.125.

Response	Predicted Mean	Predicted Median	Std Dev	SE Pred	95% PI low	Data Mean	95% PI high
XOS Concentration [g/L]	4.92166	4.92166	1.18929	1.27876	2.02891	7.37671	7.81441
AOS Concentration [g/L]	1.72404	1.72404	0.487113	0.505667	0.622287	2.00481	2.8258
Combined Yield	0.421171	0.421171	0.0957778	0.102983	0.188207	0.610495	0.654136

Table A-6: Results and predicted values for DoE verification experiment at 170 °C for 10 min and a solid to liquid ratio of 0.1.

Response	Predicted Mean	Predicted Median	Std Dev	SE Pred	95% PI low	Data Mean	95% PI high
XOS Concentration [g/L]	3.02929	3.02929	1.18929	1.28601	0.120123	0.629902	5.93846
AOS Concentration [g/L]	1.54806	1.54806	0.487113	0.513308	0.429662	1.29406	2.66647
Combined Yield	0.340942	0.340942	0.0957778	0.103568	0.106656	0.155229	0.575229

Table A-7: Results and predicted values for DoE verification experiment at 160 °C for 10 min and a solid to liquid ratio of 0.1.

Response	Predicted Mean	Predicted Median	Std Dev	SE Pred	95% PI low	Data Mean	95% PI high
XOS Concentration [g/L]	0.702518	0.702518	1.18929	1.44842	-2.57402	0.880821	3.97906
AOS Concentration [g/L]	1.51888	1.51888	0.487113	0.535577	0.351958	1.28038	2.6858
Combined Yield	0.12001	0.12001	0.0957778	0.116646	-0.14386	0.174345	0.383882

Table A-8: Xylose and arabinose concentrations obtained for scale-up experiments in 3 L LHW reactor.

Temperature [°C]	Reaction time [min]	Severity Factor [-]	Xylose concentration [g/L]	Arabinose concentration [g/L]
185	5	3.20	1.11	1.19 ± 0.05
180	5	3.05	0.42 ± 0.01	0.97 ± 0.01
180	10	3.36	0.34 ± 0.02	1.19 ± 0.04
170	20	3.36	0.36 ± 0.10	1.04 ± 0.01

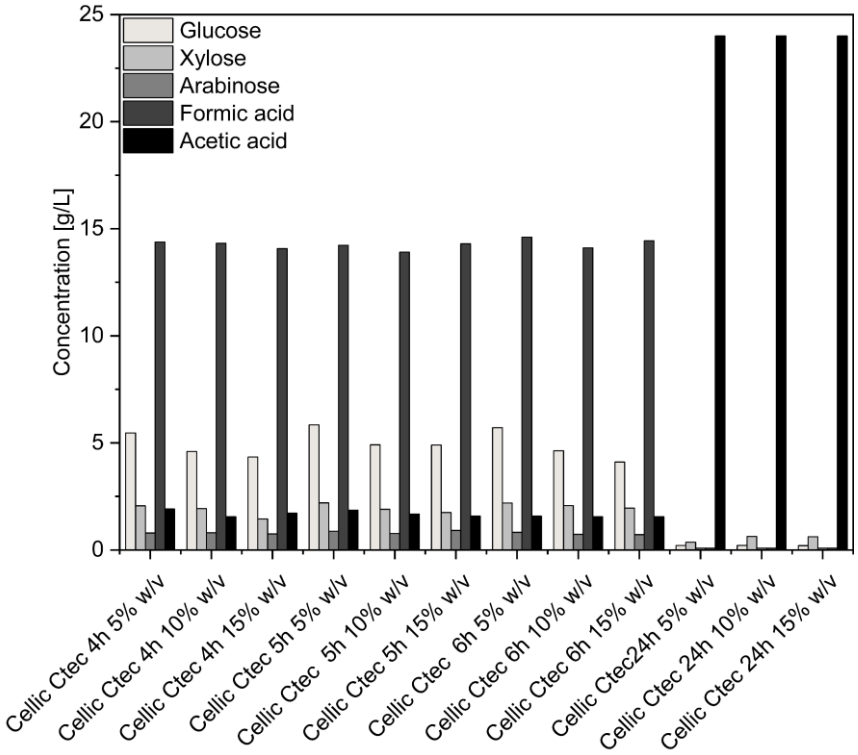

Figure A-16: Monosaccharide and organic acid concentrations for screening experiments using Cellic® Ctec at different incubation times and enzyme dosages. Activity of stock solution: 10 U/mL. Extractions performed with 5 min HSM BSG at 50 °C, pH 5 and 120 rpm.

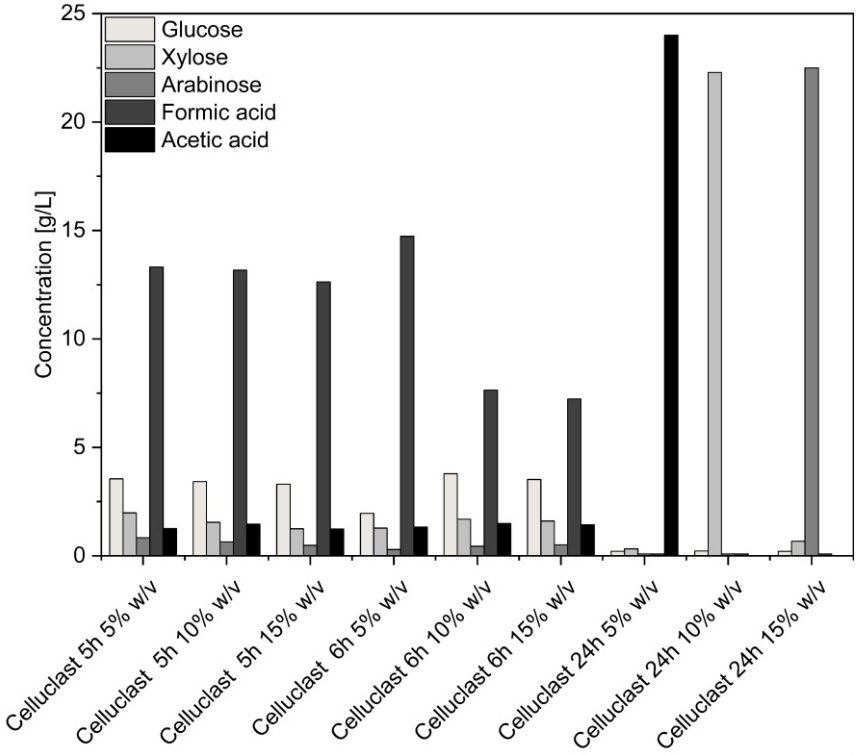

Figure A-17: Monosaccharide and organic acid concentrations for screening experiments using Celluclast® at different incubation times and enzyme dosages. Activity of stock solution: 10 U/mL. Extractions performed with 5 min HSM BSG at 50 °C, pH 5 and 120 rpm.

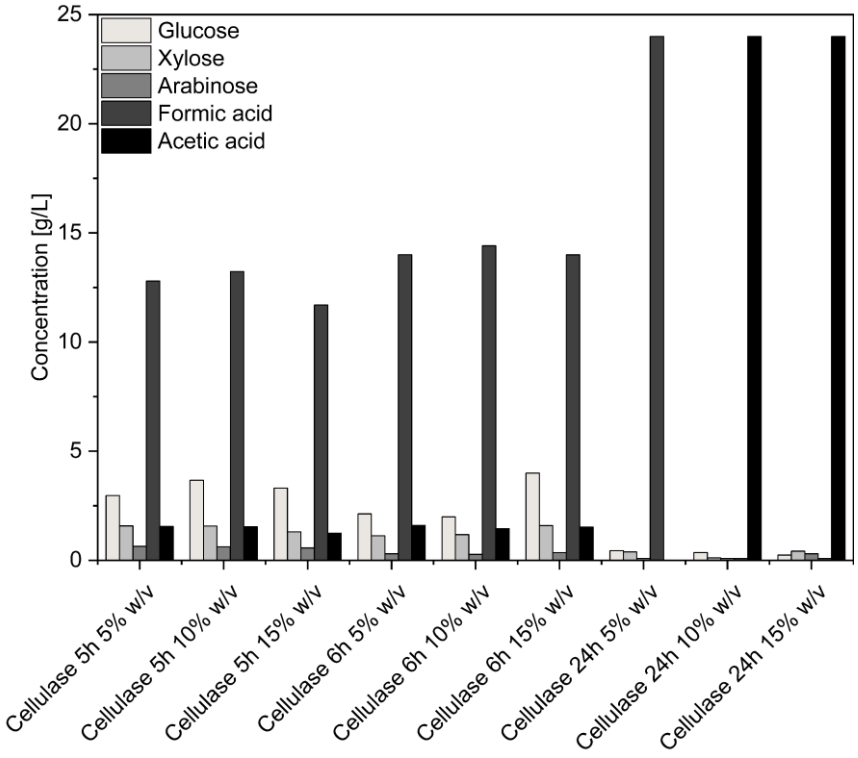

Figure A-18: Monosaccharide and organic acid concentrations for screening experiments using Cellulase at different incubation times and enzyme dosages. Activity of stock solution: 10 U/mL. Extractions performed with 5 min HSM BSG at 50 °C, pH 5 and 120 rpm.

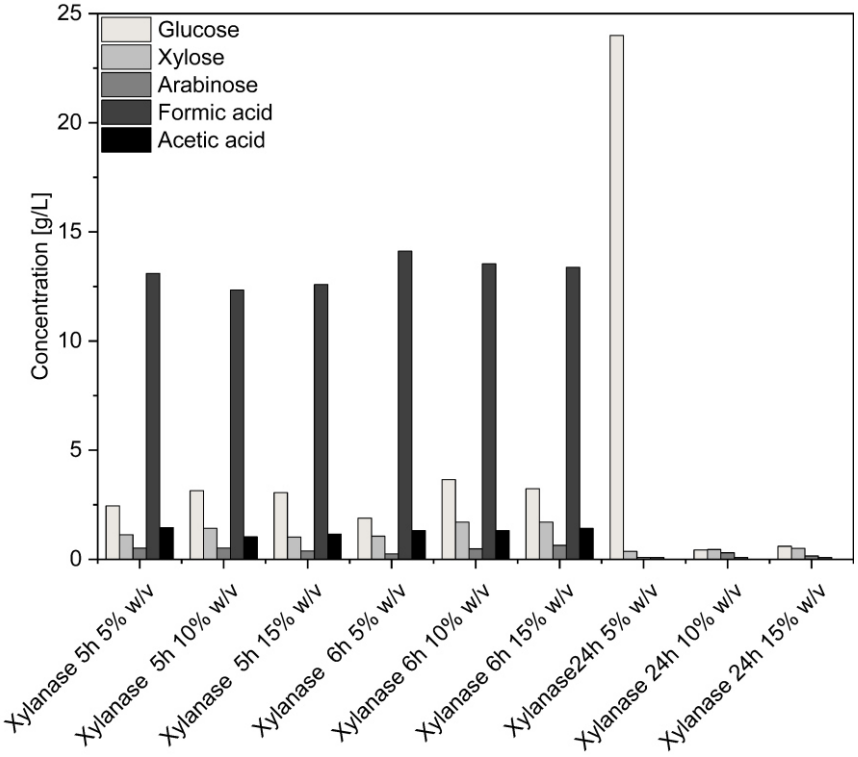

Figure A-19: Monosaccharide and organic acid concentrations for screening experiments using Xylanase at different incubation times and enzyme dosages. Activity of stock solution: 10 U/mL. Extractions performed with 5 min HSM BSG at 50 °C, pH 5 and 120 rpm.

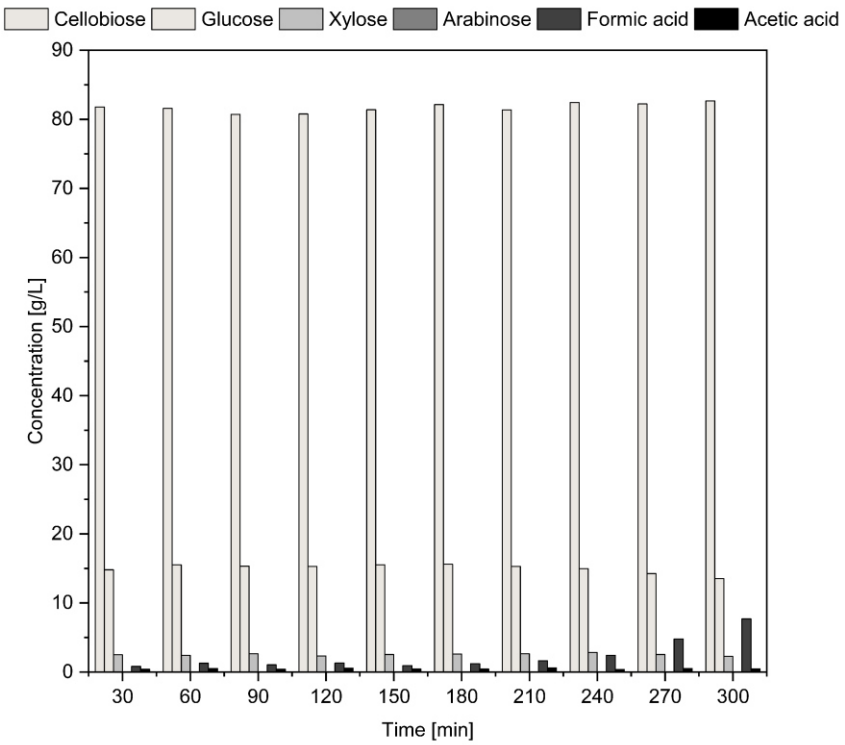

Figure A-20: Monosaccharide and organic acid concentrations for scale-up experiment using Celluclast® at 5% w/v enzyme dosage. Activity of stock solution: 10 U/mL. Extractions performed with 5 min HSM BSG at 50 °C, pH 5 and 50% power input of top-mounted agitator (27 rpm).

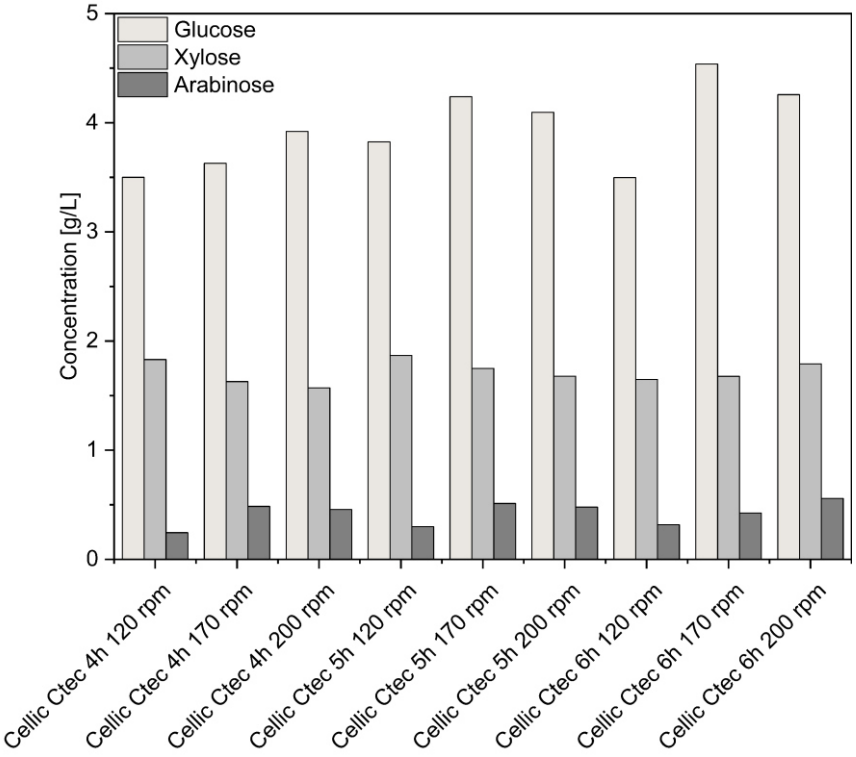

Figure A-21: Influence of mixing rpm on sugar extraction from 5% HSM BSG at 50 °C, pH 5, 5% w/v enzyme dosage with activity 100 U/mL in stock solution.

Table A-9: Experimental results for optimization DoE for C5 and C6 sugar extractions from BSG using Celluclast®.

No.	Temperature [°C]	Time [h]	S/E [%w/v]	pH	C5 yield [-]	C6 yield [-]	Arabinose conc. [g/L]	Xylose conc. [g/L]	Glucose conc. [g/L]
1	46.	8.88	5	4.5	1	0.23	0	2	5.04
2	51	11.61	5	5.5	1	0.16	0	3	3.57
3	45	6.89	10	5.5	1	0.21	0	2	4.67
4	45	12	1	5	1	0.16	0.73	3	2.93
5	45	12	10	4.5	1	0.21	0	2	4.58
6	51	11.65	10	4.5	1	0.4	0	4	8.96
7	53	6.47	1	4.5	1	0.31	0.3	3	5.7
8	54	10.6	10	5	0	0.17	0	2	3.78
9	47	10.35	1	5.5	1	0.38	0.76	4	6.89
10	47	10.32	10	5	1	0.21	0	2	4.74
11	52	7.1	10	5.5	1	0.25	0.03	3	5.59
12	47	10.35	1	5.5	1	0.38	0.76	4	6.89
13	55	12	5	4.5	0	0.02	0	0	0.5
14	52	10.35	1	4.5	1	0.3	0	3	5.53
15	49	5	10	4.5	1	0.18	0.14	2	4.09
16	55	5	5	4.5	1	0.21	0	2	4.67
17	53	11.86	10	5.5	0	0.06	0.54	1	1.39
18	52	10.28	5	5	1	0.31	0.39	4	6.87
19	55	9.2	10	4.5	1	0.2	0	2	4.45
20	55	5	1	5.5	1	0.24	0	3	4.33
21	51	6.05	1	5	1	0.31	0.35	3	5.55
22	45	5	1	4.5	1	0.24	0	3	4.33
23	46	8.85	5	4.5	1	0.23	0	2	5.04
24	55	5	10	5	1	0.18	0	2	4.04
25	47	10.32	10	5	1	0.21	0	2	4.74
26	45	5	5	5	1	0.18	5	2	4.04
27	55	9.2	5	5.5	0	0.08	0	1	1.79
28	49	5	5	5.5	1	0.19	0.11	2	4.15
29	52	10.28	5	5	1	0.23	0	2	5.04
30	51	6.05	1	5	1	0.31	0.39	4	6.87
31	55	12	1	5	1	0.31	0.35	3	5.55
32	45	12	5	5.5	0	0.01	0.01	0	0.31

Table A-10: Experimental results for optimization DoE for C5 and C6 sugar extractions from BSG using Cellic Ctec®.

No.	Temperature [°C]	Time [h]	S/E [%w/v]	pH	C5 yield [-]	C6 yield [-]	Arabinose conc. [g/L]	Xylose conc. [g/L]	Glucose conc. [g/L]
1	46.	8.88	5	4.5	0.59	0.25	0	2.44	5.53
2	51	11.61	5	5.5	0.95	0.17	0	3.93	3.75
3	45	6.89	10	5.5	0.59	0.22	0	2.46	4.81
4	45	12	1	5	1	0.54	0.34	4.34	9.76
5	45	12	10	4.5	0.56	0.21	0.02	2.27	4.63
6	51	11.65	10	4.5	0.76	0.34	0	3.14	7.46
7	53	6.47	1	4.5	1	0.64	0.04	3.94	11.63
8	54	10.6	10	5	0.73	0.42	0	3.01	9.33
9	47	10.35	1	5.5	1	0.81	0.5	5.98	14.77
10	47	10.32	10	5	0.72	0.32	0.02	2.94	7.03
11	52	7.1	10	5.5	1	0.26	1.02	2.51	5.87
12	47	10.35	1	5.5	1	0.81	0.5	5.98	14.77
13	55	12	5	4.5	0.08	0.05	0.01	0.33	1.08
14	52	10.35	1	4.5	0.97	0.49	0	3.28	8.92
15	49	5	10	4.5	0.63	0.19	0.15	2.35	4.27
16	55	5	5	4.5	0.6	0.22	0	2.46	4.81
17	53	11.86	10	5.5	0.75	0.19	0.52	2.26	4.13
18	52	10.28	5	5	1	0.63	0.36	5.44	13.87
19	55	9.2	10	4.5	0.67	0.29	0	2.79	6.54
20	55	5	1	5.5	1	0.62	0	3.76	11.28
21	51	6.05	1	5	1	0.65	0.01	3.73	11.77
22	45	5	1	4.5	1	0.62	0	3.76	11.28
23	46	8.85	5	4.5	0.59	0.25	0	2.44	5.53
24	55	5	10	5	0.61	0.23	0	2.54	5.01
25	47	10.32	10	5	0.72	0.32	0.02	2.94	7.03
26	45	5	5	5	0.62	0.23	0	2.54	5.01
27	55	9.2	5	5.5	0.66	0.16	0	2.73	3.64
28	49	5	5	5.5	0.69	0.26	0.16	2.58	5.69
29	52	10.28	5	5	1	0.63	0.36	5.44	13.87
30	51	6.05	1	5	1	0.65	0.01	3.73	11.77
31	55	12	1	5	1	0.54	0.34	4.34	9.76
32	45	12	5	5.5	0.51	0.06	0	2.12	1.26

Table A-11: Regression coefficients and their significance C5 sugar yield using Celluclast® in the central composite design model.

Source	Sum of Squares	df	Mean Square	F-value	p-value	
Model	1.94	21	0.0926	5.54	0.0040	significant
A-Temperature	0.0834	1	0.0834	4.99	0.0495	significant
B-Time	0.0614	1	0.0614	3.67	0.0842	
C-E/S	0.3330	2	0.1665	9.96	0.0042	significant
D-pH	0.0189	2	0.0094	0.5647	0.5857	
AB	0.3607	1	0.3607	21.58	0.0009	significant
AC	0.1814	2	0.0907	5.43	0.0253	Significant
AD	0.0079	2	0.0040	0.2376	0.7928	
BC	0.0573	2	0.0286	1.71	0.2291	
BD	0.0069	2	0.0034	0.2060	0.8172	
CD	0.3107	4	0.0777	4.65	0.0222	significant
A^2	0.3111	1	0.3111	18.62	0.0015	significant
B^2	0.0358	1	0.0358	2.14	0.1741	
Residual	0.1671	10	0.0167			
Lack of Fit	0.1671	5	0.0334			not significant
Pure Error	0.0000	5	0.0000			
Cor Total	2.11	31				

Table A-12: Regression coefficients and their significance C6 sugar yield using Celluclast® in the central composite design model.

Source	Sum of Squares	df	Mean Square	F-value	p-value	
Model	0.2824	21	0.0134	6.54	0.0020	significant
A-Temperature	0.0083	1	0.0083	4.05	0.0718	
B-Time	0.0112	1	0.0112	5.47	0.0415	significant
C-E/S	0.0294	2	0.0147	7.15	0.0118	significant
D-pH	0.0100	2	0.0050	2.43	0.1380	
AB	0.0220	1	0.0220	10.69	0.0084	significant
AC	0.0119	2	0.0059	2.89	0.1025	
AD	0.0115	2	0.0057	2.79	0.1086	
BC	0.0089	2	0.0045	2.18	0.1642	
BD	0.0076	2	0.0038	1.84	0.2086	
CD	0.0462	4	0.0115	5.61	0.0124	significant
A^2	0.0503	1	0.0503	24.46	0.0006	significant
B^2	0.0222	1	0.0222	10.82	0.0082	significant
Residual	0.0206	10	0.0021			
Lack of Fit	0.0206	5	0.0041			not significant
Pure Error	0.0000	5	0.0000			
Cor Total	0.3030	31				

Table A-13: Regression coefficients and their significance C5 sugar yield using Cellic Ctec® in the central composite design model.

Source	Sum of Squares	df	Mean Square	F-value	p-value	
Model	1.41	21	0.0670	5.94	0.0030	significant
A-Temperature	0.0107	1	0.0107	0.9514	0.3524	
B-Time	0.0005	1	0.0005	0.0475	0.8319	
C-E/S	0.5266	2	0.2633	23.35	0.0002	significant
D-pH	0.0972	2	0.0486	4.31	0.0447	significant
AB	0.0518	1	0.0518	4.59	0.0578	
AC	0.0181	2	0.0091	0.8029	0.4749	
AD	0.0522	2	0.0261	2.31	0.1494	
BC	0.0122	2	0.0061	0.5421	0.5977	
BD	0.0838	2	0.0419	3.72	0.0621	
CD	0.1651	4	0.0413	3.66	0.0437	significant
A^2	0.1060	1	0.1060	9.40	0.0119	significant
B^2	0.0277	1	0.0277	2.46	0.1479	
Residual	0.1128	10	0.0113			
Lack of Fit	0.1128	5	0.0226			not significant
Pure Error	0.0000	5	0.0000			
Cor Total	1.52	31				

Table A-14: Regression coefficients and their significance C6 sugar yield using Cellic Ctec® in the central composite design model.

Source	Sum of Squares	df	Mean Square	F-value	p-value	
Model	1.46	21	0.0695	74.56	< 0.0001	significant
A-Temperature	0.0008	1	0.0008	0.8634	0.3747	
B-Time	6.010E-06	1	6.010E-06	0.0064	0.9376	
C-E/S	0.8191	2	0.4095	439.42	< 0.0001	significant
D-pH	0.0732	2	0.0366	39.25	< 0.0001	significant
AB	0.0061	1	0.0061	6.58	0.0281	
AC	0.0337	2	0.0168	18.06	0.0005	significant
AD	0.0557	2	0.0278	29.86	< 0.0001	significant
BC	0.0376	2	0.0188	20.19	0.0003	significant
BD	0.0316	2	0.0158	16.97	0.0006	significant
CD	0.1809	4	0.0452	48.51	< 0.0001	significant
A^2	0.0317	1	0.0317	34.06	0.0002	significant
B^2	0.0397	1	0.0397	42.56	< 0.0001	significant
Residual	0.0093	10	0.0009			
Lack of Fit	0.0093	5	0.0019			not significant
Pure Error	0.0000	5	0.0000			
Cor Total	1.47	31				

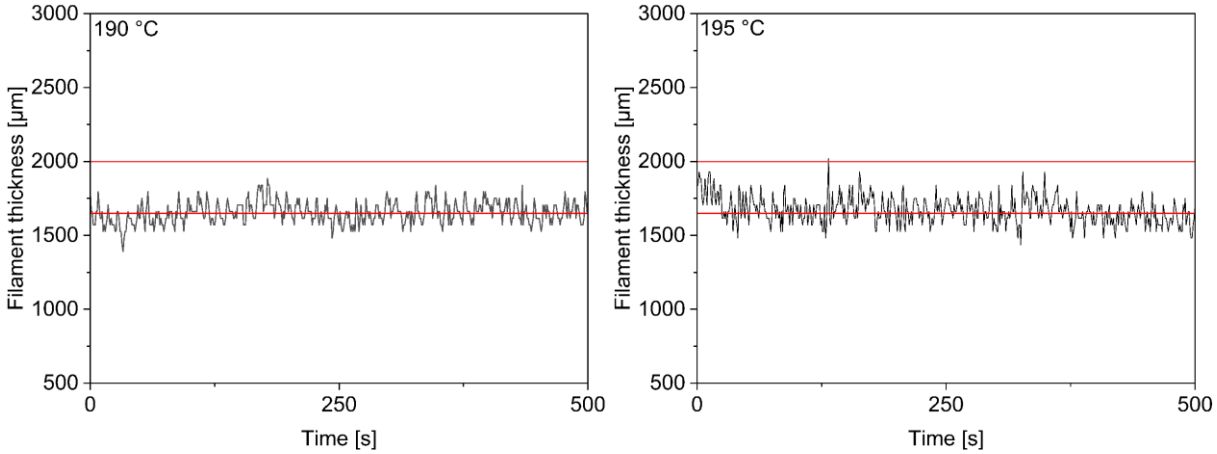

Figure A-22: Filament thickness over time during extrusion of 5% by weight BSG and PLA composite at 5.5 rpm and 65% fan speed. Left: Extrusion at 190 °C. Right: Extrusion at 195 °C.

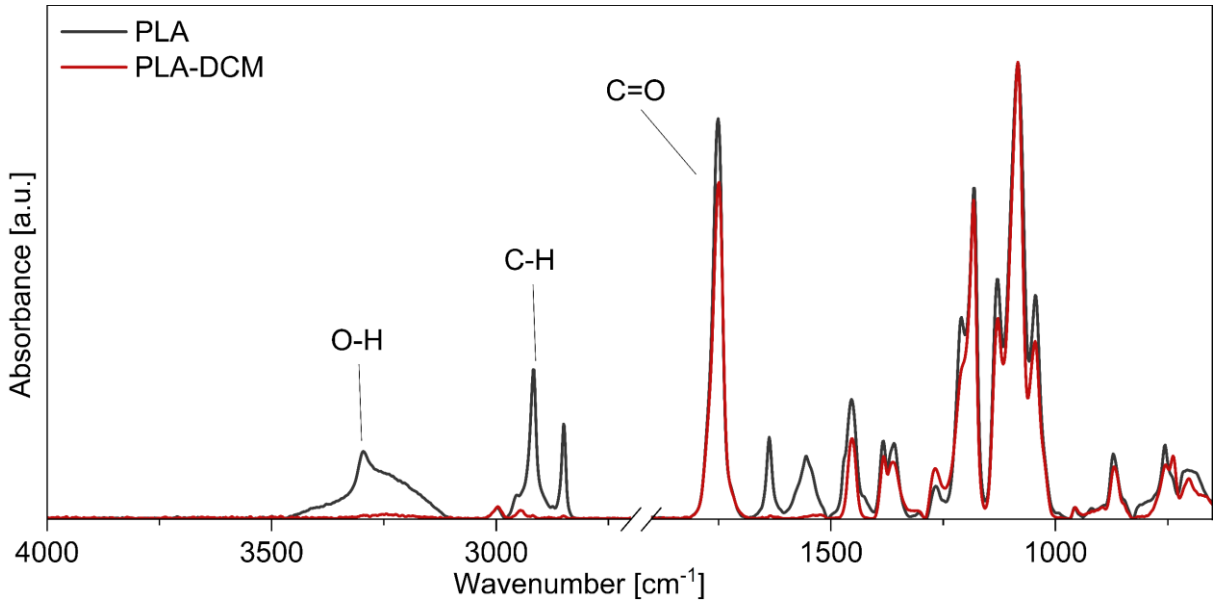

Figure A-23: FTIR spectrum of virgin PLA pellets and of PLA after dissolution in DCM.